AD-A098 683 ILLINOIS UNIV AT CHICAGO CIRCLE DEPT OF MATERIALS ENG--ETC F/G 11/4
STRESS ANALYSIS OF COMPOSITES.(U)
JAN 81 R L SPILKER, T C TING
DAAG46-79-C-0045

UNCLASSIFIED AMMRC-TR-81-8 NL

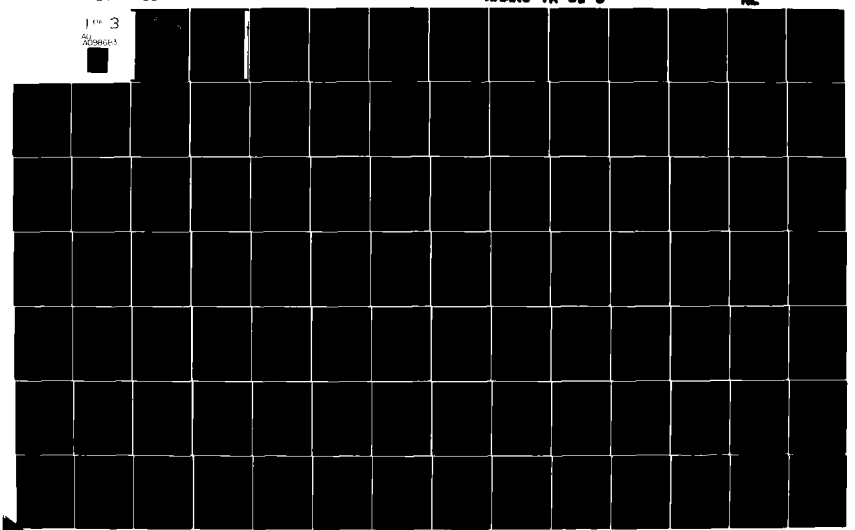

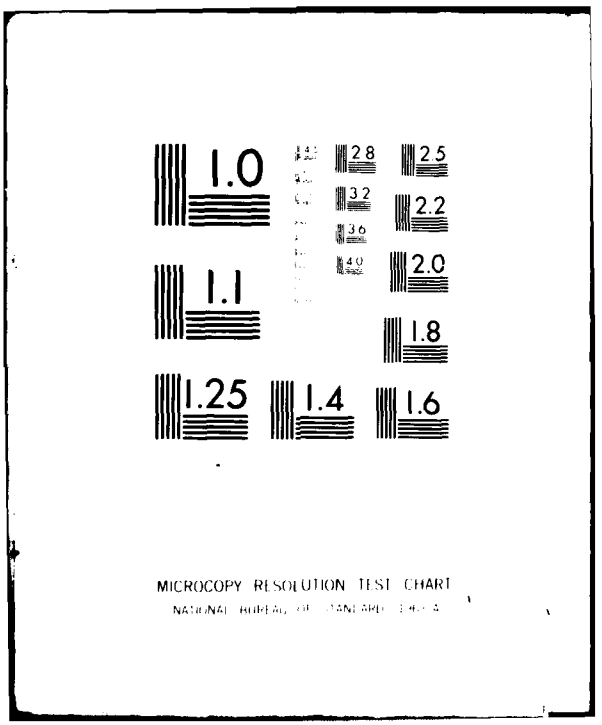
1.0
1.1
1.25
1.4
1.6
1.8
2.0
2.2
2.5
2.8
3.2
3.6
4.0
MICROCOPY RESOLUTION TEST CHART
NATIONAL BUREAU OF STANDARDS

AMMRC TR 81-5

STRESS ANALYSIS OF COMPOSITES

JANUARY 1981

R. L. SPILKER AND T. C. T. TING

DEPARTMENT OF MATERIALS ENGINEERING
UNIVERSITY OF ILLINOIS AT CHICAGO CIRCLE
CHICAGO, ILLINOIS 60680

Final Report Contract Number DAAG 46-79-C-0045

Prepared for

ARMY MATERIALS AND MECHANICS RESEARCH CENTER
Watertown, Massachusetts 02172

The findings in this report are not to be construed as an official Department of the Army position, unless so designated by other authorized documents.

Mention of any trade names or manufacturers in this report shall not be construed as advertising nor as an official indorsement or approval of such products or companies by the United States Government.

DISPOSITION INSTRUCTIONS

Destroy this report when it is no longer needed.
Do not return it to the originator.

UNCLASSIFIED

SECURITY CLASSIFICATION OF THIS PAGE (When Data Entered)

REPORT DOCUMENTATION PAGE	READ INSTRUCTIONS BEFORE COMPLETING FORM
1. REPORT NUMBER: AMMRC TR-81-5	2. GOVT ACCESSION NO.: AD-A098 683	3. RECIPIENT'S CATALOG NUMBER
4. TITLE (and Subtitle): STRESS ANALYSIS OF COMPOSITES	5. TYPE OF REPORT & PERIOD COVERED: Final Report. Aug 79 - Aug 80
	6. PERFORMING ORG. REPORT NUMBER
7. AUTHOR(s): R. L. Spilker and T. C. T. Ting	8. CONTRACT OR GRANT NUMBER(s): DAAG46-79-C-0045
9. PERFORMING ORGANIZATION NAME AND ADDRESS: Department of Materials Engineering, University of Illinois at Chicago Circle, Chicago, Illinois 60680	10. PROGRAM ELEMENT, PROJECT, TASK AREA & WORK UNIT NUMBERS: D/A Project 8X363304D215; AMCMS Code: 633304.21500.03
11. CONTROLLING OFFICE NAME AND ADDRESS: Army Materials and Mechanics Research Center, ATTN: DRXMR-AP, Watertown, Massachusetts 02172	12. REPORT DATE: January 1981
	13. NUMBER OF PAGES: 240
14. MONITORING AGENCY NAME & ADDRESS(if different from Controlling Office)	15. SECURITY CLASS. (of this report): Unclassified
	15a. DECLASSIFICATION/DOWNGRADING SCHEDULE

16. DISTRIBUTION STATEMENT (of this Report)

Approved for public release; distribution unlimited.

17. DISTRIBUTION STATEMENT (of the abstract entered in Block 20, if different from Report)

18. SUPPLEMENTARY NOTES

19. KEY WORDS (Continue on reverse side if necessary and identify by block number)

Composite materials
Finite element
Stress analysis
Wave propagation
Plastic analysis
Viscoelasticity
Transient responses

20. ABSTRACT (Continue on reverse side if necessary and identify by block number)

Static and dynamic stress analysis of laminated composites is studied. In the static analysis, the hybrid-stress finite element model is used for (1) the study of edge effects in symmetrically-stacked laminates subject to prescribed inplane strain, (2) the development and evaluation of 8-node single-layer plate bending elements for which the traction-free conditions are satisfied along a straight edge, and (3) the elastic-plastic analysis of single layer plates. An analytic study is also presented to determine the nature of the potential 2-D singularity at the intersection of a bimaterial interface and a free edge.

DD FORM 1 JAN 73 1473 EDITION OF 1 NOV 65 IS OBSOLETE

UNCLASSIFIED

SECURITY CLASSIFICATION OF THIS PAGE (When Data Entered)

40 171

Block No. 20

In the dynamic analysis, the stress response in a laminated composite due to a unit step load applied at the boundary is obtained for points which are (a) at a finite distance, and (b) at a large distance, from the impact end. For the case (a), the composite may consist of a finite number of layers.

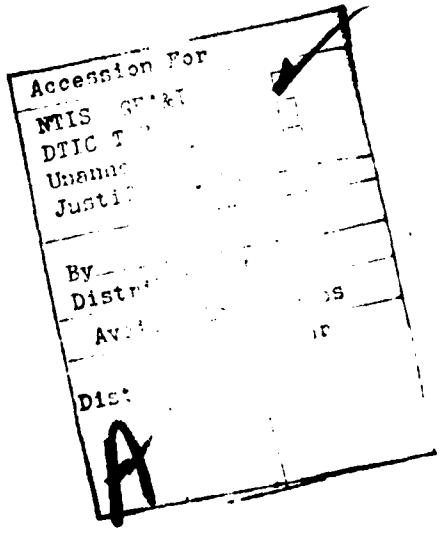

CONTENTS

FOREWORD

This research work was performed for the Army Materials and Mechanics Research Center (AMMRC), Watertown, Massachusetts under Contract No. DAAG46-79-C-0045 with the University of Illinois at Chicago Circle, Chicago, Illinois. Mr. J. F. Dignam of the AMMRC was the project manager and Dr. S. C. Chou was technical monitor. The support and encouragement of Mr. Dignam and Dr. Chou are gratefully acknowledged.

CHAPTER 1

INTRODUCTION

The use of fiber reinforced composite materials for structural components affords the designer the flexibility of choosing appropriate layer orientations to achieve required directional stiffness. These materials are particularly attractive in applications where high strength to weight ratios are important. However, this flexibility comes an increased complexity in the analysis of these structures and numerical techniques are required.

The goal of the static response portion of the present project is the nonlinear analysis of thin to moderately thick multilayer composite plate structures. These structures may include cutouts and/or other free edges; an important consideration is the possibility of severe stress gradients near these free edges.

In order to obtain accurate prediction of nonlinear structural response, accurate finite elements, coupled with an appropriate and accurate nonlinear analysis scheme will be needed. In terms of the nonlinear analysis, alternate schemes can be examined and compared using problems of elastic-plastic analysis of single layer plates; the results of such a study should then guide the selection of the nonlinear scheme for multilayer plates.

To achieve this goal, four pilot studies are described which will serve as building blocks for a future static analysis program. The studies include; (1) the analysis of edge effects in laminates under prescribed uniaxial inplane strain, (2) the development of a single layer plate element with a straight traction-free edge, (3) the elastic-plastic analysis of single layer isotropic plates, and (4) edge singularity analysis. The rationale for each of these tasks is described in the following.

The assumed-stress hybrid finite element model is used in the first three studies. Briefly, this model involves the selection of (1) an intraelement stress field which satisfies the homogeneous equilibrium equations, and (2) an intraelement (or element boundary) displacement field which yields the required interelement boundary displacement continuity. Elements based on this model are often found to yield improved convergence and intraelement stress predictions in comparison to corresponding assumed-displacement elements. The hybrid-stress model is ideally suited for multilayer plate applications since layer stress fields can be defined which satisfy exactly interlaminar traction continuity and upper/lower surface traction-free conditions exactly. In addition free-edge conditions can, inprinciple, be satisfied exactly.

The three studies identified above are described in Chapters 2 through 4 of this report. Each chapter is reasonably self-contained and includes pertinent literature survey, details of the formulations and developemnts, example problems, and summary remarks. The following is a brief summary of each study, including the relevance to the overall analysis objectives,

In order to better understand the nature of stress distributions in the vicinity of cutouts and other free-edges, it is first necessary to better understand the free-edge-vicinity stress distributions in a more well-defined (simple) problem. One such pilot problem which is used by most investigators is a multilayer strip (symmetrically stacked) of finite thickness and width which are less than the strip length. This is intended to simulate a tension test specimen. Mathematically, the problem is posed as a generalized plane strain analysis (in the cross-section of the strip)

in which the loading corresponds to a prescribed uniform inplane strain (normal to the plane of analysis). Such a problem is useful in the present study since relatively efficient 2-D generalized plane strain analysis can be performed. In any finite-element analysis certain of the elasticity field equations and boundary conditions are only approximately satisfied. The purpose of one pilot study, described in Chapter 2, is to assess the effects of enforcement of (1) traction-free edge or (2) interlayer strain continuity conditions on the predicted stress distributions near the free-edge. Although the present study utilizes pseudo 2-D elements, the results obtained should provide insight into those conditions which should be incorporated into more general 3-D multilayer plate elements designed for use near free-edge zones of a structure.

In the analysis of more general multilayer plate structures with free-edges, special-purpose multilayer plate elements may be required along the free-edges. One such element currently envisioned is a multilayer plate element for which the traction-free conditions are exactly satisfied along one edge of the element. With the hybrid-stress model, this requires that a layer stress field be defined which exactly satisfies the traction-free conditions on that edge. Numerous plausible stress fields can be defined, and numerical experimentation is required to identify the best stress field. Extensive insight toward identifying the best stress field can be obtained by considering a single layer pure bending moderately thick plate element in which all components of stress (bending contributions) are included. In Chapter 3, an 8-node moderately thick single layer plate element with a straight traction-free edge is developed. Various stress fields, each satisfying the free-edge conditions, are defined and compared for selected example problems. The best stress field (element) is identified,

and can serve as a basis for development of a special-purpose multilayer plate element including both bending and stretching contributions.

The analysis program envisioned will include material nonlinear effects. One phase of the present study is to evaluate alternate nonlinear analysis schemes in terms of accuracy and efficiency. Alternate hybrid-stress functionals are defined in Chapter 4 for material nonlinear analysis using the initial-stress procedure. In this procedure, material nonlinearities are accounted for via an equivalent nodal force vector representing the difference between an assumed elastic stress state and the actual stress state. The alternate functionals (approaches) are examined for the elastic-plastic analysis of single layer plates, and the better approach is identified. To extend the better functional to multilayer plates, the single layer element can be replaced by a multilayer element, and the elastic-plastic nonlinear material model replaced by appropriate existing failure and post-failure nonlinear models for laminated composites.

In addition to the approaches used in Chapters 2 to 4, one could also introduce a special element at the free edge point to account for the exact singular nature of the stress there. To this end, the first step is to determine analytically the order of singularity and the angular distribution of displacements and stresses near the free-edge point. Although the stress singularity analyses of the free-edge point have been done extensively for isotropic materials, there are few published works on corresponding analyses for anisotropic materials. One of the difficulties is that the Airy stress function for isotropic materials is no longer applicable to anisotropic materials. The other difficulty is the possibility of multiple eigenvalues for the elasticity constants and/or the order of singularities. In Chapter 5 we analyse the form of stress singularities near

the free-edge point of an anisotropic composite wedge. The changes in the forms of stress singularities due to multiple eigenvalues are presented.

On the dynamic response of composites, the emphasis is placed on the prediction of transient wave propagation. Although the dynamic response of a composite subject to harmonic oscillation has been studied and well understood, there seems to be no reliable way to predict the transient response of a composite. In this report we consider two problems on transient wave propagation.

In Chapter 6, we present a theory of viscoelastic analogy for wave propagation normal to the layering of a finite periodically layered bilaminate. Each layer of the bilaminate can be elastic or viscoelastic materials. The composite is modeled as an homogeneous viscoelastic material. The crux of the problem is the determination of the relaxation function of this "equivalent" homogeneous viscoelastic material. We obtain the relaxation function by comparing the solutions to the wave propagation problem in the finite layered composite and in the homogeneous viscoelastic medium. Wave propagation in the layered composite is then obtained by solving the wave propagation in the homogeneous viscoelastic medium. Numerical examples for an elastic composite show excellent agreements between the solution obtained by this theory and the exact solution by the ray theory.

The asymptotic solution in a semi-infinite bilaminate reported in the literature shows that the stress response oscillates as time increases when the bilaminate is elastic. If the bilaminate is viscoelastic, the stress response is monotonic. This presents a paradox because an elastic bilaminate is a special case of viscoelastic bilaminates; and yet the asymptotic solution is oscillatory for the special case of elastic bilaminate, not for the general case of viscoelastic bilaminate. This para-

dox is solved in Chapter 7 by considering the interaction between the dispersion and dissipation of wave propagation in general viscoelastic bilaminates. If the distance traveled by the wave is not too large, the dispersion effects dominate and the response is oscillatory. As the waves travel farther, the viscous effects eventually prevail and the response becomes monotonic. The distance beyond which wave propagation becomes monotonic is also determined in Chapter 7.

Finally, in Chapter 8 we present a brief concluding remark on this entire project.

CHAPTER 2

FINITE-ELEMENT STUDY OF EDGE-EFFECTS IN LAMINATES UNDER INPLANE STRAIN

ABSTRACT

The hybrid-stress finite-element model is used for the analysis of symmetrically-stacked arbitrary angle laminates subjected to a prescribed uniform inplane strain. The analysis reduces to a 2-D analysis in the plane of the laminate cross-section. Multilayer 2-D hybrid-stress elements are developed which utilize high-order through-thickness distribution for displacements and stresses. Three types of elements are developed: (I) Standard elements in which interlayer displacement and traction continuity, and upper / lower surface traction-free conditions are exactly satisfied, (2) Strain continuity elements in which the standard element is modified to exactly satisfy appropriate interlayer strain continuity, and (3) A traction-free edge element in which the standard element is modified to exactly satisfy free-surface conditions on a lateral edge of the element. These elements are applied to several example problems and results are compared with existing results to assess the effects of the various elements/strategies used.

1. Introduction

The cause of laminate failure in multilayer composite structures has been a source of speculation for some time. It is generally accepted that high interlaminar stress gradients exist near the free edge of these laminates which are a cause or partial cause of laminate failure. Therefore, although classical lamination theory, which does not include the effects of the interlaminar stresses, will provide accurate stress predictions away from the free edge, it is unacceptable as a means of solution for this problem near the free edge [1]. Consequently, the problem of composite laminate failure has been approached by several investigators using a wide variety of numerical techniques [2-7].

Although numerous stress results have been presented for both cross-ply and angle-ply laminates, not any set of solutions has been accepted as completely correct. Many discrepencies between solutions still exist. The effects of approximating known stress and strain conditions which exist along the surface of the laminate and across interlayer boundaries of the laminate also remain a point of interest when various solutions are compared.

In this study, a hybrid stress finite element model is used to solve the problem of a composite laminate under uniform inplane strain (Figure 1). The assumed stress hybrid formulation is well suited to this type of problem due to the fact that stresses and displacements can be assumed independently within each layer. Therefore, continuity of interlaminar stresses and continuity of inplane strains across interlayer boundaries as well as continuity of displacements need not be approximated, but can instead be exactly satisfied. In addition, the traction free edge condition along the outer surface of the laminate can be exactly enforced.

A special purpose multilayer element is developed which satisfies continuity of interlaminar stresses across interlayer boundaries and which also satisfies the traction free edge condition along the top and bottom of the laminate. A finite

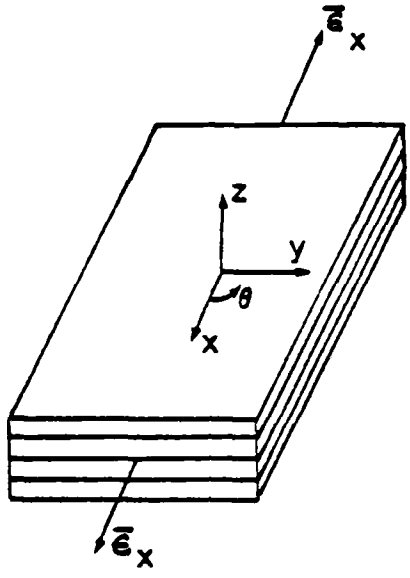

(a) LAMINATE SUBJECT TO UNIFORM INPLANE STRAIN $\bar{\epsilon}_x$

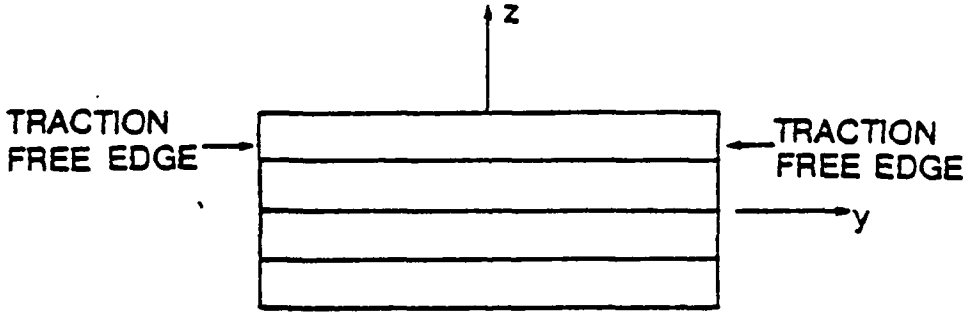

(b) PLANE OF ANALYSIS

Fig. 1 Problem Definition

element mesh composed of these multilayer elements comprises the first approach used to solve the above stated problem. Two additional analyses are also considered. The first, modifies the multilayer element to include the traction free edge condition along the lateral side of the laminate. This element is then coupled with the standard multilayer element to comprise the second approach to the problem. In the third analysis, the original (standard) multilayer element is modified to include the continuity of inplane strains (computed from stresses) across interlayer boundaries. A mesh composed of only these strain continuity elements comprises the third approach.

In the chapters to follow, the formulation of the special purpose multilayer element, including all additional modifications, is presented. Test cases, including cross-ply and angle-ply examples, are described and stress results are shown. The differences and similarities between the three approaches are discussed. Observations between the stress results for different laminate stacking sequences are also discussed where appropriate.

2. Formulation

A. Energy Functional and Element Matrix Definitions

The general formulation of the hybrid-stress model for cross-ply laminates subject to uniform inplane strain is given in [8,9]. That development will be expanded here to include the more general angle-ply laminate case. The enforcement of certain displacement and stress/strain continuities will also be incorporated into the formulation.

The basis of the assumed-stress hybrid formulation is a modified complementary energy principle. This is a two field principle for which intraelement equilibrating stresses and interelement compatible displacements can be assumed independently within each element. In the case of multilayer structures which are subdivided such that a single element is composed of a number of layers, the energy must be summed over the numbers of layers within each element as well as the number of elements. Thus, the hybrid-stress functional for multilayer structures, disregarding external forces, is given as

$$\Pi_{mc} = \sum_{n_e} \left\{ \sum_{N} \left[\tfrac{1}{2} \int_{V_{ni}} \underset{\sim}{\sigma}^{i\,T} \underset{\sim}{S}^{i} \underset{\sim}{\sigma}^{i} \, dV - \int_{V_{ni}} \underset{\sim}{\sigma}^{i\,T} \underset{\sim}{\hat{\epsilon}}^{i} \, dV \right] \right\} \tag{1}$$

$\sum_{n_e}$ = the summation over the number of elements

$\sum_{N}$ = the summation over the number of layers

V_{ni} = the volume of the i^{th} layer for the n^{th} element

$\underset{\sim}{\sigma}^{i}$ = the components of the stress vector for the i^{th} layer

$\underset{\sim}{\hat{\epsilon}}^{i}$ = the components of the strain vector in the i^{th} layer based on displacements

$\underset{\sim}{S}^{i}$ = the material property matrix for the i^{th} layer in the global x,y.z system

The effect of the uniform inplane strain, $\bar{\epsilon}_x$, will be incorporated directly into the complementary energy functional. In order to accomplish this, first consider the expression for the material property matrix, $\underset{\sim}{S}$. A material axis system is defined such that x_1 is in the fiber direction for the layer and x_2 is perpendicular to the fibers (inplane). Then the stress-strain relations in this material system are [10]:

$$\begin{Bmatrix} \epsilon_1 \\ \epsilon_2 \\ \epsilon_3 \\ \epsilon_{23} \\ \epsilon_{31} \\ \epsilon_{12} \end{Bmatrix} = \begin{bmatrix} S_{11} & S_{21} & S_{31} & 0 & 0 & 0 \\ S_{21} & S_{22} & S_{32} & 0 & 0 & 0 \\ S_{31} & S_{32} & S_{33} & 0 & 0 & 0 \\ 0 & 0 & 0 & S_{44} & 0 & 0 \\ 0 & 0 & 0 & 0 & S_{55} & 0 \\ 0 & 0 & 0 & 0 & 0 & S_{66} \end{bmatrix} \begin{Bmatrix} \sigma_1 \\ \sigma_2 \\ \sigma_3 \\ \sigma_{23} \\ \sigma_{31} \\ \sigma_{12} \end{Bmatrix} \tag{2}$$

In general, fibers are not oriented in the global coordinate direction. The material property matrix in terms of stress/strain in the global, x,y,z, system (element coordinate system) can be defined by applying the appropriate transformation laws, and is given by [10]:

$$\begin{Bmatrix} \epsilon_x \\ \epsilon_y \\ \epsilon_z \\ \epsilon_{yz} \\ \epsilon_{zx} \\ \epsilon_{xy} \end{Bmatrix} = \begin{bmatrix} \bar{S}_{11} & & & & & \\ \bar{S}_{12} & \bar{S}_{22} & & & \text{SYM.} & \\ \bar{S}_{13} & \bar{S}_{23} & \bar{S}_{33} & & & \\ 0 & 0 & 0 & \bar{S}_{44} & & \\ 0 & 0 & 0 & \bar{S}_{45} & \bar{S}_{55} & \\ \bar{S}_{16} & \bar{S}_{26} & \bar{S}_{36} & 0 & 0 & \bar{S}_{66} \end{bmatrix} \begin{Bmatrix} \sigma_x \\ \sigma_y \\ \sigma_z \\ \sigma_{yz} \\ \sigma_{zx} \\ \sigma_{xy} \end{Bmatrix} \tag{3}$$

where the $\bar{S}$'s are a function of the original terms in $\underset{\sim}{S}$ and the layer fiber orientation. The terms in $\underset{\sim}{\bar{S}}$ are defined in [10]

Imposing the condition that the inplane strain $\bar{\epsilon}_x$ calculated from stresses must equal the prescribed inplane strain $\bar{\epsilon}_x$ permits elimination of σ_x according to:

$$\sigma_x = \frac{\bar{\epsilon}_x}{\bar{S}_{11}} - \frac{\bar{S}_{12}}{\bar{S}_{11}}\sigma_y - \frac{\bar{S}_{13}}{\bar{S}_{11}}\sigma_z - \frac{\bar{S}_{16}}{\bar{S}_{11}}\sigma_{xy} \tag{4}$$

In matrix form this can be expressed as:

$$\begin{Bmatrix} \sigma_x \\ \sigma_y \\ \sigma_z \\ \sigma_{yz} \\ \sigma_{zx} \\ \sigma_{xy} \end{Bmatrix} = \begin{bmatrix} 1/\bar{S}_{11} & -\bar{S}_{12}/\bar{S}_{11} & -\bar{S}_{13}/\bar{S}_{11} & 0 & 0 & -\bar{S}_{16}/\bar{S}_{11} \\ 0 & 1 & 0 & 0 & 0 & 0 \\ 0 & 0 & 1 & 0 & 0 & 0 \\ 0 & 0 & 0 & 1 & 0 & 0 \\ 0 & 0 & 0 & 0 & 1 & 0 \\ 0 & 0 & 0 & 0 & 0 & 1 \end{bmatrix} \begin{Bmatrix} \bar{\epsilon}_x \\ \sigma_y \\ \sigma_z \\ \sigma_{yz} \\ \sigma_{zx} \\ \sigma_{xy} \end{Bmatrix} \tag{5}$$

Substituting this relationship into the first term in (1) leads to:

$$\begin{Bmatrix} \bar{\epsilon}_x \\ \sigma_y \\ \sigma_z \\ \sigma_{yz} \\ \sigma_{zx} \\ \sigma_{xy} \end{Bmatrix}^T \begin{bmatrix} \frac{1}{\bar{S}_{11}} & 0 & 0 & 0 & 0 & 0 \\ 0 & \bar{S}_{22} - \frac{\bar{S}_{12}^2}{\bar{S}_{11}} & \bar{S}_{23} - \frac{\bar{S}_{12}\bar{S}_{13}}{\bar{S}_{11}} & 0 & 0 & \bar{S}_{26} - \frac{\bar{S}_{12}\bar{S}_{16}}{\bar{S}_{11}} \\ 0 & \bar{S}_{23} - \frac{\bar{S}_{12}\bar{S}_{13}}{\bar{S}_{11}} & \bar{S}_{33} - \frac{\bar{S}_{13}^2}{\bar{S}_{11}} & 0 & 0 & \bar{S}_{36} - \frac{\bar{S}_{13}\bar{S}_{16}}{\bar{S}_{11}} \\ 0 & 0 & 0 & \bar{S}_{44} & \bar{S}_{45} & 0 \\ 0 & 0 & 0 & \bar{S}_{45} & \bar{S}_{55} & 0 \\ 0 & \bar{S}_{26} - \frac{\bar{S}_{16}\bar{S}_{12}}{\bar{S}_{11}} & \bar{S}_{36} - \frac{\bar{S}_{16}\bar{S}_{13}}{\bar{S}_{11}} & 0 & 0 & \bar{S}_{66} - \frac{\bar{S}_{16}^2}{\bar{S}_{11}} \end{bmatrix} \begin{Bmatrix} \bar{\epsilon}_x \\ \sigma_y \\ \sigma_z \\ \sigma_{yz} \\ \sigma_{zx} \\ \sigma_{xy} \end{Bmatrix} \tag{6}$$

or simplifying:

$$\begin{bmatrix} \sigma_y & \sigma_z & \sigma_{yz} & \sigma_{zx} & \sigma_{xy} \end{bmatrix} [R] \begin{Bmatrix} \sigma_y \\ \sigma_z \\ \sigma_{yz} \\ \sigma_{zx} \\ \sigma_{xy} \end{Bmatrix} + \frac{1}{\bar{S}_{11}} \bar{\epsilon}_x^2 \tag{7}$$

Using equation (5) and substituting the linear strain displacement relationships, equation (1) becomes:

$$\Pi_{mc} = \sum_{n_e} \left\{ \sum_{N} \left[\tfrac{1}{2} \int_{A_{mi}} \lfloor \sigma_y \ \sigma_z \ \sigma_{yz} \ \sigma_{zx} \ \sigma_{xy} \rfloor^i [R]^i \begin{Bmatrix} \sigma_y \\ \sigma_z \\ \sigma_{yz} \\ \sigma_{zx} \\ \sigma_{xy} \end{Bmatrix}^i dA \right.\right.$$

$$+ \bar{\epsilon}_x \int_{A_{mi}} \lfloor \sigma_y \ \sigma_z \ \sigma_{xy} \rfloor^i \begin{Bmatrix} \bar{S}_{12}/\bar{S}_{11} \\ \bar{S}_{22}/\bar{S}_{11} \\ \bar{S}_{26}/\bar{S}_{11} \end{Bmatrix}^i dA \qquad (8)$$

$$\left.\left. - \int_{A_{mi}} \lfloor \sigma_y \ \sigma_z \ \sigma_{yz} \ \sigma_{zx} \ \sigma_{xy} \rfloor^i \begin{Bmatrix} \frac{\partial v}{\partial y} \\ \frac{\partial w}{\partial z} \\ \frac{\partial w}{\partial y} + \frac{\partial v}{\partial z} \\ \frac{\partial u}{\partial z} \\ \frac{\partial u}{\partial y} \end{Bmatrix}^i dA \right] \right\}$$

where the linear strain-displacement relations are based on a displacement field corresponding to uniform inplane strain in the x direction [4]:

$$\begin{aligned} u^i(x,y,z) &= x\bar{\epsilon}_x + u^i(y,z) \\ v^i(x,y,z) &= v^i(y,z) \\ w^i(x,y,z) &= w^i(y,z) \end{aligned} \qquad (9)$$

Note that the constant terms have been dropped in view of the fact that it is the variation of Π_{mc} which is ultimately of interest.

The stresses are now expressed within each layer in terms of a set of stress parameters, $\underline{\beta}$, such that the homogeneous equilibrium equations are exactly satisfied. The reduced equilibrium equations, where the stress components are independent of the x direction (in view of equations (9)), are:

$$\frac{\partial \sigma_{xy}}{\partial y} + \frac{\partial \sigma_{xz}}{\partial z} = 0$$

$$\frac{\partial \sigma_{y}}{\partial y} + \frac{\partial \sigma_{yz}}{\partial z} = 0 \qquad (10)$$

$$\frac{\partial \sigma_{yz}}{\partial y} + \frac{\partial \sigma_{z}}{\partial z} = 0$$

The stresses are therefore given as:

$$\begin{Bmatrix} \sigma_y \\ \sigma_z \\ \sigma_{yz} \\ \sigma_{zx} \\ \sigma_{xy} \end{Bmatrix}^i = \underset{\sim}{P}^i \underset{\sim}{\beta}^i \qquad (11)$$

where the form of the matrix $\underset{\sim}{P}$ is chosen so that equilibrium is satisfied.

The displacements, also defined independently within each layer, are given in terms of nodal displacements, $\underset{\sim}{q}$:

$$\underset{\sim}{u}^i = \underset{\sim}{N}^i \underset{\sim}{q}^i \qquad (12)$$

The displacement interpolation, $\underset{\sim}{N}$, is formed such that continuity between elements is guaranteed. Using the strain displacement relations, the matrix $\underset{\sim}{B}$ is defined as:

$$\begin{Bmatrix} \frac{\partial v}{\partial y} \\ \frac{\partial w}{\partial z} \\ \frac{\partial w}{\partial y} + \frac{\partial v}{\partial z} \\ \frac{\partial u}{\partial z} \\ \frac{\partial u}{\partial y} \end{Bmatrix} = \underset{\sim}{B}^i \underset{\sim}{q}^i \qquad (13)$$

Substituting (11) and (13) into (8) leads to:

$$\pi_{mc} = \sum_{n_e} \left\{ \sum_{N} \left[\tfrac{1}{2} \int_{A_{ni}} \underset{\sim}{\beta}^{i\,T} \underset{\sim}{P}^{i\,T} \underset{\sim}{R}^i \underset{\sim}{P}^i \underset{\sim}{\beta}^i \, dA + \bar{\epsilon}_x \int_{A_{ni}} \underset{\sim}{\beta}^{i\,T} \underset{\sim}{P}_x^{i\,T} - \int_{A_{ni}} \underset{\sim}{\beta}^{i\,T} \underset{\sim}{P}^{i\,T} \underset{\sim}{B}^i \underset{\sim}{q}^i \, dA \right] \right\} \begin{Bmatrix} N_1 & 0 & N_2 & 0 & N_3 \\ 0 & N_1 & 0 & N_2 & 0 \end{Bmatrix}^i dA \qquad (14)$$

where $\underset{\sim}{P}_R^i$ represents the first, second and fifth rows of $\underset{\sim}{P}^i$.

Simplifying this expression by defining the following layer matrices:

$$\underset{\sim}{H}^i = \int_{A_{mi}} \underset{\sim}{P}^{iT} \underset{\sim}{R}^i \underset{\sim}{P}^i \, dA \tag{15a}$$

$$\underset{\sim}{G}^i = \int_{A_{mi}} \underset{\sim}{P}^{iT} \underset{\sim}{B}^i \, dA \tag{15b}$$

$$\underset{\sim}{f}_s^i = \int_{A_{mi}} \underset{\sim}{P}_R^{iT} \begin{Bmatrix} N_{11} \\ N_{12} \\ N_{22} \\ N_{66} \end{Bmatrix}^i dA \tag{15c}$$

leads to:

$$\pi_{mc} = \sum_{n_e} \left\{ \sum_{N} \left[\tfrac{1}{2} \underset{\sim}{\beta}^{iT} \underset{\sim}{H}^i \underset{\sim}{\beta}^i - \underset{\sim}{\beta}^{iT} \underset{\sim}{G}^i \underset{\sim}{q}^i + \bar{\epsilon}_x \underset{\sim}{\beta}^{iT} \underset{\sim}{f}_s^i \right] \right\} \tag{16}$$

Up to this point, $\underset{\sim}{q}^i$ and $\underset{\sim}{\beta}^i$ are independent from layer to layer. Recalling that a single element is composed of a number of layers, improved results can be found by enforcing certain continuity conditions along interlayer surfaces such as continuity of displacements, continuity of tractions, and continuity of strains from stresses. Appropriate relationships between the stress parameters, $\underset{\sim}{\beta}^i$, and nodal displacements, $\underset{\sim}{q}^i$, for a layer and stress parameters, $\underset{\sim}{\beta}_L$, and nodal displacements, $\underset{\sim}{q}_L$, for the laminate can be defined in terms of these continuity conditions. For the present case of prescribed $\bar{\varepsilon}_x$, they can be expressed in the following form:

$$\underset{\sim}{\beta}^i = \underset{\sim}{T}_s^i \underset{\sim}{\beta}_L + \underset{\sim}{C}_s^i \bar{\epsilon}_x \tag{17a}$$

$$q^i = T_L^i \, q_L \tag{17b}$$

Substituting (17a) and (17b) into (16) and defining the following laminate matrices:

$$H = \sum_{i=1}^{N} T_s^{iT} H^i T_s^i \tag{18a}$$

$$G = \sum_{i=1}^{N} T_s^{iT} G T_L^i \tag{18b}$$

$$F_s = \sum_{i=1}^{N} \left(T_s^{iT} H^i C_s^i + T_s^{iT} f_s^i \right) \tag{18c}$$

$$J_s = \sum_{i=1}^{N} T_L^{iT} G^{iT} C_s^i \tag{18d}$$

leads to:

$$\pi_{mc} = \sum_{n_e} \left\{ \tfrac{1}{2} \beta_L^T H \beta_L + \beta_L^T F_s \bar{\epsilon}_x - \beta_L^T G q_L - \bar{\epsilon}_x q_L^T J_s \right\} \tag{19}$$

Recalling that the β's are independent from element to element, the stationary condition of π_{mc} with respect to β_L eliminates the stress parameters on an element level. Therefore, for an arbitrary $\delta\beta_L \neq 0$:

$$\beta_L = H^{-1} G q_L - H^{-1} F_s \bar{\epsilon}_x \tag{20}$$

Substituting this back into equation (19) yields:

$$\bar{\pi}_{mc} = - \sum_{n_e} \left\{ \tfrac{1}{2} q_L^T k q_L - q_L^T Q \right\} \tag{21}$$

where:

$$k = G^T H^{-1} G \tag{21a}$$

$$Q = \left(G^T H^{-1} F_s - J_s \right) \bar{\epsilon}_x \tag{21b}$$

define the element stiffness matrix and the element load vector (due to $\bar{\varepsilon}_x$) respectively.

After assembly of all elements, the solution of equation (21) results in the values of the nodal displacements. Stresses can be found by using (20) to obtain the laminate β's, (17a) to obtain the layer β's, and finally using (11) for the stress field.

B. Displacement Interpolation and Enforced Displacement Continuities

The same high order through thickness displacements assumption used in [8] and [9] for the displacements v and w (in the y and z directions respectively) is utilized in this study. Furthermore, the u displacement (in the x direction) is chosen to be of the same form as the v displacement. The position of the nodal displacements for each layer is shown in figure 2b. Note in figure 2a that the total height of the laminated element is H, and the total length is ℓ. Also shown is the z coordinate for the bottom of layer i which is designated h_i, and that for the top as h_{i+1}. For convenience, a local coordinate, ζ, is defined whose origin is at the mid-surface of each layer. The local system is defined such that:

$$\zeta = \frac{1}{h_i - h_{i+1}} \left[h_i + h_{i+1} - 2z \right] \tag{22}$$

where

$\zeta = -1$ at $z = h_i$

$\zeta = 1$ at $z = h_{i+1}$

The displacement assumption in terms of the local coordinate ζ, where the displacements u and v are of order z^3 and the displacement at w is or order z^2, is given as:

$$v^i(\zeta) = \frac{1}{16}\left[(-1+\zeta+9\zeta^2-9\zeta^3)v_1^i + (9-27\zeta-9\zeta^2+27\zeta^3)v_2^i\right.$$

$$\left. + (9+27\zeta-9\zeta^2-27\zeta^3)v_3^i + (-1-\zeta+9\zeta^2+9\zeta^3)v_4^i\right]_{\text{MODEL}}\left(1-\frac{y}{\ell}\right) \tag{23}$$

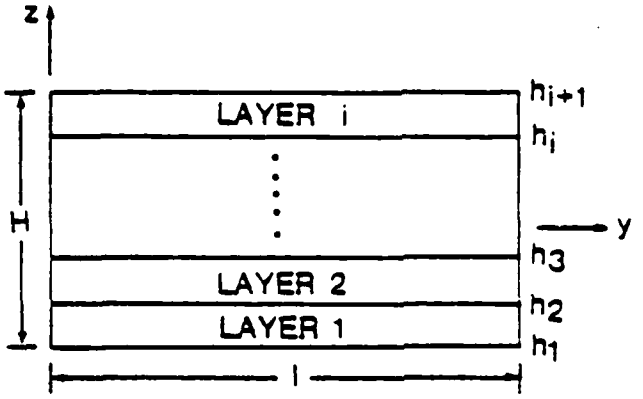

(a) ELEMENT GEOMETRY AND LAYER NUMBERING CONVENTION

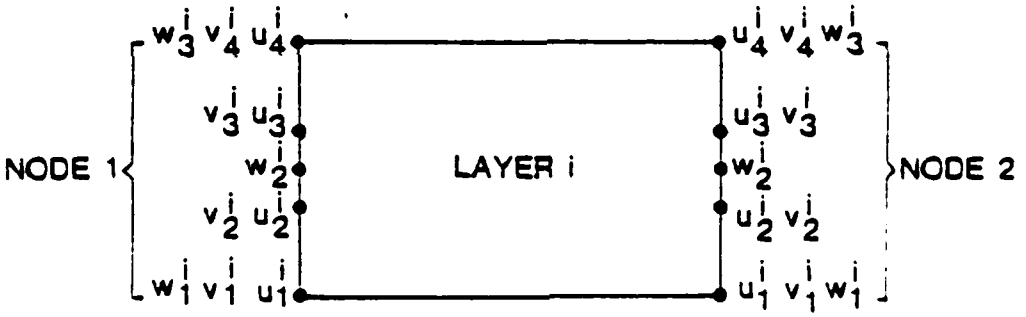

(b) ELEMENT DEGREES OF FREEDOM FOR A TYPICAL LAYER

Fig. 2 Element Geometry and Degrees of Freedom

$$+\frac{1}{16}\left[(-1+\xi+9\xi^2-9\xi^3)v_1^i+(9-27\xi-9\xi^2+27\xi^3)v_2^i\right.$$

$$\left.+(9+27\xi-9\xi^2-27\xi^3)v_3^i+(-1-\xi+9\xi^2+9\xi^3)v_4^i\right]_{\text{NODE 2}}(y/\ell)$$

$$w^i(\xi)=\left[\frac{1}{2}(-\xi+\xi^2)w_1^i+(1-\xi^2)w_2^i+\frac{1}{2}(\xi+\xi^2)w_3^i\right]_{\text{NODE 1}}(1-y/\ell)$$

$$+\left[\frac{1}{2}(-\xi+\xi^2)w_1^i+(1-\xi^2)w_2^i+\frac{1}{2}(\xi+\xi^2)w_3^i\right]_{\text{NODE 2}}(y/\ell)$$

where the u displacement, as previously noted, is of the same form as the v displacement.

This displacement interpolation insures compatibility between elements. To enforce displacement continuity between layers, however, the nodal displacements for layer i must be related to those of layer i+1. As can be seen from figures 2a and 2b, this would require:

$$(u_4, v_4, w_3)^i = (u_1, v_1, w_1)^{i+1} \tag{24}$$

This is the expression which relates the layer degrees of freedom to the laminate degrees of freedom and it defines the transformation matrix $\underset{\sim}{T}_d^i$ used in (17b). When the nodal displacements are given the ordering,

$$\underset{\sim}{q}^i = \begin{Bmatrix} \bar{\underset{\sim}{q}}^i \\ \underset{\sim}{q}^i \\ \bar{\underset{\sim}{q}}^{i+1} \end{Bmatrix} \tag{25}$$

where $\bar{\underset{\sim}{q}}^i$ represents the displacements at the bottom node of the layer and $\bar{\underset{\sim}{q}}^{i+1}$ represents the displacements at the upper most node of the layer, the matrix $\underset{\sim}{T}_d^i$ becomes a Boolean matrix. The products defined in (18b) and (18d) can therefore be accomplished by the use of assembly pointers which simply position the layer contributions into the appropriate laminate positions within $\underset{\sim}{G}$ and $\underset{\sim}{J}_s$.

It should be noted that the displacement interpolation is written in terms of the normalized coordinate, ζ, and consequently the matrix $\underset{\sim}{B}$, which is defined by this interpolation using the strain displacement relations, is also in terms of ζ. In order to perform the integral (15b), a transformation of coordinates must be defined. Furthermore, since all of the integrals will be evaluated by use of a Gauss integration scheme, the limits of the integral must be from -1 to 1. Therefore, an additional local coordinate, s, is defined in the y direction such that

$$y = \frac{-\ell}{2} + \frac{\ell}{2} s \tag{26}$$

The Jacobian of the transformation is then given as:

$$J = \frac{-\ell (h_i - h_{i+1})}{4} \tag{27}$$

Thus, the $\underset{\sim}{B}$ and $\underset{\sim}{T}_d^i$ matrices have been defined. It remains to define the stress assumption and the continuity requirements placed on stress and strain.

C. Stress Assumption and Enforced Traction Continuities

The basic stress assumption used in [8] and [9] have been employed here where σ_y, σ_z, σ_{yz} are of order z^3, z^5 and z^4 respectively. The additional stress components used here, namely σ_{xy} and σ_{xz} are chosen to be in the same form as σ_y and σ_{yz} respectively. Although the basic stress assumption is the same, it has been recast in the following form for reasons which will be discussed subsequently. Also, recall that the following stress assumption is for a typical layer i:

$$\sigma_y^i = \frac{3}{4\bar{t}_i}(\bar{\beta}_1^i - \bar{\beta}_1^{i+1})(1+s)(1-s)y + \frac{1}{8\bar{t}_i}(3\bar{\beta}_2^i y^2 + 2\bar{\beta}_3^i y^3) \tag{28a}$$

$$(1-s)(1+s)(1-5s) - \frac{1}{8\bar{t}_i}(3\bar{\beta}_2^{i+1} y^2 + 2\bar{\beta}_3^{i+1} y^3)(1-s)(1+s)(1+5s)$$

$$+ \frac{5}{8\bar{t}_i^2}\left[3(\bar{\beta}_4^i - \bar{\beta}_4^{i+1})y^2 + (\bar{\beta}_5^i - \bar{\beta}_5^{i+1})y^3\right] J(1-s)(1+s)$$

$$+\tfrac{1}{2}\hat{\beta}_1^i(1-\xi)+\tfrac{1}{2}\hat{\beta}_5^i(1+\xi)-\tfrac{1}{4}\hat{\beta}_2^i y(1-\xi)(1+3\xi)$$

$$-\tfrac{1}{4}\hat{\beta}_6^i y(1+\xi)(1-3\xi)+\tfrac{1}{4}(\hat{\beta}_3^i y^2+\hat{\beta}_4^i y^3)(1-\xi)(-1+2\xi+5\xi^2)$$

$$+\tfrac{1}{4}(\hat{\beta}_7^i y^2+\hat{\beta}_8^i y^3)(1+\xi)(-1-2\xi+5\xi^2)-\beta_1^i(1-\xi)(1+\xi)$$

$$-(\beta_2^i+\beta_3^i y)\xi(1-\xi)(1+\xi)$$

$$\sigma_2^i=-\tfrac{\bar{E}_i}{16}(\bar{\beta}_2^i+2\bar{\beta}_3^i y)(1-\xi)^3(1+\xi)(5+3\xi)+\tfrac{\bar{E}_i}{16}(\bar{\beta}_2^{i+1}+2\bar{\beta}_3^{i+1}y)(1-\xi) \quad (28b)$$

$$(1+\xi^2)(5-3\xi)+\tfrac{1}{16}(\bar{\beta}_4^i+\bar{\beta}_5^i y)(1-\xi)^3(8+9\xi+3\xi^2)$$

$$+\tfrac{1}{16}(\bar{\beta}_4^{i+1}+\bar{\beta}_5^{i+1}y)(1+\xi)^3(8-9\xi+3\xi^2)+\tfrac{\bar{E}_i^2}{8}(\hat{\beta}_3^i+3\hat{\beta}_4^i y)$$

$$(1-\xi)^2(1+\xi)^2+\tfrac{\bar{E}_i^2}{8}(\hat{\beta}_7^i+3\hat{\beta}_8^i y)(1-\xi)^2(1+\xi)^3$$

$$\sigma_{y2}^i=\tfrac{1}{4}\bar{\beta}_1^i(1-\xi)^2(2+\xi)+\tfrac{1}{4}\bar{\beta}_1^{i+1}(1+\xi)^2(2-\xi)-\tfrac{1}{16}(\bar{\beta}_2^i y+\bar{\beta}_3^i y^2)$$

$$(1-\xi)^2(7+5\xi)(1+3\xi)-\tfrac{1}{16}(\bar{\beta}_2^{i+1}y+\bar{\beta}_3^{i+1}y^2)(1+\xi)^2(7-5\xi)(1-3\xi) \quad (28c)$$

$$+\tfrac{15}{32\bar{E}_i}[2(\bar{\beta}_4^i-\bar{\beta}_4^{i+1})y+(\bar{\beta}_5^i-\bar{\beta}_5^{i+1})y^2](1-\xi)^2(1+\xi)^2$$

$$-\tfrac{\bar{E}_i}{4}\hat{\beta}_2^i(1-\xi)^2(1+\xi)+\tfrac{\bar{E}_i}{4}\hat{\beta}_6^i(1-\xi)(1+\xi)^2$$

$$+\tfrac{\bar{E}_i}{16}(2\hat{\beta}_3^i y+3\hat{\beta}_4^i y^2)(1-\xi)^2(1+\xi)(1+5\xi)-\tfrac{\bar{E}_i}{16}(2\hat{\beta}_7^i y+3\hat{\beta}_8^i y^2)$$

$$(1-\xi)(1+\xi)^2(1-5\xi]-\tfrac{\bar{E}_i}{4}\beta_3^i(1-\xi)^2(1+\xi)^2$$

$$\sigma_{xy}^{i} = \frac{3}{4\bar{t}_i}(\bar{\beta}_6^{i} - \bar{\beta}_6^{i+1})y(1-\zeta^2) + \frac{3}{8\bar{t}_i}(\bar{\beta}_7^{i} - \bar{\beta}_7^{i+1})y^2(1-\zeta^2)$$

$$+ \frac{1}{4\bar{t}_i}(\bar{\beta}_8^{i} - \bar{\beta}_8^{i+1})y^3(1-\zeta^2) + \frac{1}{2}\hat{\beta}_9^{i}(1-\zeta) \qquad (28d)$$

$$+ \frac{1}{4}(\hat{\beta}_{10}^{i}y + \hat{\beta}_{11}^{i}y^2 + \hat{\beta}_{12}^{i}y^3)(3\zeta^2 - 2\zeta - 1) + \frac{1}{2}\hat{\beta}_{13}^{i}(1+\zeta)$$

$$+ \frac{1}{4}(\hat{\beta}_{14}^{i}y + \hat{\beta}_{15}^{i}y^2 + \hat{\beta}_{16}^{i}y^3)(3\zeta^2 + 2\zeta - 1) + \beta_4^{i}(\zeta^2 - 1)$$

$$+ (\beta_5^{i} + \beta_6^{i}y + \beta_7^{i}y^2 + \beta_8^{i}y^3)(\zeta^3 - \zeta)$$

$$\sigma_{xz}^{i} = \frac{1}{4}(\bar{\beta}_6^{i} + \bar{\beta}_7^{i}y + \bar{\beta}_8^{i}y^2)(\zeta^3 - 3\zeta + 2)$$

$$+ \frac{1}{4}(\bar{\beta}_6^{i+1} + \bar{\beta}_7^{i+1}y + \bar{\beta}_8^{i+1}y^2)(-\zeta^3 + 3\zeta + 2) \qquad (28e)$$

$$+ \frac{\bar{t}_i}{4}(\hat{\beta}_{10}^{i} + 2\hat{\beta}_{11}^{i}y + 3\hat{\beta}_{12}^{i}y^2)(-\zeta^3 + \zeta^2 + \zeta - 1)$$

$$+ \frac{\bar{t}_i}{4}(\hat{\beta}_{14}^{i} + 2\hat{\beta}_{15}^{i}y + 3\hat{\beta}_{16}^{i}y^2)(-\zeta^3 - \zeta^2 + \zeta + 1)$$

$$+ \frac{\bar{t}_i}{4}(\beta_6^{i} + 2\beta_7^{i}y + 3\beta_8^{i}y^2)(-\zeta^4 + 2\zeta^2 - 1)$$

where $\bar{t}_i$ for convenience is defined as the half thickness of layer i. Also, the stresses defined above exactly satisfy the equilibrium equations (equations (10)).

The special form into which the stress assumption has been cast easily allows the identification of all the stresses at the interlayer boundaries. This greatly simplifies the enforcement of given stress/strain continuities along the layer interfaces. The interlaminar transverse shear and normal stresses are only related to appropriate $\bar{\beta}$ terms at the interlayer boundaries.

$$\text{AT } z = h_i \text{ OR } \zeta = -1 : \quad \begin{aligned} \sigma_{yz}^{i} &= \bar{\beta}_1^{i} + \bar{\beta}_2^{i}\gamma + \bar{\beta}_3^{i}\gamma^2 \\ \sigma_{z}^{i} &= \bar{\beta}_4^{i} + \bar{\beta}_5^{i}\gamma \\ \sigma_{xz}^{i} &= \bar{\beta}_6^{i} + \bar{\beta}_7^{i}\gamma + \bar{\beta}_8^{i}\gamma^2 \end{aligned}$$

$$\text{AT } z = h_{i+1} \text{ OR } \zeta = 1 : \quad \begin{aligned} \sigma_{yz}^{i} &= \bar{\beta}_1^{i+1} + \bar{\beta}_2^{i+1}\gamma + \bar{\beta}_3^{i+1}\gamma^2 \\ \sigma_{z}^{i} &= \bar{\beta}_4^{i+1} + \bar{\beta}_5^{i+1}\gamma \\ \sigma_{xz}^{i} &= \bar{\beta}_6^{i+1} + \bar{\beta}_7^{i+1}\gamma + \bar{\beta}_8^{i+1}\gamma^2 \end{aligned} \qquad (29)$$

Similarly, the inplane stresses are only related to appropriate $\hat{\beta}$ terms at the interlayer boundaries.

$$\text{AT } z = h_i \text{ OR } \zeta = -1 : \quad \begin{aligned} \sigma_{y}^{i} &= \hat{\beta}_1^{i} + \hat{\beta}_2^{i}\gamma + \hat{\beta}_3^{i}\gamma^2 + \hat{\beta}_4^{i}\gamma^3 \\ \sigma_{xy}^{i} &= \hat{\beta}_9^{i} + \hat{\beta}_{10}^{i}\gamma + \hat{\beta}_{11}^{i}\gamma^2 + \hat{\beta}_{12}^{i}\gamma^3 \end{aligned}$$

$$\text{AT } z = h_{i+1} \text{ OR } \zeta = 1 : \quad \begin{aligned} \sigma_{y}^{i} &= \hat{\beta}_5^{i} + \hat{\beta}_6^{i}\gamma + \hat{\beta}_7^{i}\gamma^2 + \hat{\beta}_8^{i}\gamma^3 \\ \sigma_{xy}^{i} &= \hat{\beta}_{13}^{i} + \hat{\beta}_{14}^{i}\gamma + \hat{\beta}_{15}^{i}\gamma^2 + \hat{\beta}_{16}^{i}\gamma^3 \end{aligned} \qquad (30)$$

In this section, only the enforcement of interlaminar stress continuities and satisfaction of traction free conditions along the top and bottom of the laminate will be considered. The purpose for casting σ_y and σ_{xy} in the above form at the layer interfaces will be discussed later.

The traction free conditions along the top and bottom of the laminate are easily satisfied as a result of the form of the given stress assumption (28). Referring to equations (29) these conditions, along the top of the laminate, result in:

$$\sigma_{yz}^{i}(z = h_{N+1}) = 0 \qquad \Rightarrow \bar{\beta}_1^{N+1} = \bar{\beta}_2^{N+1} = \bar{\beta}_3^{N+1} = 0$$

$$\sigma_z^{i}(z = h_{N+1}) = 0 \qquad \Rightarrow \bar{\beta}_4^{N+1} = \bar{\beta}_5^{N+1} = 0 \tag{31a}$$

$$\sigma_{xz}^{i}(z = h_{N+1}) = 0 \qquad \Rightarrow \bar{\beta}_6^{N+1} = \bar{\beta}_7^{N+1} = \bar{\beta}_8^{N+1} = 0$$

where N is the total number of layers. Enforcing the same condition along the bottom of the laminate leads to:

$$\bar{\beta}_1' = \bar{\beta}_2' = \bar{\beta}_3' = \bar{\beta}_4' = \bar{\beta}_5' = \bar{\beta}_6' = \bar{\beta}_7' = \bar{\beta}_8' = 0 \tag{31b}$$

This is accomplished by not assembling the contribution of these β's into the $\underset{\sim}{H}$ and $\underset{\sim}{G}$ matrices by setting the appropriate assembly pointers equal to zero. Thus, the traction free conditions along the top and bottom of the laminate are exactly satisfied.

Continuity of tractions across interlayer boundaries (i.e. σ_z, σ_{yz}, σ_{xz}) can be satisfied exactly by again considering equations (29). If the stress parameters are ordered in the following manner:

$$\begin{Bmatrix} \sigma_y \\ \sigma_z \\ \sigma_{yz} \\ \sigma_{xz} \\ \sigma_{xy} \end{Bmatrix} = \underset{\sim}{P} \begin{Bmatrix} \hat{\beta}^{i}_{(1-4,\,9-12)} \\ \bar{\beta}^{i} \\ \beta^{i} \\ \hat{\beta}^{i}_{(5-8,\,13-16)} \\ \bar{\beta}^{i+1} \end{Bmatrix} \tag{32}$$

where the form of $\underset{\sim}{P}$ is defined by the stress assumption, then the transformation matrix $\underset{\sim}{T}_s^i$ is a Boolean matrix and the matrix $\underset{\sim}{C}_s^i$ is zero (see equation (17a)). Again, since the transformation matrix is Boolean, all matrix multiplications involving the matrix $\underset{\sim}{T}_s^i$ can be accomplished, as previously noted, by the use of assembly pointers.

Also, as previously discussed, all integrals involving the $\underset{\sim}{P}$ matrix will be evaluated using a Gauss integration scheme, and therefore use will be made of an additional local coordinate, s, and the Jacobian of the transformation.

In general, therefore, the complete formulation of a multilayer structure subject to defined displacement and traction continuities across interlayer boundaries has been described. Besides the conditions already satisfied, however, use can be made of additional stress/strain conditions which can be imposed on the structure to perhaps provide a more realistic solution to the problem. Two of these more specialized conditions are the enforcement of a traction free edge condition along the right and left edges of the laminate (Figure 1), and the enforcement of certain strain continuities across interlayer boundaries. These ideas will now be discussed in more detail.

D. The Traction Free Edge Condition

The traction free edge condition along the lines $y=b$ and $y=-b$ as shown in figure (3a), is enforced in a manner similar to that of the traction free edge conditions along the top and bottom of the laminate. The stresses to be considered along $y=b$ and $y=-b$, however, are not of a special form as was the case along the top and bottom of the laminate. The y locations of the traction free edges must, therefore, be substituted into the general stress assumption (28) in order to define the β's which must be set equal to zero in order to enforce the conditions. To facilitate this procedure, a local $\bar{y}$ coordinate is adopted at the left edge of the laminate. Also, due to the symmetry of the laminate about both the y and z axis, only the upper left hand portion of the laminate need be analyzed. Therefore, as shown in figure (3b), the line $\bar{y}=0$ is the only traction free edge which need be considered. As a consequence of the translational invariance of the element being used, the stress assumptions are written in terms of $\bar{y}$ and the traction free edge condition is applied to this set of equations resulting in:

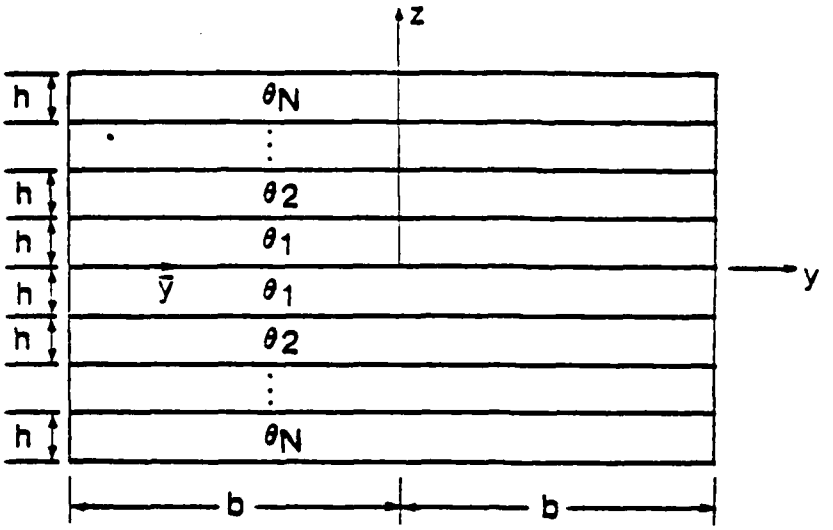

(a) PROBLEM DEFINITION: SYMMETRIC LAMINATE UNDER UNIFORM E_x

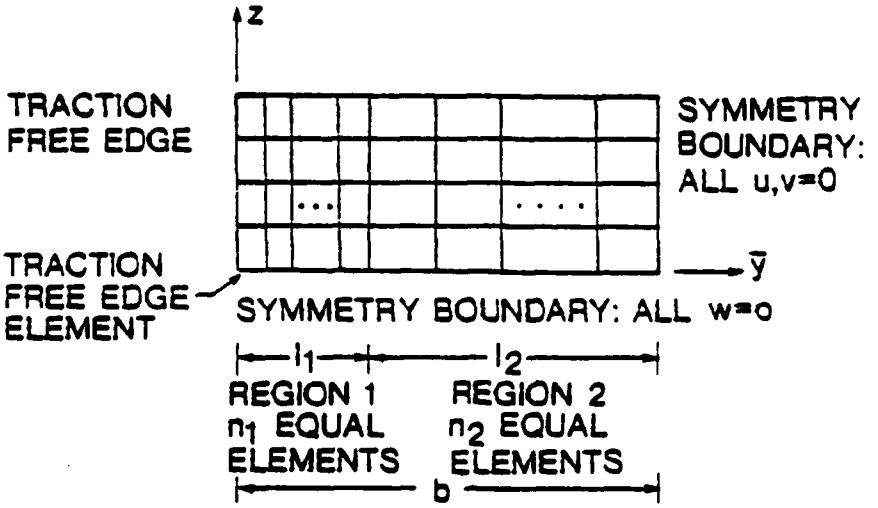

(b) FINITE ELEMENT MODEL OF THE UPPER LEFT-HAND PLANE TO BE ANALYZED

Fig. 3 Finite Element Model

$$\sigma_y(\bar{y}=0)=0 \;;\quad \hat{\beta}_1^i=\hat{\beta}_5^i=\beta_1^i=\beta_2^i=0$$
$$\sigma_{yz}(\bar{y}=0)=0 \;;\quad \beta_1^i=\bar{\beta}_1^{i+1}=\hat{\beta}_2^i=\hat{\beta}_6^i=\beta_3^i=0 \qquad (33)$$
$$\sigma_{xy}(\bar{y}=0)=0 \;;\quad \hat{\beta}_9^i=\hat{\beta}_{13}^i=\beta_4^i=\beta_5^i=0$$

Thus, if the elements are numbered from left to right (figure 3b), the contribution of the above β's (33) into the $\underset{\sim}{H}$ and $\underset{\sim}{G}$ matrices is not taken into account for the first element. Again, this is done through the use of assembly pointers. All other features of the element remain unchanged, therefore this traction free edge (TFE) element remains compatable with the other elements to be used in the mesh.

One additional consideration is of importance when using the TFE element. The work done by the tractions is given by:

$$\underset{\sim}{\beta}_L^T \underset{\sim}{G}\, \underset{\sim}{q}_L \qquad (34)$$

as it appears in equation (19). For the case of the TFE element, where no work is done along the left edge, (34) takes on the special form:

$$\underset{\sim}{\beta}_L^T \begin{bmatrix} \underset{\sim}{0} & \underset{\sim}{G}_2 \end{bmatrix} \begin{Bmatrix} \underset{\sim}{q}_L^1 \\ \underset{\sim}{q}_L^2 \end{Bmatrix} \qquad (35)$$

where $\underset{\sim}{q}_L^1$ and $\underset{\sim}{q}_L^2$ represent the displacements of nodes 1 and 2 respectively. Substituting the above form of the $\underset{\sim}{G}$ matrix into the expressions for the element stiffness matrix and the element load vector leads to:

$$\underset{\sim}{k} = \begin{bmatrix} \underset{\sim}{0} & \underset{\sim}{0} \\ \underset{\sim}{0} & \underset{\sim}{k}_{22} \end{bmatrix} \qquad \underset{\sim}{Q} = \begin{Bmatrix} \underset{\sim}{0} \\ \underset{\sim}{Q}_2 \end{Bmatrix} \qquad (36)$$

Recalling that the first element is taken to be the TFE element, the general form of the system of equations after assembly is:

$$\begin{bmatrix} \underset{\sim}{0} & \underset{\sim}{0} \\ \underset{\sim}{0} & \underset{\sim}{K}^* \end{bmatrix} \begin{Bmatrix} q_L^1 \\ q_f^* \end{Bmatrix} = \begin{Bmatrix} \underset{\sim}{0} \\ \underset{\sim}{Q}^* \end{Bmatrix} \tag{37}$$

where $\underset{\sim}{K}^*$, $\underset{\sim}{q}^*$, and $\underset{\sim}{Q}^*$ represent the assembled stiffness matrix, displacement vector, and load vector after the contributions due to node 1 are removed.

In practice, this system of equations can be solved in the conventional manner by setting the displacements at node 1 equal to zero and setting the diagonal stiffness terms equal to unity. This results in the system of non-singular equations:

$$\begin{bmatrix} \underset{\sim}{I} & \underset{\sim}{0} \\ \underset{\sim}{0} & \underset{\sim}{K}^* \end{bmatrix} \begin{Bmatrix} \underset{\sim}{0} \\ q_f^* \end{Bmatrix} = \begin{Bmatrix} \underset{\sim}{0} \\ \underset{\sim}{Q}^* \end{Bmatrix} \tag{38}$$

As can be seen from equation (20), the stress parameters will also be independent of the displacements at node 1:

$$\underset{\sim}{\beta}_L = \begin{bmatrix} \underset{\sim}{0} & \underset{\sim}{H}^{-1}\underset{\sim}{G}_L \end{bmatrix} \begin{Bmatrix} q_L^1 \\ q_L^2 \end{Bmatrix} - \underset{\sim}{H}^{-1}\underset{\sim}{F}_s \bar{\epsilon}_x \tag{39}$$

The calculation of the stresses (11) which are the quantities of interest, will not be affected by artificially constraining the degrees of freedom at node 1. Thus, the singularity which occurs in the assembled stiffness matrix, as a result of the enforcement of the traction free edge condition, can be eliminated in this way. Solutions for $\underset{\sim}{q}_L^1$ can subsequently be obtained, but they are not calculated or used in this analysis.

E. The Strain Continuity Condition

In addition to the stress continuities previously defined across layer interfaces, certain strain continuities which are known to exist, can also be exactly enforced. The layers of the laminate are assumed to be perfectly bonded and therefore, the u and v displacements along any xy plane (see Figure 1) are smooth con-

tinuous functions. If this is the case, their derivatives with respect to x and y are also continuous. Applying this to the linear strain-displacement relations, based on the displacement field given in (9), shows that both ε_y and γ_{xy} are continuous across interlayer boundaries.

Using equations (3) and (4), and the definition of the matrix $\underline{R}$ given in (6) and (7), leads to the following expressions for ε_y and γ_{xy} (from stresses):

$$\begin{aligned} \epsilon_y &= R_{11}\,\sigma_y + R_{12}\,\sigma_z + R_{15}\,\sigma_{xy} + \frac{\bar{\zeta}_{12}}{\bar{\zeta}_{11}}\,\bar{\epsilon}_x \\ \gamma_{xy} &= R_{51}\,\sigma_y + R_{52}\,\sigma_z + R_{55}\,\sigma_{xy} + \frac{\bar{\zeta}_{16}}{\bar{\zeta}_{11}}\,\bar{\epsilon}_x \end{aligned} \tag{40}$$

Continuity requires (see Figure 2a):

$$\begin{aligned} \epsilon_y^{\,i}(z = h_i) - \epsilon_y^{\,i-1}(z = h_i) &= 0 \\ \gamma_{xy}^{\,i}(z = h_i) - \gamma_{xy}^{\,i-1}(z = h_i) &= 0 \end{aligned} \tag{41}$$

Substituting (40) into (41) and recalling that σ_z is continuous across interlayer boundaries (i.e. $\sigma_z^i = \sigma_z^{i-1} = \sigma_z$) leads to:

$$\begin{aligned} &R_{11}^{\,i}\sigma_y^{\,i} - R_{11}^{\,i-1}\sigma_y^{\,i-1} + R_{15}^{\,i}\sigma_{xy}^{\,i} - R_{15}^{\,i-1}\sigma_{xy}^{\,i-1} + (R_{12}^{\,i} - R_{12}^{\,i-1})\sigma_z \\ &\qquad + \left(\frac{\bar{\zeta}_{12}^{\,i}}{\bar{\zeta}_{11}^{\,i}} - \frac{\bar{\zeta}_{12}^{\,i-1}}{\bar{\zeta}_{11}^{\,i-1}}\right)\bar{\epsilon}_x = 0 \\ &R_{51}^{\,i}\sigma_y^{\,i} - R_{51}^{\,i-1}\sigma_y^{\,i-1} + R_{55}^{\,i}\sigma_{xy}^{\,i} - R_{55}^{\,i-1}\sigma_{xy}^{\,i-1} + (R_{52}^{\,i} - R_{52}^{\,i-1})\sigma_z \\ &\qquad + \left(\frac{\bar{\zeta}_{16}^{\,i}}{\bar{\zeta}_{11}^{\,i}} - \frac{\bar{\zeta}_{16}^{\,i-1}}{\bar{\zeta}_{11}^{\,i-1}}\right)\bar{\epsilon}_x = 0 \end{aligned} \tag{42}$$

where all stresses are evaluated at $z = h_i$

Further, substituting (30) into (42), and collecting coefficients in y, results in four sets of two simultaneous equations in $\hat{\beta}$'s and $\bar{\beta}$'s. Solving each set of equations, eight of the $\hat{\beta}$'s are expressed in terms of the remaining $\hat{\beta}$'s and $\bar{\beta}$'s. This results in the following relationships between betas of layer i and i-1 required to satisfy the strain continuity condition:

$$\begin{aligned} \hat{\beta}_1^{\,i} &= RF\,\hat{\beta}_5^{\,i-1} + RG\,\hat{\beta}_{13}^{\,i-1} + RH\,\bar{\beta}_1^{\,i} + RI\,\bar{\epsilon}_x \\ \hat{\beta}_3^{\,i} &= RF\,\hat{\beta}_6^{\,i-1} + RG\,\hat{\beta}_{14}^{\,i-1} + RH\,\bar{\beta}_5^{\,i} \end{aligned} \tag{43}$$

$$\hat{\beta}_3^i = RF\,\hat{\beta}_7^{i-1} + RG\,\hat{\beta}_{15}^{i-1}$$

$$\hat{\beta}_4^i = RF\,\hat{\beta}_8^{i-1} + RG\,\hat{\beta}_{16}^{i-1}$$

$$\hat{\beta}_9^i = RA\,\hat{\beta}_5^{i-1} + RB\,\hat{\beta}_{13}^{i-1} + RC\,\bar{\beta}_4^i + RD\,\bar{\epsilon}_x$$

$$\hat{\beta}_{10}^i = RA\,\hat{\beta}_6^{i-1} + RB\,\hat{\beta}_{14}^{i-1} + RC\,\bar{\beta}_5^i$$

$$\hat{\beta}_{11}^i = RA\,\hat{\beta}_7^{i-1} + RB\,\hat{\beta}_{15}^{i-1}$$

$$\hat{\beta}_{12}^i = RA\,\hat{\beta}_8^{i-1} + RB\,\hat{\beta}_{16}^{i-1}$$

where:

$$R1 = \frac{-R_{15}^i R_{51}^i}{R_{11}^i} + R_{66}^i \qquad R2 = \frac{R_{51}^i R_{11}^{i-1}}{R_{11}^i} - R_{51}^{i-1}$$

$$R3 = \frac{R_{15}^{i-1} R_{51}^i}{R_{11}^i} - R_{55}^{i-1}$$

$$R4 = \frac{-(R_{12}^i - R_{12}^{i-1}) R_{51}^i}{R_{11}^i} + (R_{52}^i - R_{52}^{i-1}) \qquad (44)$$

$$R5 = \frac{-\left(\frac{\bar{S}_{12}^i}{\bar{S}_{11}^i} - \frac{\bar{S}_{12}^{i-1}}{\bar{S}_{11}^{i-1}}\right) R_{51}^i}{R_{11}^i} + \left(\frac{\bar{S}_{16}^i}{\bar{S}_{11}^i} - \frac{\bar{S}_{16}^{i-1}}{\bar{S}_{11}^{i-1}}\right)$$

$$RA = \frac{-R2}{R1} \qquad RB = \frac{-R3}{R1} \qquad RC = \frac{-R4}{R1} \qquad RD = \frac{-R5}{R1}$$

$$RF = \frac{R_{11}^{i-1}}{R_{11}^i} + \frac{R_{15}^i}{R_{11}^i}\frac{R2}{R1} \qquad RG = \frac{R_{15}^{i-1}}{R_{11}^i} + \frac{R_{15}^i}{R_{11}^i}\frac{R3}{R1}$$

$$RH = \frac{-(R_{12}^i - R_{12}^{i-1})}{R_{11}^i} + \frac{R_{16}^i}{R_{11}^i}\frac{R4}{R1}$$

$$RI = \frac{\left(\frac{-\bar{S}_{12}^{\,i}}{\bar{S}_{11}^{\,i}} + \frac{\bar{S}_{12}^{\,i-1}}{\bar{S}_{11}^{\,i-1}} \right)}{R_{11}^{\,i}} + \frac{R_{15}^{\,i}}{R_{11}^{\,i}} \frac{RS}{RI}$$

The laminate betas correspond to the set of stress parameters remaining after the interlayer traction and strain continuity conditions have been satisfied. Equations (43) define the transformation matrices $\underset{\sim}{T}_S^i$ and $\underset{\sim}{C}_S^i$ shown in (17a). Again, the calculations given in (18) are accomplished both by use of the transformation matrices and by the use of assembly pointers. All displacement calculations are now done with respect to a complete set of laminate betas.

Recall that stresses however are assumed independently within each layer and, therefore, must be calculated independently for each layer. This requires that the original set of layer betas (for each layer where stresses are calculated) must be calculated using (17a) where all quantities on the right hand side are known. Prior to the consideration of the strain continuity condition, the transformation matrix $\underset{\sim}{T}_S^i$ is a Boolean matrix and all terms in $\underset{\sim}{C}_S^i$ are zero. When this is the case, the actual values of the layer betas remain unchanged, and it is only a matter of identifying those betas in the laminate set of betas which correspond to each subsequent layer by use of the assembly pointers. In the case where strain continutiy is enforced, however, β_{1-4} and β_{9-12} have been redefined in terms of the set of laminate betas. The relationship given in (17a) must, therefore, be used in conjunction with the assembly pointers to recalculate the layer betas to be used in the stress calculation. After the layer betas have been identified, the calculation of stresses is identical to that previously described (11).

3. Example Problems and Numerical Results

Three basic approaches can be defined for the analysis of cross-ply and angle-ply laminates. Each approach exactly satisfies traction free edge conditions along the top and bottom of the laminate and continuity of displacement and interlaminar stresses across layer interfaces. The element which satisfies these conditions will be termed the standard element. Other special stress and strain conditions are then imposed in addition to the above continuities and traction free conditions. The three analysis used are: 1) NO SPECIAL ELEMENT (NSE) analysis where the standard element is used throughout the mesh, 2) TRACTION FREE EDGE (TFE) analysis where one special element exactly satisfying free edge conditions along the side of the laminate is used in conjunction with the standard element throughout the remainder of the mesh, and 3) STRAIN CONTINUITY (SC) analysis where the continuity of inplane strains across interlayer boundaries is exactly satisfied for all elements.

Five test cases have been chosen to illustrate the effects of exactly satisfying different stress and strain conditions. Due to the symmetry of the plane of analysis, only one quarter of the cross section need be modeled. As previously stated, the upper left hand plane is analyzed in order to facilitate imposing the traction free edge condition. To be consistent with available results on this topic, results corresponding to the upper right hand portion of the cross section are plotted. Thus, the center line is along y=0 and the traction free edge is along the line y=b (Figure 3a). The test cases, shown in figure 4, are the 4-layer cross-plys $[90/0]_s$ and $[0/90]_s$, the 4-layer angle-plys $[45/-45]_s$ and the 8-layer laminates $[90/0/-45/45]_s$ and $[45/-45/0/90]_s$.

The finite element model is shown in figure 3b. The plane of analysis is broken into two regions. More elements of a smaller size are placed in region one near the traction free edge where the stress distributions are of the greatest interest.

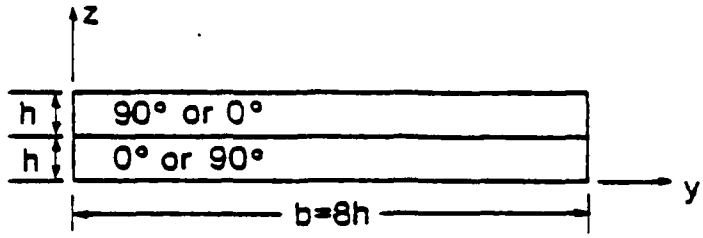

(a) FOUR LAYER LAMINATE: $(0/90)_s$, $(90/0)_s$

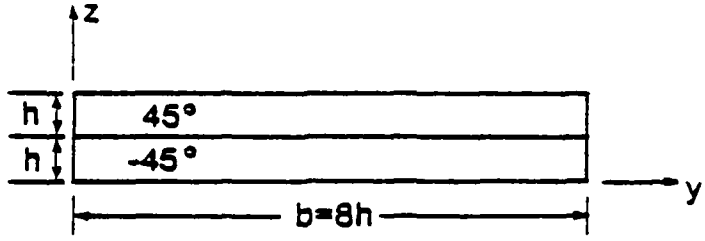

(b) FOUR LAYER LAMINATE: $(45/-45)_s$

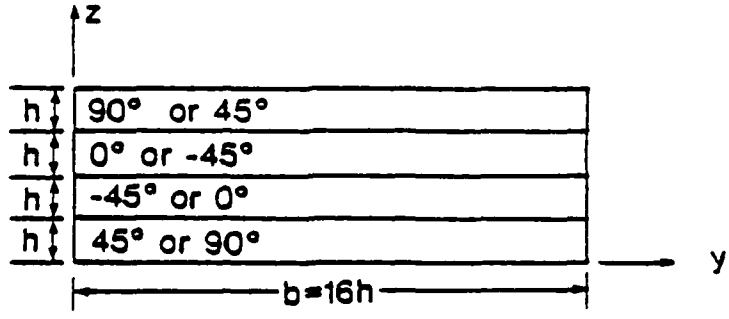

(c) EIGHT LAYER LAMINATE: $(90/0/-45/45)_s$, $(45/-45/0/90)_s$

Fig. 4 Test Cases

In the 4-layer cases considered, region one, where ℓ_1 = .25 b, is subdivided into 25 equal elements, and region two, where ℓ_2 = .75 b, is subdivided into 5 equal elements. This mesh was chosen on the basis of convergence studies which illustrated that the use of additional elements showed no appreciable change in the predicted stresses [9]. In analyzing the 8-layer cases, the use of 30 elements is computationally prohibative. In order to retain accurate stress predictions near the free edge, the size of region one is reduced such that ℓ_1 = .1b and ℓ_2 = .9b. Region one is then subdivided into 5 equal elements and region two is subdivided into 6 equal elements. Additional convergence results, based on a 4-layer laminate, show that only slight changes occur in the stress predictions when a more refined mesh is utilized. No subdivisions are needed in the z direction, because the element is developed to be multilayered.

The total width of the ply is 2b while the height of each layer is h. The ratio of width to height for both the 4-layer and 8-layer laminates considered is 4.

The boundary conditions are also shown in figure 3b. Symmetry conditions along $\bar{y}$=b (all u and v=0) and along z=0 (all w=0) are imposed. The elastic constants with respect to the principal material axes of each ply for all cases considered are:

$$E_{11} = 20.0 \times 10^6 \text{ psi}$$
$$E_{22} = 2.1 \times 10^6 \text{ psi}$$
$$\nu_{12} = \nu_{31} = \nu_{23} = 0.21$$
$$G_{12} = G_{31} = G_{23} = 0.85 \times 10^6 \text{ psi}$$

The first case considered is that of the cross-ply laminates, $[90/0]_s$ and $[0/90]_s$. For the cross-ply case, the u displacement is a function of x only. Consequently, referring to the expressions for the v and w displacement given in (9), the inplane stresses vanish (i.e. $\sigma_{xz} = \sigma_{xy} = 0$). Distributions of all stresses (i.e. σ_x (90^o layer), σ_x (0^o layer), σ_y (90^o layer), σ_y (0^o layer), σ_z and σ_{yz}) versus y along the 0/90 interface are shown in figures 5 and 6 for NO SPECIAL ele-

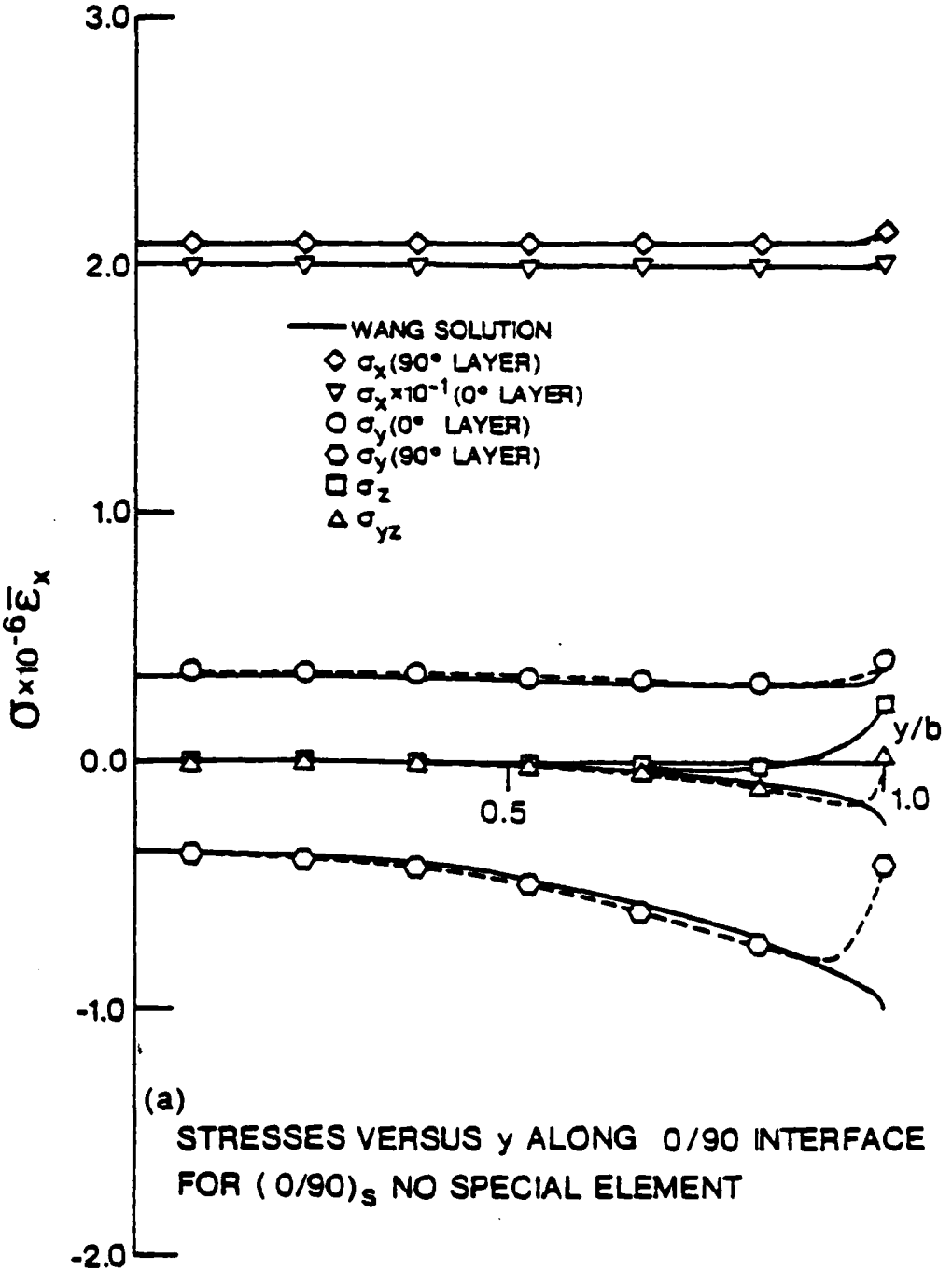

Fig. 5 Stress Results for $[0/90]_s$ laminate

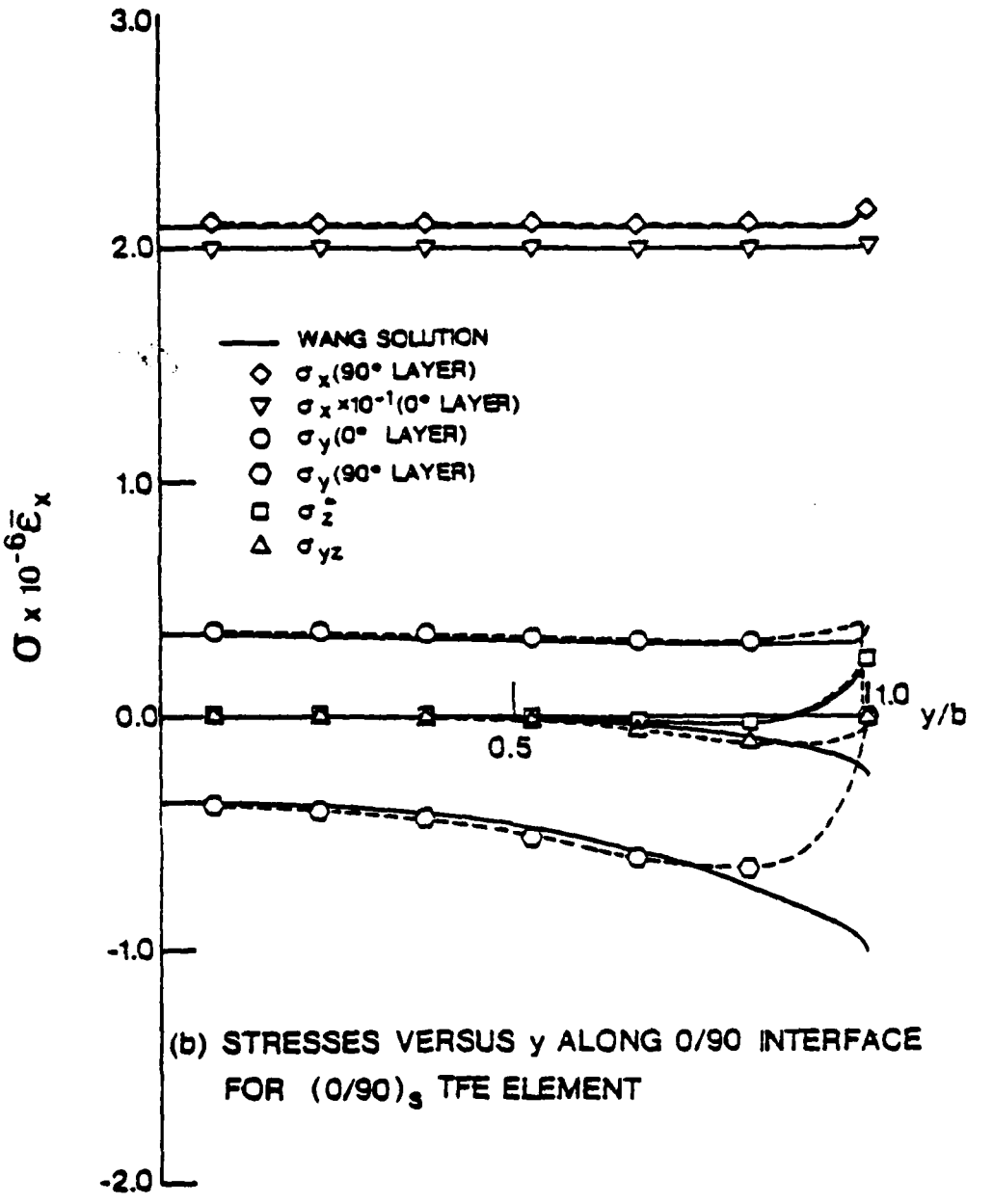

(b) STRESSES VERSUS y ALONG 0/90 INTERFACE FOR $(0/90)_s$ TFE ELEMENT

Fig. 5 (Continued)

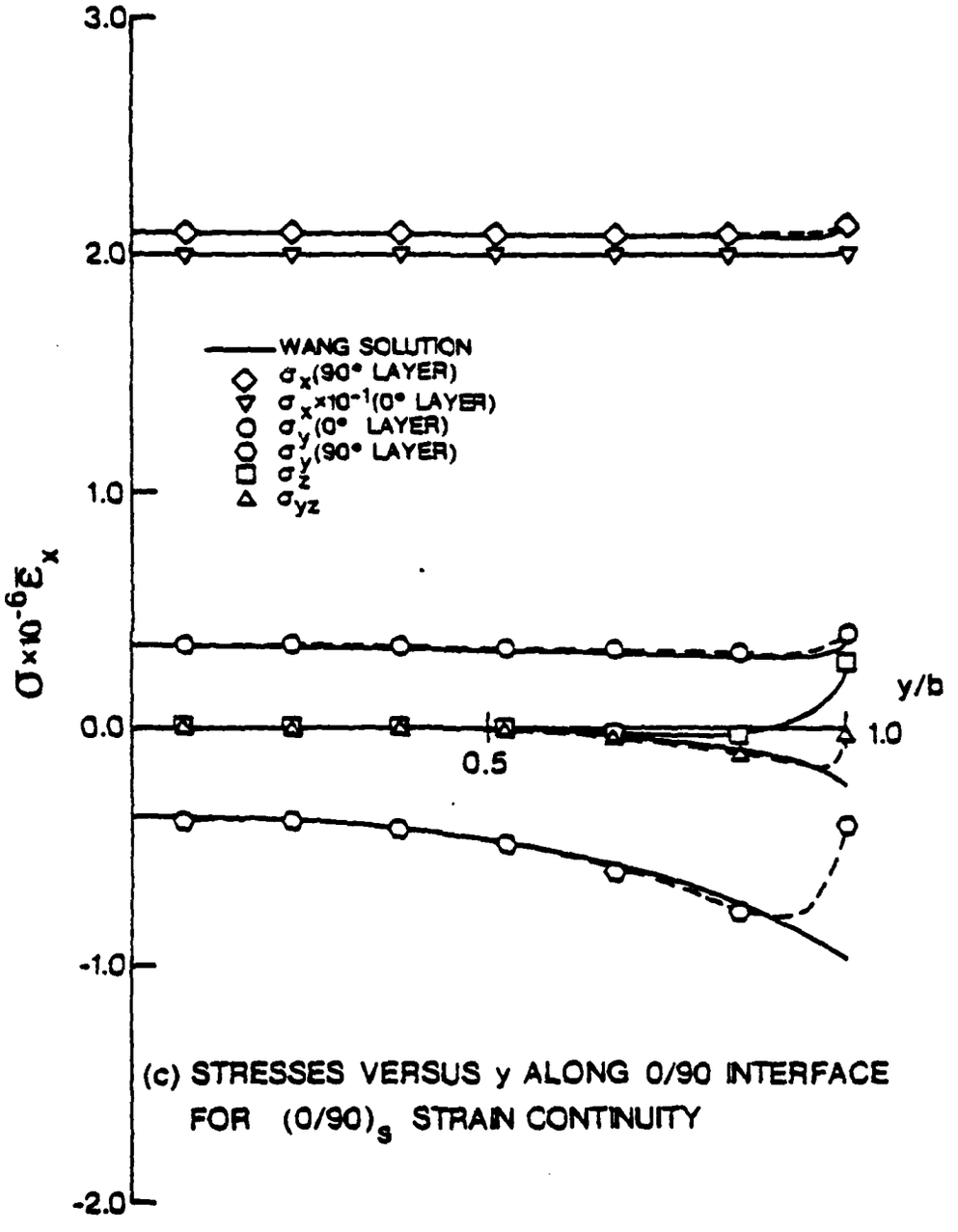

Fig. 5 (Concluded)

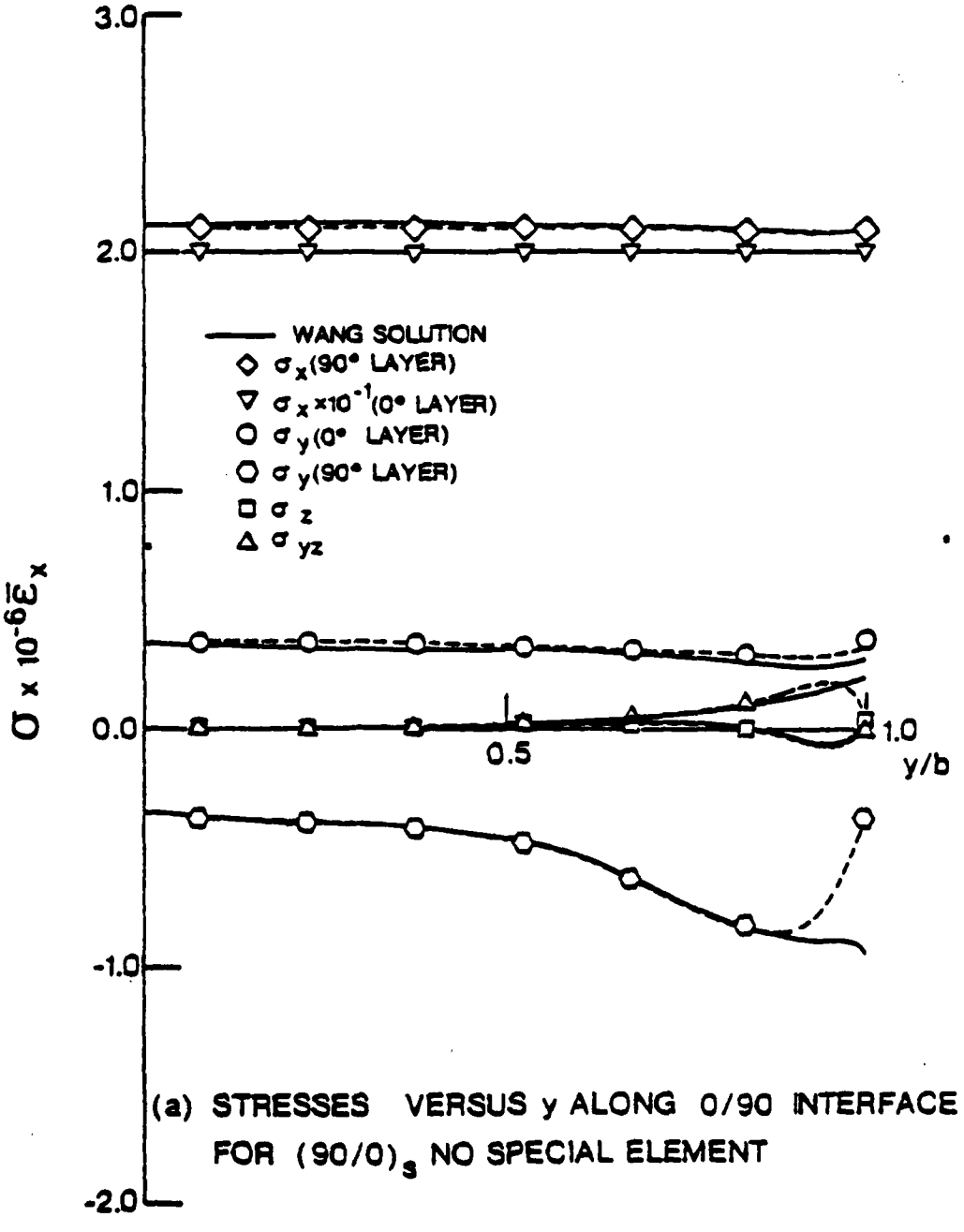

Fig. 6 Stress Results for $[90/0]_s$ laminate

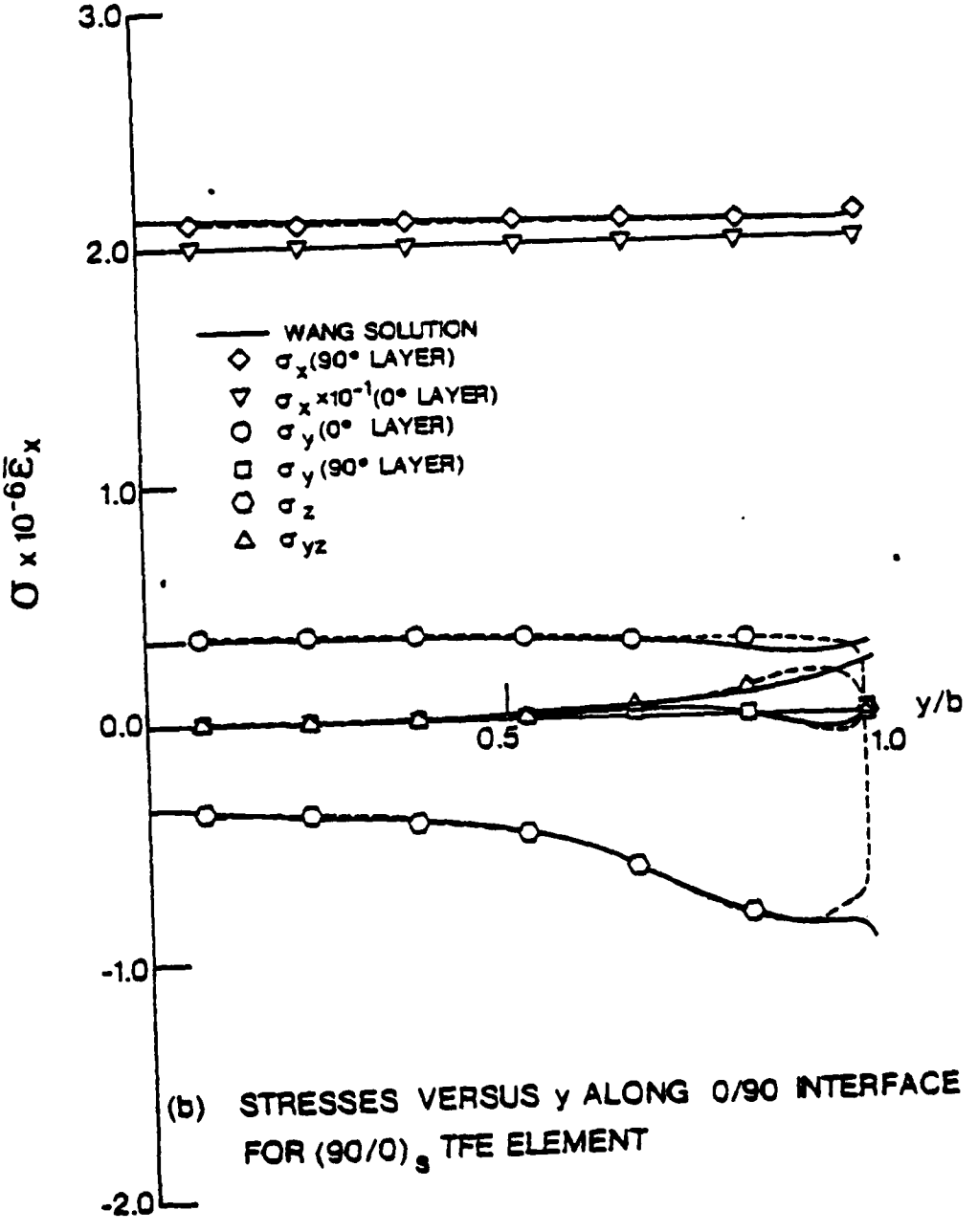

Fig. 6 (Continued)

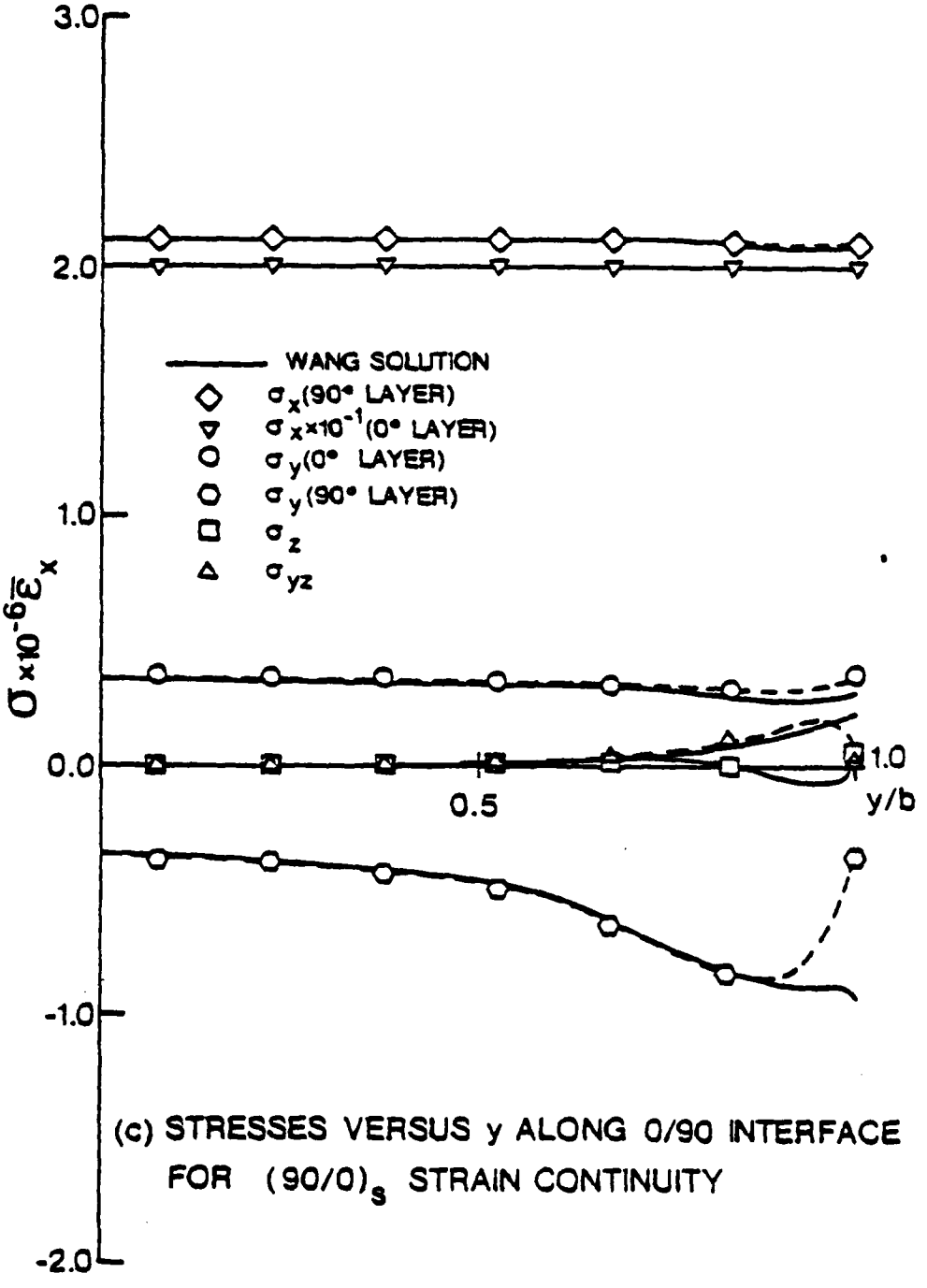

Fig. 6 (Concluded)

ment, the TFE element and the SC element. Also shown as a basis of comparison, is a solution by Wang based on a singularity eigenfunction expansion with boundary point collocation [11].

For both the $[90/0]_s$ and $[0/90]_s$ cases all three approaches agree with lamination theory away from the free edge which is expected. The differences between the solutions become apparent as the free edge is approached. For the $[0/90]_s$ case (Figures 5a through 5c), the solutions for σ_x in the 90^o and 0^o layers agree for the 3 analyses. The solution for σ_z essentially agrees, although σ_z for the TFE element deviates slightly from the other two approaches after approximately $y/b = .9$. Solutions for σ_y and σ_{yz} are nearly identical for the NSE and the SC approaches. In the TFE analysis, these stresses are forced to zero. In the other two cases, both σ_y in the 90^o layer and σ_{yz} tend toward zero despite the fact that this condition is not exactly enforced. The value of σ_y in the 0^o layer, however, stays near its constant value near the free edge for the NSE and the SC approaches and does not tend toward zero.

Similar results are observed for the $[90/0]_s$ cases shown in figures 6a through 6c. Again the results for σ_x are similar for all three approaches, and the results for σ_z are similar although slightly different after approximately $y/b = .9$. Also, σ_y in the 0^o layer and σ_{yz} for the NSE and SC element again tend toward zero, although they are not forced to do so as in the TFE element case, whereas σ_y in the 0^o layer does not.

Notable differences between the $[90/0]_s$ and $[0/90]_s$ cases occur in the results for σ_z and σ_{yz}. For the stacking sequence $[0/90]_s$, σ_{yz} is predominantly negative and rises to around the zero point near the free edge, while for the $[90/0]_s$ case, the opposite occurs; however the two curves are not mirror images. σ_z for the $[0/90]_s$ case dips negative between about $y/b = .6$ and $y/b = .9$ and then rises up from $y/b = .9$ to the free edge. For the stacking sequence $[90/0]_s$, σ_z is positive up to about $y/b = .8$ and then dips negative, rising again to about zero at the free edge.

The important differences between the two different stacking sequences, and the three different approaches is illustrated by looking at through thickness stress distributions. σ_z, σ_y and σ_{yz} are plotted through the thickness in Figures 7 and 8. Delamination of these multilayer structures is believed to be caused by a combination of stresses near the free edge. Consequently these distributions are of interest.

For the $[0/90]_s$ laminate, the distribution of σ_z shows about the same shape for all three cases. The maximum positive value is larger for the NSE and SC analyses than for the TFE case, where as the maximum negative value is larger for the SC and TFE approaches. The NSE analysis remains negative within the second layer, while the other two cases become positive and then become zero at the top of the laminate along with the NSE approach. The stresses σ_y and σ_{yz} shown in Figures 7b and 7c respectively are forced to zero in the TFE element case. σ_y agrees very closely for the other two approaches, tending toward a large negative value in the 90^o layer at the interface, and a large positive value in the 0^o layer. The distribution of σ_{yz} oscillates about the zero point. The agreement between the two approaches, NSE and SC, appears poor, but note that σ_{yz} is an order of magnitude less than the other stresses in question.

The $[90/0]_s$ laminate shows a much different distribution of σ_z. Again, however, the three approaches show the same general distribution with some disagreement in the first layer. The distribution, however, is predominantly compressive, whereas the distribution of σ_z for the $[0/90]_s$ laminate is predominantly tensile. The shape of σ_y for the $[90/0]_s$ laminate is the reverse of that for the $[0/90]_s$ laminate. The two appraches, NSE and SC, agree well. Recall that σ_y and σ_{yz} for the TFE case are set equal to zero along the free edge. The distribution of σ_{yz} again oscillates about zero, and is an order of magnitude smaller than the other stresses.

Recall that high order through thickness stress distributions have been assumed within each layer; σ_y is of order z^3, σ_z is of order z^5 and σ_{yz} is of order z^4. If

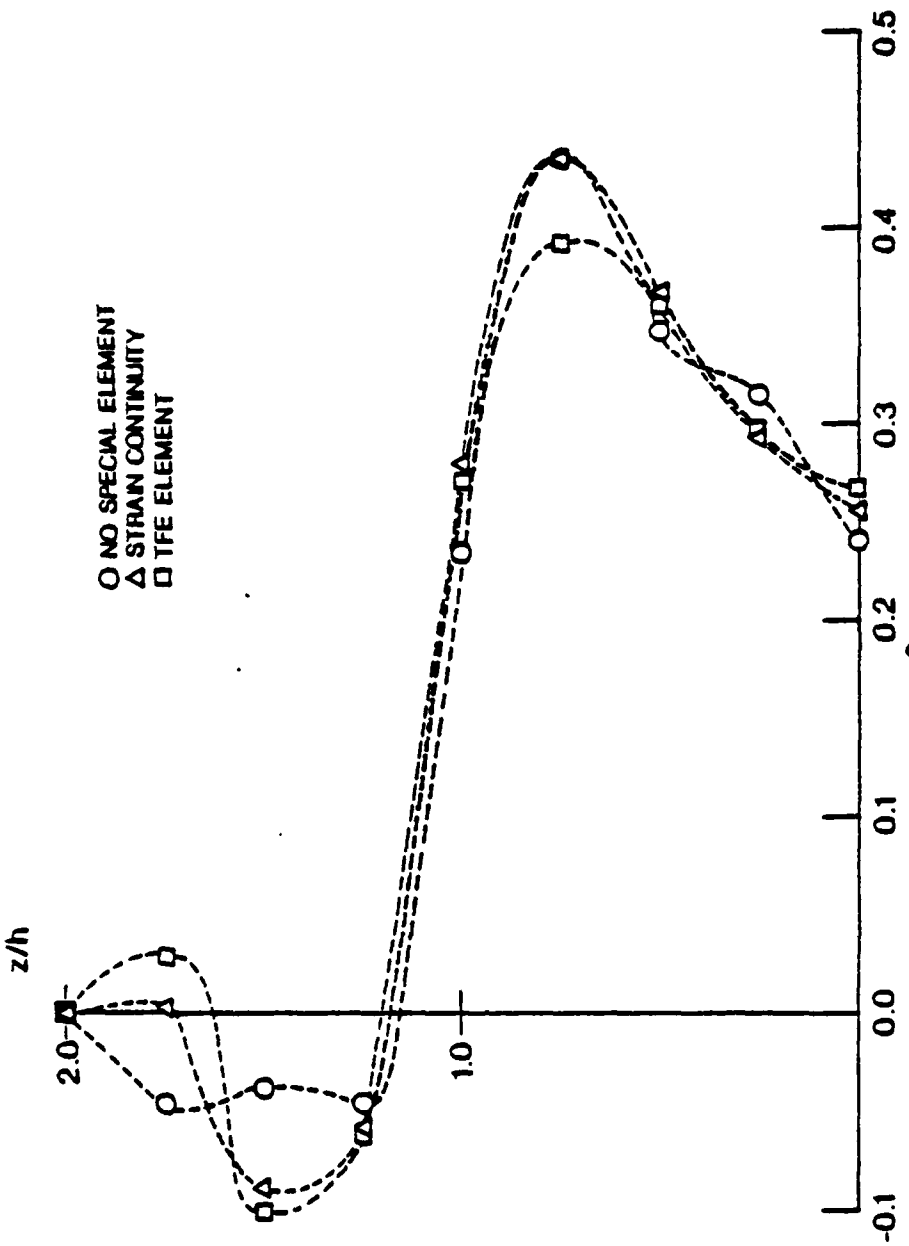

(a) σ_z VERSUS z AT y=b FOR $(0/90)_s$

Fig. 7 Through thickness stress results at the traction free edge for $[0/90]_s$ laminate

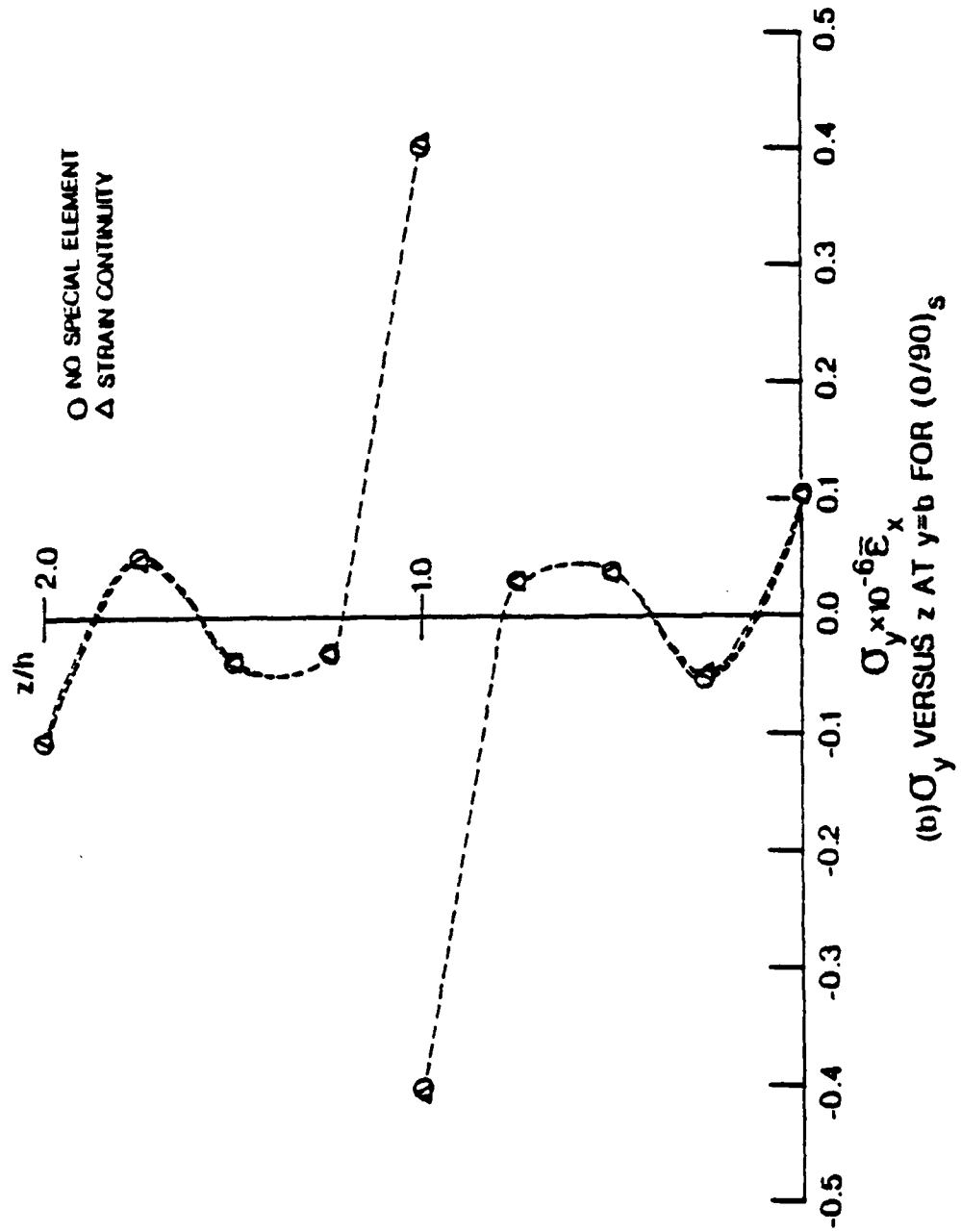

Fig. 7 (Continued)

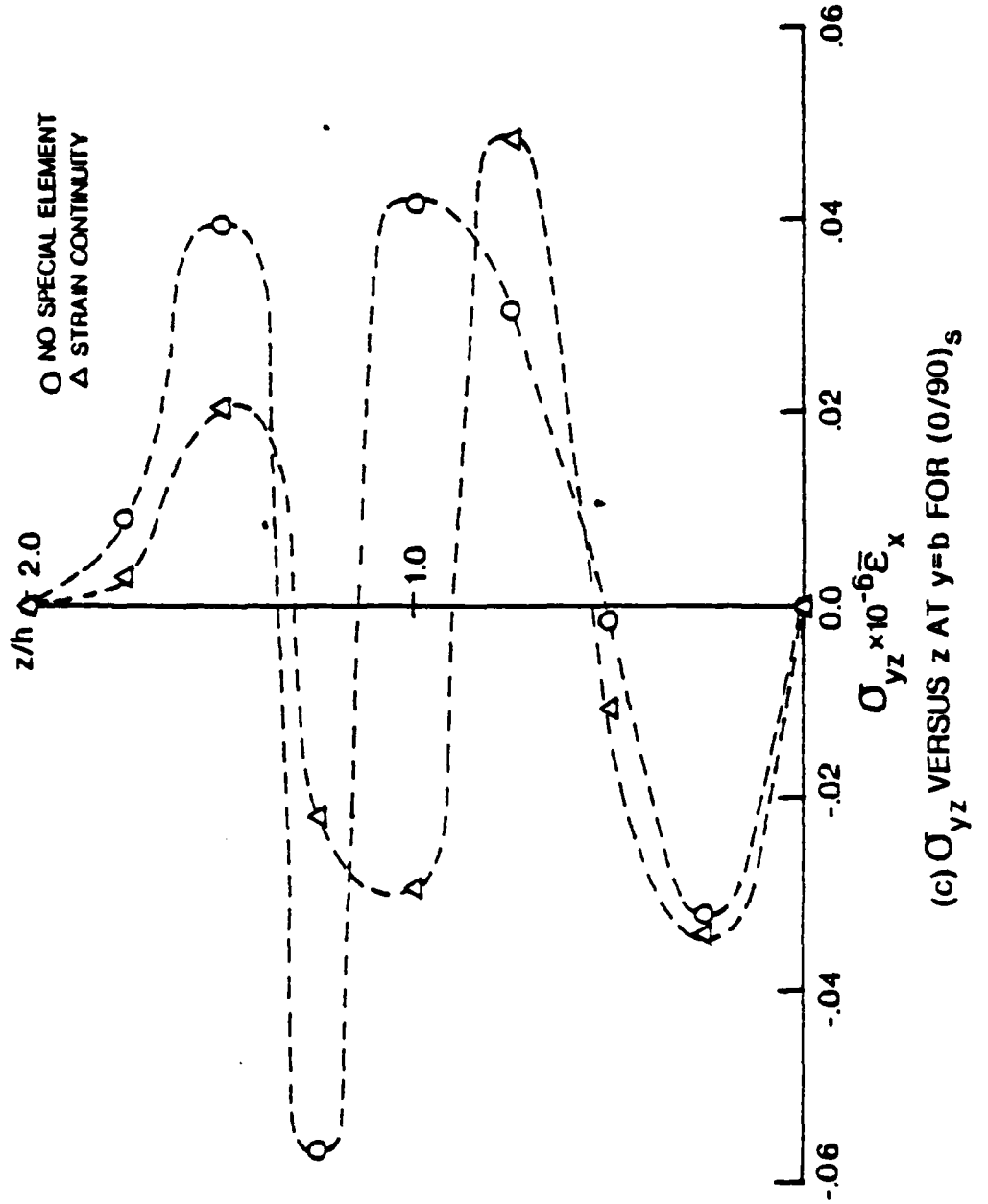

(c) σ_{yz} VERSUS z AT y=b FOR $(0/90)_s$

Fig. 7 (Concluded)

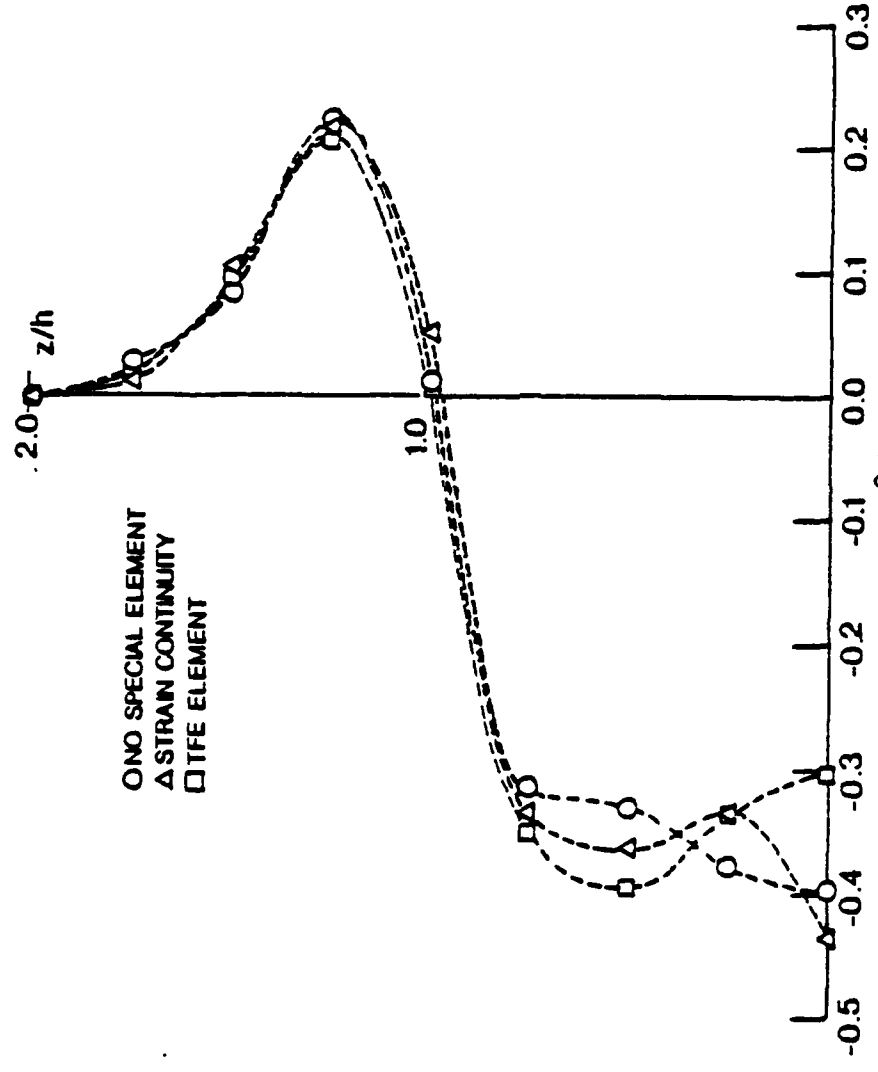

Fig. 8 Through thickness stress results at the traction free edge for $[90/0]_s$ laminate

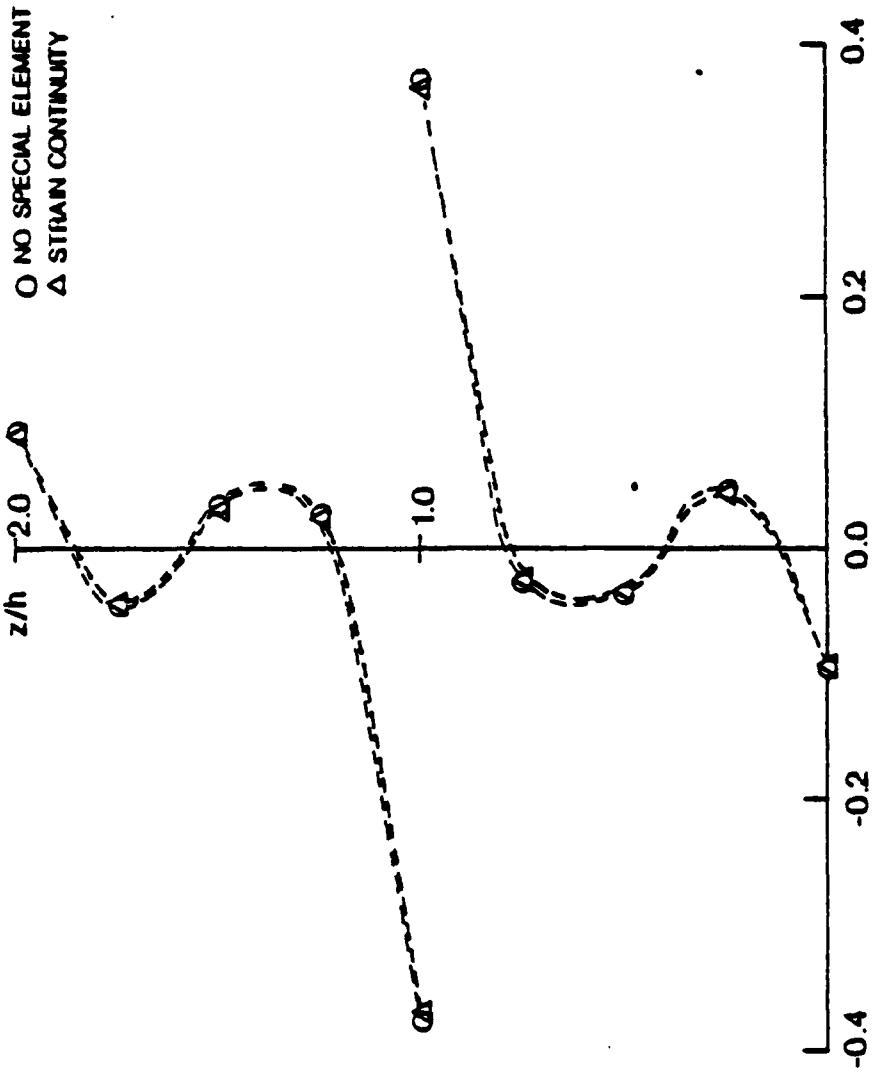

(b) σ_y VERSUS z AT y=b FOR $(90/0)_s$

Fig. 8 (Continued)

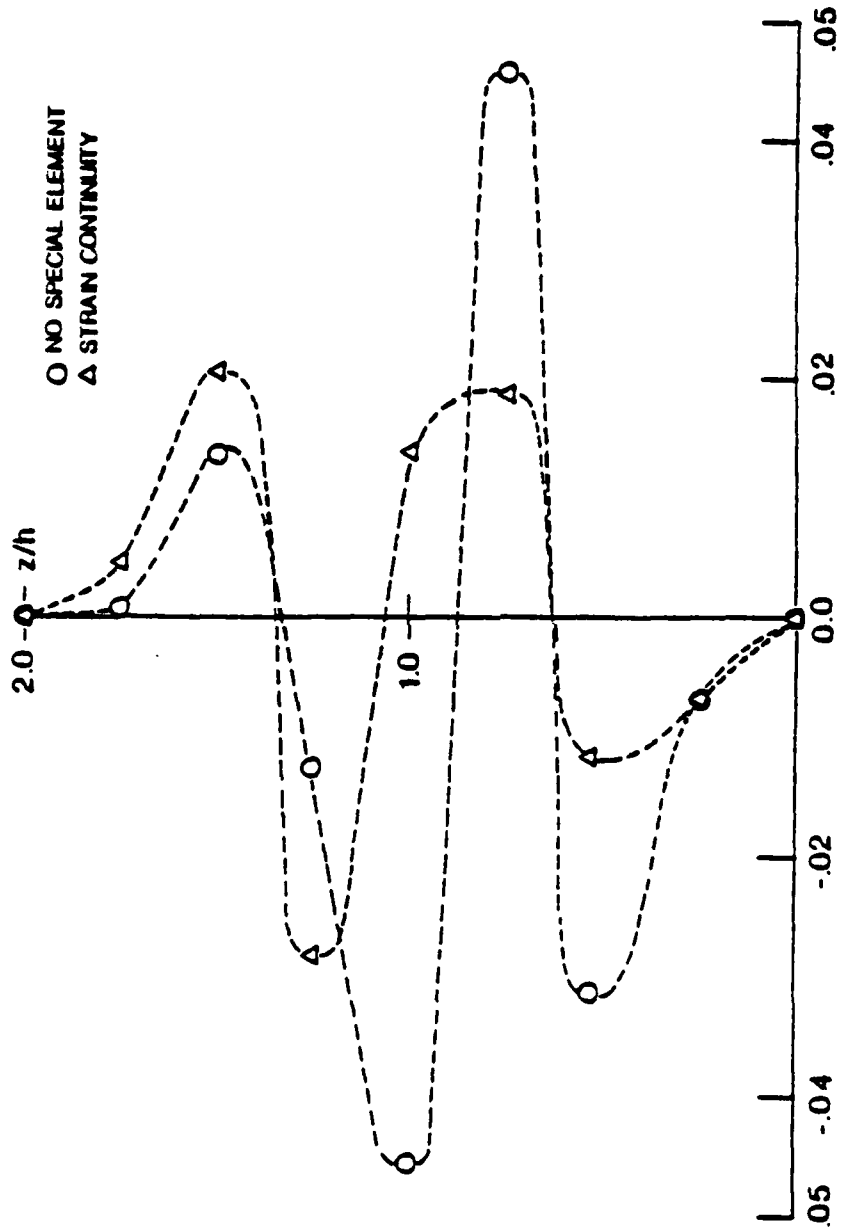

Fig. 8 (Concluded)

lower order assumed stress distributions could accurately predict the actual stress distributions, computation time could be reduced without effecting the results of the analysis. If it is possible to reduce the order of the stress assumptions, from equilibrium considerations, each stress component must be reduced by the same order. It is evident from Figures 7b and 8b that the order of σ_y can not be reduced without loss of accuracy. Therefore, the high order stress distibutions which have been used are in fact necessary.

The high order displacement interpolations might also be lowered to save on computation time. Through thickness distributions of v and w displacements along the free edge and away from the free edge for the NSE and SC approaches are shown in Figures 9a through 9c. In this analysis the v displacement is of order z^3 and the w displacement is of order z^2. The v displacement is chosen one order higher than the w displacement so that their relative through thickness contributions to γ_{yz} will be of the same order. Away from the traction free edge (Figure 9c) the w displacement is only of order z. To be consistent, therefore, the v displacement would be of order z^2 although it appears almost constant in Figure 9c. At the traction free edge, however, it appears that both the v and w displacement could be reduced by one order of z without appreciably effecting the accuracy of the displacement and stress distributions.

The next case considered is the angle ply $[45/-45]_s$ case. In this case, results by Wang and Crossman [4] are presented as a basis of comparison where available. In that analysis, constant strain triangles were used to model the problem. Later results by Herakovich, Nagarker, and O'Brien [7] , also using constant strain triangles, show results which differ somewhat from Wang and Crossman when a more refined mesh is used. The results for this case are presented in Figures 10a through 10f. Included are distributions of σ_z, σ_{yz}, σ_{xz} and σ_{xy} along the 45/-45 interface and through thickness distributions of σ_{xz} and σ_z along the free edge.

Figure 10a shows the distribution of σ_z along the 45/-45 interface. Results

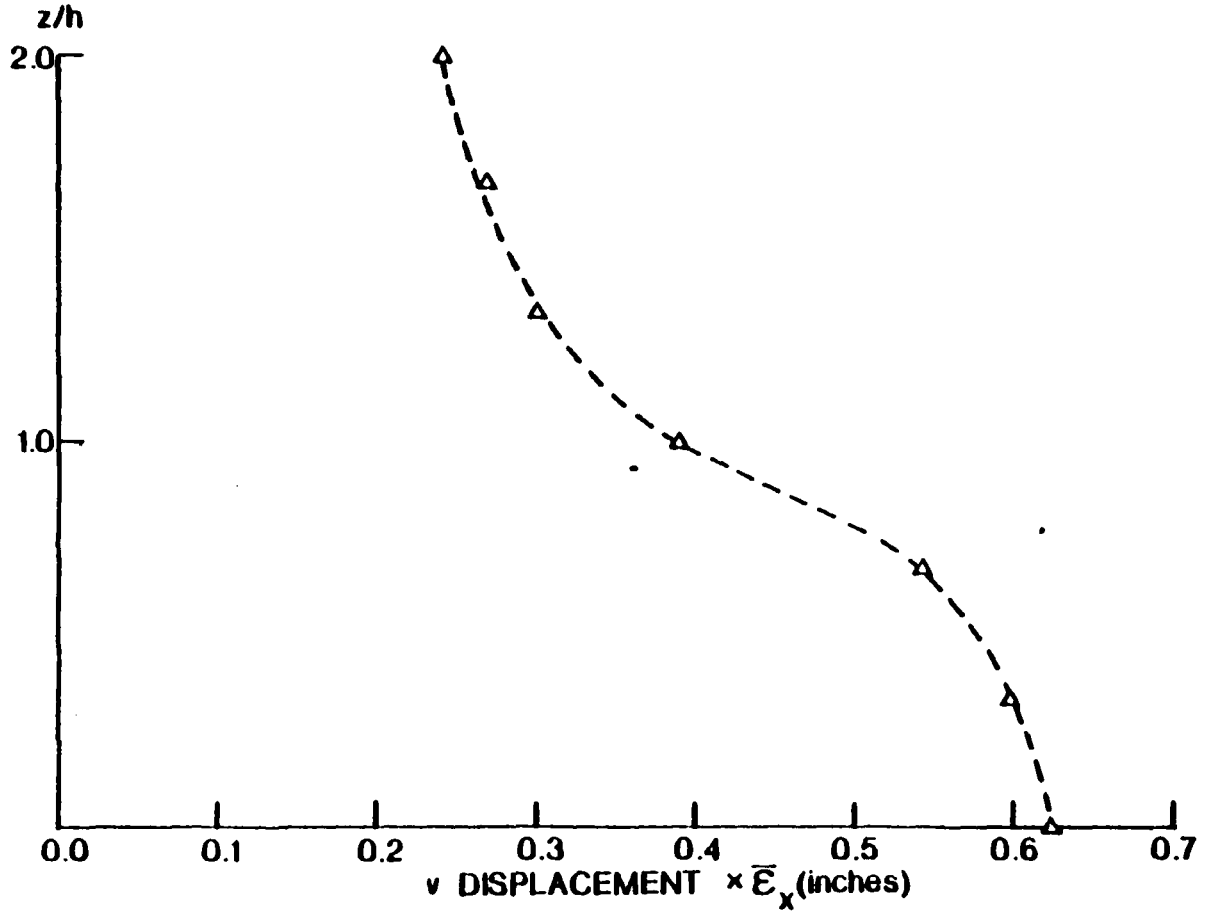

(a)v DISPLACEMENT VERSUS z AT THE TRACTION FREE EDGE FOR $(90/0)_s$
(NO SPECIAL ELEMENT; STRAIN CONTINUITY)

Fig. 9 Displacement Results

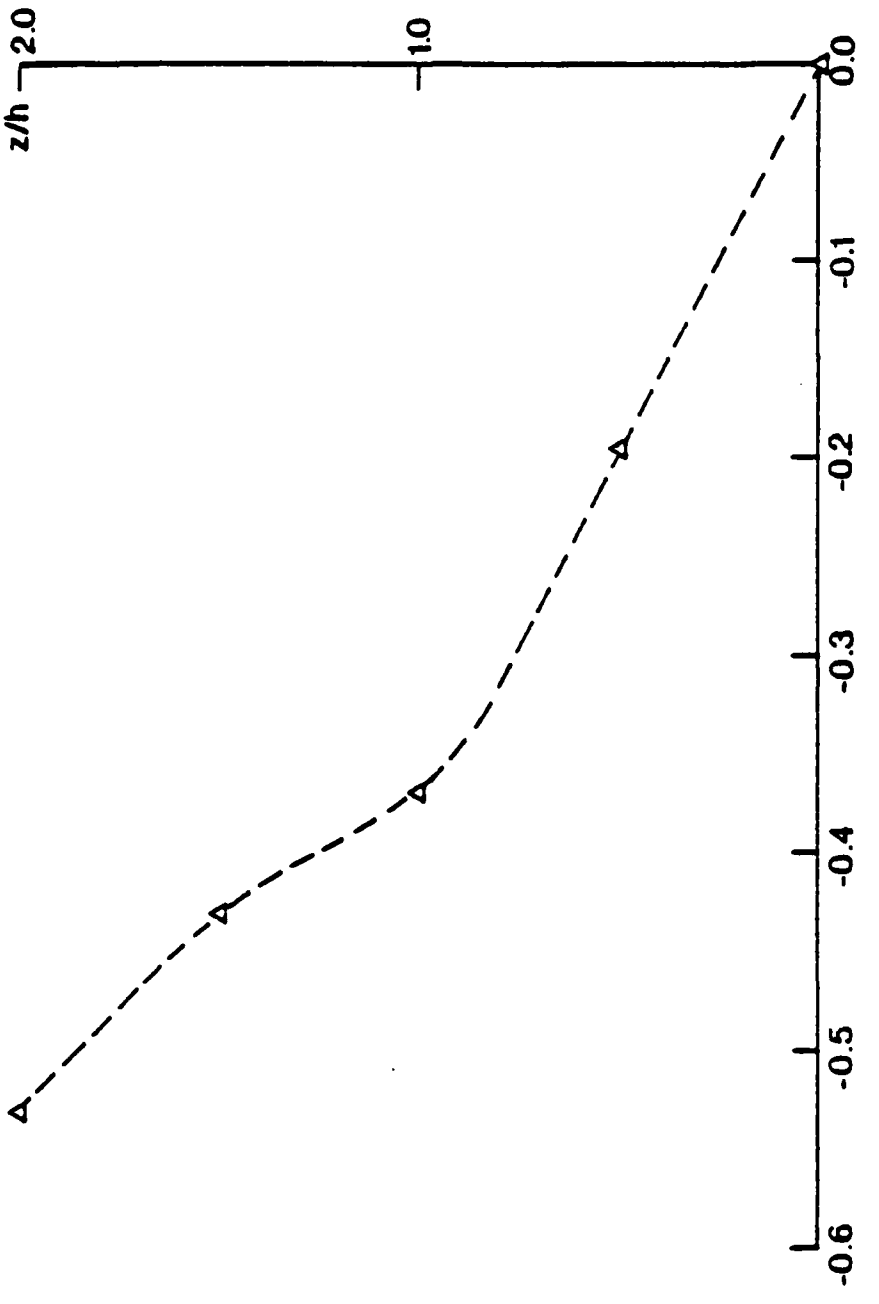

Fig. 9 (Continued)

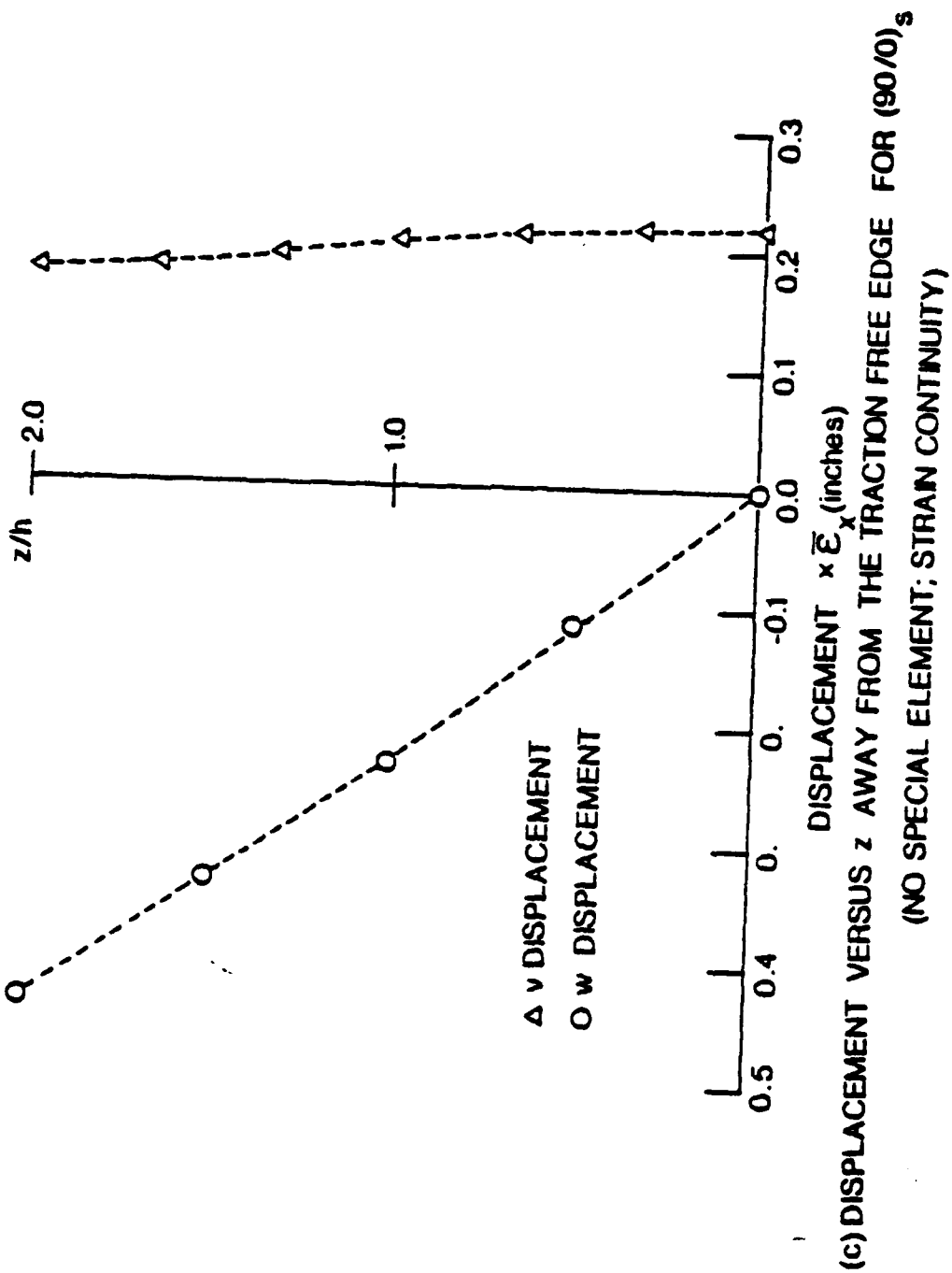

Fig. 9 (Concluded)

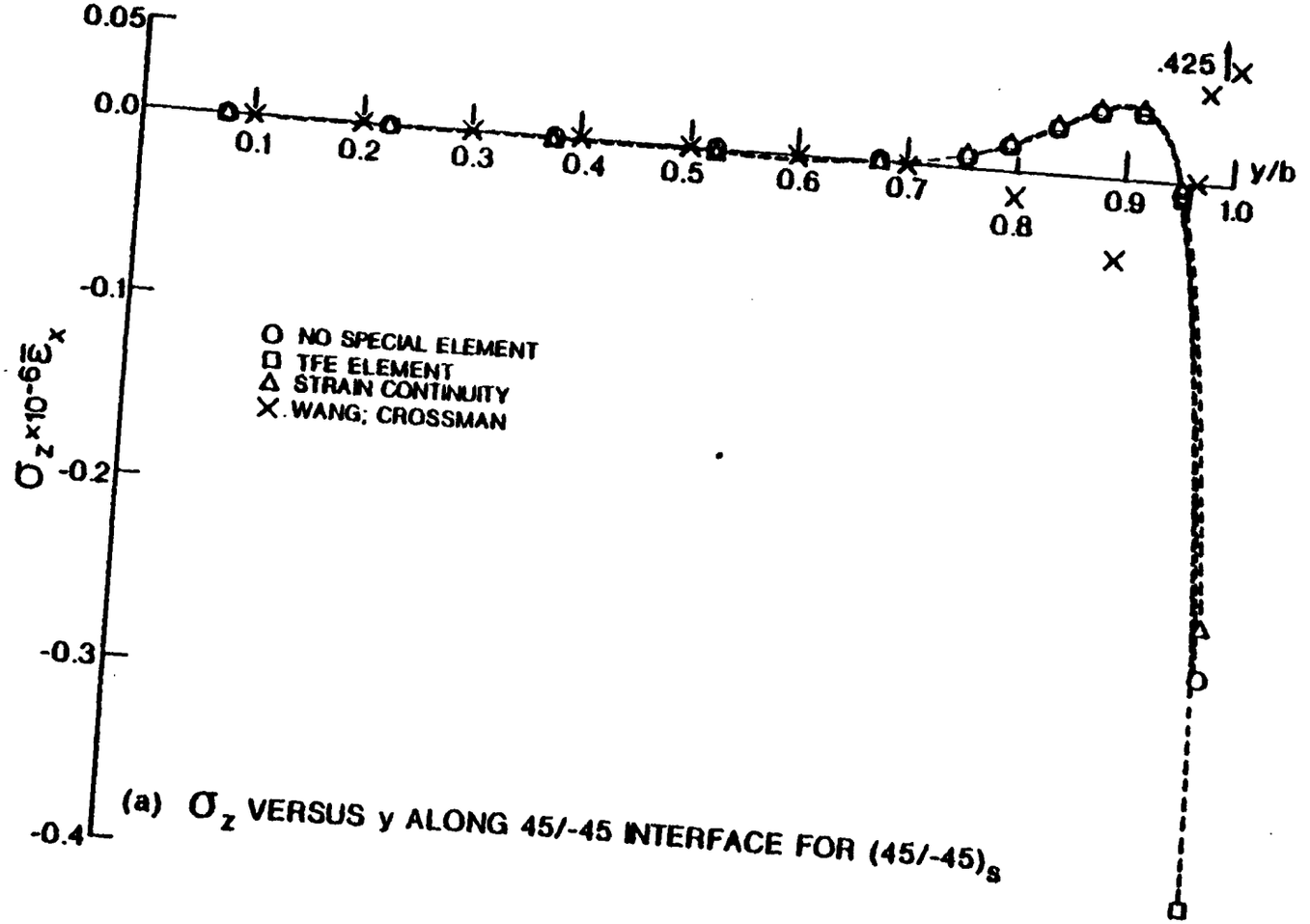

Fig. 10 Stress Results for $[45/-45]_s$ laminate

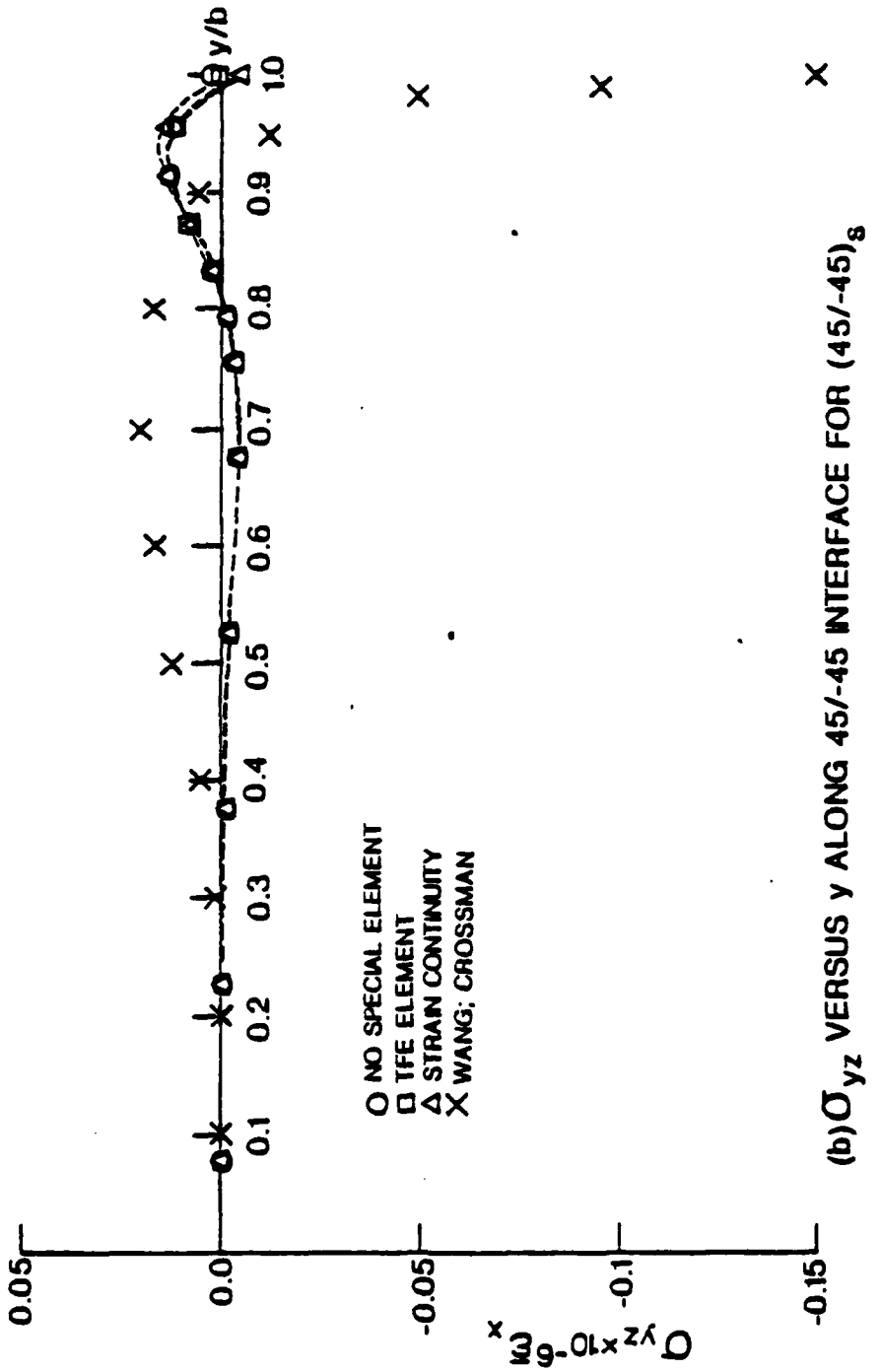

Fig. 10 (Continued)

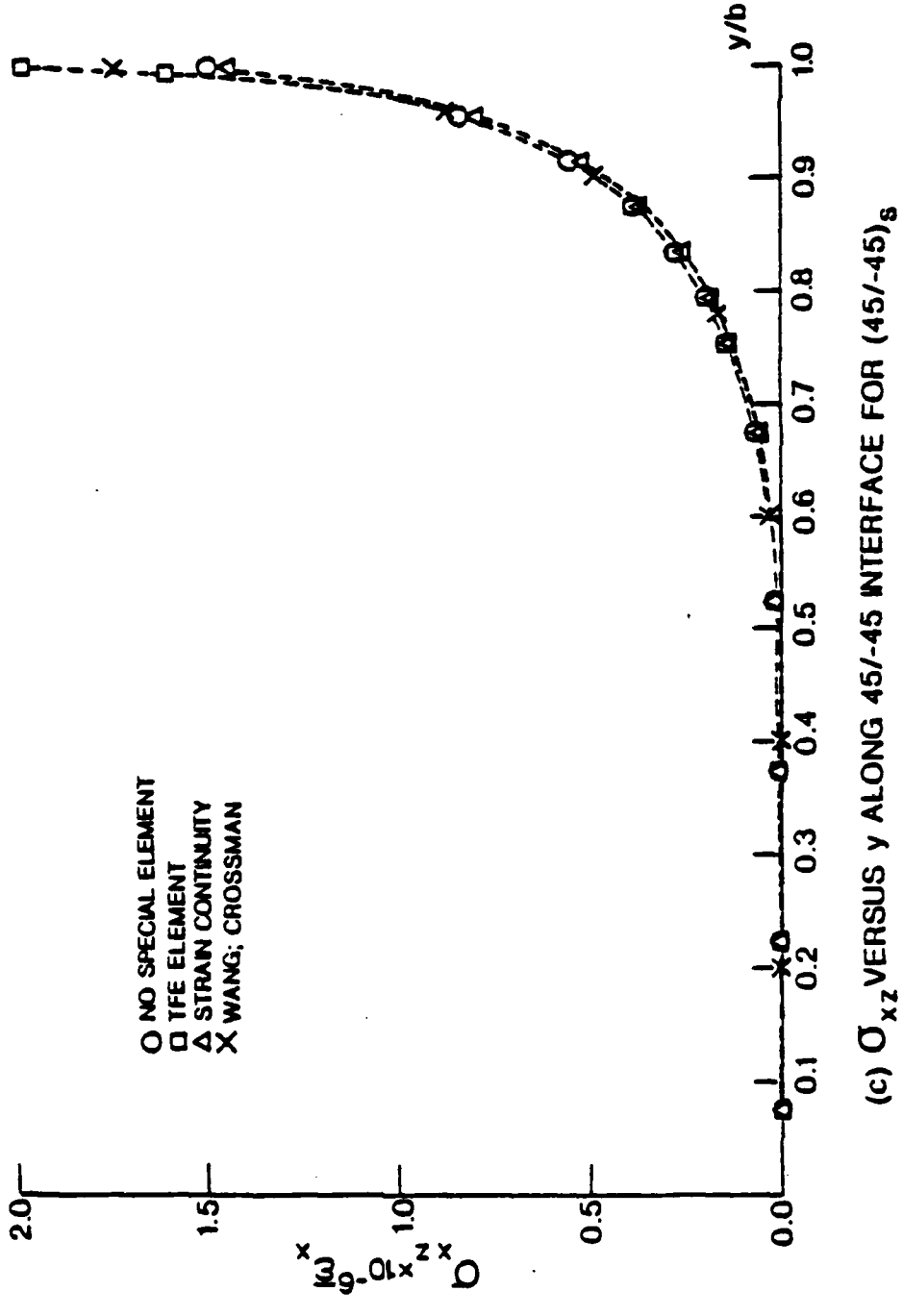

(c) σ_{xz} VERSUS y ALONG 45/-45 INTERFACE FOR $(45/-45)_s$

Fig. 10 (Continued)

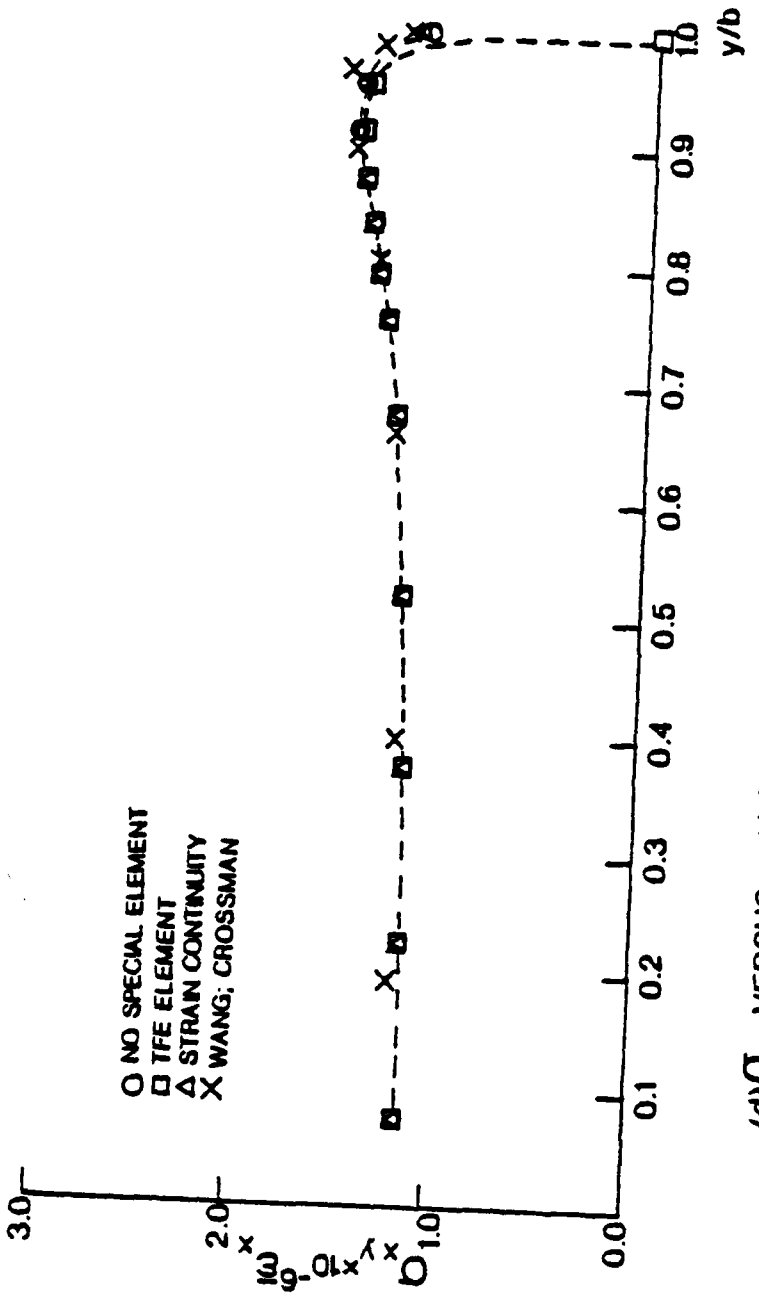

Fig. 10 (Continued)

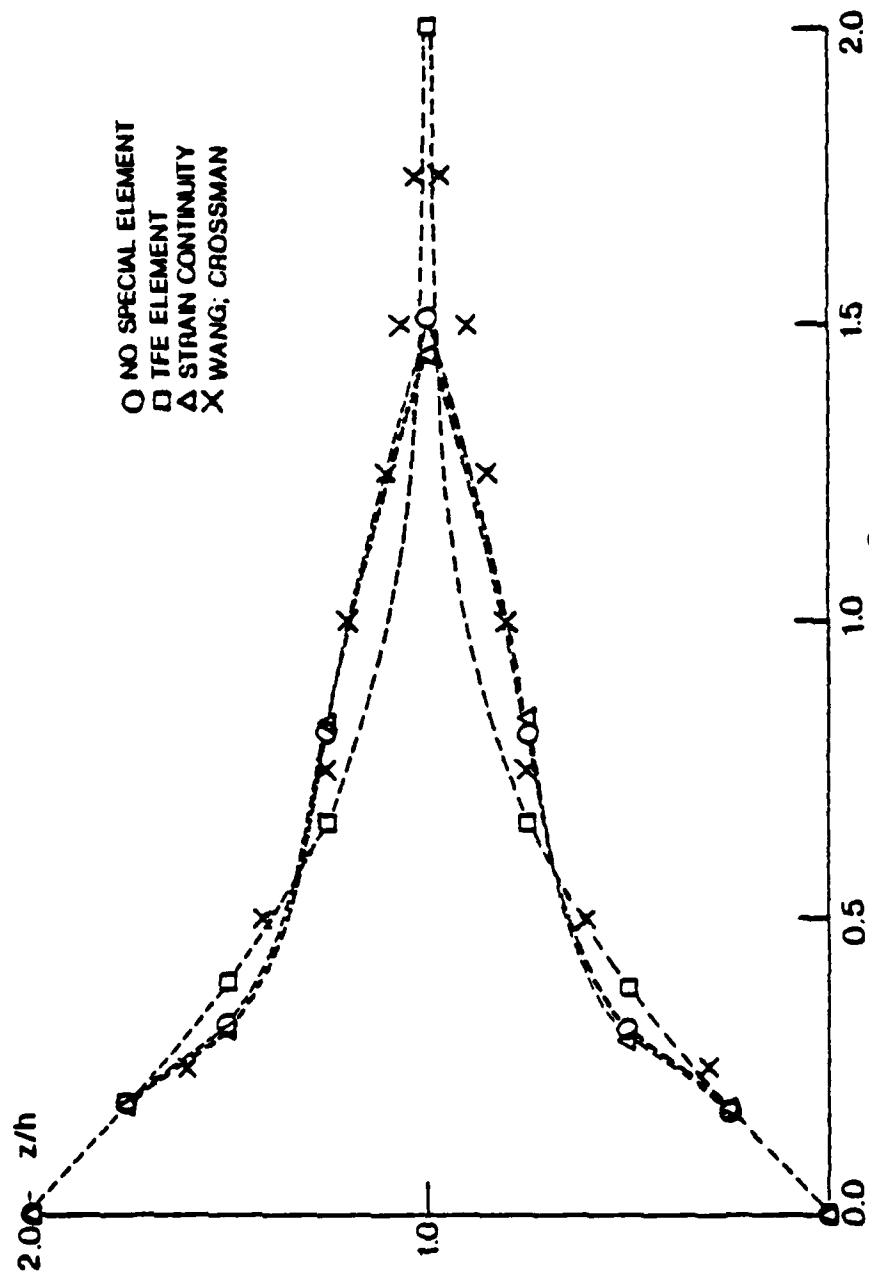

Fig. 10 (Continued)

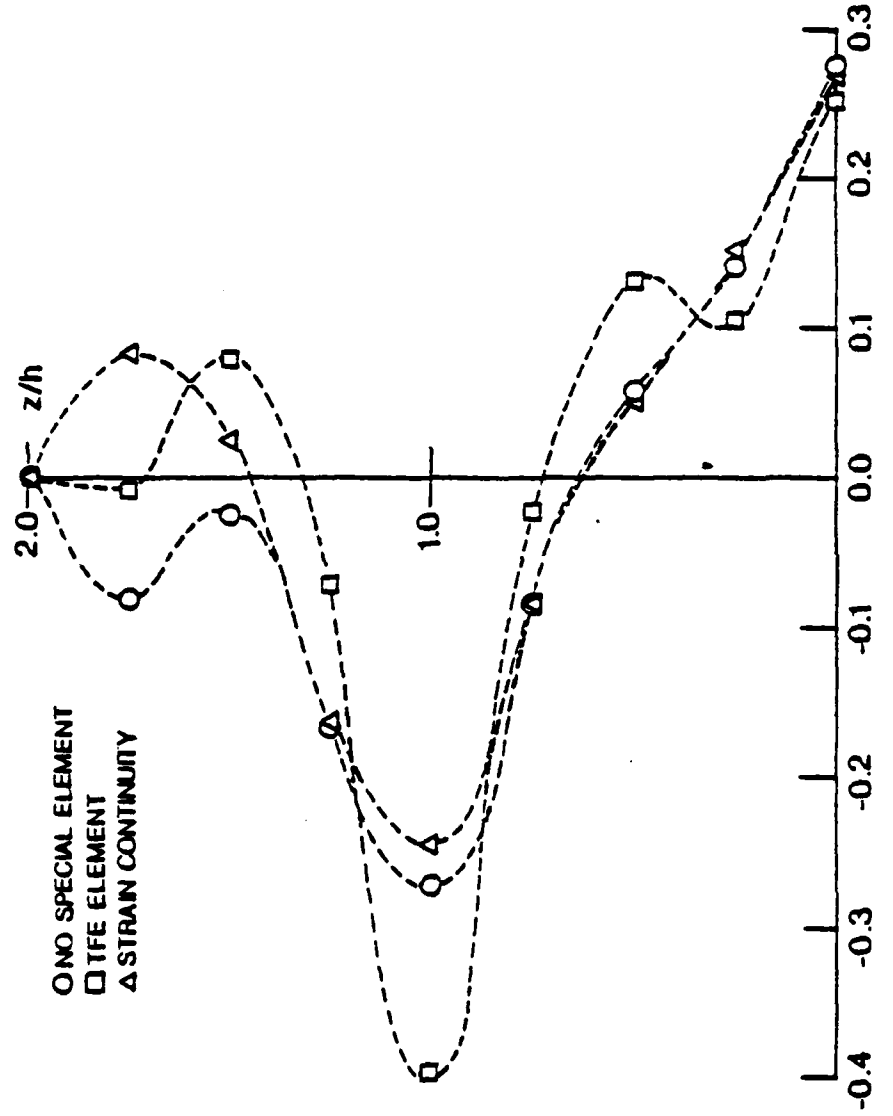

(l) σ_z VERSUS z AT y=b FOR (45/-45)s

Fig. 10 (Concluded)

for the three analyses are very similar. At the traction free edge all the solutions reach a large negative value. The TFE element reaches the greatest value while the NSE and SC analyses give similar results at the traction free edge. It is of interest to note that the Wang and Crossman results tend to a large positive value while all of the results presented here show a large negative value at the traction free edge.

The three approaches also show very similar results for the distributions of σ_{yz}, σ_{xz}, and σ_{xy} along the 45/-45 interface. Small discrepancies appear near the traction free edge for the distribution of σ_{yz}. The TFE element is forced to have a value of zero at this point, while the NSE analysis shows a small positive value and the SC analysis shows a small negative value. The results for σ_{xz} show that the TFE approach again gives the largest value at the free edge, while the results for the other two analyses are smaller and in better agreement. Note also that the results for the SC analysis are slightly lower than the other approaches from about y/b = .6 to the traction free edge. The differences observed in the distribution of σ_{xy} between the three approaches is also near the traction free edge. Here the TFE analysis is again forced to be zero. It also shows lower values from about y/b = .85 to the traction free edge when compared to the other two analysis. The NSE and SC analyses give essentially the same results but do not reach zero at the traction free edge.

The three approaches again show similar results for the through thickness distributions of σ_{xz} and σ_z at the free edge. The values of σ_{xz} through the thickness (Figure 10c) are all positive. The TFE element reaches a greater value at the 45/-45 interface than either the NSE or SC analyses, but the relative shapes of the distribution for the three appraches is the same. Again, some dissimilarities are observed between the three analysis for the distribution of σ_z (Figure 10f). They do agree well at the midsurface, where the maximum positive value of σ_z occurs. The maximum negative value occurs at the 45/-45 interface, where the TFE element again

reaches the greatest value while the NSE and SC approaches tend to have smaller negative values.

The final cases analyzed are the $[45/-45/0/90]_s$ and $[90/0/-45/45]_s$ laminates. Again, Wang and Crossman results are included on the graphs where available. Figures 11a through 11f show the results for the $[45/-45/0/90]_s$ case. The distribution of σ_z along the 0/90 interface and along the midsurface are plotted in Figures 11a and 11b respectively. The three approaches give essentially the same results up to the traction free edge where the NSE analysis drops off slightly. The results for the distributions of σ_{yz} along the 0/90 interface (Figure 11c) and the distribution of σ_{xz} along the 45/-45 interface (Figure 11d), again show that the three analysis agree well up to the traction free edge. The distribution of σ_{yz} shows the NSE approach dropping off again at the free edge. The TFE element drops down, but then is forced back up to zero at the traction free edge, whereas the SC approach rises smoothly to zero. All the results for σ_{xz} rise smoothly at the free edge. The TFE element rises to the highest value while the NSE and SC approaches rise to smaller values which are again in better agreement.

Through thickness distributions of σ_z and σ_{xz} for the $[45/-45/0/90]_s$ laminate are shown in Figures 11e and 11f. The TFE and SC approaches show tensile stress for σ_z in the 90° and 0° layers, and primarily compressive values of σ_z in the -45° and 45° layers. The NSE analysis gives smaller tensile values in the 90° layer, but remains tensile up to the top of the 45° layer. Agreement between the three approaches is slightly better for σ_{xz}. Here only the value at the 0/-45 interface, where the TFE analysis shows a larger negative value, and the value at the 45/-45 interface, where the TFE analysis shows a much higher positive value, differ significantly between the three analysis.

Results for σ_z along the 0/90 interface, and σ_z along the midsurface are shown in Figures 12a and 12b for the $[90/0/-45/45]_s$ laminate. Again the three analysis agree well up the traction free edge. The NSE approach drops off to give a negative value

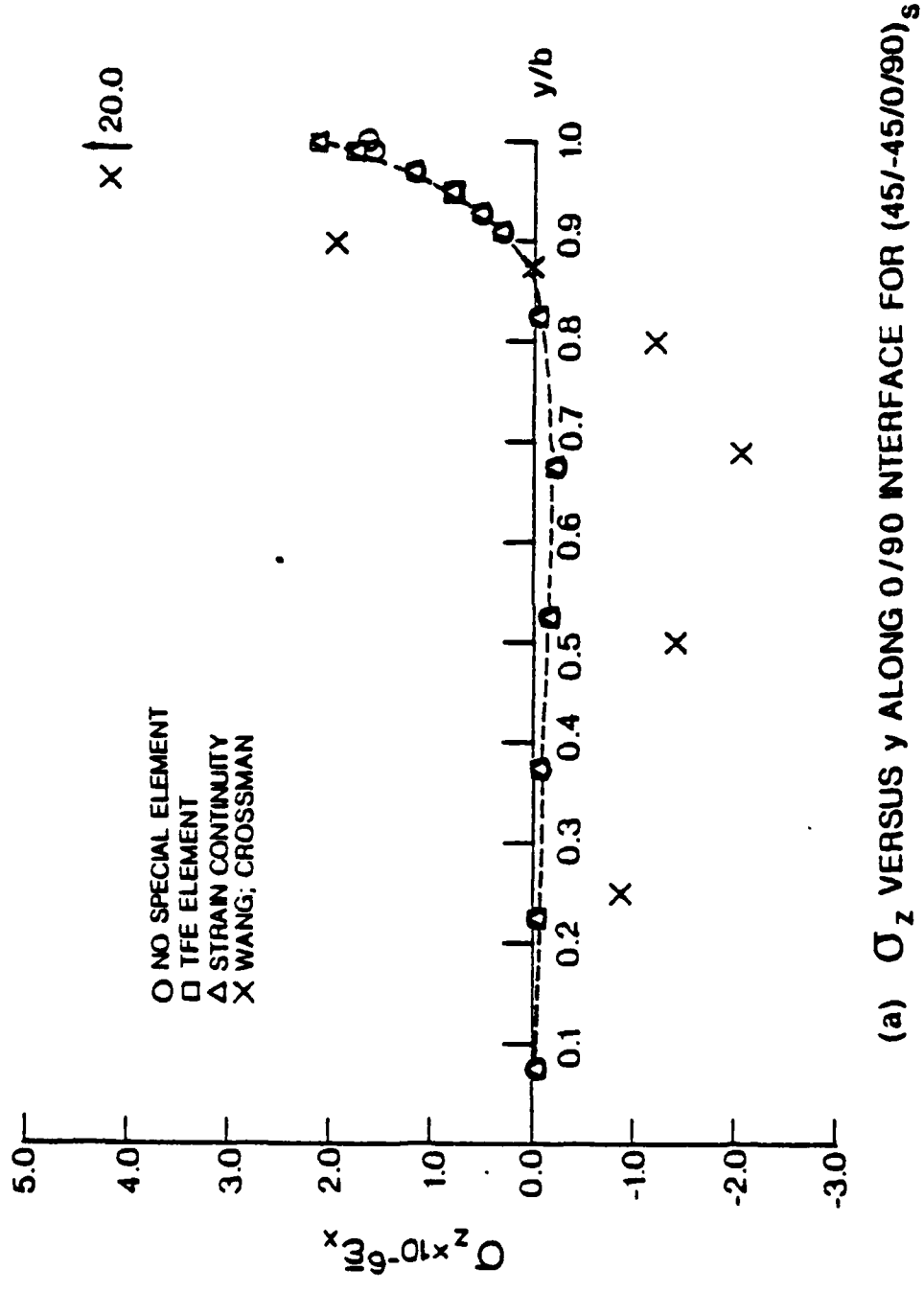

Fig. 11 Stress Results for $[45/-45/0/90]_s$ laminate

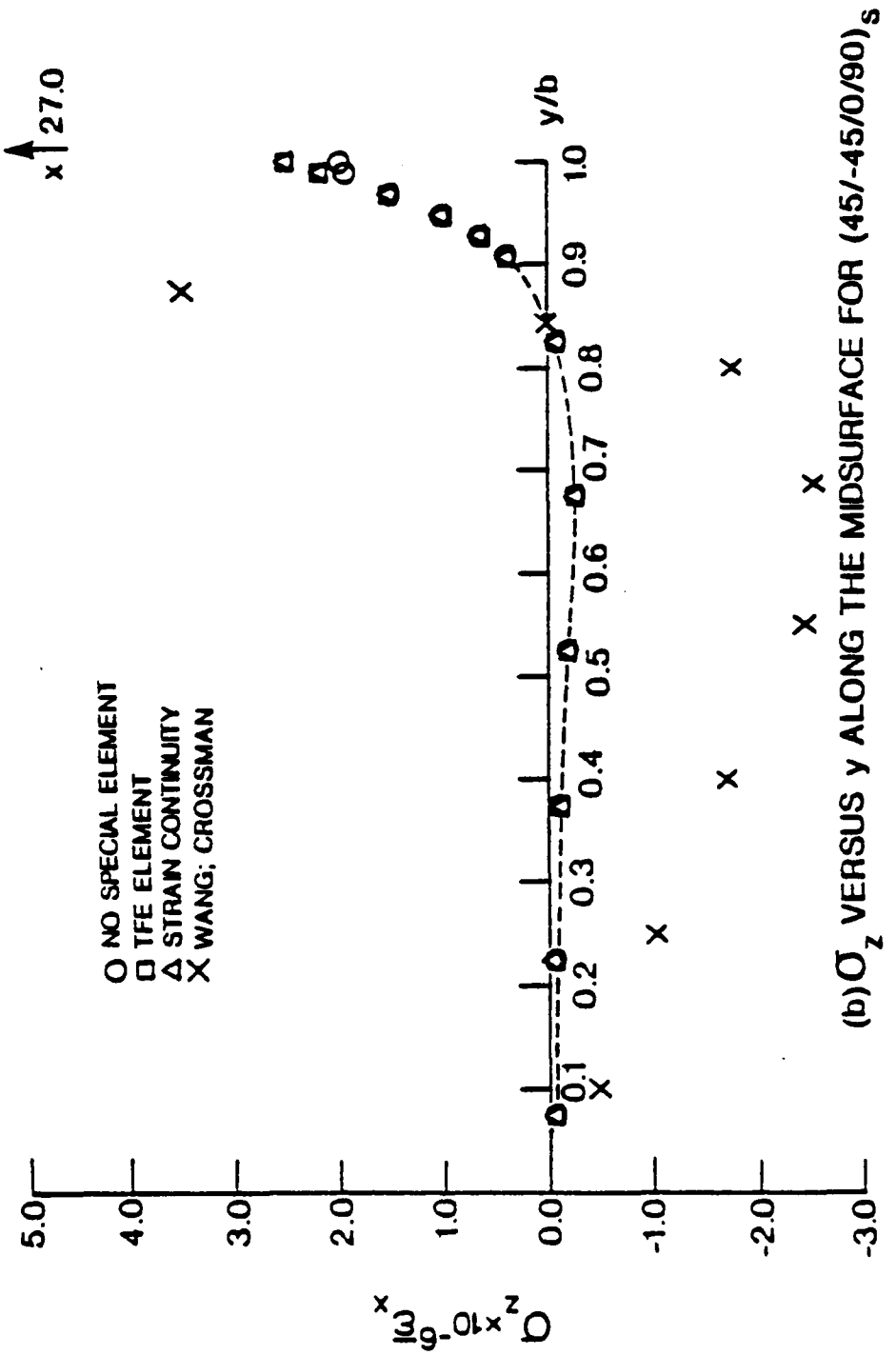

Fig. 11 (Continued)

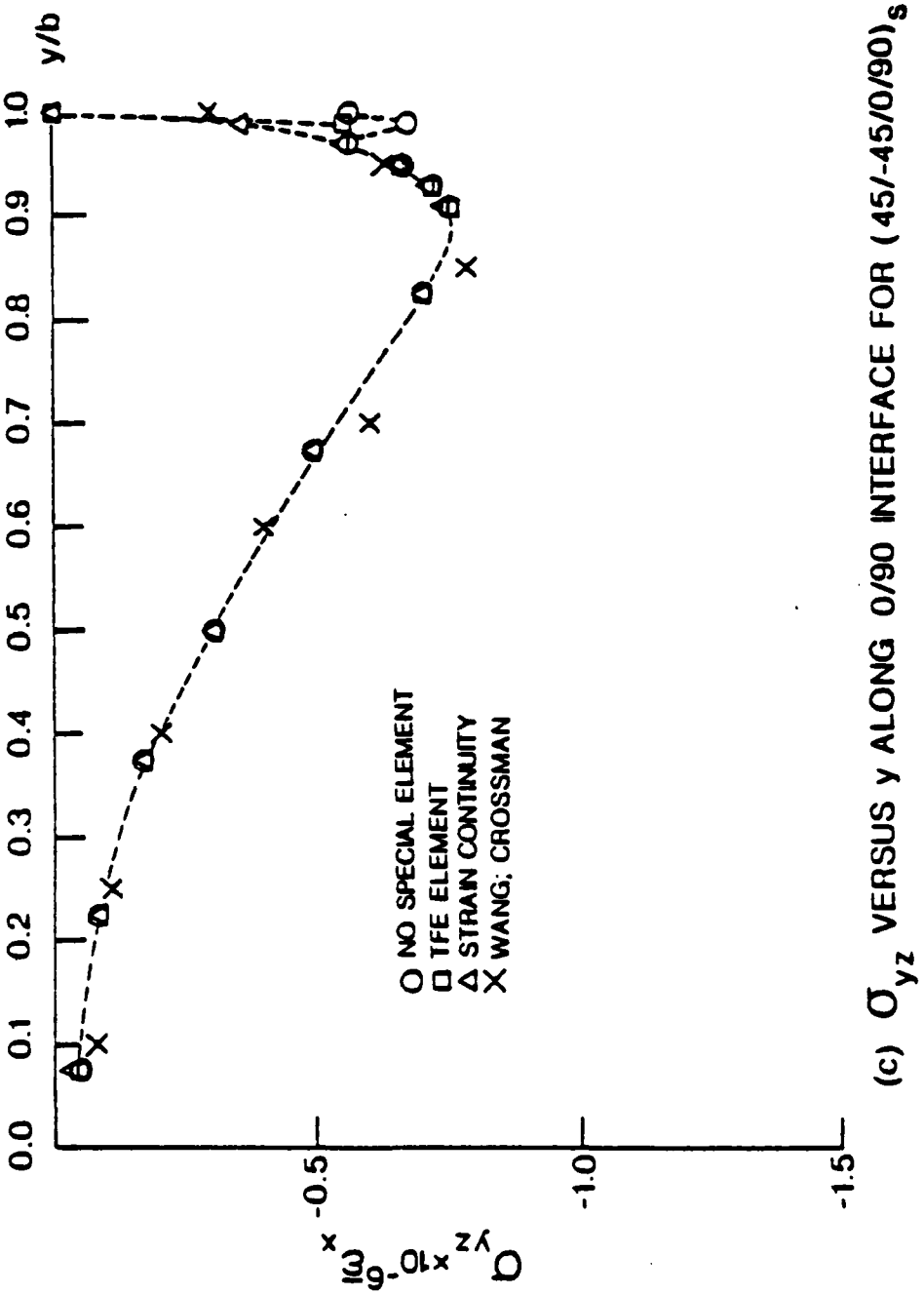

(c) σ_{yz} VERSUS y ALONG 0/90 INTERFACE FOR $(45/-45/0/90)_s$

Fig. 11 (Continued)

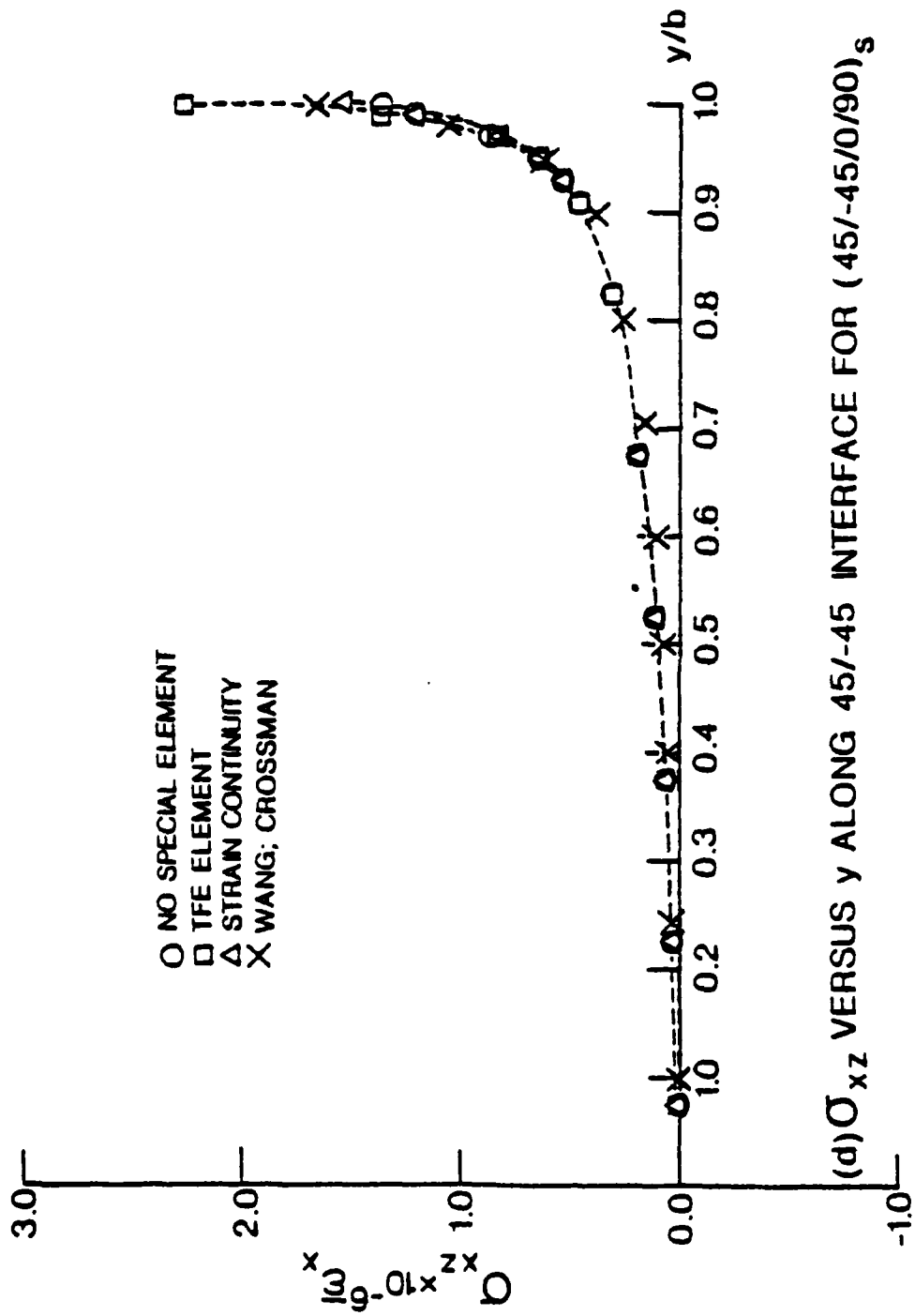

Fig. 11 (Continued)

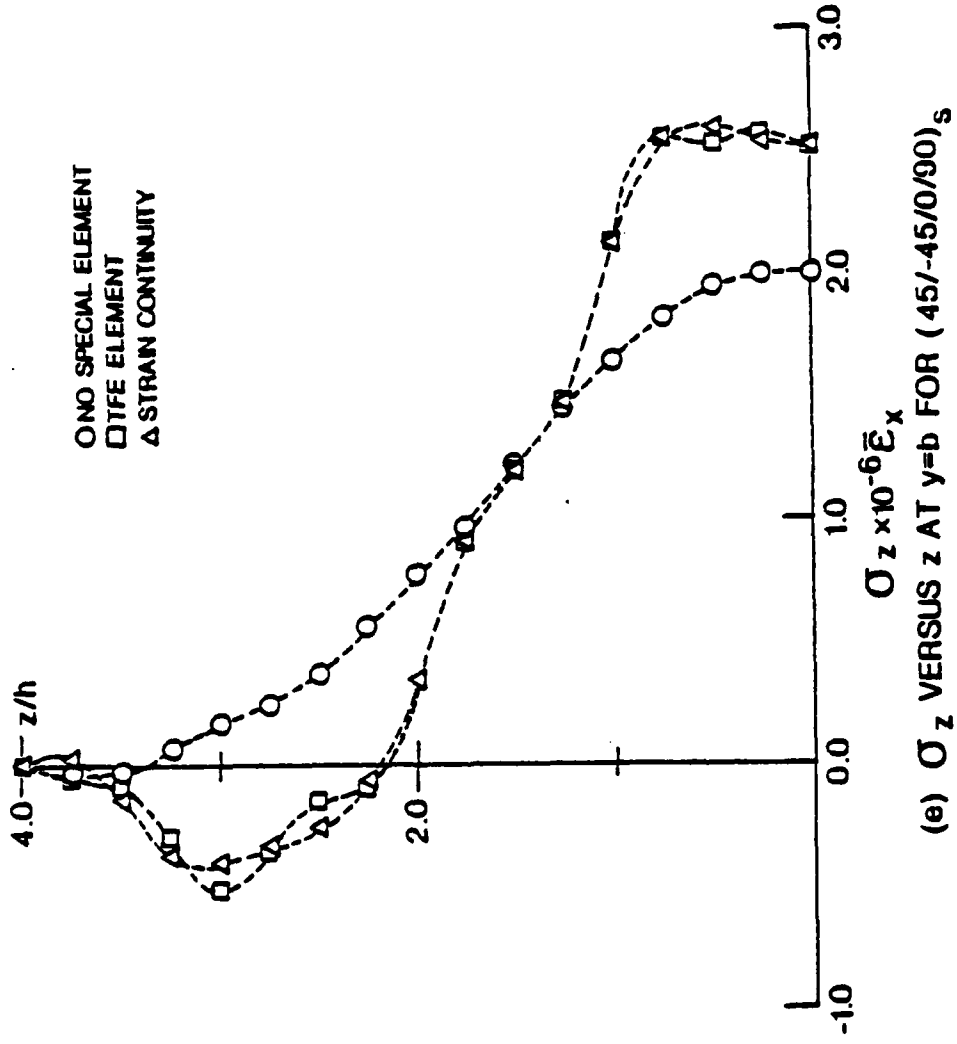

(e) σ_z VERSUS z AT y=b FOR $(45/-45/0/90)_s$

Fig. 11 (Continued)

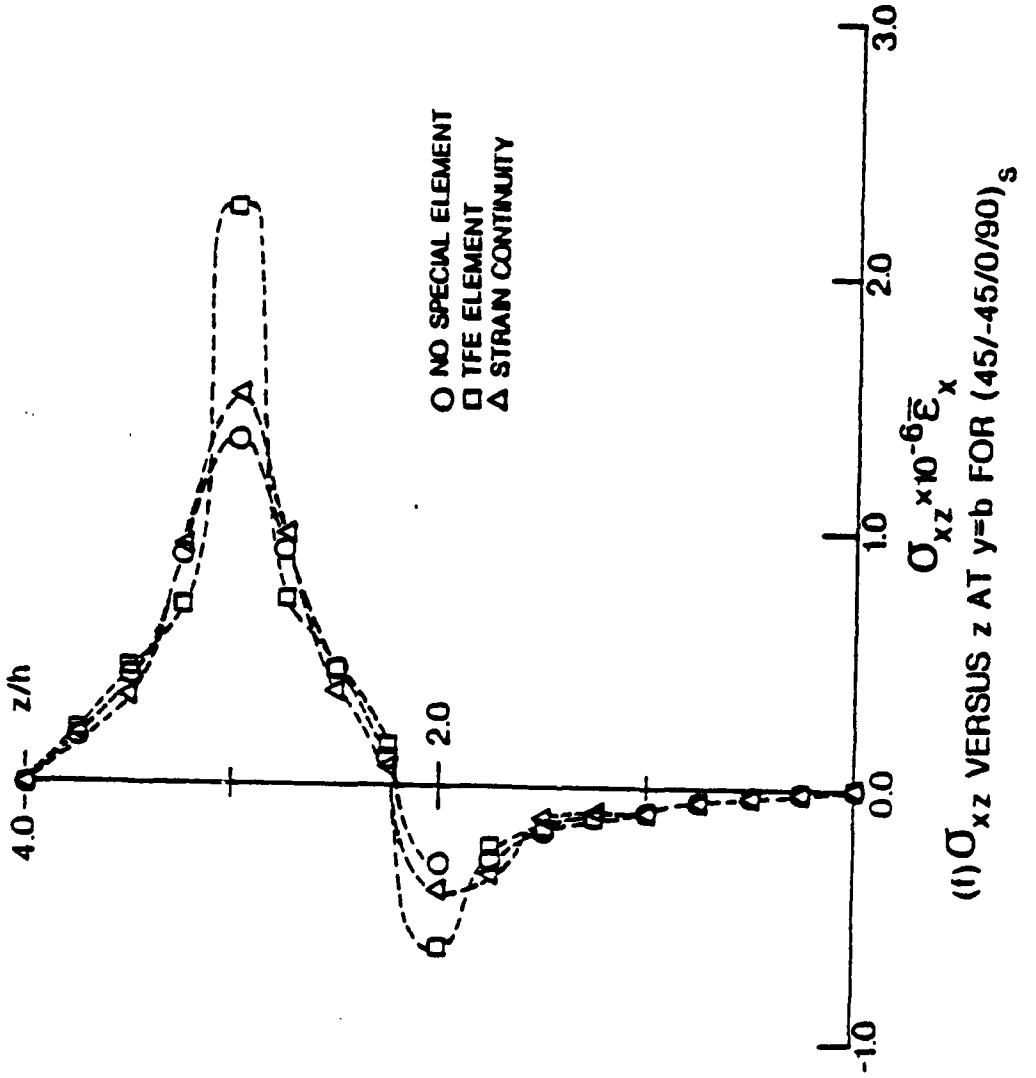

Fig. 11 (Concluded)

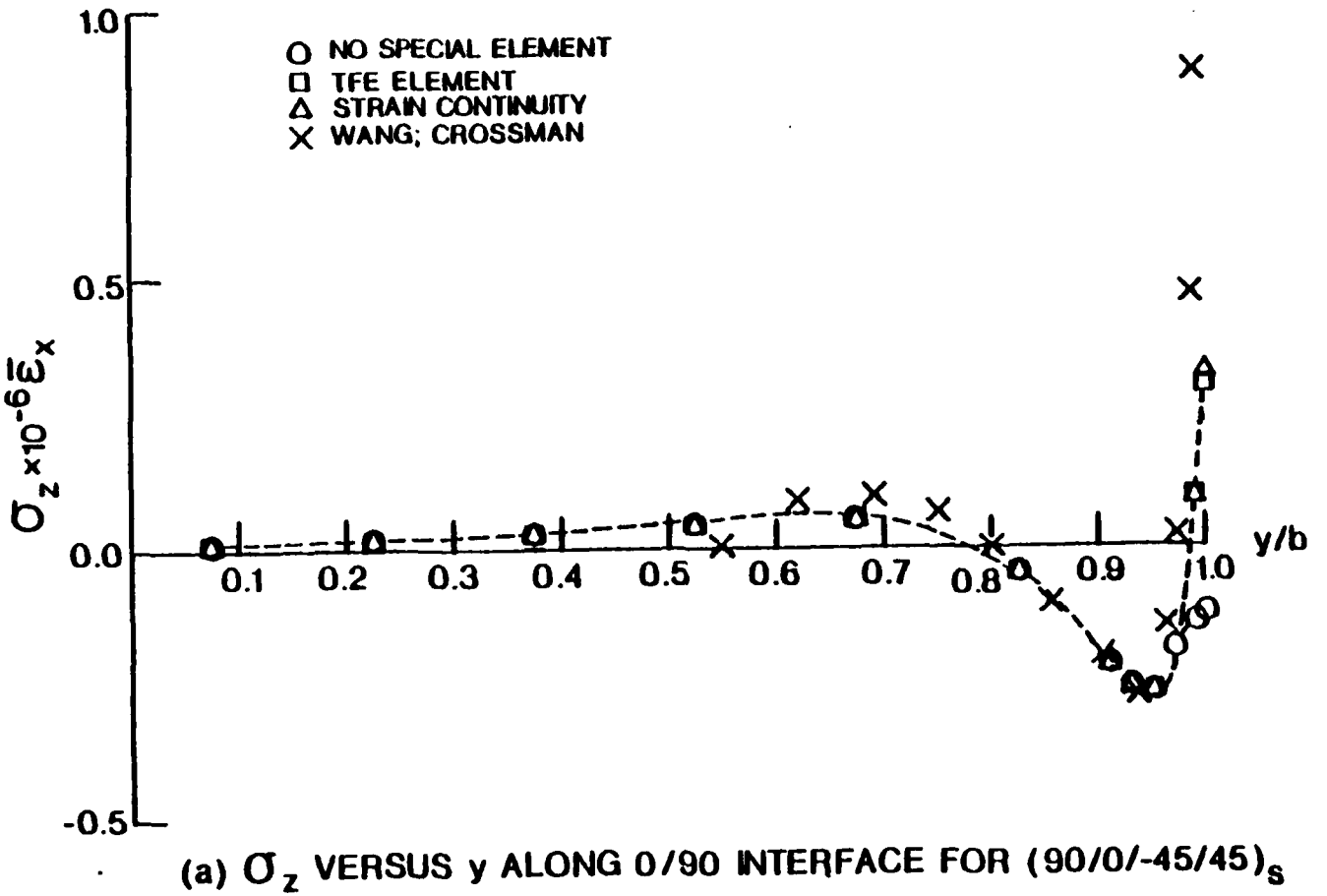

(a) σ_z VERSUS y ALONG 0/90 INTERFACE FOR $(90/0/-45/45)_s$

Fig. 12 Stress results for $[90/0/-45/45]_s$ laminate

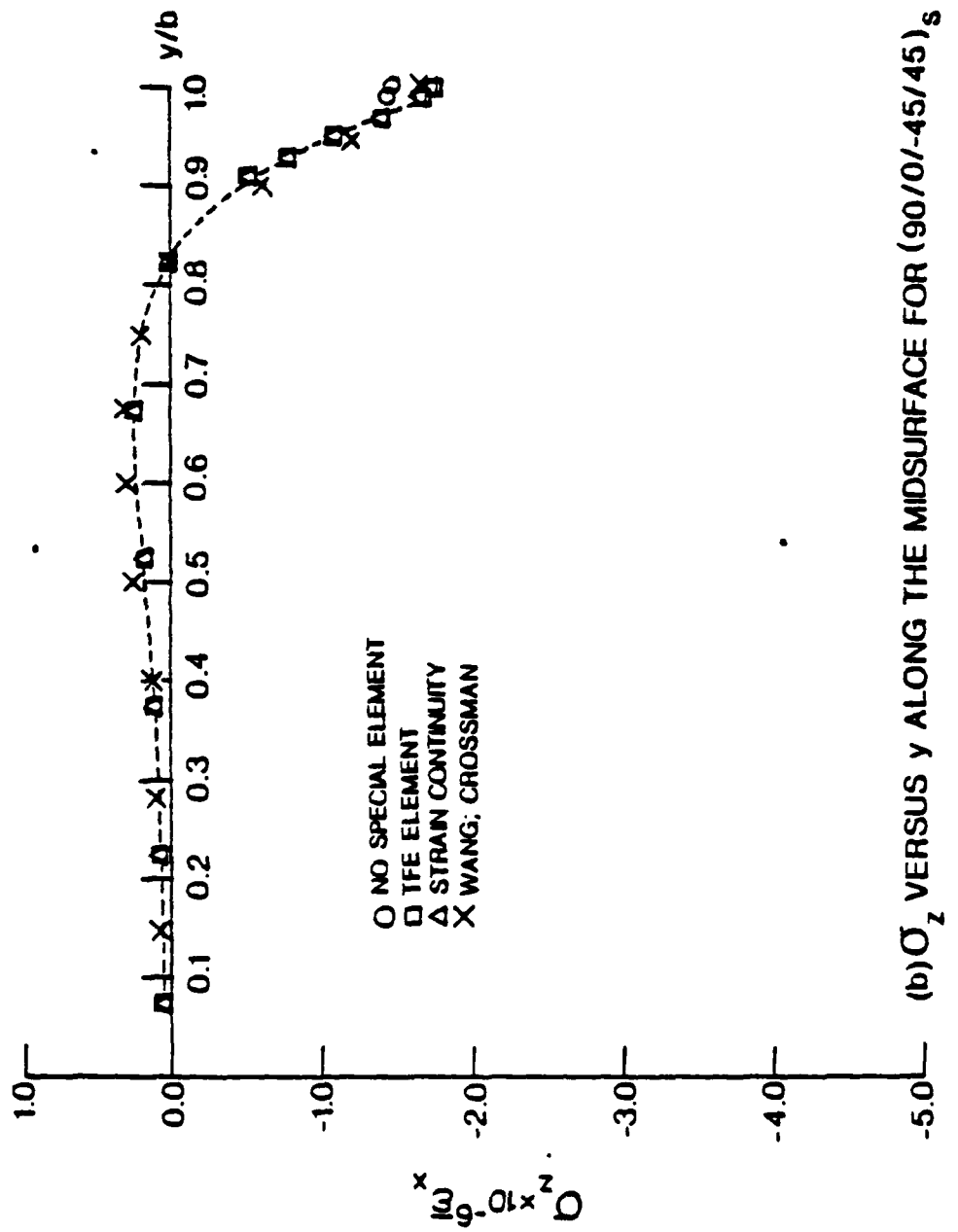

Fig. 12 (Continued)

for σ_z along the 0/90 interface while the TFE and SC analysis rise to positive values. Along the midsurface, the TFE and SC approaches reach larger negative values than the NSE anlaysis at the free edge.

Distributions of σ_z and σ_{xz} through the thickness at the traction free edge for the $[90/0/-45/45]_s$ case are shown in Figures 12c and 12d. The NSE analysis again shows smaller values throughout the laminate for σ_z. Just as in the $[45/-45/0/90]_s$ case it does not show the more definite peaks which are found in the distributions for the TFE and SC approaches. The results for the TFE and SC analysis show that σ_z is compressive throughout the first three layers and becomes tensile in the 90^o layer. The NSE analysis remains compressive up to the top of the 90^o layer, but its value remains small. The distribution for σ_{xz} demonstrates the same behavior as that of the $[45/-45/0/90]_s$ case between the three approaches. Large negative values, again for which the TFE analysis shows the largest occur at the 45/-45 interface. The TFE approach also shows the largest positive value at the 0/-45 interface where all three approaches reach the maximum positive value through the thickness.

The differences in results observed between the $[45/-45/0/90]_s$ and the $[90/0/-45/45]_s$ laminates are best illustrated by considering the through thickness distributions of σ_{xz} and σ_z. The laminate stacking sequence where the 90^o layer is on the outside shows predominantly compressive behavior and the most significant peaks in stress are compressive. The stacking sequence where the 90^o layer is on the inside, however, shows predominently tensile stresses and all significant peaks are tensile. These are very important observations considering that the interlaminar stresses near the free edge are believed to be the cause of delamination in these types of laminates.

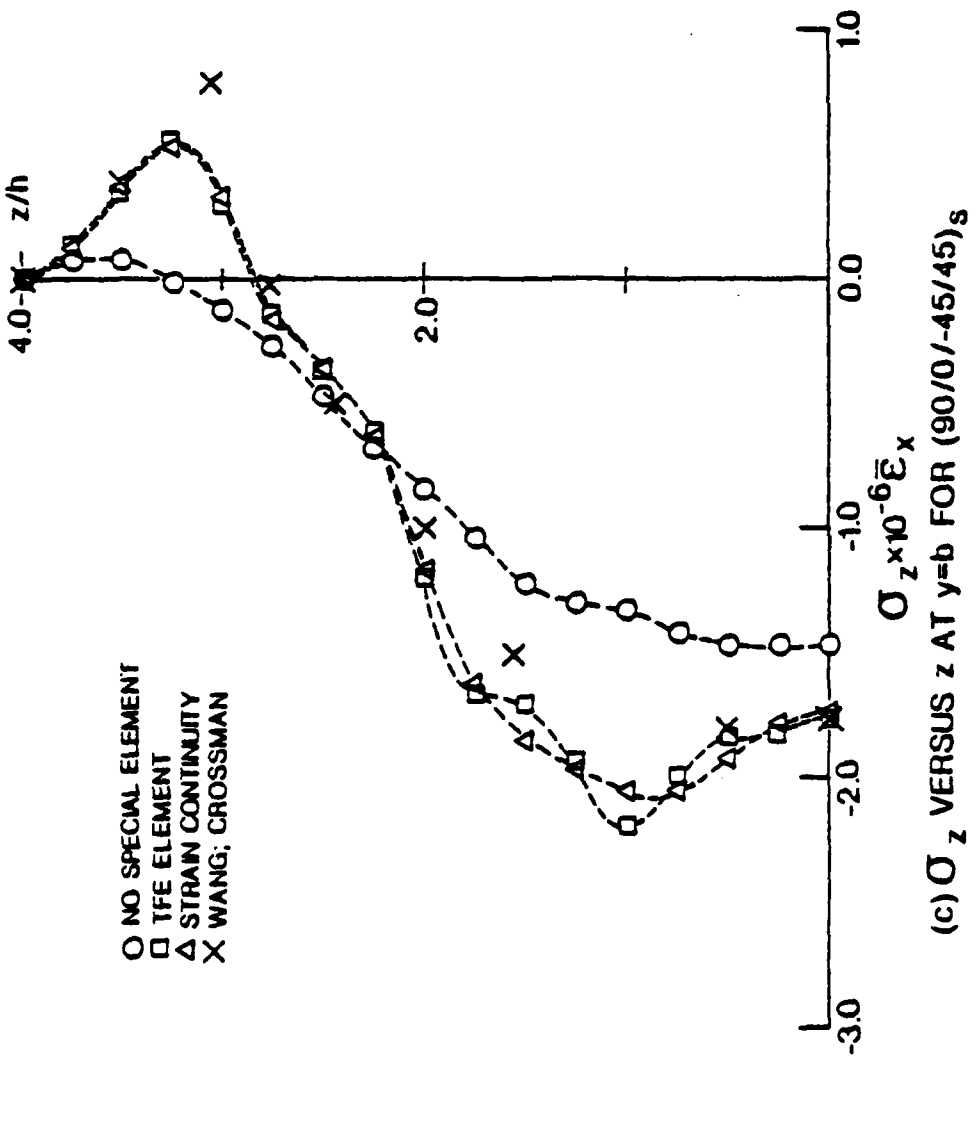

(c) σ_z VERSUS z AT y=b FOR $(90/0/-45/45)_s$

Fig. 12 (Continued)

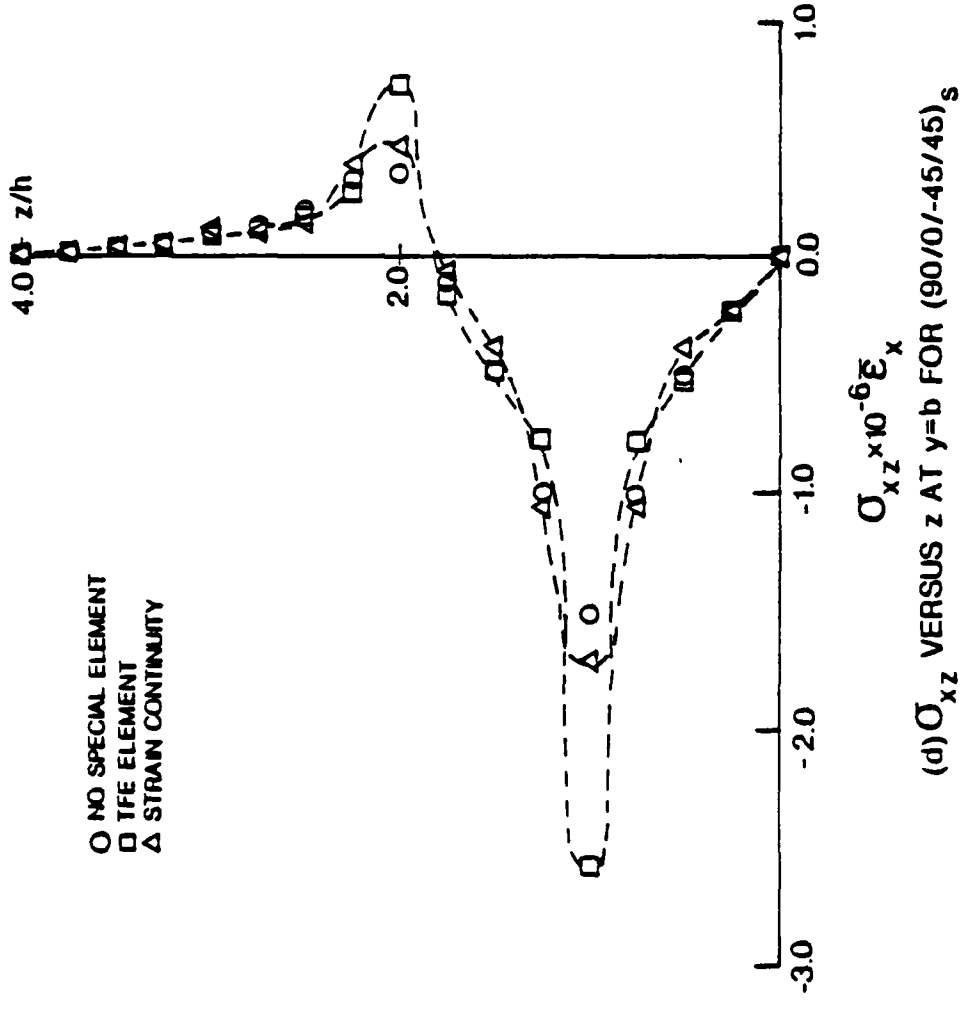

(d) σ_{xz} VERSUS z AT y=b FOR $(90/0/-45/45)_s$

Fig. 12 (Concluded)

4. Summary and Concluding Remarks

An assumed stress hybrid formulation has been presented for the problem of composite laminates under uniform inplane strain. A special purpose multilayer element has been developed which satisfies various stress and strain conditions exactly. The multilayer element has been used in conjunction with three basic approaches to the problem; 1) NSE: a mesh of so called standard elements which satisfy continuity of interlaminar stresses across interlayer boundaries and traction free edge conditions along the top and bottom of the laminate are used thoughout the mesh, 2) TFE: the first element in the mesh is modified to satisfy the traction free edge condition while the remainder of the mesh consists of the standard element, and 3) SC: the standard element is modified to satisfy continuity of inplane strain along interlayer boundaries and the entire mesh is comprised of these elements.

Stress results for five laminate test cases, $[90/0]_s$, $[0/90]_s$, $[45/-45]_s$, $[90/0/-45/45]_s$ and $[45/-45/0/90]_s$, have been presented and discussed. Basically the three approaches show consistent results, The stress contributions which are forced to zero in the TFE analysis in most cases also tend toward zero in the NSE and SC analysis even though they have not been forced to zero. Exceptions to this are σ_y (0° layer) for the $[0/90]_s$, $[90/0]_s$ laminates and σ_{xy} for the $[45/-45]_s$ laminate. In general, the TFE analysis displays the most severe distributions, exhibiting the highest peaks in both the negative and positive directions. The NSE approach behaves well except in the analysis of the $[90/0/45/-45]_s$ and $[45/-45/0/90]_s$ laminates where the results for the NSE approach drop off at the traction free edge and therefore do not agree with the TFE and SC approaches. Looking at the through thickness plots of σ_z and σ_{xz} along the traction free edge, also for the $[90/0/45/-45]_s$ and $[45/-45/0/90]_s$ laminates, it is apparent that the peaks in stress exhibited by the TFE and SC approaches are smoothed out by the NSE anlaysis. This

suggests that in the analysis of more complicated laminate stacking sequences, some special conditions must be exactly satisfied in order to obtain conclusive stress distributions.

Some general observations can also be made concerning the differences between laminate stacking sequences. It is observed when the 90° layer is on the outside (i.e., both for $[90/0]_s$ and $[90/0/45/-45]_s$ laminates) the through thickness distributions for σ_z and σ_{xz} (for the angle-ply only) show predominantly compressive stress values. Conversely, when the 90° layer is on the inside the distributions for these stresses are predominantly tensile. This suggests that a laminate stacking sequence with a 90° layer on the outside will be less likely to delaminate under an inplane tensile load than one which has a 90° layer on the inside.

Three approaches have been used to solve the problem of composite laminates under uniform inplane strain. All three analysis show basically the same results. Observed differences do occur in the vicinity of the free edge. It is not possible at this time to claim that one or the other of the analysis provides the correct detailed stress distributions for the problem in question. Conclusions of this nature must await an independent analytical solution to the problem which, thus far, does not exist.

5. References

1. R. M. Jones, Mechanics of Composite Materials, McGraw-Hill, New York, 1975.

2. R. B. Pipes and N. J. Pagano, "Interlaminar Stresses in Composite Laminates under Uniform Axial Extension," Journal of Composite Materials, Vol. 4 (1970), p. 538.

3. N. J. Pagano, "On the Calculation of Interlaminar Normal Stress in Composite Laminates," Journal of Composite Materials, Vol. 8 (1974), p. 65.

4. A. S. D. Wang and F. W. Crossman, "Some New Results on Edge Effect in Symmetric Composite Laminates," Journal of Composite Materials, Vol. 11 (1977), p. 92.

5. J. T. S. Wang and J. N. Dickson, "Interlaminar Stresses in Symmetric Composite Laminates," Journal of Composite Materials, Vol. 12 (1978), p. 390.

6. A. Harris, O. Orringer and E. A. Witmer, "A Multilayer, Traction-Free Edge, Quadrilateral Warping Element for the Stress Analysis of Composite Plates and Shells," MIT-ASRL-TR-193-1, AMMRC TR 79-26 (1979).

7. C. T. Herakonich, A. Nagorkar and D. A. O'Brien, "Failure Analysis of Composite Laminates With Free Edges," Modern Developments in Composite Materials and Structures, Winter ASME Mtg, 1979, p. 53.

8. R. L. Spilker, "A Hybrid Stress Finite-Element Formulation for Thick Multilayer Laminates," Computers and Structures, Vol. 11 (1980), pp. 507-514.

9. R. L. Spilker, "A Traction-Free-Edge Hybrid-Stress Element for the Analysis of Edge Effects in Cross-Ply Laminates," Computers and Structures, Vol. 12 (1980), pp. 167-179.

R. M. Christensen, Mechanics of Composite Materials, John Wiley and Sons, New York, 1979.

11. S. S. Wang, Department of Theoretical and Applied Mechanics, University of Illinois at Champaign-Urbana (private communications).

CHAPTER 3

A STUDY OF 8-NODE SINGLE LAYER PLATE ELEMENTS WITH A STRAIGHT TRACTION-FREE EDGE

ABSTRACT

The elements developed and tested in the last chapter were based on a plane 2-D theory. For general multilayer plate problems involving free edges, a multilayer plate element is required which satisfies the traction-free conditions along one of its edges. The present chapter describes a study which is needed to establish the basis for development of such a multilayer element. Here eight-node single layer pure bending plate elements are developed for which the traction-free conditions are exactly satisfied along one straight edge. Transverse shear deformation and transverse shear and normal stresses are included so that the elements are applicable to both thin and moderately-thick single layer plates. Various plausible stress fields are defined, and the best stress field (element) is identified by comparison of results for selected example problems. The results obtained in the computationally efficient pure bending study can then guide the development of a multilayer element, where stresses and displacements are assumed independent within each layer. In such an element, the present stress/displacement fields must be extended to include stretching contributions.

1. Introduction

In the analysis of multi-layer, laminated, composite plate structures, it has been observed [1,2] that near the traction-free edges of such structures severe gradients in the interlaminar stresses may exist. These gradients can lead to delamination as well as other forms of laminate failure. Therefore, it is necessary that accurate representation of the stress fields near traction-free edges be obtained. In employing the finite element method to solve this class of problems, accurate analysis in the vicinity of traction-free edges appears to require the developement of a special purpose, multi-layer, plate element which exactly satisfies the traction-free conditions along at least one edge. (i.e. normal and shear stresses are zero along one edge of the element.)

Historically, plate elements have been based on the assumed-displacement formulation. In this approach, displacement boundary conditions are exactly satisfied while stress conditions are satisfied only in an approximate (weighted, integral) sense. Alternatively, in the assumed-stress hybrid formulation both stress and displacement boundary conditions can be satisfied exactly. The hybrid-stress model is a two-field principle in which equilibriating intraelement stress fields and compatible displacement fields are assumed independently. The stress parameters are eliminated on the element level and a conventional stiffness matrix results [3]. In view of the independent assumption of stresses within each element, it is possible to exactly satisfy traction-free conditions by appropriate choice of the stresse fields. This feature establishes the assumed-stress hybrid formulation as a viable approach for developing such special purpose elements. In many cases [4,5],,hybrid-stress elements have been found to yield improved convergence and intraelement stress predictions in comparison with analagous assumed-displacment elements.

The hybrid-stress model is also well suited to the development of multi-layer, laminated, composite, plate elements. Stresses and displacements may be assumed in-

dependently within each layer and appropriate interlayer displacment and stress continuity conditions satisfied exactly [6,7]. Such elements have been shown to be applicable for up to moderately thick laminates [8]. Transverse shear effects can also be included in a less general manner (i.e. on the laminate level [9]). These hybrid-stress elements have been found to be more accurate than comparable assumed-displacment elements [10,11].

Based on these observations, the hybrid-stress model appears to be the ideal choice for the development of a special purpose, multi-layer, traction-free edge, plate element. However, before this element can be developed, it is necessary to examine the possible stress fields assumed in the element interior which satisfy the traction-free conditions along an edge. This is best accomplished by first considering single-layer, isotropic, plate elements. Once the best stress fields are identified for single-layer plates; the results can then be extended to multi-layer plates.

In general, the elements cited earlier in this discussion have been based on 4-node bilinear displacement fields. But, in a recent series of articles [12,13,14] a family of single-layer, isotropic, plate elements based on the hybrid-stress model have been developed and tested. These elements use displacement distributions based on Mindlin plate theory [15] and include all components of stress. Their advantage over analagous assumed-displacement elements is that the element stiffness matrix exhibits correct rank and accurate solutions can be obtained for arbitrarily thin to moderately thick plates. That is, difficulties regarding excessive stiffening (i.e. locking) observed in Mindlin-type assumed-displacment elements are avoided in the hybrid-stress elements. Similar advantages should be expected if multi-layer versions of these elements are developed for the analysis of laminated, composite plates.

In the present study a single-layer, isotropic plate element is developed for which traction-free conditions are exactly satisfied along one edge. After choosing an appropriate displacement field, various plausible intraelement stress fields are de-

fined. The resulting special purpose elements are coupled with the compatible standard element to perform the analysis of several plate problems which include a traction-free edge. The performance of the special purpose elements is evaluated and their potential value is assessed for the development of a special purpose, multilayer, plate element.

2. Formulation, Displacement and Stress Interpolations

A. Basic Equations

To establish a basis for the present work, the assumed-stress hybrid formulation for plate [12] will be summarized here. The hybrid-stress functional can be written as:

$$\Pi_{mc} = \sum_{n} \left\{ \tfrac{1}{2} \int_{V_n} \underset{\sim}{\sigma}^T \underset{\sim}{S} \underset{\sim}{\sigma} dV - \int_{V_n} \underset{\sim}{\sigma}^T \hat{\underset{\sim}{\varepsilon}} dV + \int_{S_{\sigma_n}} \underset{\sim}{u}^T \bar{\underset{\sim}{T}} \, ds \right\} \tag{1}$$

where:

$\underset{\sim}{\sigma}$	. . . .	stress vector
$\hat{\underset{\sim}{\varepsilon}}$	. . . .	strain vector calculated from displacements, $\underset{\sim}{u}$.
$\underset{\sim}{u}$	. . . .	displacement vector
$\bar{\underset{\sim}{T}}$	. . . .	prescribed tractions
$\underset{\sim}{S}$	. . . .	material property matrix
V_n	. . . .	volume of the nth element
S_{σ_n}	. . . .	boundary of the nth element over which tractions prescribed

Based on Mindlin plate theory [15], the through-thickness displacement distributions are assumed in the form (*pure bending only*):

$$\begin{aligned} u(x,y,z) &= z\theta_y(x,y) \\ v(x,y,z) &= -z\theta_x(x,y) \\ w(x,y,z) &= w(x,y) \end{aligned} \tag{2}$$

where positive sign conventions for displacements and rotations are shown in Figure 1.

From (2), the generalized displacements $\theta_y(x,y)$, $\theta_x(x,y)$, and $w(x,y)$ can be expressed in terms of a set of nodal degrees of freedom θ_{yi}, θ_{xi}, and w_i by constructing a set of C^o continuous shape functions to use as displacement interpolations. Applying the linear strain-displacement relations yields:

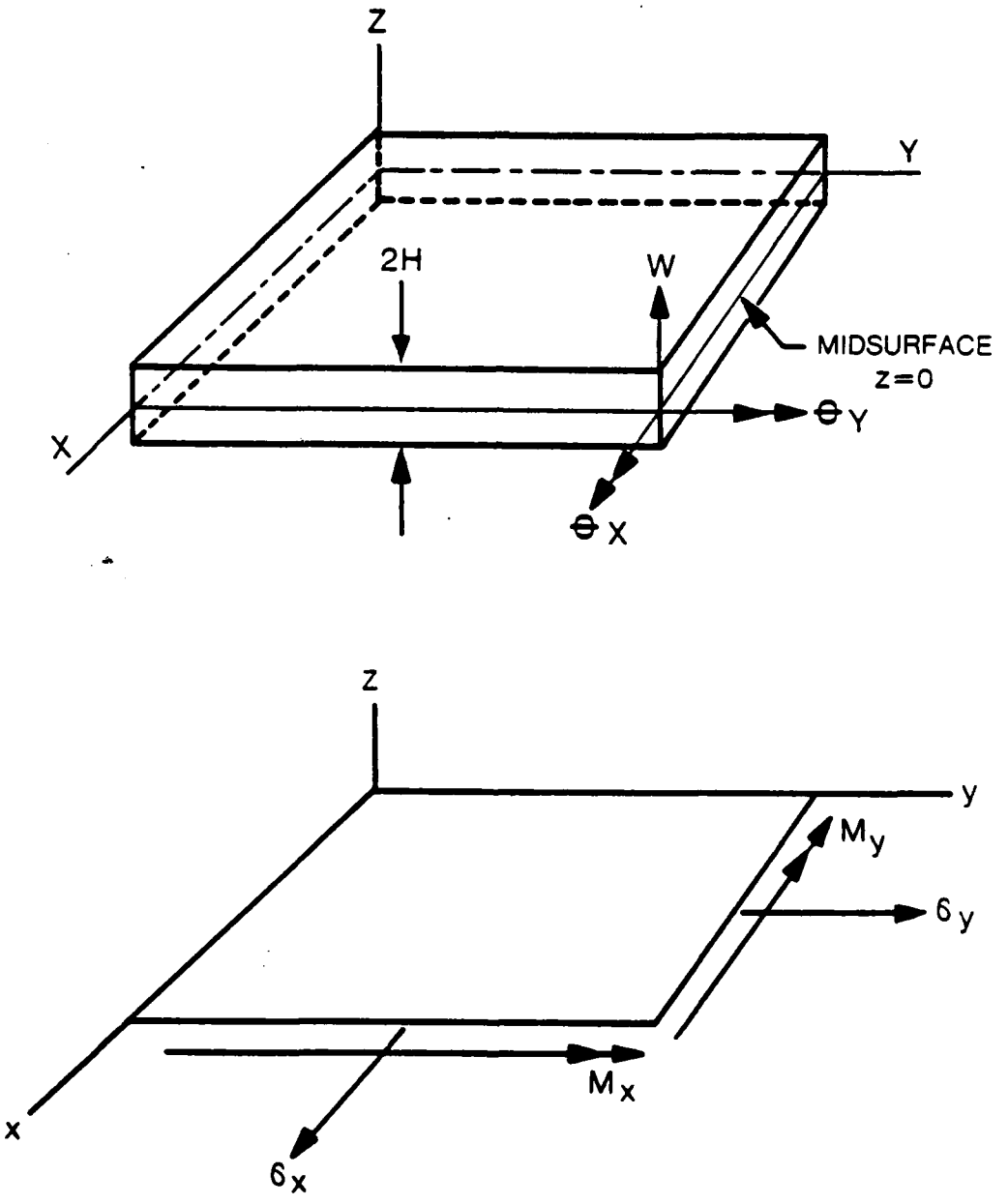

Figure 1. Orientation and Sign Convention for Plates

$$\hat{\underline{\varepsilon}} = \begin{Bmatrix} \hat{\underline{\varepsilon}}_f \\ \hat{\underline{\varepsilon}}_s \end{Bmatrix} = \begin{bmatrix} -\frac{\partial \theta_y}{\partial x} \\ -\frac{\partial \theta_x}{\partial y} \\ 0 \\ \frac{\partial \theta_y}{\partial y} - \frac{\partial \theta_x}{\partial x} \\ \hline \frac{\partial w}{\partial x} + \theta_y \\ \frac{\partial w}{\partial y} - \theta_x \end{bmatrix} = \begin{bmatrix} \underline{B}_f \\ \hline \underline{B}_s \end{bmatrix} \underline{q} = \underline{B}\underline{q} \qquad (3)$$

where $\underline{q}$ is the vector of nodal degrees of freedom for an element, and the subscripts "f" and "s" refer, respectively, to flexural and transverse shear contributions.

The stresses are expressed polynomial form in terms of a set of stress parameters, $\underline{\beta}$. The stress assumption is required to satisfy the 3-D homogenious equilibrium equations. Moreover, for a plate loaded transversely at z=h (see Figure 1) the free-surface conditions can be expressed as:

$$\begin{aligned} \sigma_{xz}(x,y,\pm h) &= 0 \\ \sigma_{yz}(x,y,\pm h) &= 0 \\ \sigma_z(x,y,-h) &= 0 \end{aligned} \qquad (4)$$

Based on the equilibrium equations and the free-surface conditions of (4), the through-thickness distribution of stresses is assumed in the form (corresponding to pure bending contributions only):

$$\begin{aligned} \sigma_x &= z\bar{\sigma}_x(x,y) \\ \sigma_y &= z\bar{\sigma}_y(x,y) \\ \sigma_{xy} &= z\bar{\sigma}_{xy}(x,y) \\ \sigma_{xz} &= \left(\frac{h^2-z^2}{2}\right)\left[\frac{\partial \bar{\sigma}_x}{\partial x} + \frac{\partial \bar{\sigma}_{xy}}{\partial y}\right] = \left(\frac{h^2-z^2}{2}\right)\bar{\sigma}_{xz}(x,y) \\ \sigma_{yz} &= \left(\frac{h^2-z^2}{2}\right)\left[\frac{\partial \bar{\sigma}_{xy}}{\partial x} + \frac{\partial \bar{\sigma}_y}{\partial y}\right] = \left(\frac{h^2-z^2}{2}\right)\bar{\sigma}_{yz}(x,y) \\ \sigma_z &= 1/6(z^3-3h^2z-2h^3)\left[\frac{\partial \bar{\sigma}_{xz}}{\partial x} + \frac{\partial \bar{\sigma}_{yz}}{\partial y}\right] = 1/6(z^3-3h^2z-2h^3)\bar{\sigma}_z(x,y). \end{aligned} \qquad (5)$$

From (5), it is observed that first the polynomials for $\bar{\sigma}_x$, $\bar{\sigma}_y$, $\bar{\sigma}_{xy}$ are defined,

after which $\bar{\sigma}_{xz}$, $\bar{\sigma}_{yz}$, $\bar{\sigma}_z$ are calculated from the last half of (5). Note that this guarantees satisfaction of the 3-D homogeneous equilibrium equations. The stress assumption can then be cast in the form:

$$\underset{\sim}{\bar{\sigma}} = \begin{Bmatrix} \underset{\sim}{\bar{\sigma}_f} \\ \hline \underset{\sim}{\bar{\sigma}_s} \end{Bmatrix} = \begin{bmatrix} \bar{\sigma}_x \\ \bar{\sigma}_y \\ \bar{\sigma}_z \\ \bar{\sigma}_{xy} \\ \hline \bar{\sigma}_{xz} \\ \bar{\sigma}_{yz} \end{bmatrix} = \begin{bmatrix} \underset{\sim}{\bar{P}_f} \\ \hline \underset{\sim}{\bar{P}_s} \end{bmatrix} \underset{\sim}{\beta} = \underset{\sim}{\bar{P}} \underset{\sim}{\beta} \tag{6}$$

Substituting (3) and (6) into (1) and manipulating the result (described in detail in [12]) yields the stiffness matrix for the plate element:

$$\underset{\sim}{k} = \left(\frac{2h^3}{3}\right)\left(\underset{\sim}{G}_f + \underset{\sim}{G}_s\right)^T \left(\underset{\sim}{H}_f + \frac{2h^2}{5}\underset{\sim}{H}_s\right)^{-1}\left(\underset{\sim}{G}_f + \underset{\sim}{G}_s\right) \tag{7}$$

where:

$$\underset{\sim}{G}_f = \int_{A_n} \underset{\sim}{\bar{P}}_f^T \underset{\sim}{B}_f \, dA \qquad \underset{\sim}{H}_f = \int_{A_n} \underset{\sim}{\bar{P}}_f^T \underset{\sim}{\bar{S}}_f \underset{\sim}{\bar{P}}_f \, dA$$

$$\underset{\sim}{G}_s = \int_{A_n} \underset{\sim}{\bar{P}}_s^T \underset{\sim}{B}_s \, dA \qquad \underset{\sim}{H}_s = \frac{2(1+\nu)}{E} \int_{A_n} \underset{\sim}{\bar{P}}_s^T \underset{\sim}{\bar{P}}_s \, dA \tag{8}$$

$$\underset{\sim}{\bar{S}}_f = 1/E \begin{bmatrix} 1 & -\nu & \nu\frac{2h^2}{5} & 0 \\ -\nu & 1 & \nu\frac{2h^2}{5} & 0 \\ \nu\frac{2h^2}{5} & \nu\frac{2h^2}{5} & \frac{52}{105}h^4 & 0 \\ 0 & 0 & 0 & 2(1+\nu) \end{bmatrix} \tag{9}$$

and A_n is the area of the midsurface of the nth element.

To implement this numerically, it is common practice to combine the flexural and transverse shear parts such that: $\underset{\sim}{G} = \underset{\sim}{G}_f + \underset{\sim}{G}_s$

$$\underset{\sim}{H} = \frac{2h^3}{3}\left(\underset{\sim}{H}_f + \frac{2h^2}{5}\underset{\sim}{H}_s\right) \tag{10}$$

where:

$$\underline{G} = \int_{A_n} \overline{\underline{P}}^T \underline{B}\, dA \tag{11a}$$

$$\underline{H} = \int_{A_n} \overline{\underline{P}}^T \overline{\underline{S}}\, \overline{\underline{P}}\, dA \tag{11b}$$

Then, the stiffness matrix is simply:

$$\underline{k} = \underline{G}^T \underline{H}^{-1} \underline{G} \tag{12}$$

The integrals in (11) are mapped from the x-y plane into the ξ-η plane and numerically integrated by Gauss quadrature.

With this information as a basis, we will next look into the formulation of the displacement interpolation ($\hat{\underline{\epsilon}} = \underline{B}\underline{q}$) and the stress assumption ($\overline{\sigma} = \overline{\underline{P}}\underline{\beta}$) necessary to yield a single-layer, traction-free edge, plate element.

B. Displacement Interpolation

In the work presented in references [12,13,14], a family of isoparametric plate elements based on the assumed-stress hybrid formulation and using the Serendipity family of displacement interpolations was developed and tested. Comparison of the elements in the family shows the 8-node and 12-node elements to be more accurate per degree of freedom than the 4-node element [14]. However, 12-node elements are generally perceived as too complex for practical applications and in applications such as nonlinear analysis where computation time is strongly dependent on element-level operations. In light of this, the 8-node element (element QH1 [13]) was chosen to interface with the special purpose element.

In order to insure that displacements are continuous between elements, the displacement interpolation of the special purpose element must be identical to the displacement interpolation of the 8-node element; that is, the quadratic, Serendipity shape functions. In the ξ-η plane, they are in the form:

$$\hat{w}(\xi,\eta) = \sum_{i=1}^{8} N_i(\xi,\eta) w_i \tag{13}$$

$$\theta_x(\xi,\eta) = \sum_{i=1}^{8} N_i(\xi,\eta)\theta_{x_i}$$

$$\theta_y(\xi,\eta) = \sum_{i=1}^{8} N_i(\xi,\eta)\theta_{y_i}$$

where N_i are the shape functions and θ_{yi}, θ_{xi}, w_i are the degrees of freedom (generalized displacements) at node i.

For isoparametric elements, the coordinate mapping is of the same form as (13) (i.e. quadratic); but, for the special purpose element, only bilinear mapping is allowed. This permits it to take on a general, quadrilateral shape, but insures that its sides remain straight. (This is a requirement of the stress assumption, and will be explained shortly). So, the mapping is given by the bilinear shape functions:

$$x = \sum_{i=1}^{4} N_i(\xi,\eta)x_i$$

$$y = \sum_{i=1}^{4} N_i(\xi,\eta)y_i \qquad (14)$$

where (x_i, y_i) are the coordinates of node i.

Recasting (3) into the ξ-η plane results in:

$$\hat{\underset{\sim}{\varepsilon}} = \frac{1}{|J|} \begin{bmatrix} 0 & 0 & \left(\frac{\partial y}{\partial \eta}\frac{\partial}{\partial \xi} - \frac{\partial y}{\partial \xi}\frac{\partial}{\partial \eta}\right) \\ 0 & -\left(\frac{\partial x}{\partial \xi}\frac{\partial}{\partial \eta} - \frac{\partial x}{\partial \eta}\frac{\partial}{\partial \xi}\right) & 0 \\ 0 & 0 & 0 \\ 0 & -\left(\frac{\partial v}{\partial \eta}\frac{\partial}{\partial \xi} - \frac{\partial v}{\partial \xi}\frac{\partial}{\partial \eta}\right) & \left(\frac{\partial x}{\partial \xi}\frac{\partial}{\partial \eta} - \frac{\partial x}{\partial \eta}\frac{\partial}{\partial \xi}\right) \\ \hline \left(\frac{\partial y}{\partial \eta}\frac{\partial}{\partial \xi} - \frac{\partial y}{\partial \xi}\frac{\partial}{\partial \eta}\right) & 0 & |J| \\ \left(\frac{\partial x}{\partial \xi}\frac{\partial}{\partial \eta} - \frac{\partial x}{\partial \eta}\frac{\partial}{\partial \xi}\right) & -|J| & 0 \end{bmatrix} \begin{Bmatrix} w(\xi,\eta) \\ \theta_x(\xi,\eta) \\ \theta_y(\xi,\eta) \end{Bmatrix} \qquad (15)$$

where $|J|$ is the Jacobian of the coordinate transformation.

Substituting (13) into (15) yields the $\underline{B}$ matrix ($\hat{\underline{\epsilon}} = \underline{B}\underline{q}$) which is used in the integral of (11a).

C. Stress Assumption

The choice of a stress assumption for the special purpose element is not obvious. In this section, several plausible stress fields are developed. Subsequently, they will be subject to numerical tests in order to identify the better stress fields.

First, consider a rectangular element with sides parallel to the x and y axes as shown in Figure 2a. Letting x=0 be the traction-free edge leads to the requirement that:

$$\begin{aligned} \sigma_x(0,y,z) &= 0 \\ \sigma_{xy}(0,y,z) &= 0 \\ \sigma_{xz}(0,y,z) &= 0 \end{aligned} \tag{16}$$

Since these conditions must hold for all values of z, the relations in (5) can be used to specifically require that:

$$\bar{\sigma}_x(0,y) = 0 \tag{17a}$$

$$\bar{\sigma}_{xy}(0,y) = 0 \tag{17b}$$

$$\bar{\sigma}_{xz}(0,y) = 0 \tag{17c}$$

Notice, that these conditions simply require that $\bar{\sigma}_x$, $\bar{\sigma}_{xy}$, and $\bar{\sigma}_{xz}$ be zero along the line x=0 for all y. For all other x and y the stresses can vary according to the polynomials which represent them in the stress assumption. In fact, for an element of general, quadrilateral shape, it is possible, in a finite-element analysis, to define a local coordinate system for that element such that its traction-free edge is on the line $\bar{x}$=0 (see Figure 2b). Then the conditions of (17) can be applied (replacing x by $\bar{x}$ and y by $\bar{y}$) in the local system and $\underline{k}$ can be formed in that system. Finally, $\underline{k}$ can be transformed into the global system by the standard transformation of displacements [16]. Furthermore, equation (17) requires $\bar{\sigma}_x$, $\bar{\sigma}_{xy}$, and $\bar{\sigma}_{xz}$ to be zero on the line x = 0 ($\bar{x}$=0) which is a straight line. Therefore, the sides of

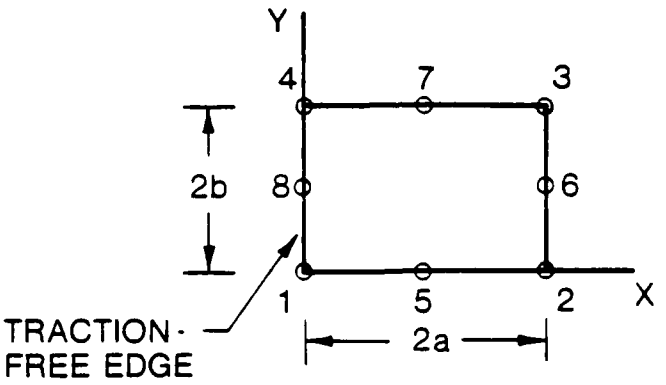

(A)

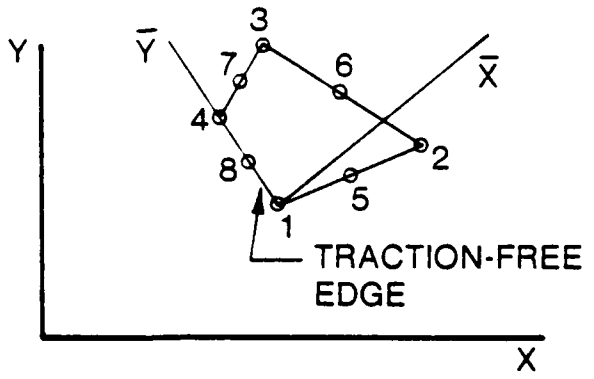

(B)

Figure 2. Typical Traction-Free Edge Plate Elements

the element must remain straight in order for these conditions to apply. This explains why the coordinate mapping was defined to be bilinear: to allow the element to take on a general, quadrilateral shape, but insure that its sides remain straight.

Another criterion which the special purpose element is subject to is: the number of stress parameters, n_β, must be greater than or equal to the number of degrees of freedom, n_q, minus the number of rigid body modes, n_r, i.e.:

$$n_\beta \geq n_q - n_r \tag{18}$$

This relation is a necessary but not sufficient codition to guarantee an element stiffness matrix of correct rank [17].

To summarize, the stress assumption for the special purpose element is defined by first defining the interpolations for $\bar{\sigma}_x$, $\bar{\sigma}_y$, and $\bar{\sigma}_{xy}$ as functions of in-plane coordinates, x and y, such that the conditions specified by (17) and (18) are met. The forms of the remaining stress components, $\bar{\sigma}_{xz}$, $\bar{\sigma}_{yz}$, and $\bar{\sigma}_z$, are then determined from the last three equations of (5). This guarantees that the equilibrium equations and the free-surface conditions of (4) are satisfied exactly.

As a starting point, consider the following stress field:

$$\begin{aligned}
\bar{\sigma}_x &= \beta_1 + \beta_2 x + \beta_3 y + \beta_4 x^2 + \beta_5 xy + \beta_6 y^2 + \beta_7 x^3 + \beta_8 x^2 y + \beta_9 xy^2 + \beta_{10} y^3 + \\
&\quad \beta_{11} x^4 + \beta_{12} x^3 y + \beta_{13} x^2 y^2 + \beta_{14} xy^3 + \beta_{15} y^4 \\
\bar{\sigma}_{xy} &= \beta_{16} + \beta_{17} x + \beta_{18} y + \beta_{19} x^2 + \beta_{20} xy + \beta_{21} y^2 + \beta_{22} x^3 + \beta_{23} x^2 y + \\
&\quad \beta_{24} xy^2 + \beta_{25} y^3 + \beta_{26} x^4 + \beta_{27} x^3 y + \beta_{28} x^2 y^2 + \beta_{29} xy^3 + \beta_{30} y^4 \\
\bar{\sigma}_y &= \beta_{31} + \beta_{32} x + \beta_{33} y + \beta_{34} xy + \beta_{35} x^2 + \beta_{36} y^2 + \beta_{37} xy^2 + \beta_{38} x^2 y
\end{aligned} \tag{19}$$

Note that $\bar{\sigma}_x$ and $\bar{\sigma}_{xy}$ are full quartic polynomials, while $\bar{\sigma}_y$ is identical to that used in element QH1 [13] (a reasonable starting point since $\bar{\sigma}_y$ is not constrained by (17)).

Applying equations (17a), (17b), and (17c) (after calculation of $\bar{\sigma}_{xz}$) yields, re-

AD-A098 683 ILLINOIS UNIV AT CHICAGO CIRCLE DEPT OF MATERIALS ENG--ETC F/G 11/4
STRESS ANALYSIS OF COMPOSITES.(U)
JAN 81 R L SPILKER, T C TING DAAG46-79-C-0045
UNCLASSIFIED ARMRC-TR-81-8 NL

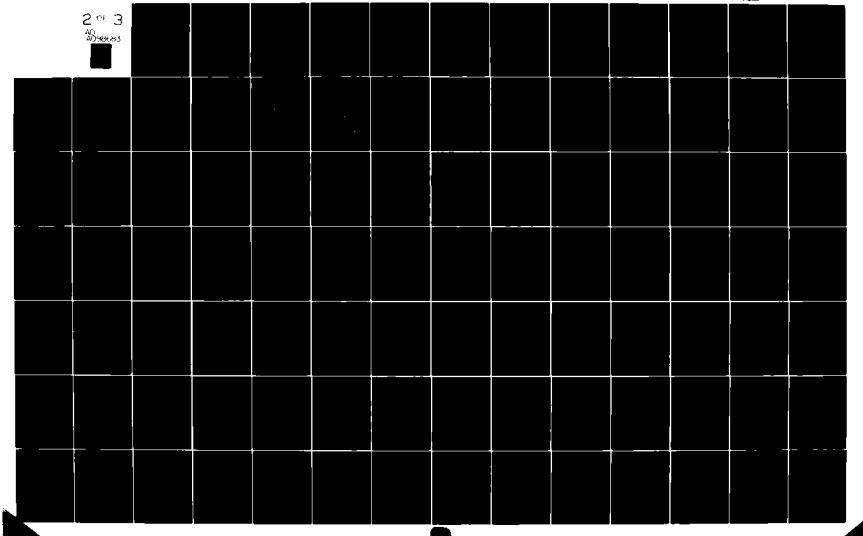

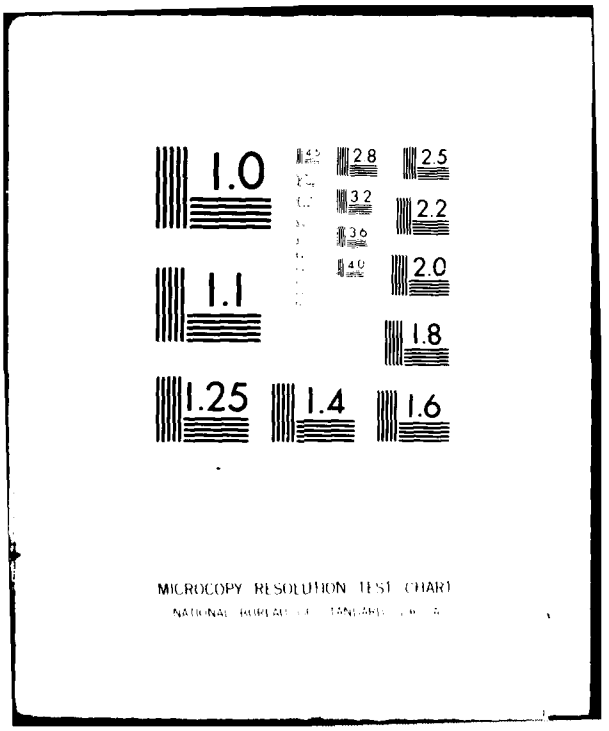
1.0
1.1
1.25
1.4
1.6
1.8
2.0
2.2
2.5
2.8
3.2
3.6
4.0
MICROCOPY RESOLUTION TEST CHART

spectively:

$$\beta_1=\beta_3=\beta_6=\beta_{10}=\beta_{15} = 0 \tag{20a}$$

$$\beta_{16}=\beta_{18}=\beta_{21}=\beta_{25}=\beta_{30} = 0 \tag{20b}$$

$$\beta_2=\beta_5=\beta_9=\beta_{14} = 0 \tag{20c}$$

After imposing equations (20) and renumbering the β_i, the stress field becomes:

$$\begin{aligned}
\bar{\sigma}_x &= \beta_1x^2 + \beta_2x^2y + \beta_3x^2y^2 + \beta_4x^3 + \beta_5x^3y + \beta_6x^4 \\
\bar{\sigma}_{xy} &= \beta_7x + \beta_8xy + \beta_9xy^2 + \beta_{10}xy^3 + \beta_{11}x^2 + \beta_{12}x^3y + \beta_{13}x^2y^2 + \beta_{14}x^3 + \beta_{15}x^3y + \beta_{16}x^4 \\
\bar{\sigma}_{yz} &= \beta_7 + \beta_8y + \beta_9y^2 + \beta_{10}y^3 + 2\beta_{11}x + 2\beta_{12}xy + 2\beta_{13}xy^2 + 3\beta_{14}x^2 + 3\beta_{15}x^2y + \\
&\quad 4\beta_{16}x^3 + \beta_{19} + \beta_{20}x + 2\beta_{22}y + 2\beta_{23}xy + \beta_{24}x^2 \\
\bar{\sigma}_z &= 2\beta_1 + 2\beta_2y + 2\beta_3y^2 + 6\beta_4x + 6\beta_5xy + 12\beta_6x^2 + 2\beta_8 + 4\beta_9y + 6\beta_{10}y^2 + 4\beta_{12}x + \\
&\quad 8\beta_{15}xy + 6\beta_{15}x^2 + 2\beta_{22} + 2\beta_{23}x \\
\bar{\sigma}_y &= \beta_{17} + \beta_{18}x + \beta_{19}y + \beta_{20}xy + \beta_{21}x^2 + \beta_{22}y^2 + \beta_{23}xy^2 + \beta_{24}x^2y \\
\bar{\sigma}_{xz} &= 2\beta_1x + 2\beta_2xy + 2\beta_5xy^2 + 3\beta_4x^2 + 3\beta_5x^2y + 4\beta_6x^3 + \beta_8x + 2\beta_9xy + 3\beta_{10}xy^2 + \\
&\quad \beta_{12}x^2 + 2\beta_{13}x^2y + \beta_{15}x^3
\end{aligned} \tag{21}$$

The β-q relation of equation (18) for the 8-node plate elements is:

$$n_\beta \geq n_q - n_r = 24 - 3 = 21 \tag{22}$$

Therefore, with 24 stress parameters, the stress assumption given by (21) satisfies the criteria established in equation (17) and (18) for the special purpose element. Equation (21) can be cast in the form of (6) to yield the $\bar{P}$ matrix which is used in the integrals of (11).

The single-layer, traction-free edge plate element based on the 24-β field of (21)

will be denoted as element PL24.

In any finite-element formulation, a necessary first test of an element is to check its rank by calculating the eigenvalues of the element stiffness matrix, $\underset{\sim}{k}$. The number of zero eigenvalues should equal the number of rigid body modes in the element. Any additional zero eigenvalues correspond to spurious zero energy modes (i.e. additional kinematic modes, AKM) which must be eliminated or constrained before the element can be safely used in a general finite-element analysis [18].

Eigenanalysis of $\underset{\sim}{k}$ for element PL24 shows 5 zero eigenvalues. With 3 rigid body modes, this indicates the presence of 2 AKM. Inspection of $\underset{\sim}{k}$ reveals that the rotational degrees of freedom at the center node along the traction-free edge (i.e. node 8 in Figure 2) receive no stiffness contributions. This result is more apparent by considering the more conventional expression for $\underset{\sim}{G}$ (equation (11a)) calculated as an integral of tractions (from stresses) times displacements along the element surfaces. All tractions (traction-free edge and upper/lower surfaces) which multiply θ_{y_8} and θ_{x_8} (rotational degrees of freedom at node 8) are zero. Hence, the columns in $\underset{\sim}{G}$ corresponding to θ_{y_8} and θ_{x_8} are zero, and the corresponding rows/columns in $\underset{\sim}{k}$ will be zero. Since these 2 degrees of freedom have no stiffness associated with them, they can be eliminated from $\underset{\sim}{k}$. Numerically, this is done by artificially constraining these degrees of freedom to be zero. Note that this operation is equivalent to redefining the interpolations for θ_y and θ_x to be linear along the traction-free edge. This resulting stiffness matrix essentially has two fewer degrees of freedom so that, in this case, $n_q = 24 - 2 = 22$. This changes the requirement on number of stress parameters given by (22) to:

$$n_\beta \geq n_q - n_r = 22 - 3 = 19 \tag{23}$$

A subsequent eigenanalysis of $\underset{\sim}{k}$ for element PL24 with θ_{y_8} and θ_{x_8} constrained yielded 3 zero eigenvalues corresponding to the 3 rigid body modes. With the 2 AKM eliminated through the constraint of θ_{y_8} and θ_{x_8}, element PL24 is a viable candidate for

use as a single-layer, traction-free edge, plate element.

Numerical experience of several authors [19,20] suggests that the "optimum" number of β_i is near the minimum. Since $n_\beta \geq 19$ and $n_\beta = 24$ in element PL24, it seems reasonable to explore ways to reduce the number of β_i. Eliminating certain β_i can result in the introduction of AKM, however. To determine which β_i can be safely eliminated, one must investigate the equation:

$$\underset{\sim}{G}\,\underset{\sim}{\alpha} = 0 \tag{24}$$

where $\underset{\sim}{G}$ is given in (11a) and $\underset{\sim}{\alpha}$ is a vector of generalized displacement parameters (coefficients of the polynomial interpolations for displacement which can be uniquely related to the actual degrees of freedom) for an element. The solution $\underset{\sim}{\alpha} = 0$ corresponds to the rigid body modes; any other non-trivial solution corresponds to AKM [21].

Equation (24) was evaluated for element PL24 using a square of side length 2 (this is a sufficiently critical geometry for investigating AKM). Based on the result, the following observations were made:

1) β_8 and β_{10} are redundant; β_{10} can be eliminated since it represents a higher order term in $\bar{\sigma}_{xy}$.
2) 2 of the following β_i can be eliminated: β_1, β_3, β_4, β_6, β_8, β_{12}, β_{15}. By arguments of completeness, only consider eliminating two of the highest order terms: β_3, β_6 in $\bar{\sigma}_x$, β_{15} in $\bar{\sigma}_{xy}$.
3) 2 of the following β_i can be eliminated: β_9, β_{13}, β_{14}, β_{16}. Again, only consider eliminating two of the highest order terms: β_{13}, β_{14}, β_{16} in $\bar{\sigma}_{xy}$.

With no further information, the task of eliminating β_i from (21) and identifying the "best" traction-free eleement is one of trial and error. Numerous candidate stress fields can be defined by elmination of combinations of stress parameters (while preserving correct stiffness rank); however, certain of these fields have been eliminated on the basis of preliminary numerical experimentation. The observations made in these preliminary tests will be briefly summarized.

First, from 1), setting $\beta_{10} = 0$ in (21) yields a 23-β element which behaves almost identically to element PL24. This is expected since β_{10} represents a redundant

equation in the solution of equation (24). (For this reason, β_{10} will not be considered in any subsequent elements.) Second, removing all the quartic terms from $\bar{\sigma}_{xy}$ (i.e. $\beta_{10}=\beta_{13}=\beta_{15}=\beta_{16} = 0$) results in a 20-$\beta$ element. This element has correct rank as expected; but yielded poor moment distributions in the preliminary tests. It therefore seems advisable to have some quartic terms in $\bar{\sigma}_{xy}$. Based on these observations, the candidate stress assumptions are reduced to the following few which will be described and assessed in more detail:

ELEMENT PL21: Remove the highest order terms present in equation (21) (x^4 in $\bar{\sigma}_x$ and $\bar{\sigma}_{xy}$) by setting $\beta_6=\beta_{16} = 0$. (Also, $\beta_{10} = 0$)

ELEMENT PL19: Since the traction-free edge condition of (17) removes the constant and linear terms in x from $\bar{\sigma}_x$ and only the constant terms in x from $\bar{\sigma}_{xy}$, it seems reasonable to expect $\bar{\sigma}_x$ to be one order higher in x than $\bar{\sigma}_{xy}$. Therefore, by removing β_6 from $\bar{\sigma}_x$ to make it cubic in x, $\bar{\sigma}_{xy}$ should be reduced to a quadratic form in x by removing β_{14}, β_{15}, and β_{16}. So, set $\beta_6=\beta_{14}=\beta_{15}=\beta_{16} = 0$ and $\beta_{10} = 0$.

ELEMENT PL20: The traction free-edge condition forces $\frac{\partial\bar{\sigma}x}{\partial x}$ as well as $\bar{\sigma}_x$ to be zero along the free edge. With these strict constraints, $\bar{\sigma}_x$ may have to be of thehighest order possible in x in order to accurately predict the stress field. So, referring to equation (21), retain all terms in $\bar{\sigma}_x$ and remove β_{14}, β_{15}, and β_{16} from $\bar{\sigma}_{xy}$ as in element PL19; i.e.: $\beta_{14}=\beta_{15}=\beta_{16}= 0$ and $\beta_{10} = 0$.

Though several other stress assumptions were considered, the elements described above are the best candidates to use as single-layer, traction-free edge plate elements.

In closing, it should be mentioned that attempts were made to develop traction-free elements with arbitrary curved traction-free edges. In this approach, the elements were mapped into ξ-η space where the stress assumptions were to be applied. However, the stress assumptions are required to satisfy the 3-D equilibrium equa-

tions; which, in this case, had to be written in a non-orthogonal system, since the elements had arbitrarily curved edges. Using a tensor analysis approach, it was found that writing a stress assumption which satisfied the equilibrium equations in a non-orthogonal space was not only an extremely long and difficult task, but, could not guarantee greatly improved results for the additional effort. In fact, as will be seen in the next chapter, approximating curved edges with straight segments yields good results in most cases.

3. Example Problems and Numerical Results

In the last section, several plausible single-layer, traction-free edge, plate elements were developed. (Summarized in Table 1). All the elements satisfy the traction-free edge conditions of (17) as well as the β-q relation of (18). Also, the stiffness matrix of each element, $\underset{\sim}{k}$, is of correct rank. (i.e., three zero eigenvalues corresponding to rigid body motion after elimination of the two AKM associated with θ_{y_8} and θ_{x_8}).

In order to determine the better elements, it is necessary to assess their performance in the numerical solution of a few, selected, example problems. This will not only identify the better special purpose elements, but, determine whether a need exists for such elements in the analysis of single-layer, isotropic plates. Moreover, this may provide insight as to the potential value of these elements in subsequent development of multi-layer, traction-free edge, plate elements.

In this section, two example problems are considered. The performance of the special purpose elements of Table 1 is compared with exact solutions as well as with the non-traction-free edge element, QH1. (Note, that element PL24 is not considered since, as mentioned earlier, it has too many stress parameters).

The first example problem is shown in Figure 3. It is a square plate (length, L; thickness, 2h) with two opposite edges simply-supported and the other two free, subject to a transverse uniform load, p[21]. By symmetry, it is possible to model a quarter of the plate in the FEM analysis using an NxN mesh of elements. The special purpose elements are situated along line AC. Results are presented for the case: L=10.0 in, h=0.05 in, p_o=5.0 psi, E=3.0x10^7 psi, and ν=0.3.

In Table 2 deflections at the center and left edge (free edge) of the plate are compared. Notice, that even for the coarsest mesh, deflections are within 4% of the exact solution, and as the mesh is refined the deflections converge to less than 1% error. Also, in the coarser meshes, the special purpose elements predict displacements slight-

ELEMENT	ZEROED β'S	NUMBER OF β'S
PL19	$\beta 6, \beta 10, \beta 14, \beta 15, \beta 16$	19
PL20	$\beta 10, \beta 14, \beta 15, \beta 16$	20
PL21	$\beta 6, \beta 10, \beta 16$	21
PL24	———	24

NOTE: β'S BASED ON EQUATIONS (21)

Table 1. Single-Layer, Traction-Free Edge, Plate Elements

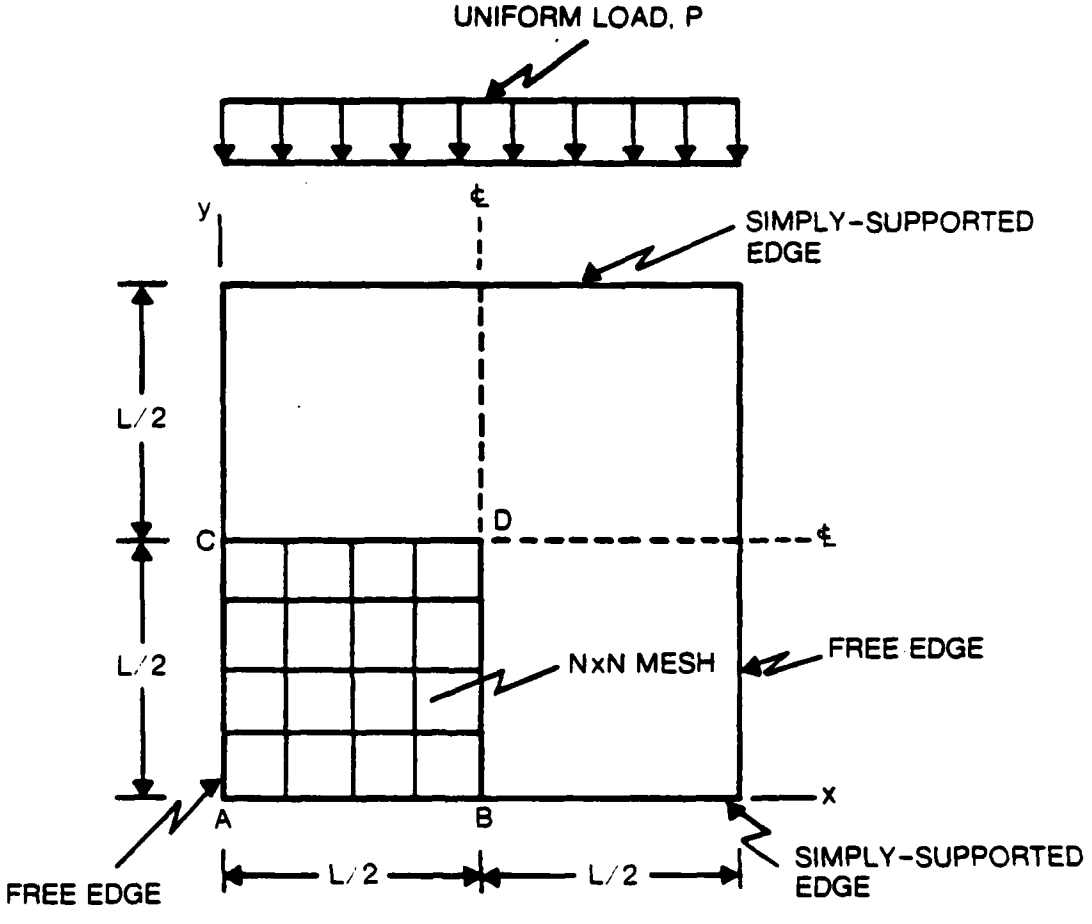

Figure 3. Problem 1. Rectangular Plate

1x1 MESH

ELEMENT	W_D		%ERROR	W_C		% ERROR
	EXACT	FEM		EXACT	FEM	
QH1	0.23824	0.2407	-1.033	0.27464	0.2848	-3.699
PL19	↓	0.2403	-0.865	↓	0.2826	-2.898
PL20		0.2372	0.437		0.2753	-0.240
PL21		0.2373	0.395		0.2753	-0.240

2x2 MESH

ELEMENT	W_D		%ERROR	W_C		% ERROR
	EXACT	FEM		EXACT	FEM	
QH1	0.23824	0.2386	-0.151	0.27464	0.2776	-1.078
PL19	↓	0.2384	-0.067	↓	0.2772	-0.932
PL20		0.2383	-0.025		0.2750	-0.131
PL21		0.2383	-0.025		0.2750	-0.131

4x4 MESH

ELEMENT	W_D		% ERROR	W_C		%ERROR
	EXACT	FEM		EXACT	FEM	
QH1	0.23824	0.2384	-0.067	0.27464	0.2753	-0.240
PL19	↓	0.2384	-0.067	↓	0.2753	-0.240
PL20		0.2384	-0.067		0.2743	0.124
PL21		—	—		—	—

NOTE: %ERROR=(1- FEM/EXACT)X 100%

Table 2. Problem 1. Deflection Comparisons

ly better than element QH1; but, in general, all of the elements converge quite well and the special purpose elements show no particular advantage at this point.

The largest moments and stresses in Problem 1 occur along line CD. (Note: See Figure 1 for sign convention for moments and stresses). To further assess the elements, Problem 1 was run with a 2x2 mesh and the moments, M_y and M_x, along line CD were plotted (Graphs 1 and 2, respectively). M_y along CD is a maximum at the free edge and decreases to a normalized value at the plate center. Notice, that all the special purpose elements show some deficiency: either they over estimate the moment at the free edge or underestimate the moment at the interface of the special purpose elements and regular elements.Of the special purpose elements, PL19 provides the best solution; however, the standard element, QH1, also yields a reasonable prediction.

M_x is calculated from σ_x and so is zero at the free edge. Along line CD, it goes from zero at the free edge to a normalized value at the center of the plate (Graph 2). Here, the first clear advantage of the special purpose elements manifests itself. Element QH1 only approximates the traction-free edges condition (20% error) while all the special prupose elements exactly satisfy this condition. Among the traction-free elements, PL20 follows the exact solution very well, while PL21 tails off at the special element/regular element interface and the curve for PL19 has increasing slope rather than decreasing slope as in the exact solution.

With no further quantities of interest in Problem 1 and too small a basis for making any broad observations, a second example problem will be considered.

Shown in Figure 4 is a circular, annular plate (inner radius, b; outer radius,a; thickness, 2h) with the inner edge free and the outer edge clamped. It is subject to a transverse load of magnitude P distributed as a line load along the inner edge such that: $P=2\pi bQ_o$ [21]. Again, by symmetry, it is possible to model a quarter of the plate in an FEM analysis. Only one mesh size is necessary (since displacements were shown to converge in Problem 1): 4 elements in the radial direction and 6 ele-

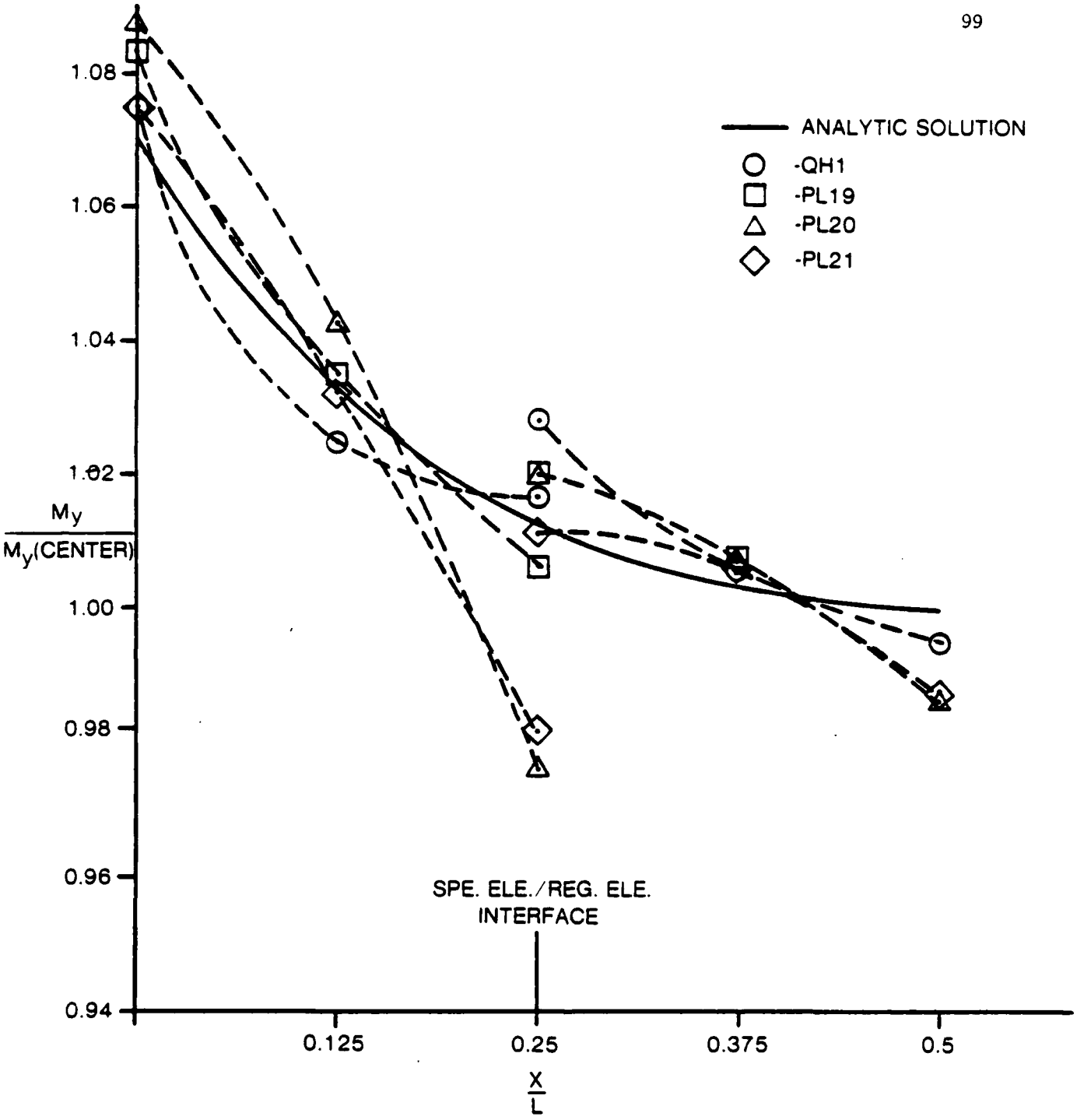

Graph 1. Problem 1. M_y Along CD (Normalized)

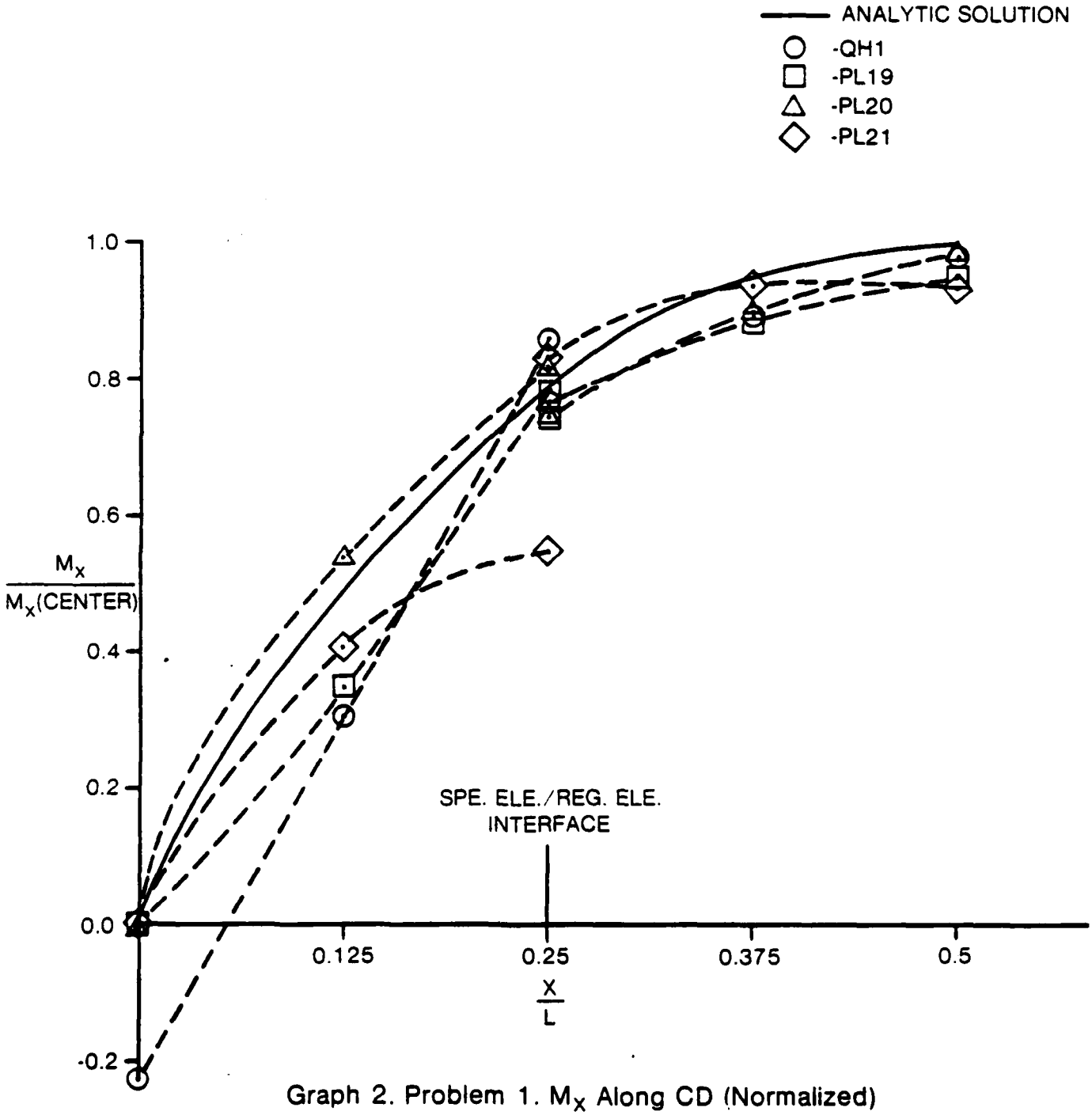

Graph 2. Problem 1. M_X Along CD (Normalized)

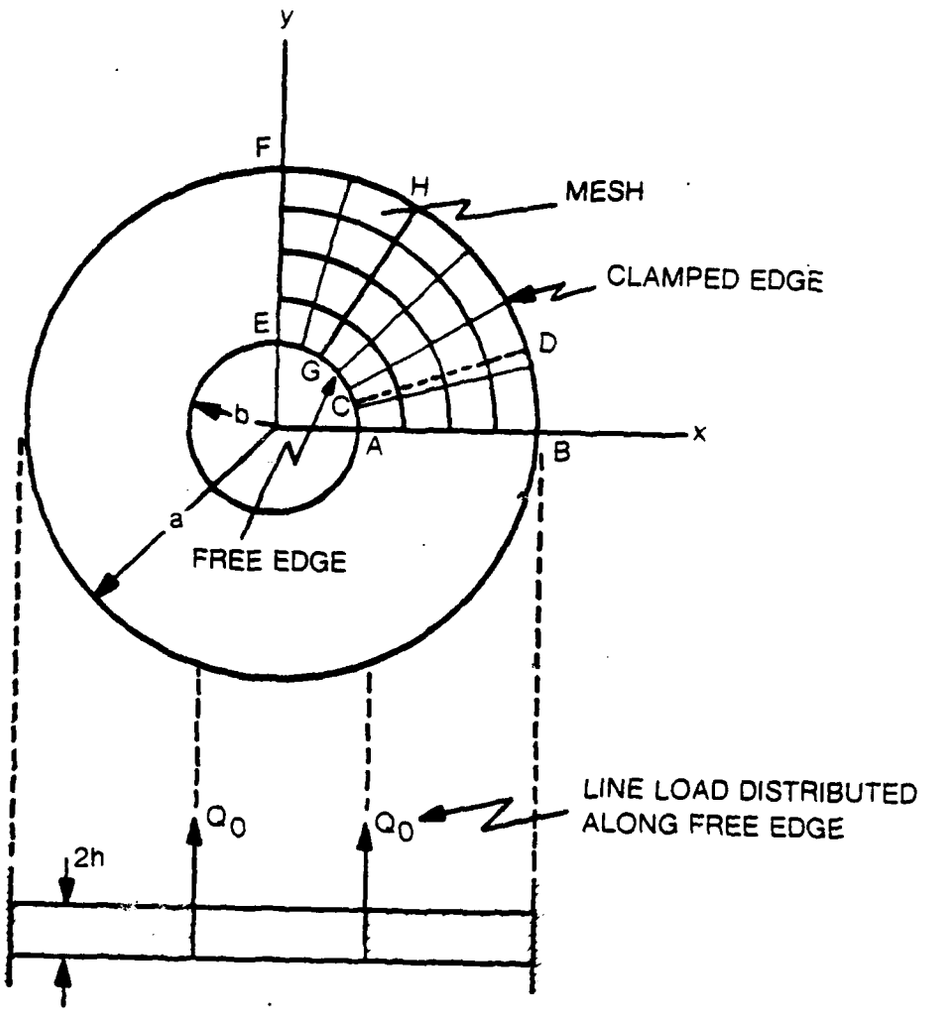

NOTE: $a=12.0,\ b=4.0,\ h=0.5,\ Q_0=1.0$

Figure 4. Problem 2. Annular Plate

ments in the circumferential direction. The traction-free edge elements are placed along the inner edge ACGE. Note, this problem also tests the performance of the elements as general quadrilaterals which approximate the circular edge with straight line segments. All results are presented for the case: a=12.0 in, b=4.0 in, Q_o= 1.0, E=1.0 x 10^7 psi, h = 0.5 in and ν = 0.3.

Since this problem is axisymmetric, a closed form solution can be readily obtained, and various quantities of interest can be compared with numerical solutions. In Graph 3, the deflections along line AB are plotted. As before, all the elements predict this quantity well. Furthermore, along any other radial line (e.g., CD, GH), the curves should not change and this is verified in the numerical results. The rotation about the y-axis, θ_y, along line AB is shown in Graph 4. Notice, that traction-free elements PL19 and PL20 underpredict the rotations at the free edge. This is undesirable in itself and may affect the predictions of moments and stresses subsequently.

Graph 5 shows the variation of M_y along line AB. M_y starts as a positive quantity, passes through zero, and is negative at the clamped edge. Observe that PL19 and PL20 behave poorly in terms of predicting the moment at the free edge and at the special element/regular element interface. Element PL21 does well at the free edge but shows slight difficulty at the special element/regular element interface. On the other hand, the non-traction-free element, QH1, follows the analytic curve very closely at all points.

The other moment of interest, M_x along line AB, is plotted in Graph 6. This moment is zero at the free edge and increases to a maximum negative value at the clamped edge. Here, all the elements predict the moment well at the free edge, but at the special element/regular element interface all the special purpose elements are poor. PL19 and PL20 grossly overestimate the moments (over 300% error) while PL21 exhibits an error of about 50% at the interface. Also, PL19 and PL20 cause the regular element at the interface to predict the moment poorly. Finally, at the

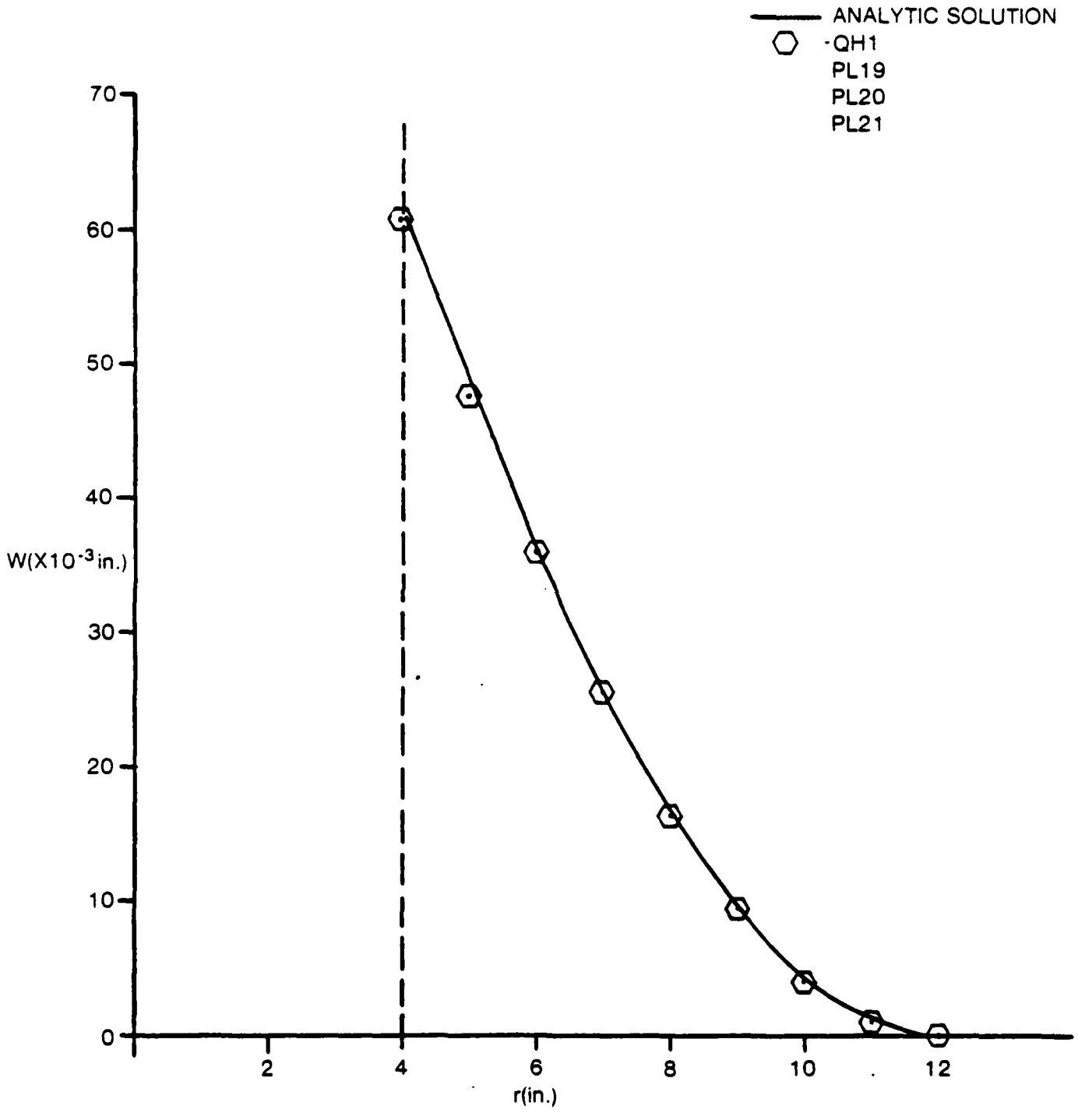

Graph 3. Problem 2. Deflection Along AB

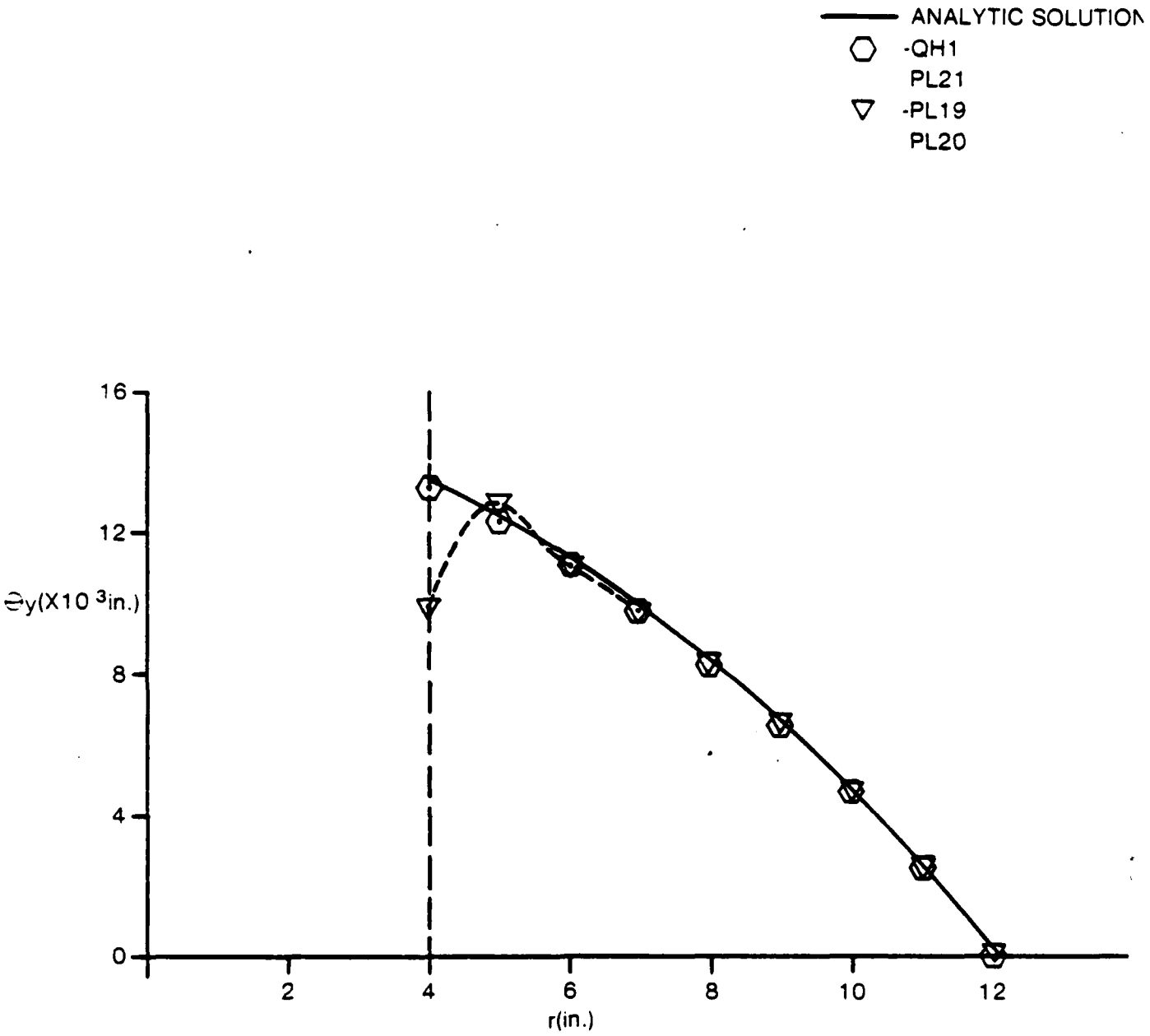

Graph 4 Problem 2. Rotation Along AB

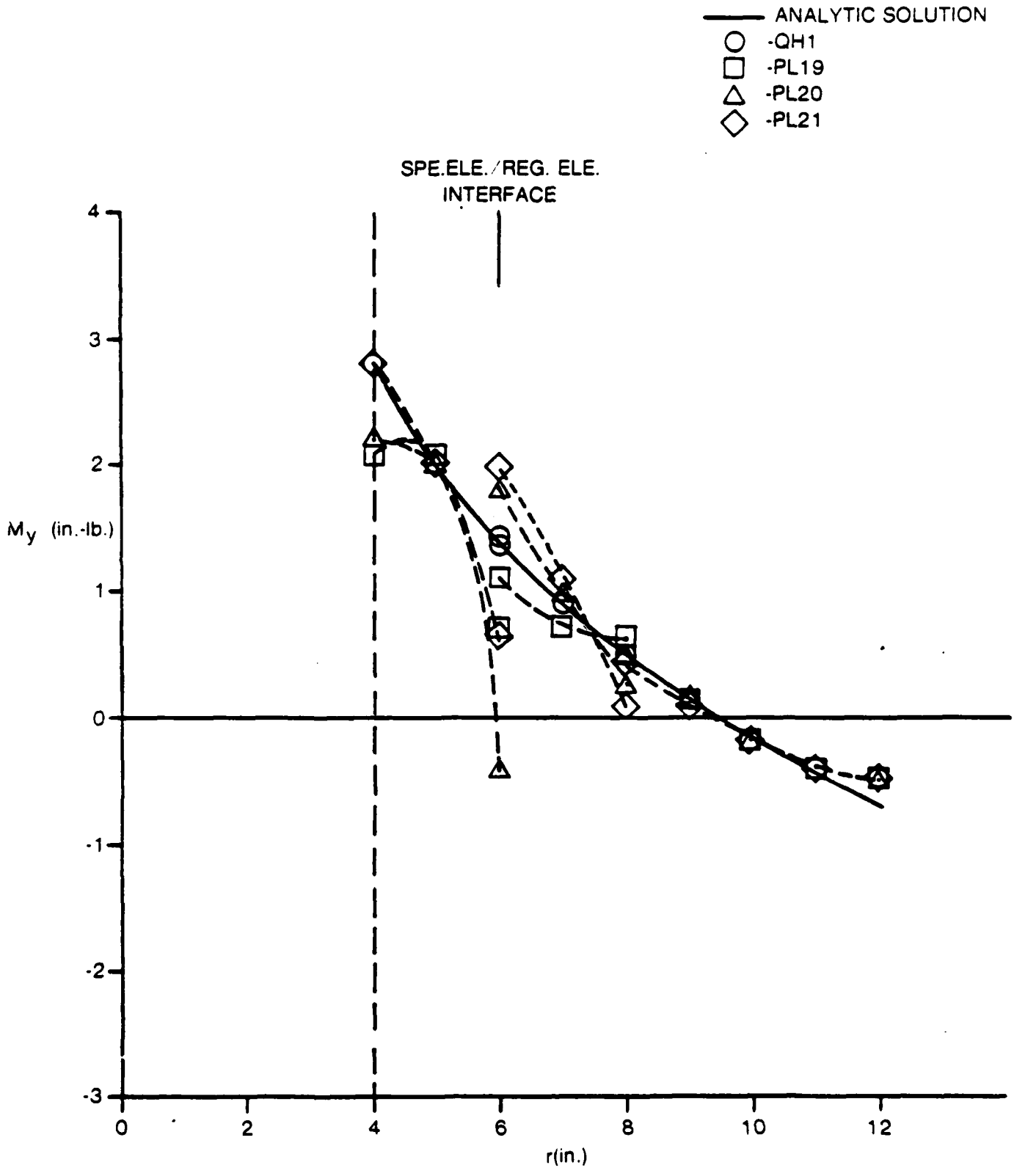

Graph 5. Problem 2. M_y Along AB

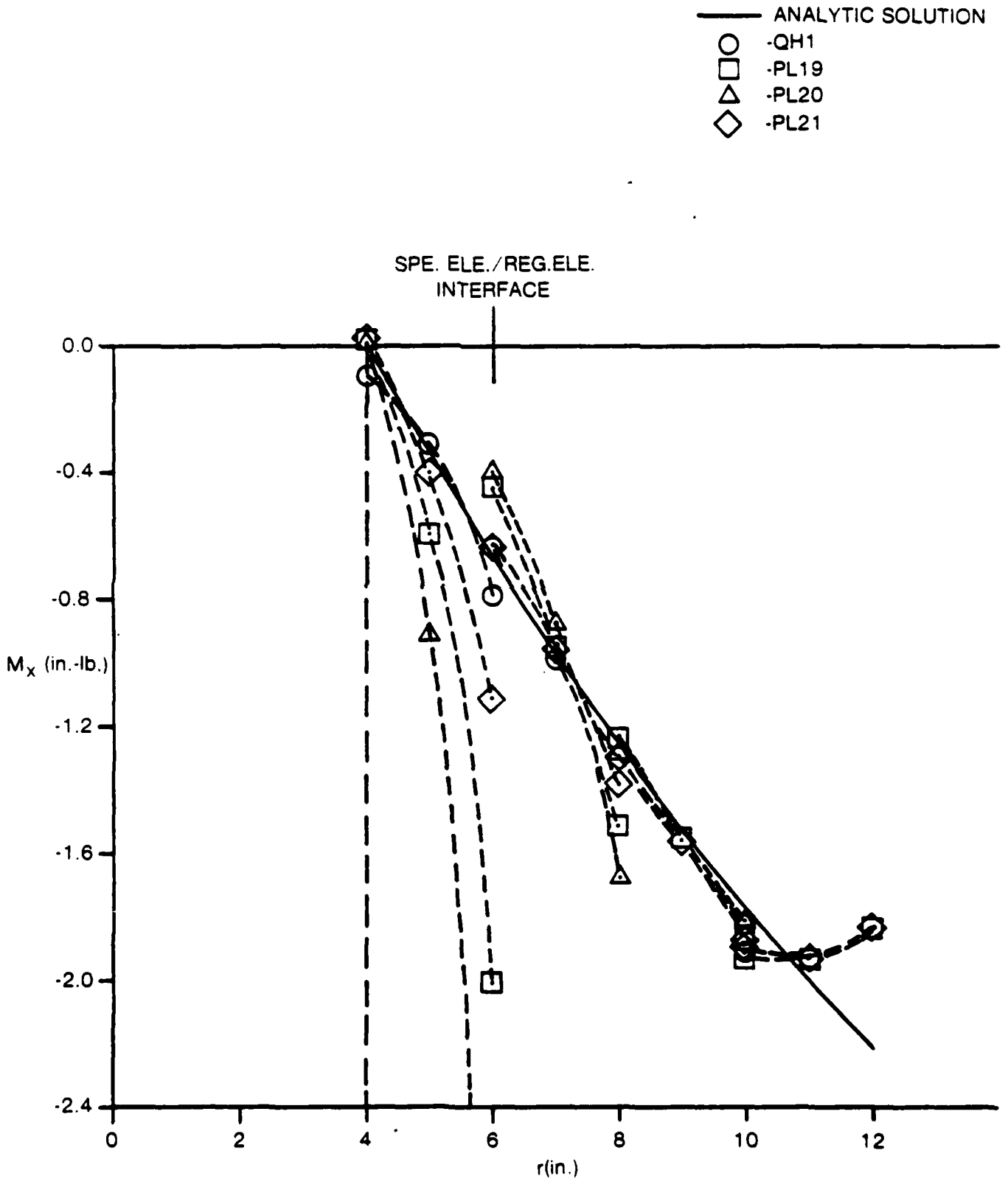

Graph 6. Problem 2. M_x Along AB

clamped edge (where element QH1 is always used), the moment, M_x, is underestimated in all cases. More will be said on this shortly.

In assumed-displacement elements, much work has been done to determine those locations within an element at which the stress (and moment) predictions are best [23,24,16]. These points are called "optimal sampling" points and depend on the order of the polynomials used in the displacement interpolations for the elements. Though such points have not been rigorously defined for hybrid-stress elements, it is at least reasonable to assume that these points will not lie on the edges of these elements. Therefore, in Problem 2, line AB (Figure 4) is not expected to be a line of "optimal sampling". Moreover, if the "optimal sampling" behavior of hybrid-stress elements is like that in assumed-displacement elements, then for 8-node elements, the "optimal sampling" points are the points used for 2x2 Gauss Quadrature.

Referring to Figure 4, line CD is a typical radial line which contains the 2x2 Gauss points. In Graphs 7 and 8, the normal and targential moments, respectively, along line CD are plotted. Notice that even along a line of "optimal sampling" traction-free elements PL19 and PL20 are unable to predict moments well. The large moment at the free edge in Graph 7 is largely underestimated by PL19 and PL20, while at the special element/regular element interface both moments are predicted poorly. On the other hand, special purpose element PL21 and regular element QH1 both follow the analytic solutions remarkably well along this line; though QH1 still only approximates the traction-free condition since the tangential moment is not exactly zero at the free edge (Graph 8).

Recall, that in Graph 6, the tangential moment was underestimated at the clamped edge. Along a line of "optimal sampling" this discrepancy vanishes; as shown in Graph 8 this moment is predicted adequately at the clamped edge in all cases. This gives further credibility to the idea of evaluating stresses at "optimal sampling" points rather than arbitrary or convenient points in an element.

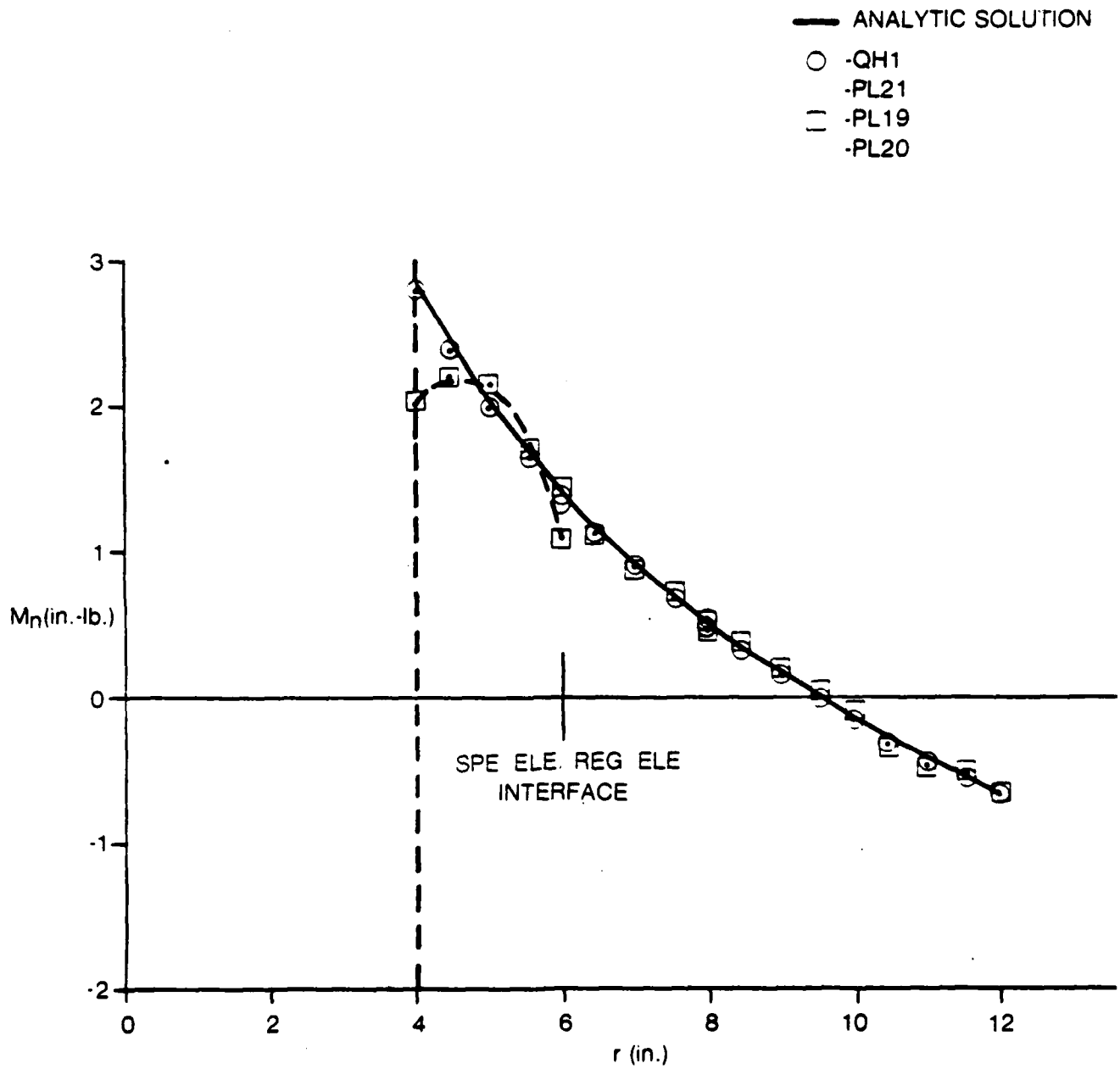

Graph 7. Problem 2. Normal Moment (M_n) Along CD

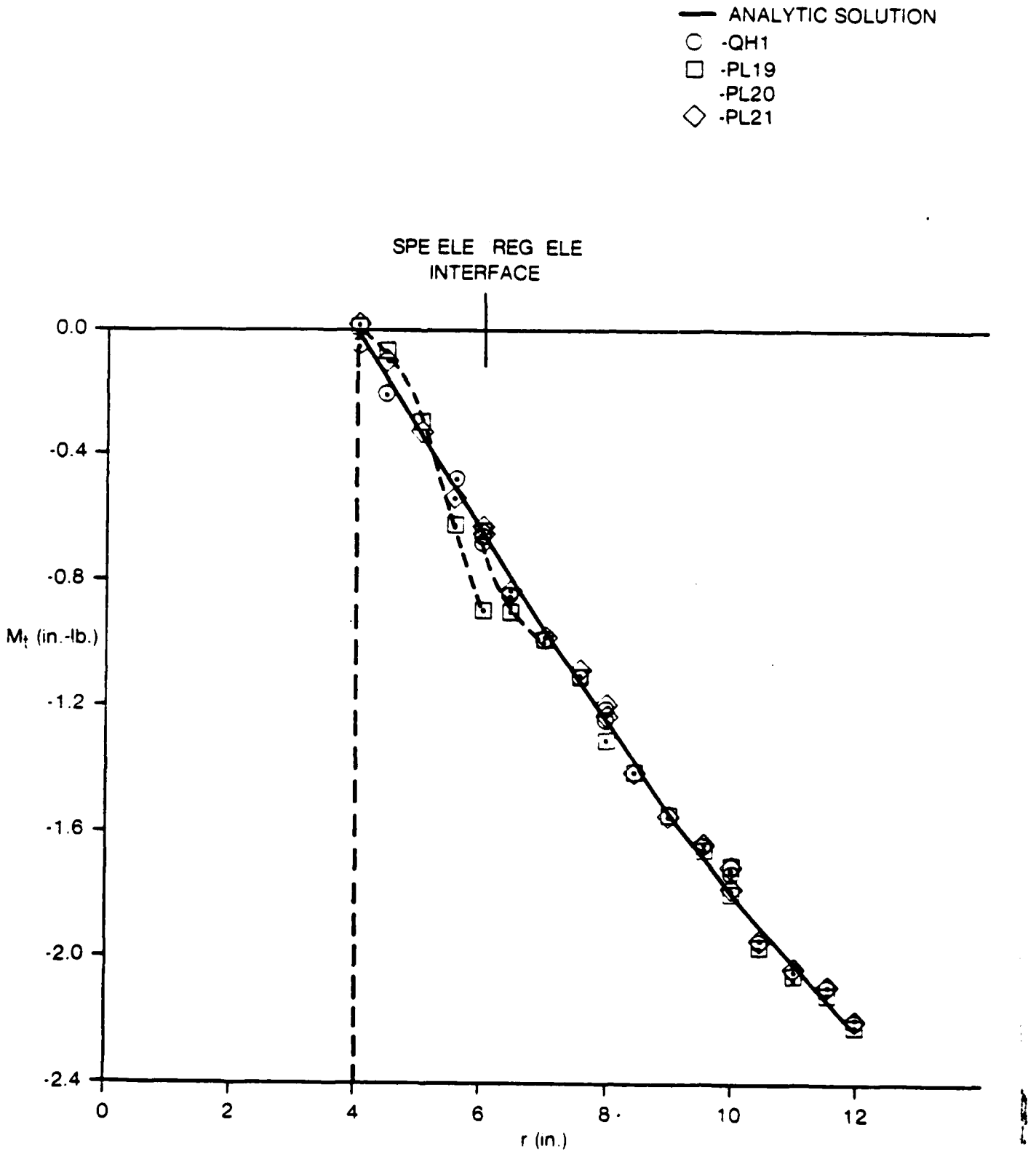

Graph 8. Problem 2. Tangential Moment (Mt) Along CD

Based on these observations, element PL21 seems the best candidate to use as a single-layer, traction-free edge plate element. Unlike PL19 and PL20, it predicts both rotations and displacements well. Though it predicts moments better than PL19 and PL20 in general; along a line of "optimal sampling" it predicts moments extremely well and shows a clear advantage over those elements. As far as element QH1 is concerned, ignoring its inherent deficiency of approximating the traction-free edge condition, it performs extremely well in all cases.

4. Summary and Concluding Remarks

In this study, a single-layer, isotropic plate element with a straight traction-free edge has been developed based on the hybrid-stress model. It can be coupled with the regular version of this element (element QH1 [13]) to perform the numerical analysis of isotropic, arbitrary thin to moderately thick plates with traction-free edges.

The element assumes a Mindlin-type displacement behavior which not only results in displacement interpolations that are only required to be C^0 continuous but facilitates satisfying the 3-D equilibrium equations and the free-surface conditions of the element. By including all components of stress, the transverse shear stresses are present for the analysis of moderately thick plates where their contributions are significant. The stress assumption for the element is chosen so that along one of its edges the tractions (i.e. appropriate stresses) are zero; and, the β-q relation, a necessary condition in the assumed-stress hybrid formulation, is satisfied. The element mapping is such that it can take on a general, quadrilateral shape.

Though the number of stress fields which satisfy these conditions is theoretically limitless, arguements of minimizing the number of stress parameters quickly narrows the choices. Extensive numerical experimentation and testing results in the conclusion that, of the numerous stress fields considered, the 21-β stress field of element PL21 is the best for the applications considered.

Element PL21 yields a stiffness matrix which exhibits correct rank, avoids "locking" in the thin plate limit, and yields displacements which converge as the number of degrees of freedom increases. Moreover, in a numerical analysis, element PL21 predicts displacements, rotations, and stresses (moments) quite well in general, and especially well along lines containing the 2x2 Gauss points which appear to be "optimal sampling" points from which to obtain or extrapolate stress (moment)

information.

However, it is important to realize that in all cases element QH1 performs well in predicting displacements and stresses; and, its only shortcoming is its inherent inability to satisfy the traction-free condition exactly along an edge. This seems to indicate that in single-layer, isotropic plates, the traction-free edge condition is not crucial when trying to obtain a numerical solution and that the extra effort to develop and use special elements to better model this condition may not be necessary.

On the other hand, the stresses which dominate the solution of multi-layer, laminated, composite plates (i.e. $\sigma_z, \sigma_{xz}, \sigma_{yz}$) have minimal effects in single-layer, isotropic plates. In fact, these stresses have not even been considered in any great length in this study. For this reason, the advantages of the traction-free edge elements over element QH1 may not be evident in single-layer plates.

Therefore, a multi-layer, traction-free edge, plate element based on element PL21 should be developed and tested. This element when compared to the multi-layer version of QH1 should prove to perform better and exhibit obvious advantages when analyzing laminated, composite plate structures with traction-free edges.

5. References

1. R.B. Pipes and N.J. Pagano, "Interlaminar Stresses in Composite Laminates Under Uniform Axial Extension," J. Comp. Materials, 4 , 538 (1970).

2. N.J. Pagano, "On the Calculation of Interlaminar Normal Stress in Composite Laminates," J. Comp. Materials, 8, 65, (1974).

3. T.H.H. Pian, "Derivation of Element Stiffness Matrix by Assumed Stress Distribution", AIAA J., 2, 1333-1336 (1964).

4. T.H.H. Pian, "Element Stiffness Matrices for Boundary Compatibility and for Prescribed Boundary Stresses", Proc. Conf. Matrix Meth. In Structural Mech., AFFDL-TR-66-80, 457-477, (1966).

5. T.H.H. Pian and P. Tong, "Rationalization in Deriving Element Stiffness Matrix Assumed-Stress Approach", Proc. 2nd Conf. Matrix Meth. in Structural Mech., AFFDL-TR-68-150, 441-469 (1969).

6. S.T. Mau, P. Tong and T.H.H. Pian, "Finite Element Solutions for Laminated Thick Plates", J. Comp. Materials, 6, 304-311 (1972).

7. R.L. Spilker and S.C. Chou and O. Orringer, "Alternate Hybrid-Stress Elements for Analysis of Multilayer Composite Plates", J. Comp. Materials, 11, 51-70, (1977).

8. R.L. Spilker, "A Hybrid-Stress Finite-Element Formulation for Thick Multilayer Laminates," Computers and Structures 11, 507-514 (1980).

9. K.H. Lo, R.M. Christensen and E.M. Wu, "A High-Order Theory of Plate Deformation, Part 2: Laminated Plates," J. Appl. Mech., 44, 669-676, (1977).

10. R.L. Spilker, "A Finite Element Model for Laminated Plates Including Transverse Shear Deformation," AMMRC CTR 72-12 (also MIT ASRL TR 169-1), July 1972.

11. S.T. Mau and E.A. Witmer, "Static, Vibration and Thermal Stress Analysis of Laminated Plates and Shells by the Hybrid-Stress Finite-Element Method, with Transverse Shear Deformation Effects Included," AMMRC CTR 72-24 (also MIT ASRL TR 169-2), Oct. 1972.

12. R.L. Spilker and N.I. Munir, "The Hybrid-Stress Model for Thin Plates," Int. J. Num. Meth. Engng., 15, 1239-1260 (1980).

13. R.L. Spilker and N.I. Munir, "A Hybrid-Stress Quadratic Serendipity Displacement Mindlin Plate Bending Element," Computers and Structures, 12, 11-21 (1980).

14. R.L. Spilker and N.I. Munir, "A Serendipity Cubic-Displacement Hybrid-Stress Element for Thin and Moderately Thick Plates," Int. J. Num. Meth. Engng., 15, 1261-1278 (1980).

15. R.D. Mindlin, "Influence of Rotary Inertial and Shear on Flexural Motion of Isotropic Elastic Plates," J. Appl. Mech., 18, 31-38, (1951).

16. O.C. Zienkiewicz, The Finite Element Method, 3rd Edition, McGraw-Hill, New York and London, 1977.

17. P. Tong and T.H.H. Pian, "A Variational Principle and the Convergence of Finite Element Method Based on Assumed Stress Distribution", Int. J. Solids Structures, 5, 463-472, (1969).

18. R.D. Cook and S.G. Ladkany, "Observations Regarding Assumed-Stress Hybrid Plate Elements", Int. J. Num. Meth. in Engng., 8, 513-519, (1974).

19. T.H.H. Pian, "Hybrid Elements", Numerical and Computer Methods in Stuctural Mechanics (edited by S.H. Fenves, N. Perrone, A.R. Robinson, and W.C. Schnobrich), Academic Press, New York, 59-78 (1973).

20. R.D. Henshell, "On Hybrid Finite Elements", in Mathematics of Finite Elements and Applications (edited by J.R. Whiteman), Academic Press, 299-312 (1973).

21. R.L. Spilker, "High-Order Three-Dimensional Hybrid-Stress Elements for Thick Plate Analysis", Int. J. for Num. Meth. in Engng., 17, 53-69 (1981).

22. S. Timoshenko and S. Woinowsky-Krieger, Theory of Plates and Shells, 2nd Edition, McGraw-Hill, New York (1959).

23. E. Hinton, F.C. Scott, and R.E. Ricketts, "Local Least Squares Stress Smoothing for Parabolic Isoparametric Elements", Int. J. Num. Meth. Engng., 9, 235-256 (1975).

24. J. Barlow, "Optimal Stress Locations in Finite Element Models", Int. J. Num. Meth. in Engng., 10, 243-251, (1976).

CHAPTER 4

ELASTIC-PLASTIC ANALYSIS OF SINGLE-LAYER PLATES

ABSTRACT

Two alternate hybrid-stress-based functionals are examined for the incremental elastic-plastic static analysis of single layer plates. Material nonlinear effects are incorporated via the initial-stress approach so that an equivalent nodal force vector is defined and the stiffness remains constant throughout the incremental loading. The alternate functionals differ in the incremental stress which is assumed to satisfy equilibrium; in the first, it is the actual stress increment, and in the second it is the elastic stress increment. Results are presented for two example problems, and comparisons of the alternate functionals and plausible iteration schemes are given. The effects of variation of pertinent solution parameters are also shown. A 4-node hybrid-stress plate element based on a Mindlin-type displacement field is used for most cases; however, limited results are also presented using an 8-node plate element, thus permitting comparisons of the relative efficiences of the two elements.

1. Introduction

In the elastic-plastic analysis of structures by the finite-element method, three incremental procedures are most commonly used; the tangent stiffness, initial-strain, and initial-stress methods. In the first, nonlinear effects are incorporated via an updated stiffness, whereas in the latter two methods, the structure stiffness remains constant and plasticity effects are included as equivalent nodal loads. In most cases, the analyses are based on assumed-displacement formulations; textbook accounts and appropriate references may be found, for example, in References 1 and 2.

A viable alternative to the assumed-displacement model for both linear and nonlinear analyses is the hybrid-stress nodel. This model is based on a modified complementary energy principle. Compatible boundary displacements and equilibrating intraelement stresses are independently interpolated; the stress parameters are eliminated on the element level resulting in a conventional element stiffness matrix. Elastic-plastic analyses based on the hybrid-stress model [3-10] have been reported by Yamanda et al [3], Luk [4], Spilker and Pian [5,7], Horrigmoe and Eidsheim [8], and Barnard and Sharman [9]; these include applications of all three elastic-plastic procedures. A survey of incremental hybrid-stress formulations for nonlinear problems has been presented by Pian [10].

The initial-stress procedure was first used in conjunction with the assumed-displacement model by Zienkiewicz et al [11]. In this approach, the effects of material nonlinearity are accounted for by a fictitious initial stress, $\underset{\sim}{\sigma}^f$, equal to the difference between an assumed elastic stress increment, $\Delta\underset{\sim}{\sigma}^e$, and the actual stress increment, $\Delta\underset{\sim}{\sigma}_{ep}$ (see Figure 1). The equivalent load vector is calculated by a weighted integral of $\underset{\sim}{\sigma}^f$, and therefore the accuracy of the numerical scheme will be dependent on the accuracy of intraelement stress distributions. Since the hybrid-stress model yields improved intraelement stress predictions compared with analagous assumed-displacement elements in many cases [e.g. 12,13], this model appears to be ideally suited for use in conjunction with the initial-stress approach.

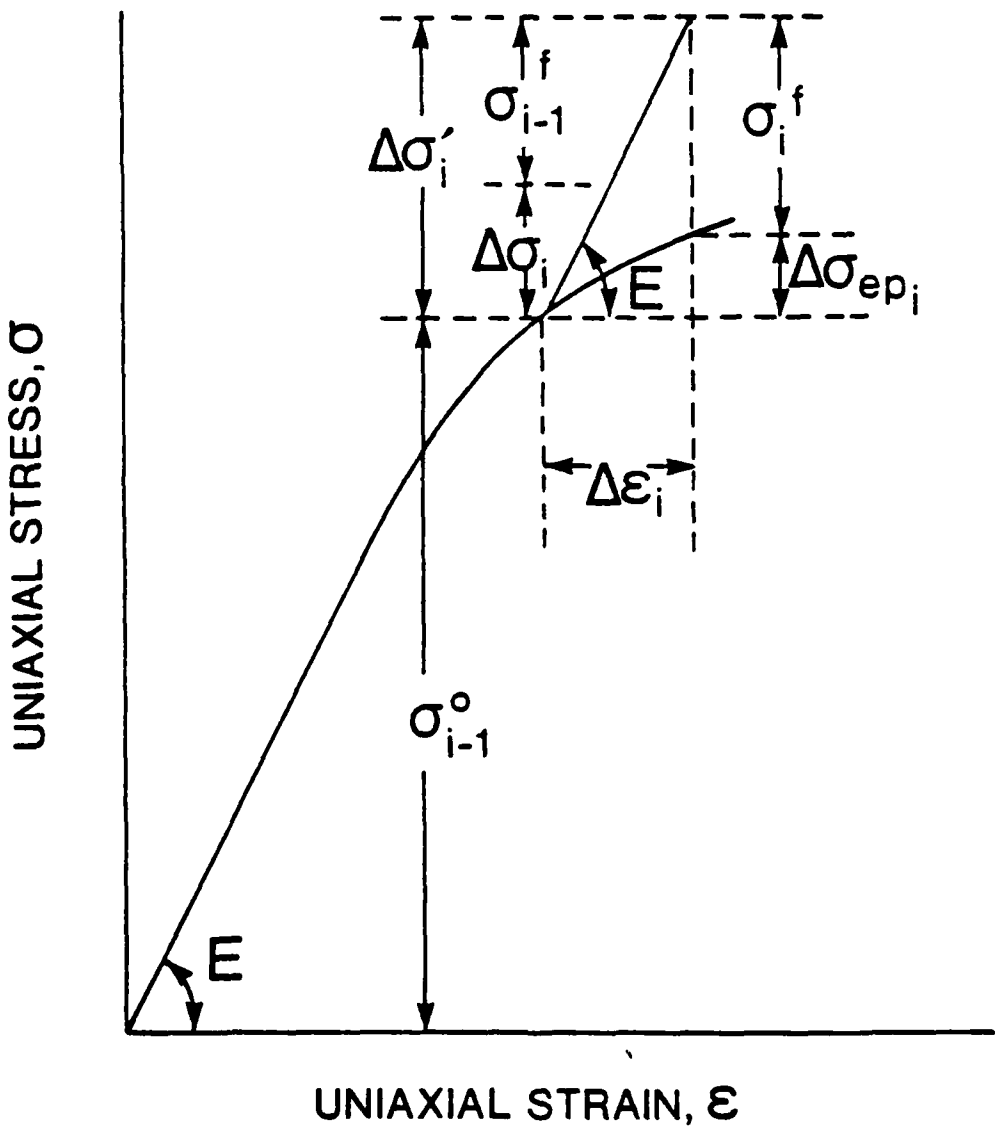

Figure 1. Schematic representation and definition of stress and strain quantities for the initial-stress approach for a 1-D problem.

Alternate hybrid-stress functionals using the initial-stress approach have been derived in References 5 and 7. These functionals, denoted by Π_{mc}^{I} and Π_{mc}^{II}, differ in the stress increment assumed to satisfy equilibrium; in Π_{mc}^{I}, it is the (approximate) actual stress increment ($\Delta\underset{\sim}{\sigma}$ in Figure 1), while in Π_{mc}^{II}, it is the elastic stress increment, $\Delta\underset{\sim}{\sigma}'$. Extensive numerical studies for axisymmetric structures, also including equilibrium imbalance corrections, suggest that Π_{mc}^{II} is the more accurate and efficient approach [5, 7].

However, a potential disadvantage of Π_{mc}^{II} is the need for intraelement compatible displacement interpolations (not required in Π_{mc}^{I}). For plate elements based on classical thin plate theory, the required C^1 continuity intraelement displacement fields are not easily constructed and a Π_{mc}^{II} approach would therefore be intractable. Applications of the hybrid-stress model to elastic-plastic plate bending, using classical plate theory elements, have been reported in References 8 and 9. In these approaches, as in Π_{mc}^{I}, displacements are interpolated only on the element boundaries and thus no difficulties are encountered in defining the C^1 continuity interpolations.

Recently, a family of hybrid-stress plate elements have been developed for which independent transverse displacement and rotations are assumed, and in which all components of stress are included [14-16]; the elements are thus applicable for thin and moderately thick plates. Because only C^o displacement continuity is required, intraelement displacements/rotation interpolations are easily constructed, and thus the Π_{mc}^{II} approach is possible. The family of elements are based on 4-node, 8-node, and 12-node Serendipity shape functions. In each case, the element stiffness is of correct rank, and the plate thickness may be taken arbitrarily small without inducing solution 'locking'. In numerical comparisons, these elements, in general, yield superior displacement and intraelement stresses in comparison with analagous reduced or selectively reduced integration assumed-displacement Mindlin plate elements. Because the hybrid-stress plate elements do not require a formal separation of flexural and transverse shear stiffness contributions, the

application of these elements to nonlinear problems will be straightforward and no special modifications will be required in order to analyze plates from moderate to arbitrarily small thickness.

In the present study, the plate elements of [14,15] are used with Π^{I}_{mc} and Π^{II}_{mc} for elastic-plastic analysis. Equilibrium imbalance corrections are included in all cases, and the effects of solution refinement and integration sampling points are explored, primarily using Π^{II}_{mc} and a 4-node plate element. Comparisons of Π^{II}_{mc} and Π^{I}_{mc} (using alternate iteration schemes) are presented which again show Π^{II}_{mc} to be the better approach. Also, limited comparisons of the 4-node and 8-node elements are presented to assess the relative efficiency and accuracy of these elements in nonlinear analysis.

2. Hybrid-Stress Functionals and Matrix Formulation

Details of the derivation of the alternate hybrid functionals from the incremental virtual work expression are found in Reference 5; only the final forms and element matrix definitions will be given here for the sake of completeness. In vector form, Π^{I}_{mc} and Π^{II}_{mc} may be expressed as:

$$\Pi^{I}_{mc}(\Delta\underset{\sim}{\sigma},\Delta\underset{\sim}{u}) = \sum_{n}\Big\{1/2\int_{V_n}(\Delta\underset{\sim}{\sigma}+\underset{\sim}{\sigma}^{f})\,\underset{\sim}{S}\,(\Delta\underset{\sim}{\sigma}+\underset{\sim}{\sigma}^{f})\,dV - \int_{V_n}\Delta\underset{\sim}{\sigma}^{T}\,\Delta\hat{\underset{\sim}{\varepsilon}}\,dV + \int_{S_{\sigma_n}}\Delta\overline{\underset{\sim}{T}}^{T}\,\Delta\underset{\sim}{u}\,dS + R^{*}_{n}\Big\} \tag{1}$$

$$\Pi^{II}_{mc}(\Delta\underset{\sim}{\sigma}',\Delta\underset{\sim}{u}) = \sum_{n}\Big\{1/2\int_{V_n}\Delta\underset{\sim}{\sigma}'^{T}\underset{\sim}{S}\,\Delta\underset{\sim}{\sigma}'\,dV - \int_{V_n}(\Delta\underset{\sim}{\sigma}'-\underset{\sim}{\sigma}^{f})^{T}\,\Delta\hat{\underset{\sim}{\varepsilon}}\,dV + \int_{S_{\sigma_n}}\Delta\overline{\underset{\sim}{T}}^{T}\Delta\underset{\sim}{u}\,dS + R^{*}_{n}\Big\} \tag{2}$$

where

V_n = volume of the nth element.

S_{σ_n} = portion of the boundary of the nth element over which tractions are prescribed.

$\underset{\sim}{S}$ = material elastic compliance matrix ($\underset{\sim}{\varepsilon} = \underset{\sim}{S}\underset{\sim}{\sigma}$).

$\underset{\sim}{\sigma}'$ = elastic stress vector

$\underset{\sim}{\sigma}^f$ = fictitious initial stress vector (a prescribed quantity).

$\underset{\sim}{\sigma}$ = actual stress vector (i.e. $\Delta\underset{\sim}{\sigma} = \Delta\underset{\sim}{\sigma}' - \underset{\sim}{\sigma}^f$).

$\underset{\sim}{u}$ = displacement vector

$\underset{\sim}{\varepsilon}$ = "strains" calculated from displacements, $\underset{\sim}{u}$, via the linear strain-displacement relations.

$\overline{\underset{\sim}{T}}$ = prescribed tractions.

$\Delta(\ )$ = increment in the quantity ( ).

$(\ )^o$ = total value of the quantity ( ).

The term R_n^* appearing in both functionals corresponds to the equilibrium imbalance correction[5] and is given by (for no body forces):

$$R_n^* = -\int_{V_n} \underset{\sim}{\sigma}^{oT} \Delta\hat{\underset{\sim}{\varepsilon}}\, dV + \int_{S_{\sigma_n}} \overline{\underset{\sim}{T}}^{oT} \Delta\underset{\sim}{u}\, dS \tag{3}$$

If the total stress at the beginning of an increment satisfies equilibrium, and the total tractions satisfy the mechanical boundary conditions, R_n^* vanishes.

In Π_{mc}^I, the actual stress increment, $\Delta\underset{\sim}{\sigma}$, must satisfy the equilibrium equation;

$$\underset{\sim}{E}\,\Delta\underset{\sim}{\sigma} = \underset{\sim}{E}(\Delta\underset{\sim}{\sigma}' - \underset{\sim}{\sigma}^f) = \underset{\sim}{0} \tag{4}$$

where $\underset{\sim}{E}$ is the differential operator matrix corresponding to the homogeneous equilibrium equations. In Π_{mc}^{II}, the elastic stress increment, $\Delta\underset{\sim}{\sigma}'$, must satisfy equilibrium:

$$\underset{\sim}{E}\,\Delta\underset{\sim}{\sigma}' = \underset{\sim}{E}(\Delta\underset{\sim}{\sigma}_{ep} + \underset{\sim}{\sigma}^f) = \underset{\sim}{0} \tag{5}$$

where $\Delta\underset{\sim}{\sigma}_{ep}$ is the actual elastic-plastic stress increment (see Figure 1). In view of equations (4) and (5), Π_{mc}^I appears to be the more "consistent" hybrid-stress approach, and Π_{mc}^{II} may be viewed as a modified Hellinger-Reissner approach since only a portion of the actual stress increment satisfies equilibrium. It should also be noted that the second integral in Π_{mc}^I appears as a surface integral over the ele-

ment boundary in the original formulation [5,7] (by applying the Divergence theorem to this term, with equation (4)), so that displacements need be defined only on the element boundary (if R_n^* is elminated). However, for the present application where intraelement displacements are easily interpolated, the present form is preferred. Note also that an intraelement displacement field is always required when using Π_{mc}^{II}, and when R_n^* is retained in Π_{mc}^{I}.

In the element formulations, stresses are expressed in terms of stress parameters, $\underset{\sim}{\beta}$ (usually in polynomial form);

$$\Delta\underset{\sim}{\sigma} = \underset{\sim}{P}\,\Delta\underset{\sim}{\beta} \quad \text{for } \Pi_{mc}^{I} \tag{6a}$$

$$\Delta\underset{\sim}{\sigma}' = \underset{\sim}{P}\,\Delta\underset{\sim}{\beta} \quad \text{for } \Pi_{mc}^{II} \tag{6b}$$

such that the appropriate equilibrium equations (equations (4) and (5)) are exactly satisfied. The intraelement displacements, $\underset{\sim}{u}$, are interpolated in terms of nodal displacements, $\underset{\sim}{q}$, such that appropriate interelement continuity is guaranteed;

$$\Delta\underset{\sim}{u} = \underset{\sim}{N}\,\Delta\underset{\sim}{q} \tag{7}$$

The linear strain-displacement relations are applied to equation (7) to give

$$\Delta\hat{\underset{\sim}{\epsilon}} = \underset{\sim}{B}\,\Delta\underset{\sim}{q} \tag{8}$$

Equations (6) through (8) are substituted into equations (1) and (2), and the following element matrices are defined

$$\underset{\sim}{H} = \int_{V_n} \underset{\sim}{P}^T \underset{\sim}{\underset{\sim}{S}}\,\underset{\sim}{P}\; dV \tag{9a}$$

$$\underset{\sim}{G} = \int_{V_n} \underset{\sim}{P}^T \underset{\sim}{B}\; dV \tag{9b}$$

$$\underset{\sim}{F}^I = \int_{V_n} \underset{\sim}{P}^T \underset{\sim}{\underset{\sim}{S}}\,\underset{\sim}{\sigma}^f\; dV \tag{9c}$$

$$\underset{\sim}{F}^{II} = \int_{V_n} \underset{\sim}{B}^T \underset{\sim}{\sigma}^f \, dV \tag{9d}$$

$$\underset{\sim}{F}^{o} = \int_{V_n} \underset{\sim}{B}^T \underset{\sim}{\sigma}^o \, dV \tag{9e}$$

$$\Delta\underset{\sim}{Q} = \int_{S_{\sigma_n}} N^T \, \Delta\overline{\underset{\sim}{T}} \, dS \tag{9f}$$

$$\underset{\sim}{Q}^{o} = \int_{S_{\sigma_n}} \underset{\sim}{N}^T \, \overline{\underset{\sim}{T}}^{o} \, dS \tag{9g}$$

Following [5,7] , the stress parameters are eliminated on the element level from the resulting functionals according to;

$$\Delta\underset{\sim}{\beta} = \underset{\sim}{H}^{-1}\underset{\sim}{G} \, \Delta\underset{\sim}{q} - \underset{\sim}{H}^{-1}\underset{\sim}{F}^{I} \qquad \text{for } \Pi_{mc}^{I} \tag{10a}$$

$$\Delta\underset{\sim}{\beta} = \underset{\sim}{H}^{-1}\underset{\sim}{G} \, \Delta\underset{\sim}{q} \qquad \text{for } \Pi_{mc}^{II} \tag{10b}$$

When equations (10) are substituted back into the functionals, both Π_{mc}^{I} and Π_{mc}^{II} may be put in the form;

$$\Pi_{mc}^{I,II} = \sum_{n} \left[1/2 \, \Delta\underset{\sim}{q}^T \underset{\sim}{k} \, \Delta\underset{\sim}{q} - \Delta\underset{\sim}{q}^T (\Delta\underset{\sim}{Q} + \underset{\sim}{Q}^f + \underset{\sim}{R}^o) \right] \tag{11}$$

where

$\underset{\sim}{k} = \underset{\sim}{G}^T\underset{\sim}{H}^{-1}\underset{\sim}{G}$ = element elastic stiffness matrix. (12a)

$\Delta\underset{\sim}{Q}$ = incremental element external load vector. (12b)

$\underset{\sim}{R}^o = \underset{\sim}{Q}^o - \underset{\sim}{F}^o$ = equivalent element load vector corresponding to the equilibrium imbalance correction. (12c)

The vector $\underset{\sim}{Q}^f$ is the equivalent element load vector corresponding to the fictitious

initial stress and differs for the two functionals:

$$\underset{\sim}{Q}^f = \underset{\sim}{G}^T \underset{\sim}{H}^{-1} \underset{\sim}{F}^I \qquad \text{for } \Pi_{mc}^I \tag{13a}$$

$$\underset{\sim}{Q}^f = \underset{\sim}{F}^{II} \qquad \text{for } \Pi_{mc}^{II} \tag{13b}$$

Following the usual assembly operations, the stationary condition of Π_{mc} yields the following system of equations, written for the ith increment (from applied load i-1 to applied load i):

$$\underset{\sim}{K}\, \Delta \underset{\sim}{q}_i^* = \Delta \underset{\sim}{Q}_i^* + \underset{\sim}{Q}_i^{f*} + \underset{\sim}{R}_i^{o*} \tag{14}$$

where the starred ( )* quantitites refer to the assembed system and $\underset{\sim}{K}$ is the global elastic stiffness matrix.

To solve equations (14), $\underset{\sim}{K}$ is factored prior to the first load increment, after which $\Delta \underset{\sim}{q}_i^*$ can be calculated at each increment by the forward/backward substitution operations. Note that $\underset{\sim}{Q}_i^{f*}$ is not known for the ith increment, but can be extrapolated or estimated from data at the previous increment. In the present applications $\underset{\sim}{Q}_i^{f*} = \underset{\sim}{Q}_{i-1}^{f*}$ is used in conjunction with iteration within a load increment. The equilibrium correction vector, $\underset{\sim}{R}_i^{o*}$, is calculated from the total stresses and total external load at the beginning of an increment, which are known.

3. Elastic-Plastic Material Relations

The effects of material nonlinearity are incorporated in the fictitious initial stress, $\underset{\sim}{\sigma}^f$. In order to calculate $\underset{\sim}{\sigma}^f$, the correct "elastic-plastic" stress increment, $\Delta \underset{\sim}{\sigma}_{ep}$, corresponding to an increment in total strain, $\Delta \underset{\sim}{\varepsilon}$, is required (Figure 1). This relation is given by

$$\Delta \underset{\sim}{\sigma}_{ep} = \underset{\sim}{D}_{ep}\, \Delta \underset{\sim}{\varepsilon} \tag{15}$$

where $\underset{\sim}{D}_{ep}$ is termed the elastic-plastic material matrix.

The matrix $\underset{\sim}{D}_{ep}$ is determined from the flow theory of plasticity, assuming a yield surface $F(\underset{\sim}{\sigma},\kappa) = 0$ and an associated flow rule. It can be shown that [e.g. 5, 11]

$$\underset{\sim}{D}_{ep} = \underset{\sim}{D} - \underset{\sim}{D}\left(\frac{\partial F}{\partial \underset{\sim}{\sigma}}\right)\left(\frac{\partial F}{\partial \underset{\sim}{\sigma}}\right)^T \underset{\sim}{D} \left[E_t^P + \left(\frac{\partial F}{\partial \underset{\sim}{\sigma}}\right)^T \underset{\sim}{D}\left(\frac{\partial F}{\partial \underset{\sim}{\sigma}}\right)\right]^{-1} \tag{16}$$

where $\underset{\sim}{D}$ is the elasticity matrix ($\underset{\sim}{\sigma} = \underset{\sim}{D}\,\underset{\sim}{\varepsilon}$) and E_t^P is the slope of the equivalent stress versus equivalent plastic strain curve. $\underset{\sim}{D}_{ep}$ is symmetric and positive definite and equation (16) is valid also for elastic, perfectly-plastic materials (i.e. $E_t^P = 0$). Note also that $\underset{\sim}{D}_{ep}$ is stress-history dependent and must therefore be evaluated for each sampling station at each incremental step.

In the present analysis, the Huber-Mises-Hencky initial yield criterion is adopted. For 3-D stress states (as in the plate elements to be used here), the yield surface is:

$$F(\underset{\sim}{\sigma},\kappa) = \frac{1}{\sqrt{2}}\left[(\sigma_x - \sigma_y)^2 + (\sigma_x - \sigma_z)^2 + (\sigma_y - \sigma_z)^2 + 6\sigma_{xy}^2 + 6\sigma_{xz}^2 + 6\sigma_{yz}^2\right]^{1/2} - \bar{\sigma}_o = 0 \tag{17}$$

and therefore

$$\frac{\partial F}{\partial \underset{\sim}{\sigma}} = \frac{1}{\bar{\sigma}_o}\begin{bmatrix} 1 & -1/2 & -1/2 & 0 & 0 & 0 \\ -1/2 & 1 & -1/2 & 0 & 0 & 0 \\ -1/2 & -1/2 & 1 & 0 & 0 & 0 \\ 0 & 0 & 0 & 3 & 0 & 0 \\ 0 & 0 & 0 & 0 & 3 & 0 \\ 0 & 0 & 0 & 0 & 0 & 3 \end{bmatrix} \underset{\sim}{\sigma} \tag{18}$$

where $\bar{\sigma}_o$ is the uniaxial yield stress.

The examples considered herein assume elastic, perfectly-plastic material behavior. For strain hardening materials, various mathematical models [e.g. 17-19] could be incorporated.

4. Calculation of Equivalent Element Loads

The expressions for the equivalent element loads, $\underset{\sim}{Q}^f$ and $\underset{\sim}{F}^o$, require the distributions of $\underset{\sim}{\sigma}^f$ and $\underset{\sim}{\sigma}^o$ which, in the plastic range, can only be determined numerically. Thus, $\underset{\sim}{Q}^f$ and $\underset{\sim}{F}^o$ are evaluated using a numerical integration rule (Gauss quadrature in the present case) so that $\underset{\sim}{\sigma}^f$ and $\underset{\sim}{\sigma}^o$ (and appropriate matrices) are evaluated at numerical integration stations. A flow chart indicating the steps required for $\underset{\sim}{Q}^f$ and $\underset{\sim}{F}^o$ for an element and for both Π^I_{mc} and Π^{II}_{mc} is given in Figure 2. Note that steps unique to Π^I_{mc} or Π^{II}_{mc} have been prefaced by "I" or "II", respectively; otherwise the steps are identical for both functionals.

A comparison of the two precedures shows that Π^I_{mc} requires more core storage (both $\underset{\sim}{H}^{-1}\underset{\sim}{G}$ and $\underset{\sim}{H}^{-1}$ must be stored for each element) and more operations. As a rough benchmark estimate of the relative computation times required for the evaluation of $\underset{\sim}{Q}^f$ and $\underset{\sim}{F}^o$ for Π^I_{mc} and Π^{II}_{mc} (for one element), the number of multiplications required for the matrix operations in Figure 2 can be determined. Table 1 gives the multiplication counts for each of the operations in Figure 2; note that it has been assumed that all matrix operations are done in full without accounting for symmetry or zeroes. Summing the contributions, and ignoring the equilibrium correction, the total multiplications (for one element), M^I and M^{II}, for Π^I_{mc} and Π^{II}_{mc}, respectively, are:

$$M^I = 3n_3n_q + n_xn_yn_zn_s \left\{ n_s + n_3 + \alpha(3n_s^2 + 3n_s + n_3) \right\} \tag{19a}$$

$$M^{II} = n_3n_q + n_xn_yn_zn_s \left\{ n_s + n_3 + \alpha(3n_s^2 + 2n_s + n_q) \right\} \tag{19b}$$

where α is the ratio of the number of integration stations per element at which yielding occurs to the total number of integration stations per element. The remaining parameters have been defined in Table 1. These expressions will be used later to compare various solution strategies. Further discussion of the alternate functionals and solution procedures is found in Reference [5].

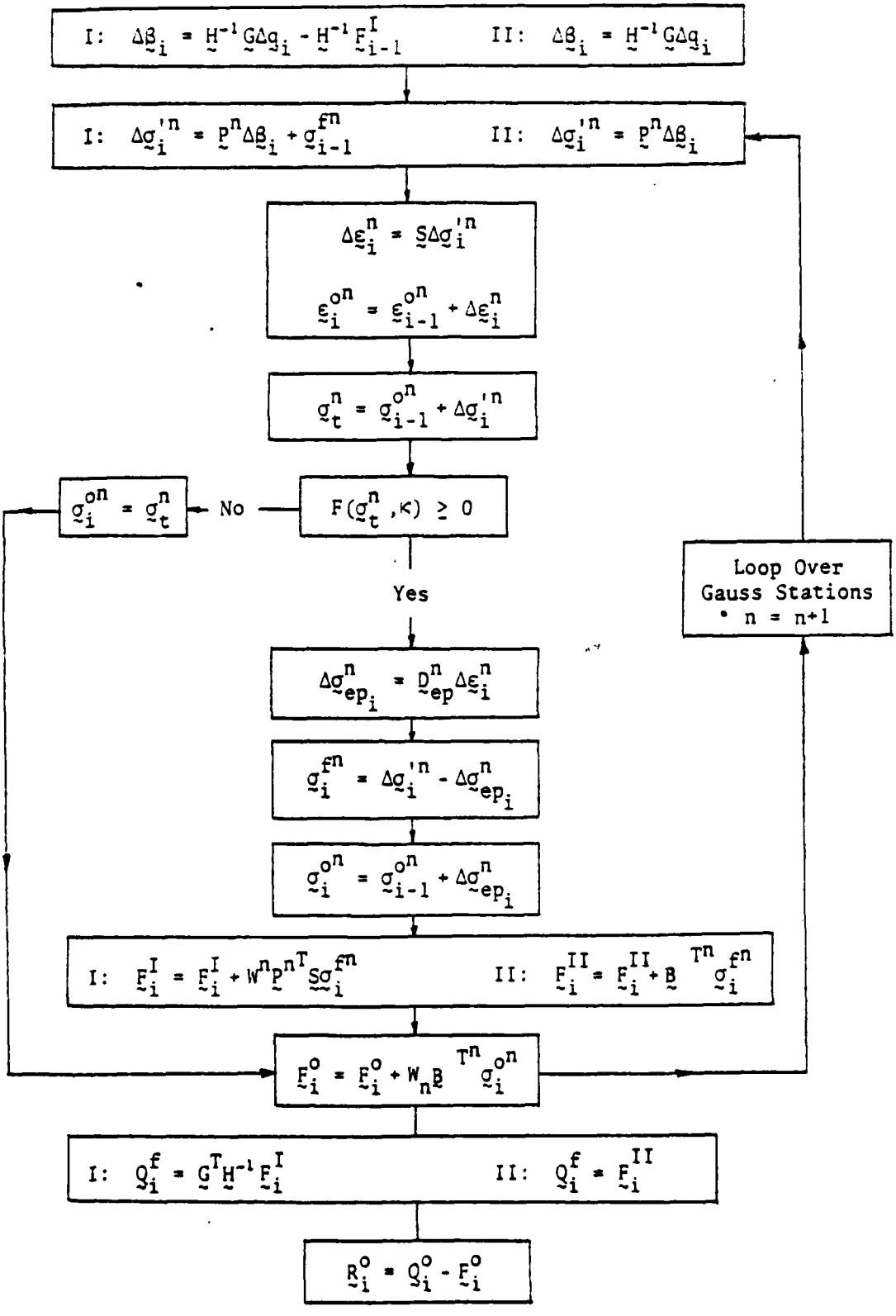

Figure 2. Flow chart for the calculation of equivalent loads for an element. Note that subscript t implies a temporary quantity.

Table 1. Benchmark multiplication counts per element for the evaluation of the equivalent load vector corresponding to material nonlinearity.

	Computations	Π^{I}_{mc}	Π^{II}_{mc}
	$\Delta\underset{\sim}{\beta}$	$2n_\beta n_q$	$n_\beta n_q$
At each integration station	$\Delta\underset{\sim}{\sigma}'$	$n_s n_\beta$	$n_s n_\beta$
	$\Delta\underset{\sim}{\varepsilon}$	n_s^2	n_s^2
	$\underset{\sim}{D}_{ep}$ (1)	$3n_s^3$	$3n_s^3$
	$\Delta\underset{\sim}{\sigma}_{ep}$ (1)	n_s^2	n_s^2
	$\underset{\sim}{F}^{I,II}$ (1)	$n_s^2 + n_s n_\beta$	$n_s n_q$
	$\underset{\sim}{Q}^{f}$	$n_q n_\beta$	———

(1) These computations are necessary only if yielding occurs at that station.

Legend:

n_β = number of β's per element.

n_q = number of degrees of freedom per element.

n_s = number of stress components.

n_z = number of z integration stations.

n_x = number of x (or ξ) integration stations.

n_y = number of y (or η) integration stations.

Finally it should be noted that the operations and computation time when using the assumed-displacement model with the initial-stress approach [11] is roughly equivalent to that required for Π_{mc}^{II} [5].

5. Iteration Schemes

Typically, nonlinear schemes make use of a combination of load increments with iteration within each load increment cycle. In the present study, two alternate iteration schemes are used. In both, equation (14) is first solved for Δq_i^* corresponding to an applied increment in external load and including any fictitious forces, Q^{f*}, remaining from the previous step and, if desired, the load corresponding to equilibrium imbalance. In the first iteration scheme, a series of iterations, governed by the equation (for the kth iteration within the ith external loading increment).

$$K \Delta q_k^* = Q_{k-1}^{f*} \tag{20}$$

are performed until the equivalent load corresponding to the fictitious initial stress is sufficiently small; ie. until

$$\frac{\left|Q_{k-1}^{f*}\right|}{\left|Q_o^{f*}\right|} \leq \text{RCONV} \tag{21}$$

where RCONV is a small parameter (e.g. 0.01), $|(\ )|$ denotes the magnitude (squared) of the vector ( ), and Q_o^{f*} corresponds to the equivalent load vector prior to the first iteration (computed for the applied external load increment). This scheme is termed iteration scheme A, and is depicted for a one-dimensional stress-strain curve in Figure 3a. Note that displacments, stresses, and strains are continually updated during the iteration cycle. When equation (21) is satisfied, the solution proceeds with equation (14) for the next increment in external loading.

Scheme A has been applied to both Π_{mc}^{I} and Π_{mc}^{II} in Reference [5,7]+.

+ Note that equation (36) in Reference [11] is incorrectly stated and should correspond to the present equation (21).

However, it is believed that scheme A is best suited for Π_{mc}^{II}, as verified in the studies of [5,7]. In those studies, the use of Π_{mc}^{I} and scheme A yielded poor predictions of strain. From Figure 3a, it is apparent that, with Π_{mc}^{II}, $\underset{\sim}{\sigma}^f$ must vanish in order for the assumed stress increment, $\Delta\underset{\sim}{\sigma}$, to be equal to the actual stress increment, $\Delta\underset{\sim}{\sigma}_{ep}$. In addition, from equation (5), $\underset{\sim}{\sigma}^f = 0$ is required if $\Delta\underset{\sim}{\sigma}_{ep}$ is to satisfy equilibrium. In contrast, from Figure 1 and equation (4) for Π_{mc}^{I}, it is observed that $\underset{\sim}{\sigma}^f = 0$ is not required in order for the interpolated stress $\Delta\underset{\sim}{\sigma}$ to be equal to the actual stress, $\Delta\underset{\sim}{\sigma}_{ep}$, and therefore $\Delta\underset{\sim}{\sigma}_{ep}$ to satisfy equilibrium.

An alternate iteration scheme, termed scheme B [5,7], would therefore appear to be more appropriate for Π_{mc}^{I}. In this scheme, the equation governing the kth iteration within the ith external loading increment is

$$\underset{\sim}{K}\,\Delta\underset{\sim}{q}_k^* = \Delta\underset{\sim}{Q}_i^* + \underset{\sim}{Q}_{k-1}^{f*} \tag{22}$$

where $\underset{\sim}{Q}_o^{f*}$ (i.e. k=1) is zero. This scheme (see Figure 3b for an illustrative 1-D case) seeks to satisfy the condition

$$\underset{\sim}{\sigma}_k^f = \underset{\sim}{\sigma}_{k-1}^f \tag{23}$$

which, if satisfied, implies that

$$\Delta\underset{\sim}{\sigma}_i = \Delta\underset{\sim}{\sigma}_{ep_i} \tag{24}$$

for the ith external loading increment. The iteration process is determined to be converged when

$$\frac{\left|\underset{\sim}{Q}_k^{f*} - \underset{\sim}{Q}_{k-1}^{f*}\right|}{\left|\underset{\sim}{Q}_k^{f*}\right|} \leq \text{RCONV} \tag{25}$$

is satisfied. In scheme B, total displacements, stresses, and strains are updated only after equation (25) is satisfied, using the incremental quantities computed

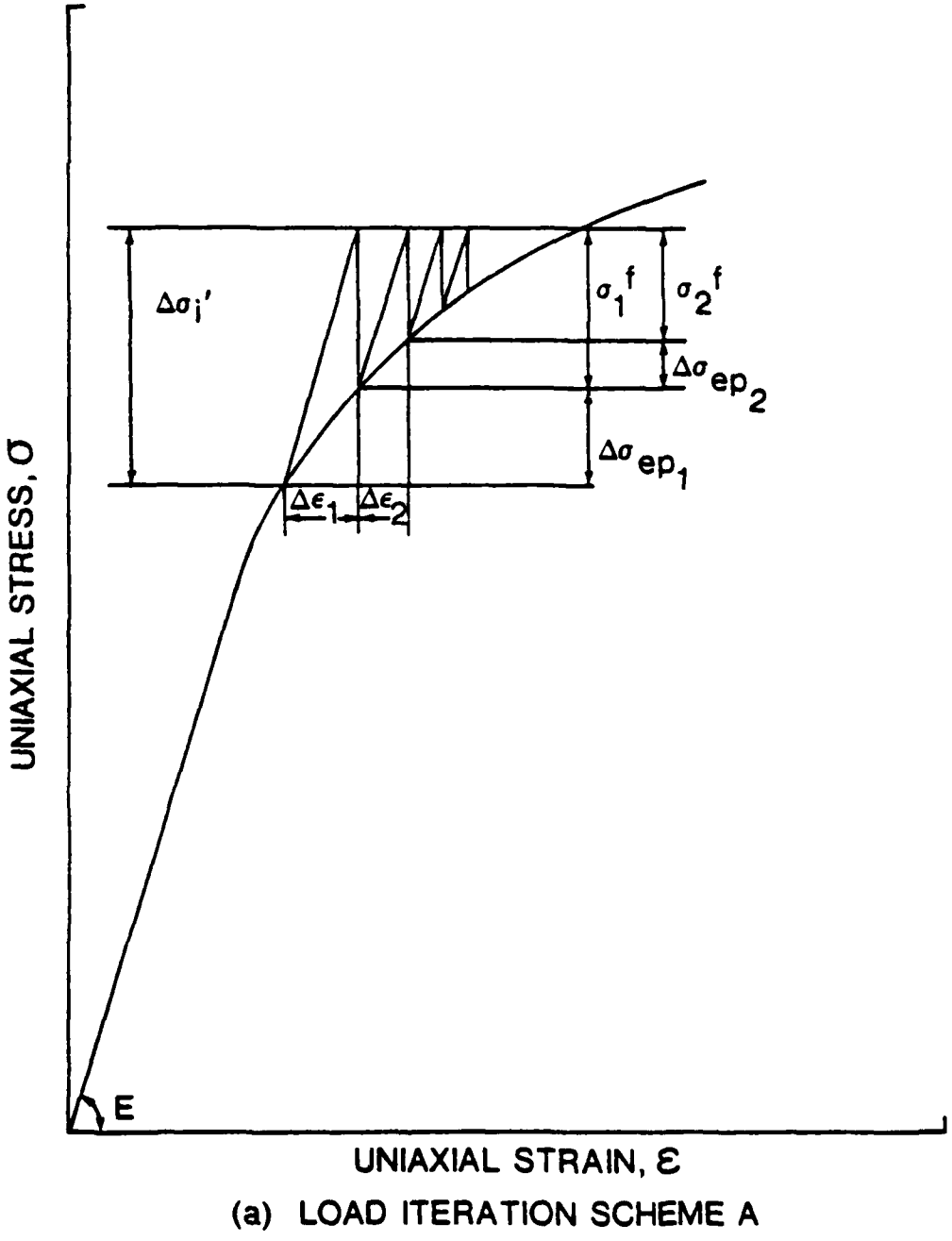

Figure 3. Schematic 1-D representation of iteration schemes A and B.

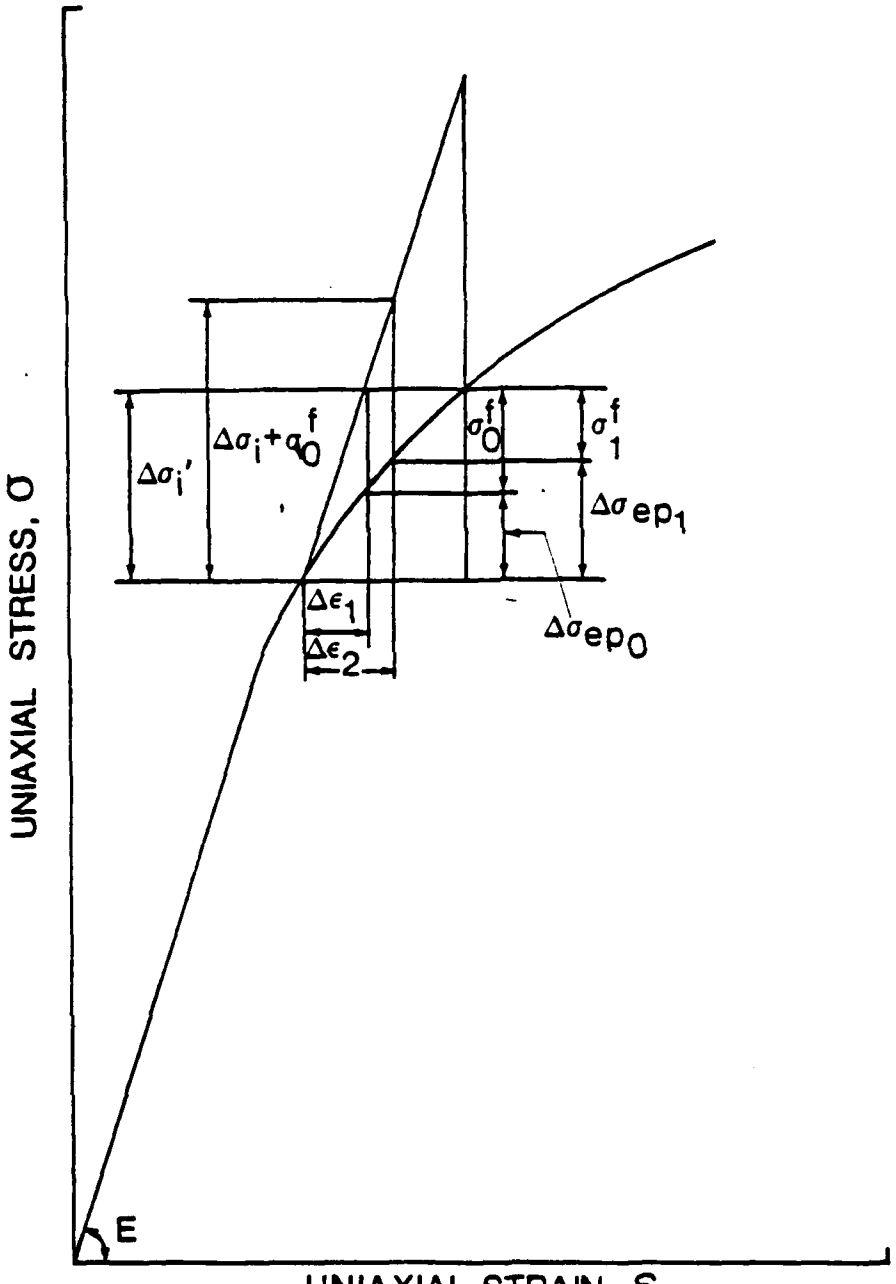

(b) LOAD ITERATION SCHEME B

Figure 3. (concluded)

for the final iteration step.

An advantage of scheme B with Π^I_{mc} is that, in view of equation (24), total stresses may be updated using $\Delta\underset{\sim}{\sigma}$. Since $\Delta\underset{\sim}{\sigma}$ satisfies equilibrium, the total stress, $\underset{\sim}{\sigma}^o$, will be in equilibrium and no equilibrium imbalance correction is needed. If $\underset{\sim}{R}^o$ can be ignored, no interior displacement field need be defined when using Π^I_{mc}. This is particularly important for elements requiring C^1 continuity, but is of no real consequence for C^o continuity elements (as in the present application).

6. Description of Plate Elements

The plate elements to be used are taken from a recently-developed family (4,8, and 12 node) of hybrid-stress plate elements [14-16]. The elements utilize independent interpolations for the transverse displacement, w, and cross-section rotations, θ_x and θ_y, so that any of the C^o continuity families of shape functions may be used (in these cases, the Serendipity shape functions). In general, all components of stress are included, allowing for the analysis of moderately-thick plates.

Results presented in References 14-16 show these elements to yield comparable or superior results when compared to the analogous assumed-displacement plate element (also based on a Mindlin-type displacement behavior and utilizing reduced or selective-reduced integration). Each of the hybrid-stress elements of this family has a stiffness of correct rank (i.e. no spurious zero energy modes) and the elements will not 'lock' for arbitrarily thin plates, independent of machine precision used.

Comparisons made in Reference 16 suggest that the 8-node and 12-node elements are the more accurate per degree-of-freedom in the assembled structure. However, 12-node elements may be impractical for general applications. Also, for nonlinear analyses, where computation time is strongly dependent on element-level operations, the 4-node element may be preferred. In the present study, both the 4- and 8-node elements will be used (with most emphasis on the 4-node element).

The elements, both of which allow for isoparametric planforms, are shown in Figure 4. Briefly, the 4-node element (termed LH4 [14]), contains 12 degrees of free-

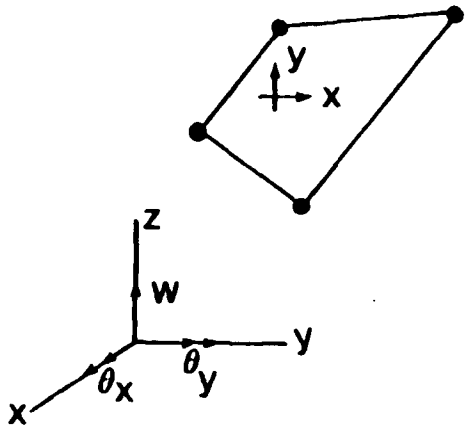

W_i, θ_{x_i}, θ_{y_i} at each node.
n_g=12
n_β=11
No spurious zero energy modes.

(a) ELEMENT LH4

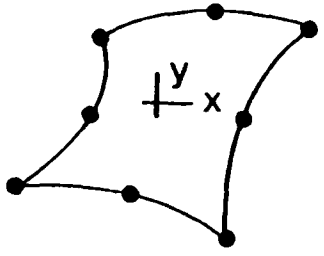

W_i, θ_{x_i}, θ_{y_i} at each node.
n_g=24
n_β= 22
No spurious zero energy modes

(b) ELEMENT QHI

Figure 4. Summary of plate elements LH4 and QH1.

dom and is based on a 11β stress field (bilinear x,y variation for inplane stresses). Note that $\sigma_z = 0$ in LH4. The 8-node element (termed QH1 [15]), contains 24 degrees-of-freedom and is based on a 23β stress field (bicubic x,y variation for inplane stresses) with $\sigma_z \neq 0$.

It is important to observe that a criticism [8] of Π_{mc}^{II} for plate analyses - - - the requirement of an interior displacement field yielding C^1 interelement continuity - - - is no longer valid. The interior displacement fields for the present plate elements (C^o continuity) are easily constructed, and Π_{mc}^{II} does not present any formulation or computational difficulties.

7. Example Problems and Numerical Results

The problem of a simply-supported thin beam subjected to a uniformly distributed transverse load of magnitude, P, has been chosen as a first test. An analytic solution for this problem is available [20] under the assumption of elastic, perfectly-plastic material behavior. Here, the beam length is 10.0 in, depth is 1.0 in., thickness is 0.1 in. The elastic material constants are $E = 10^7$ psi, and $\nu = 0.3$, with a uniaxial yield stress of 10^4 psi. First yielding will occur at the beam center at a load of 1.33 psi, and the fully-plastic load is $P_{FP} = 2.0$ psi.

For initial comparisons, the 4-node plate element, LH4 [14], is used and half of the beam span is modelled by a mesh of NDX by NDY equal-sized elements (see Figure 5).

For a given functional, effects of various parameters can be examined; these include iteration scheme (A or B), number of equal-size load increments in the load range from initial to full plasticity, NINC (i.e. the load corresponding to first yield, P=1.33 psi, is applied first, after which increments in load corresponding to ΔP=(2.0-1.33)/NINC are applied. Loading ceases at the theoretical fully plastic load), convergence ratio, RCONV, maximum number of iteration permitted per load step, MAXIT, mesh size (NDX, NDY), and integration stations for computing the equivalent loads (NGX,NGY,NGZ). Unless otherwise stated, NDX = 4, NDY = 1 is used;

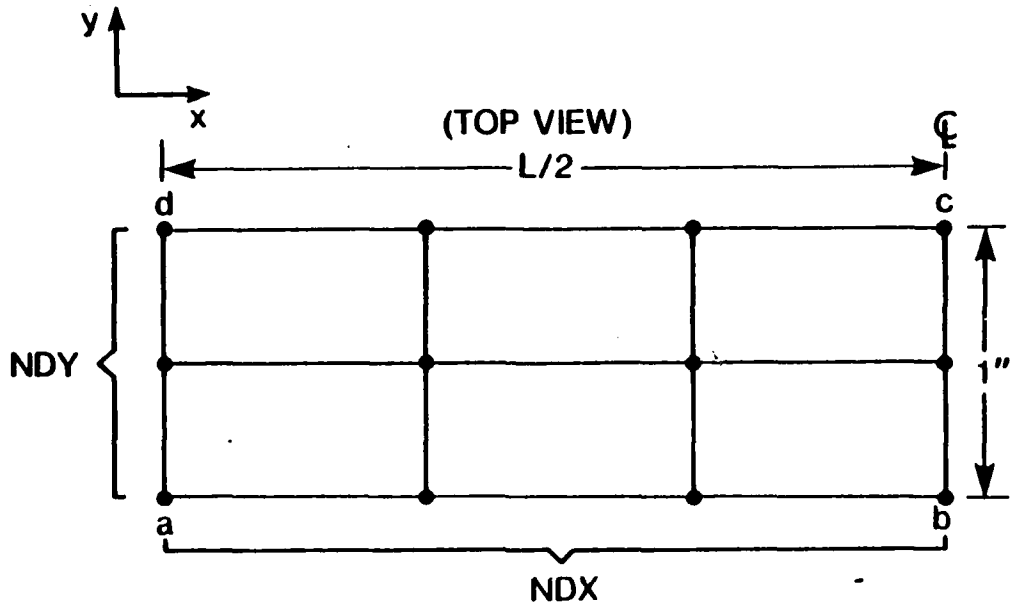

BOUNDARY CONDITIONS:

W=0 along ad

θ_y=0 along bc

θ_x=0 along ad

LOADING: UNIFORM LOAD

NDX: Number of Divisions in x direction.

NDY: Number of Divisions in y direction.

Figure 5. Geometry, mesh, and boundary conditions for the example problem of a simply-supported beam (modeled by plate elements) subject to uniform load.

remaining parameters are defined on each figure. In all cases, the predicted normalized center transverse displacement (normalized by the center deflection at first yield) versus the applied load (normalized by the fully-plastic load, P_{FP}) is compared with the analytic result. In a first series of tests, only Π_{mc}^{II} will be used (determined to be the superior functional in [5,7]). In all cases the equilibrium imbalance correction is included and iteration scheme A is used.

The effects of NINC (number of load steps from first to full plasticity) is shown in Figure 6 where MAXIT = 1 so that no iteration is used. Decreasing load step sizes lead to an improved response, particularly near the fully-plastic load. The effects of maximum permitted iterations per load step, MAXIT, for load increments NINC = 8,4, and 2 are shown in Figures 7a through 7c, respectively. In each case, MAXIT = 1 (no iteration), 10 and 20 are used. For smaller load steps (NINC = 8, Figure 7a), iteration has a major effect only near the fully plastic load; however, increasing MAXIT from 10 to 20 has no effect on the solution. For increasing load step size (NINC = 4, Figure 7b), MAXIT has a greater effect and differences are observed between MAXIT = 10 and 20. For large load steps (NINC = 2, Figure 7c), solutions are poor even when MAXIT = 20.

The effects of convergence ratio, RCONV, are shown in Figure 8 for NINC = 4 and MAXIT = 20; a value of RCONV = .01 has been used previously. Increasing RCONV to .1 has a discernable effect at all load levels, whereas decreasing RCONV to .001 produces significant effects only for the last load step. Arbitrary decreases in RCONV without a corresponding increase in MAXIT will not, in general, lead to a significantly improved solution as MAXIT will terminate the iteration cycle for load steps in severely nonlinear regions. For practical purposes, values of RCONV = .01 and MAXIT = 10 are believed to be adequate. Converging results can then be sought by increasing the number of load steps (smaller load increments).

The computation time required to compute the equivalent load vector is nearly proportional to the number of integration stations employed (see Table 1 and equation (19b)). The question of through-thickness and inplane stations can, however,

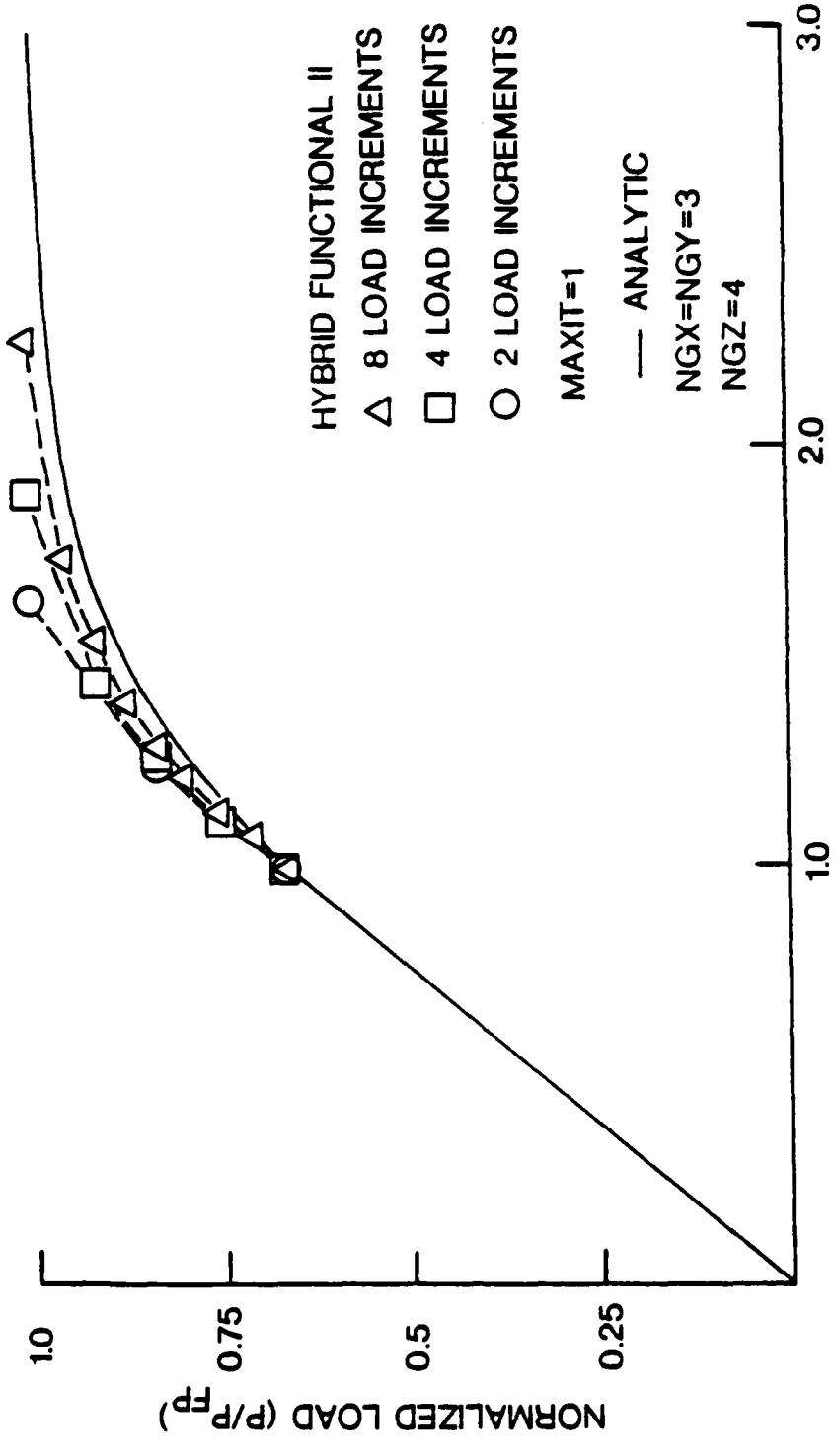

Figure 6. Effect of post-yield load step size for the beam problem.

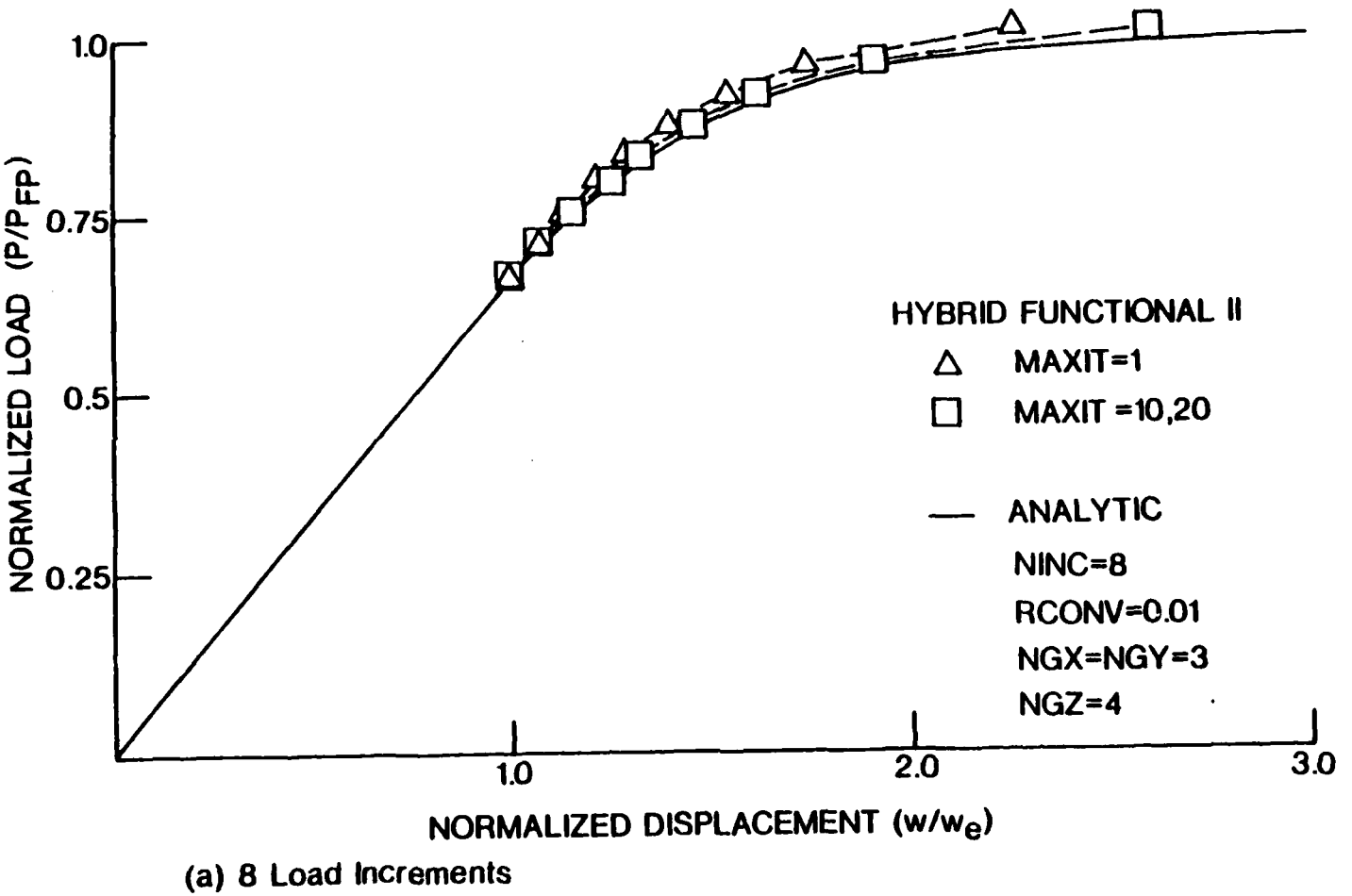

(a) 8 Load Increments

Figure 7. Effect of maximum permitted iterations per load step for the beam problem.

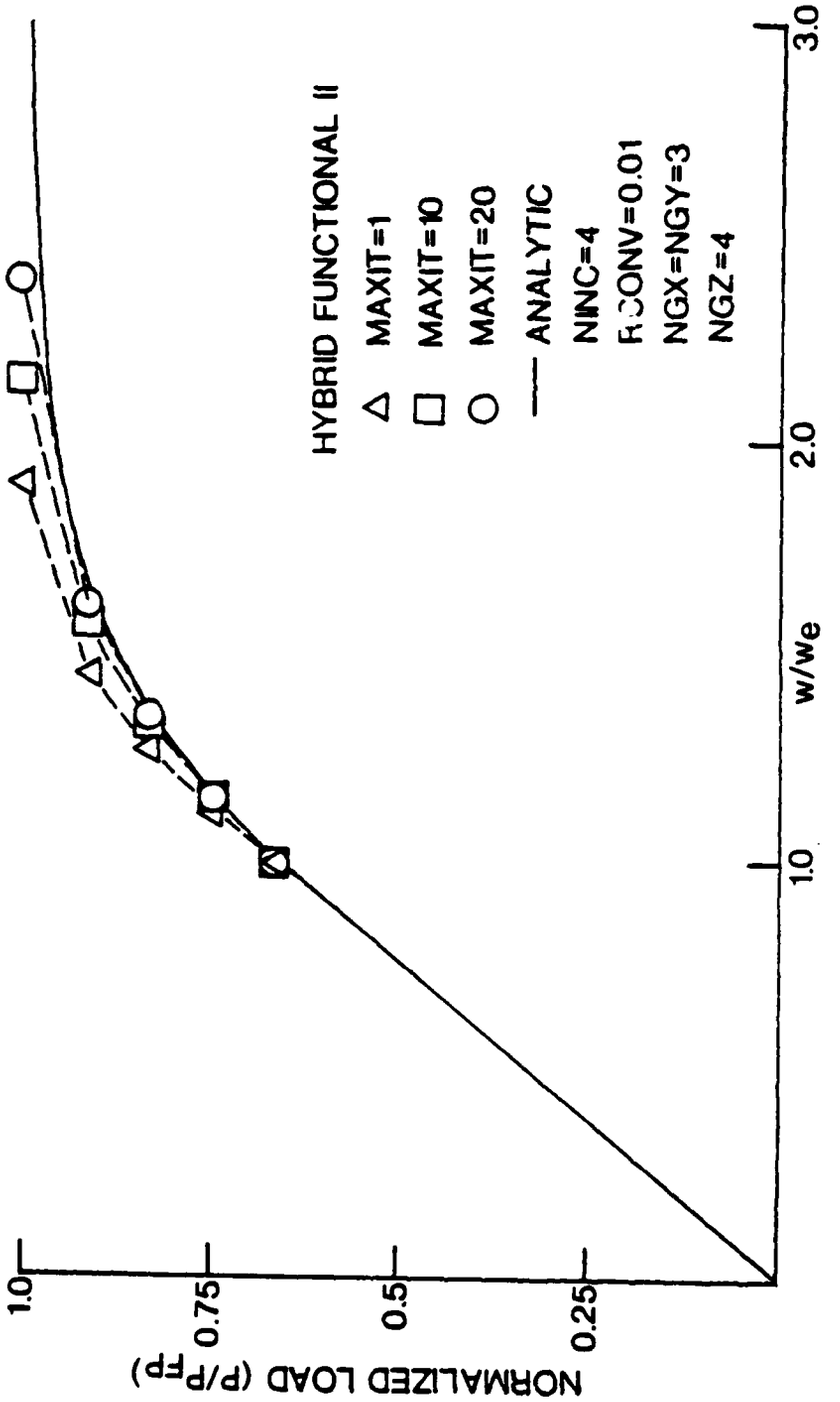

(b) 4 Load Increments

Figure 7 (continued)

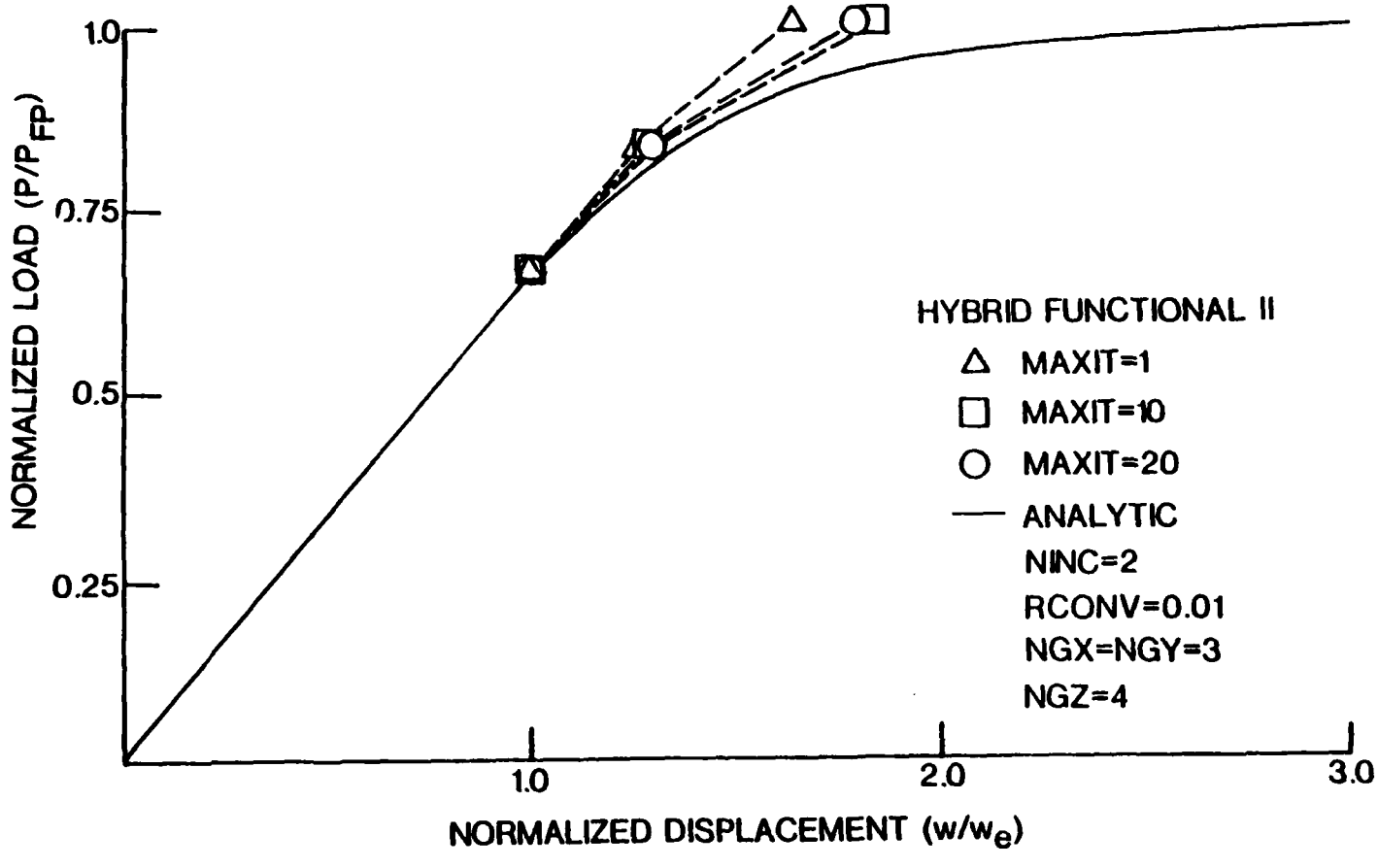

(c) 2 Load Increments

Figure 7 (concluded)

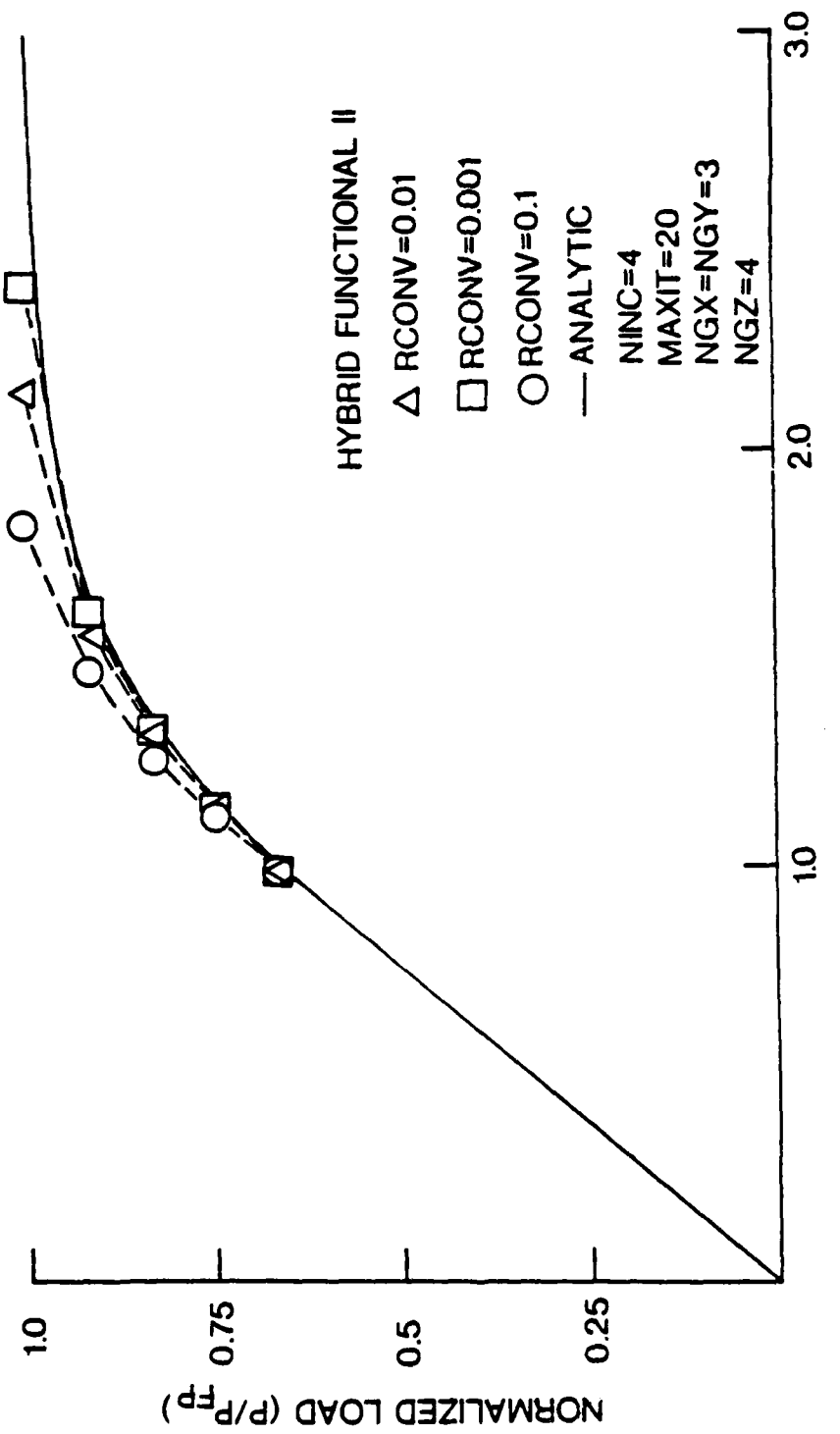

Figure 8. Effect of convergence tolerance parameter, RCONV, for the beam problem.

be examined independently. The through-thickness distributions used for all stress components in the present hybrid-stress plate elements should correspond to the 'exact' distributions for thin to moderately-thick plates in the linear elastic region. Yielding will, in general, initiate at and progress from the plate upper/lower surfaces, resulting in discontinuous through-thickness stress distributions (for σ_x, σ_y, and σ_{xy}). This, in principle, requires that increasing numbers of z integration stations be used (which therefore locates stations closer to the upper/lower surfaces). The effects of NGZ (number of z stations) are shown in Figure 9a where NGX=NGY=3 and NINC=4. Decreasing NGZ from 3 (used in all previous cases) to 2 severely stiffens the solution, whereas increasing from NGZ=3 to NGZ=4 produces only a slightly improved solution. In view of the increased computation time associated with NGZ=4 compared with NGZ=3 with only marginal improvement in the results obtained, the value NGZ=3 would appear to be the appropriate choice.

The selection of the number of inplane stations, NGX and NGY, is dependent on the accuracy of the predicted x-y intraelement stress distribution; i.e. there is no merit in sampling stresses (from which equivalent loads are calculated) at locations where predicted stresses may be severely in error. For assumed-displacement elements, optimal sampling points can be defined [e.g.21,22] and used. No such points have been rigorously defined for hybrid-stress elements; however, stress results given in [14] for linear analyses suggest that LH4 yields good intraelement stress predictions throughout the element, and therefore increasing NGX and NGY should produce improved results. Figure 9b shows the effects of NGX and NGY (for NGZ = 3). The results for NGX=NGY=3 are marginally improved compared with NGX=NGY=2. The solution for NGX=NGY=1 is slightly stiffer until the final load step where an excessively flexible solution is obtained; once this point is fully yielded, the entire element is assumed to be yielded and a mechanism forms producing the excessive flexibility. In view of the results obtained and computational considerations, NGX=NGY=2 is recommended.

The 1 point inplane integration can lead to acceptable results if a more refined

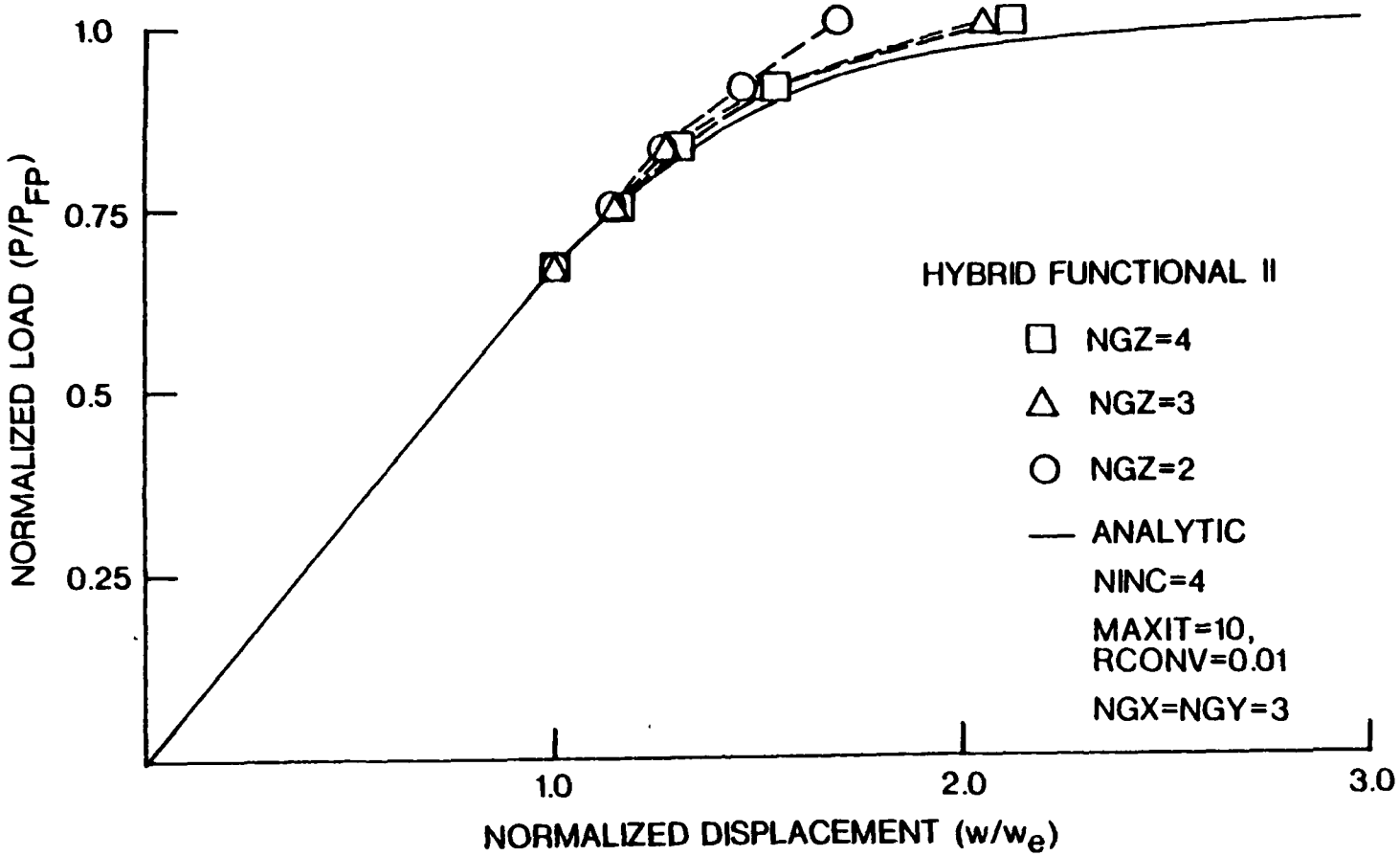

(a) Effects of Through-Thickness Integration Stations

Figure 9. Effect of the number of integration stations to compute the equivalent load vector for the beam problem.

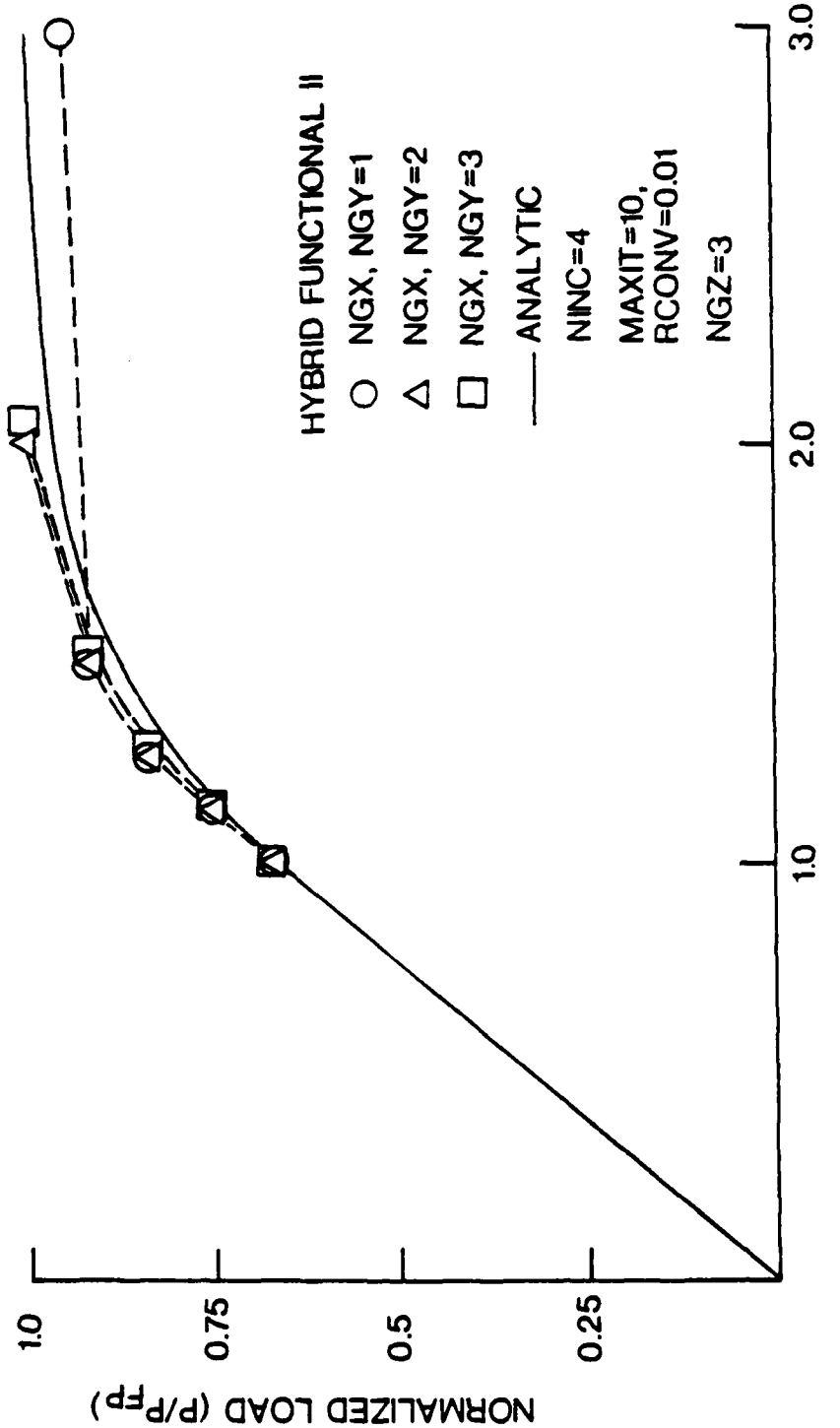

(b) Effects of Inplane Integration Stations

Figure 9 (concluded)

mesh is used, as shown in Figure 10. Using the NDX=4, NDY=1 case as a basis for comparison (with NGX=NGY=1), the excessive flexibility no longer appears when NDX=8, NDY=1 is used (note that a fully plastic zone has not yet been reached in this solution at $P=P_{FP}$). Increasing to NDX=8, NDY=2 shows a slight improvement.

Using the benchmark multiplication counts given in Table 1, total multiplications (for a load increment or iteration cycle, and a specified number of elements, assuming yielding occurs at all integration stations) have been computed for a number of cases of interest and are given in Table 2. Based on these benchmark counts, the use of a 2 by 2 block of elements with NGX=NGY=1 in each element should require a similar computational effort compared with 1 element and NGX=NGY=2. This is analogous to an 8x2 mesh with NGX=NGY=1 and a 4x1 mesh with NGX=NGY=2. Results for these two cases, shown in Figure 11, indicate that the first approach is superior, despite the fact that the predicted elastic center deflecion is nearly identical for both meshes. This improvement would therefore appear to correspond to superior stress accuracy at the element centroid compared with the 2x2 Gauss stations.

The results presented thus far have been obtained using Π_{mc}^{II}. Similar studies have been carried out using Π_{mc}^{I} which verify the general trends (with regard to NINC, MAXIT, RCON, and integration stations) observed for Π_{mc}^{II}. A more important consideration is the effect of iteration scheme. Figure 12a shows results obtained using iteration scheme A for a coarse load/iteration solution (NINC=4, MAXIT=1) versus a refined solution (NINC=8, MAXIT=10). In both cases, NDX=4, NDY=1, RCONV=.01, NGX=NGY=2, NGZ=3 are used. The coarse solution is stiff (as expected) whereas excessive flexibility is observed for the refined solution; the predicted center displacement exceeds the exact value for $P/P_{FP} > 0.75$. Such behavior is judged unacceptable and it would appear that iteration scheme A is not well suited to Π_{mc}^{I}. Note that further solution refinement (results not shown) leads to increased flexibility.

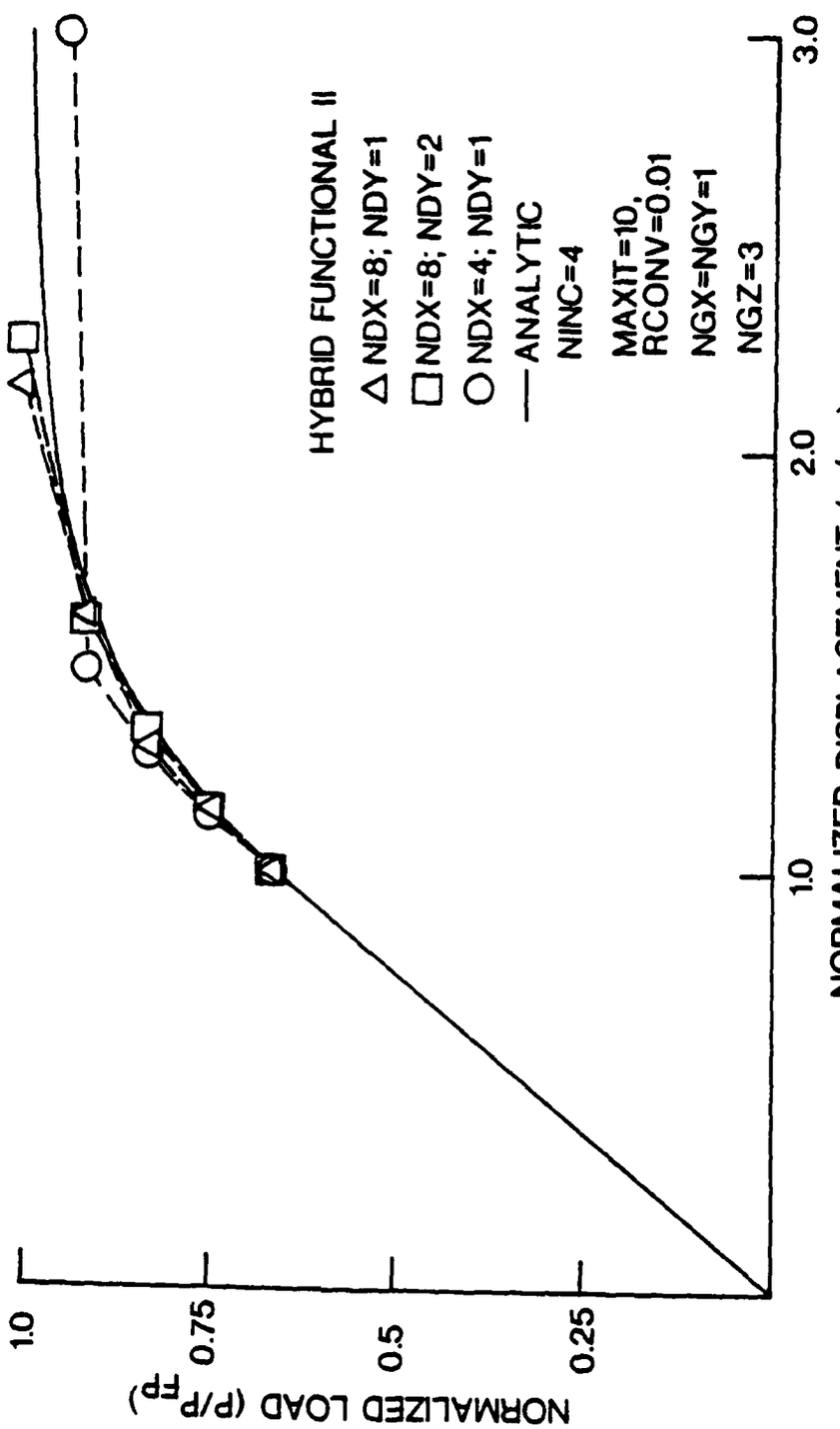

Figure 10. Effect of mesh, using a 1 point inplane integration, for the beam problem.

Table 2. Multiplication count comparisons for various cases of interest.

Functional (1)	Element (2)	n_s	n_x, n_y	n_z	#elems.(3)	Mults.
I	LH4	6	2	3	1	11,484
I	LH4	6	1	3	1	3,168
I	LH4	3	2	3	1	2,592
I	LH4	3	1	3	1	945
II	LH4	6	2	3	1	10,860
II	LH4	6	1	3	1	2,814
II	LH4	3	2	3	1	2,256
II	LH4	3	1	3	1	663
II	LH4	6	2	4	1	14,436
II	LH4	6	1	3	4	12,672
II	QH1	6	2	3	1	13,008
II	QH1	6	3	3	1	28,578
II	QH1	3	2	3	1	3,540

Notes: (1) "I" and "II" correspond to Π_{mc}^{I} and Π_{mc}^{II}, respectively.

(2) For element LH4, $n_q = 12$ and $n_\beta = 11$.
For element QH1, $n_q = 24$ and $n_\beta = 22$.

(3) Number of elements for which the equivalent load is computed. It is assumed that yielding occurs at all integration stations.

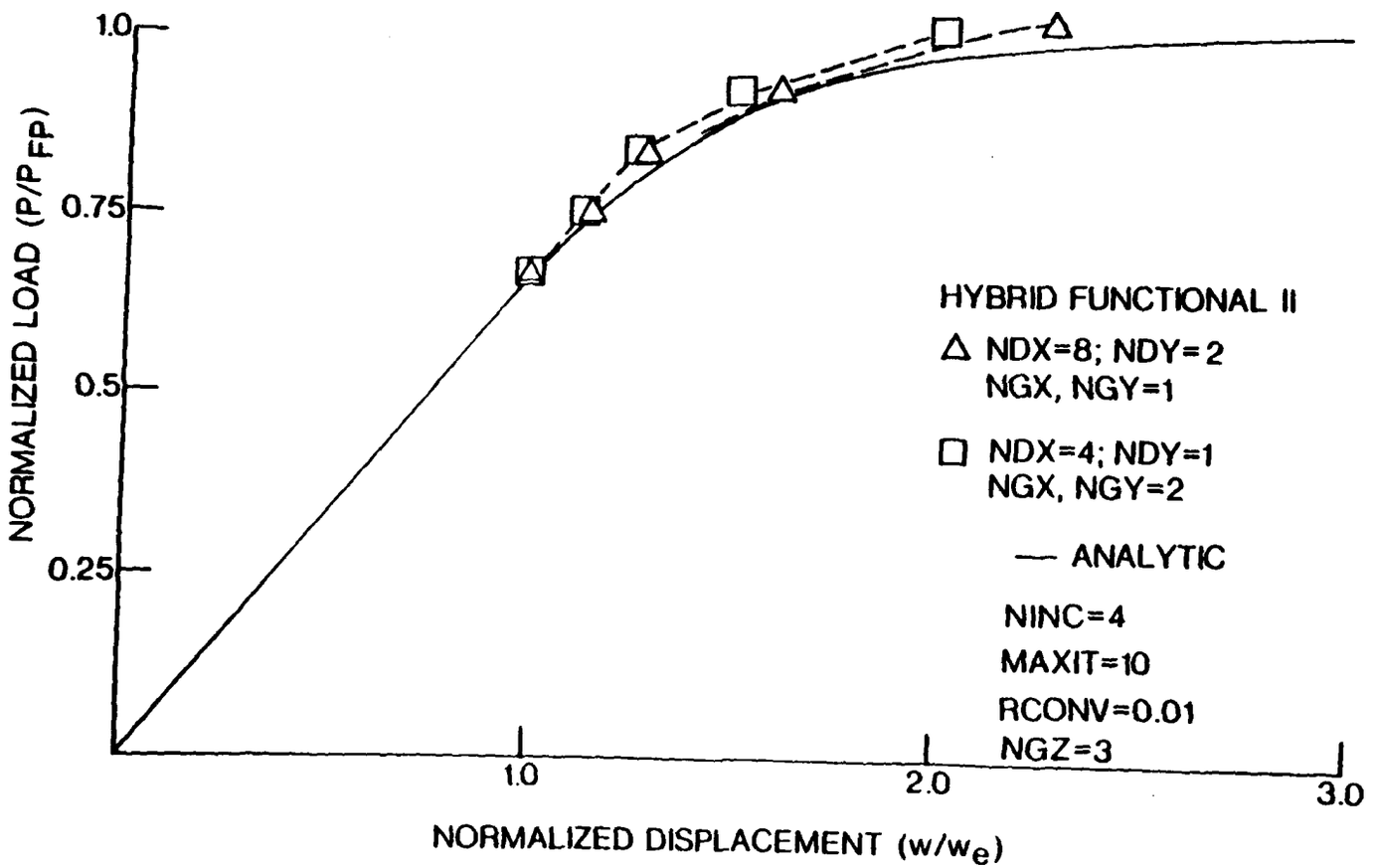

Figure 11. Comparison of alternate mesh/integration rule strategies for the beam problem.

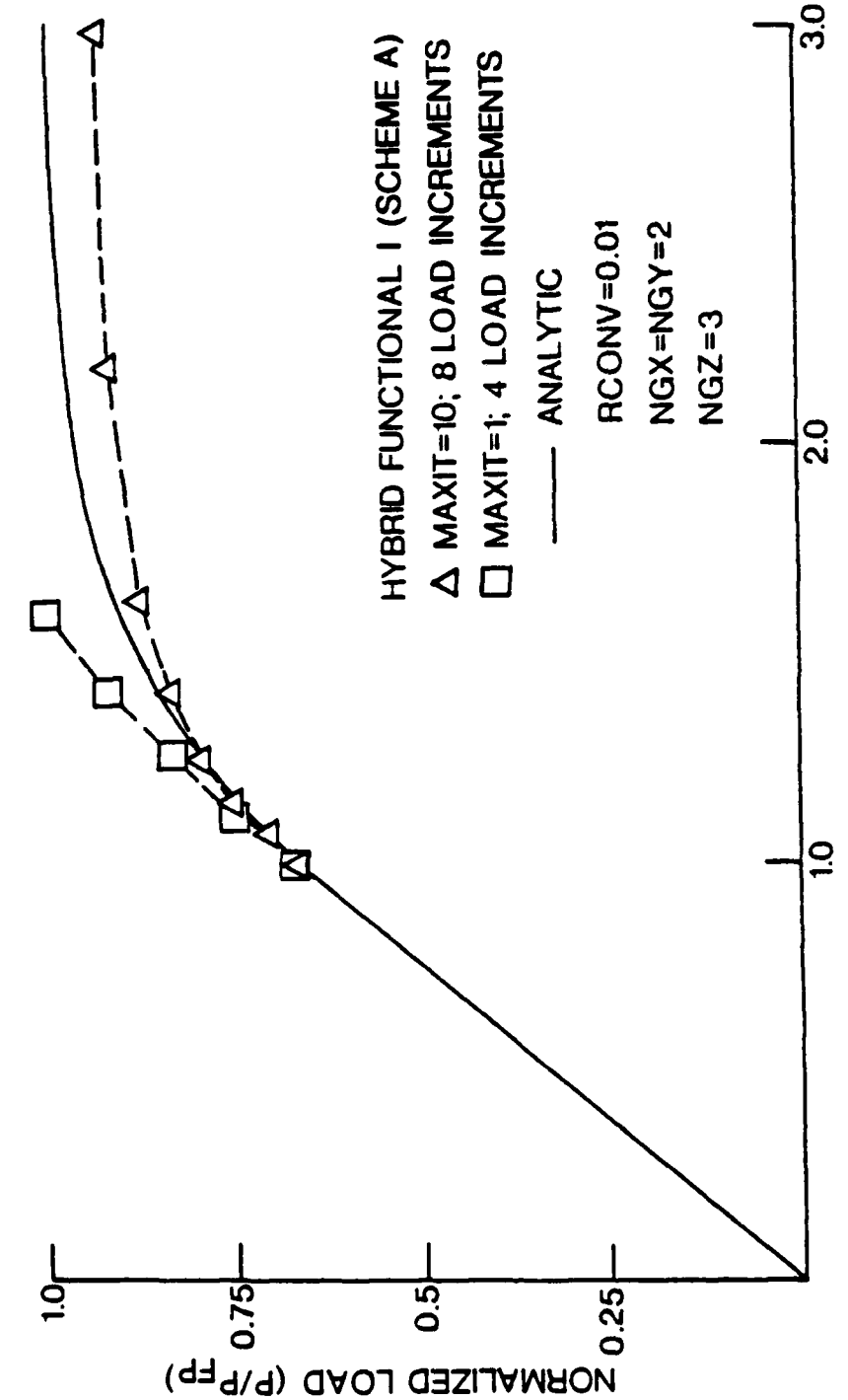

(a) Results using Iteration Scheme A

Figure 12. Beam example results obtained using hybrid functional I and iteration schemes A and B.

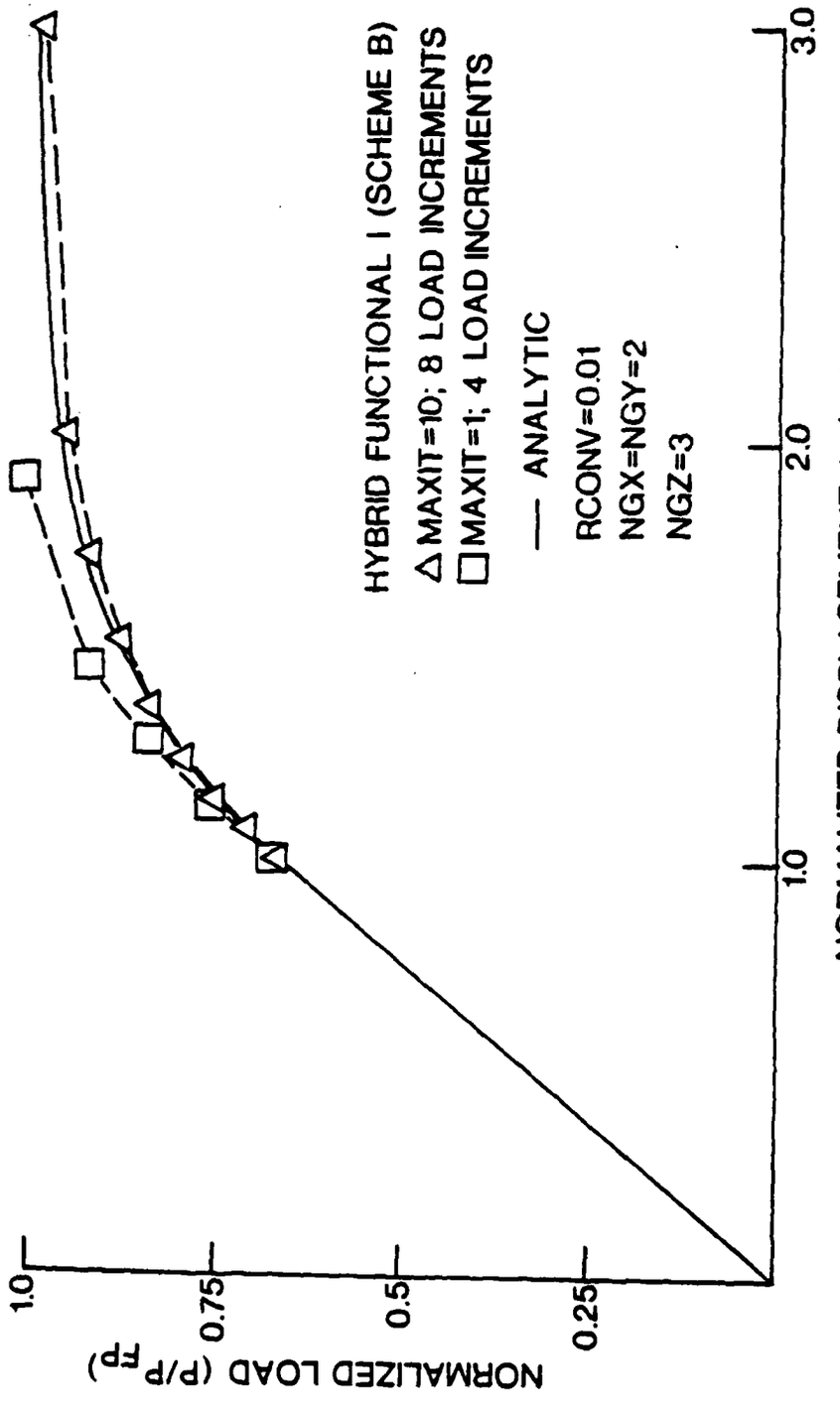

(b) Results using Iteration Scheme B

Figure 12 (concluded)

By comparison, results obtained by using Π^{I}_{mc} with iteration scheme B for the coarse and refined solutions are shown in Figure 12b. For the coarse solution, scheme B yields a more flexible solution compared with scheme A, whereas the refined solution by scheme B is stiffer than that of scheme A. The scheme B refined solution is in good agreement with the analytic solution, although slightly more flexible than the analytic solution, and is therefore the preferred scheme with Π^{I}_{mc}. Note that further refinement of the scheme B solution yields no discernable change.

A comparison of Π^{I}_{mc} with scheme B and Π^{II}_{mc} with scheme A for coarse and refined solutions is shown in Figure 13. Recall that for all cases, load has been applied only up to the theoretical fully-plastic load, P_{FP}. Thus, for example, the refined Π^{II}_{mc} run, which underestimates the displacements, would produce, effectively, infinite displacements by application of an additional small increment in external load beyond $P = P_{FP}$.

Both functionals (with an appropriate iteration scheme) appear to lead to convergence to the analytic solution. Such observations were also made in References 5 and 7 for axisymmetric structures. However, Π^{II}_{mc} requires less computation time per cycle; see References [5,7] and benchmark multiplication counts in Table 2. Therefore, Π^{II}_{mc} would again appear to be the preferred functional.

Before presenting results for a more general plate problem, several observations related to computation time should be made. In the cases considered here, all components of stress have been included (i.e. $n_s = 6$). For moderately thick plates, all components should be retained, whereas for thin plates σ_{xz}, σ_{yz}, and σ_z are negligible and could be ignored in the computation of equivalent loads. From Table 1, total multiplications are strongly influenced by the number of stress components retained, n_s, and for selected cases computed in Table 2, it is apparent that a reduction from $n_s = 6$ to $n_s = 3$ can lead to substantial reductions in multiplications (i.e. by a factor of 4-5 times). Results (not shown) for the beam problems (thin plate) show the two solutions ($n_s = 3,6$) to be essentially iden-

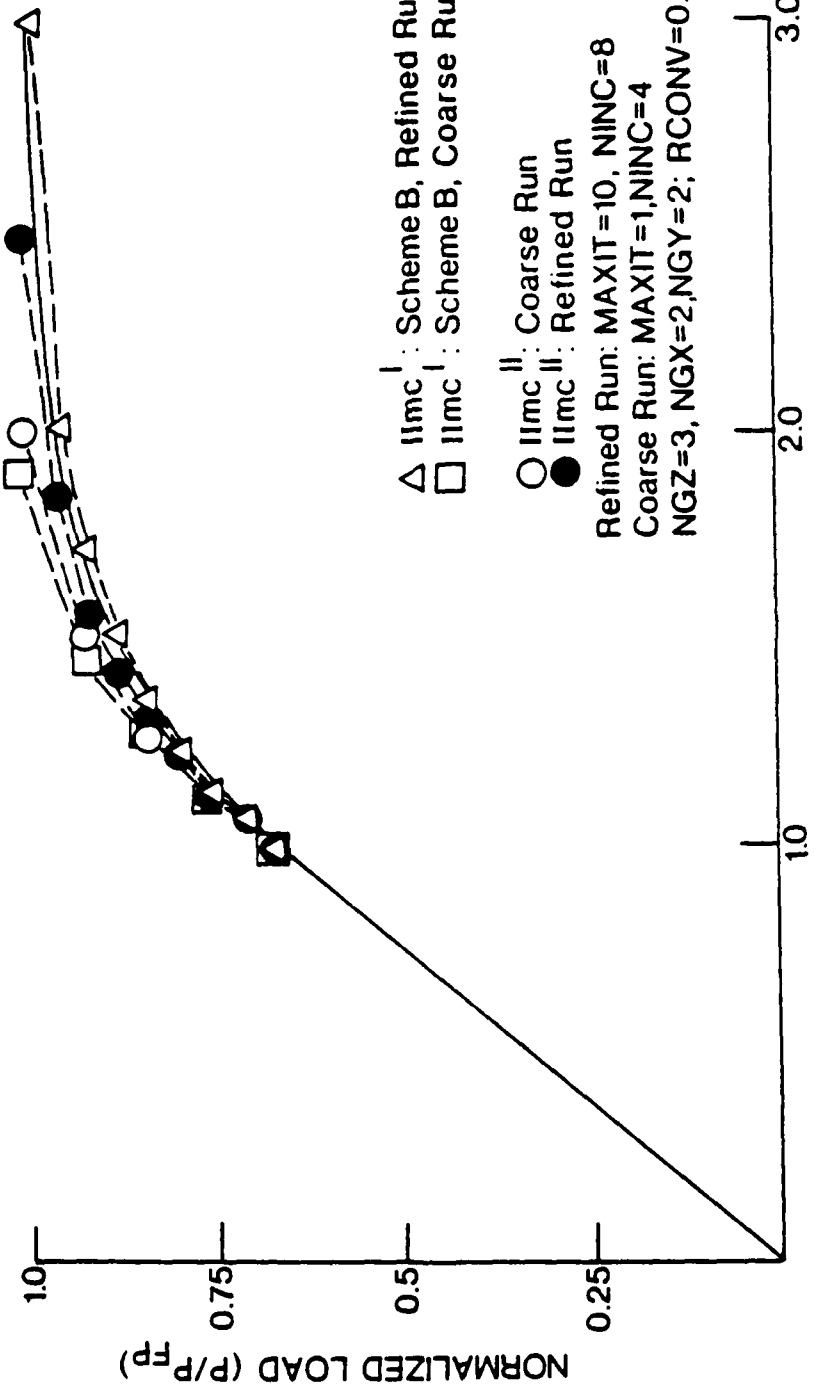

Figure 13. Comparison of results obtained using functional I with iteration scheme B against functional II with iteration scheme A for the beam problem.

tical.

Results presented also suggest that NGZ=3 is adequate for through-thickness integration. If the plate is thin so that $n_s = 3$ can be used, the remaining stresses $(\sigma_x, \sigma_y, \sigma_{xy})$ are zero at z=0, corresponding to the center integration station for NGZ=3, and this point can be skipped in the integration loop. The result is a reduction of multiplications by approximately 33%. Finally, it is noted that in the elastic-plastic plate analysis of Horrigmoe and Eidsheim [8], the yield surface has been expressed in terms of moments, thereby avoiding through-thickness numerical integration. There is no difficulty in adopting such a procedure with the present element and functionals by operating with analytically integrated stresses. However this approach has not been pursued because of the inherent smearing of actual partial yielding effects through the plate thickness.

The second example problem is a simply supported square plate of side length 10.0 in., thickness 0.1 in. subjected to uniform load of magnitude P (Figure 14). The material is assumed to be elastic perfectly plastic with $E = 10^7$ psi, $\nu = 0.3$, and $\bar{\sigma}_o = 10^4$ psi. Upper/lower bounds for this problem correspond to loads of 6.63 and 6.23 psi, per Hodge and Belytschko [23]. Symmetry is utilized and a quarter of the plate is modelled by a uniform NDX by NDY mesh.

Because Π^{II}_{mc} is the computationally preferred scheme, only Π^{II}_{mc} with iteration scheme A and including equilibrium imbalance correction is used in this example. In view of the parametric studies for the beam problem, the parameters MAXIT=10, RCONV=.01, NGX=NGY=2, and NGZ=3 are used unless otherwise stated. A load corresponding to P = 3.47 psi is applied first, after which the range P = 3.47 to 6.63 psi is divided into NINC equal increments in load. Results are presented in terms of the normalized center transverse displacement $\frac{W_c D}{M_p L^2}$, (where D is the flexural stiffness, and M_p is the plastic moment at full yield) versus the normalized total load $\varphi = \frac{PL^2}{M_p}$.

The effects of iteration (using a 2 by 2 element mesh for which the elastic tip deflection is in error by less than 2%) are shown in Figure 15.

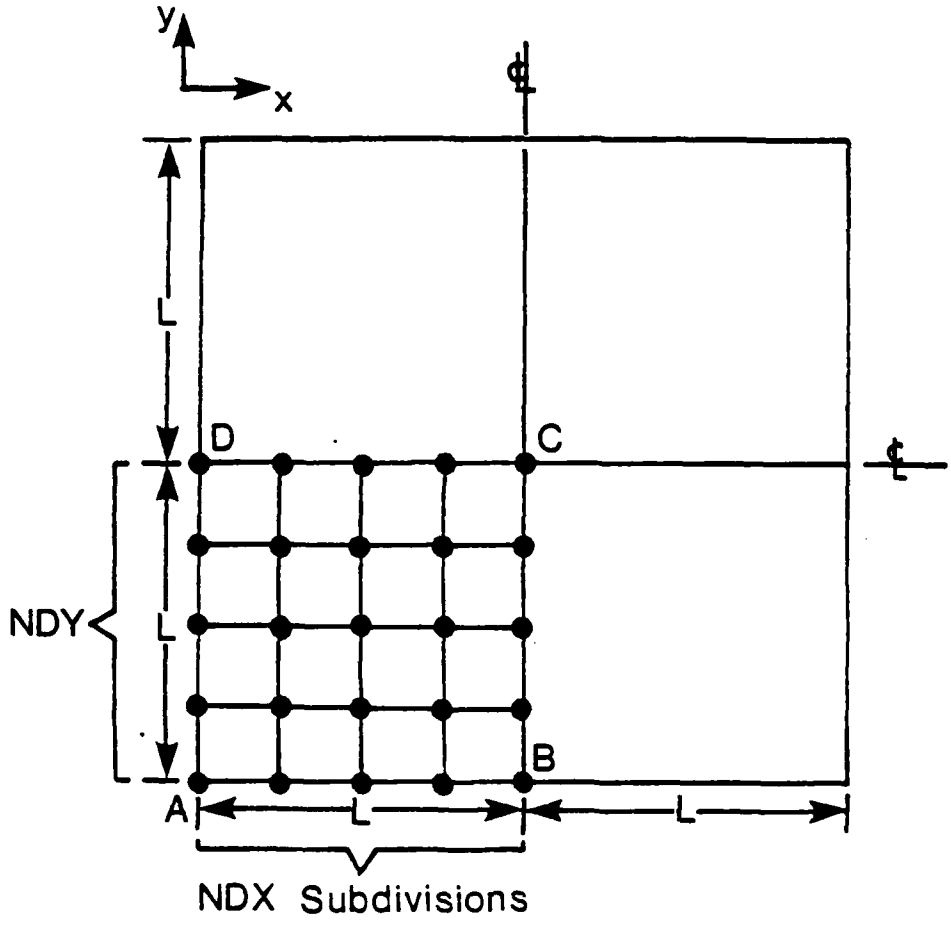

Boundary Conditions:

Sides AB and AD: $w=\theta_n=0$

Side BC: $\theta_y=0$

Side DC: $\theta_x=0$

Loading: Uniform of magnitude P (lb/in)

Mesh: NDX by NDY mesh of elements LH4 (shown) or QHI.

Figure 14. Mesh, geometry, and boundary conditions for the example problem of a square plate under uniform load.

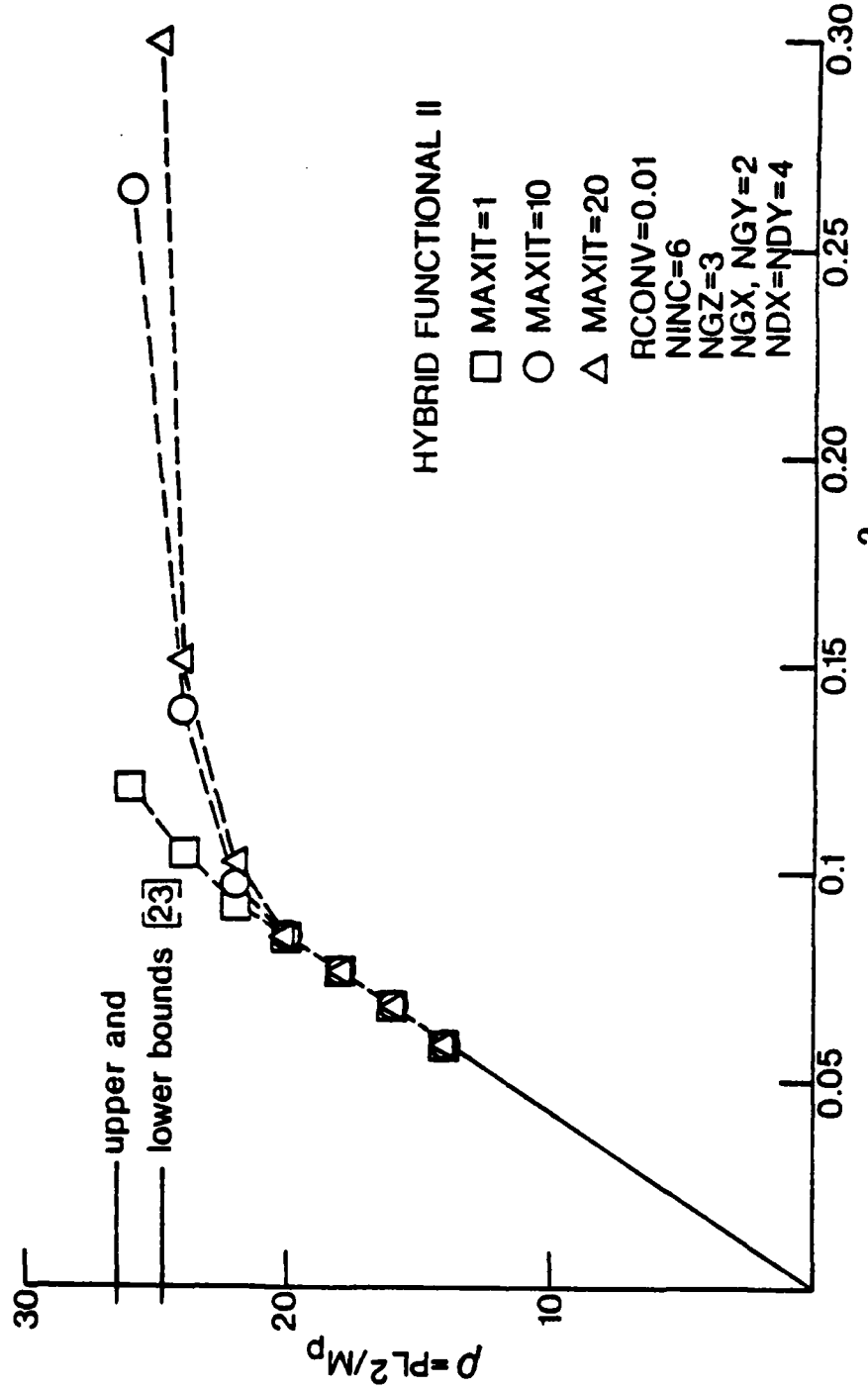

Figure 15. Effects of maximum permitted iterations per load step for the plate problem.

Increasing MAXIT yields a more flexible solution. The MAXIT=10 solution will produce a fully-plastic load slightly above the upper bound value, whereas the MAXIT=20 solution will fall within the upper/lower bounds.

The effects of mesh size and inplane integration stations are shown in Figures 16a and 16b. The comparison between the case of a 2 by 2 mesh with NGX=NGY=2, and the case of a 4 by 4 mesh with NGX=NGY=1 (approximately equivalent in terms of computational effort), Figure 16a, suggests that the latter approach is superior; although the predicted fully-plastic loads will not differ substantially, details of the load-deflection results are clearly different beyond a normalized load of $\rho > 18.0$. The effects of mesh (NDX,NDY), for NGX=NGY=1 (Figure 16b) show little change in predicted response beyond a 3 by 3 mesh.

In Reference [16], comparisons of the hybrid-stress family of plate elements suggest that the 8-node element, QH1, is in general more accurate than the 4-node element, LH4, per degree of freedom in the assembled mesh (an exception is the simply-supported plate under uniform load). A reasonable comparison of these two elements for elastic-plastic analysis corresponds to a 2 by 2 block of LH4 elements with NGX=NGY=1 replaced by one QH1 element with NGX=NGY=2. Benchmark multiplication estimates in Table 2 suggest that the LH4 analysis will require slightly less computational effort. Results obtained using a 4x4 mesh of LH4 elements with NGX=NGY=1, compared with a 2x2 mesh of QH1 elements with NGX=NGY=2 are shown in Figure 17. The two schemes are found to produce nearly identical results. Actual CPU times show that the LH4 analysis requires approximately 80% of the time required for the QH1 analysis. It should be noted that for the elastic analysis of a simply-supported uniform loaded plate, LH4 is more efficient than QH1. However for other boundary conditions/loading, QH1 is more accurate per degree of freedom [16] and advantages of QH1 over LH4 in the elastic-plastic analysis may be found.

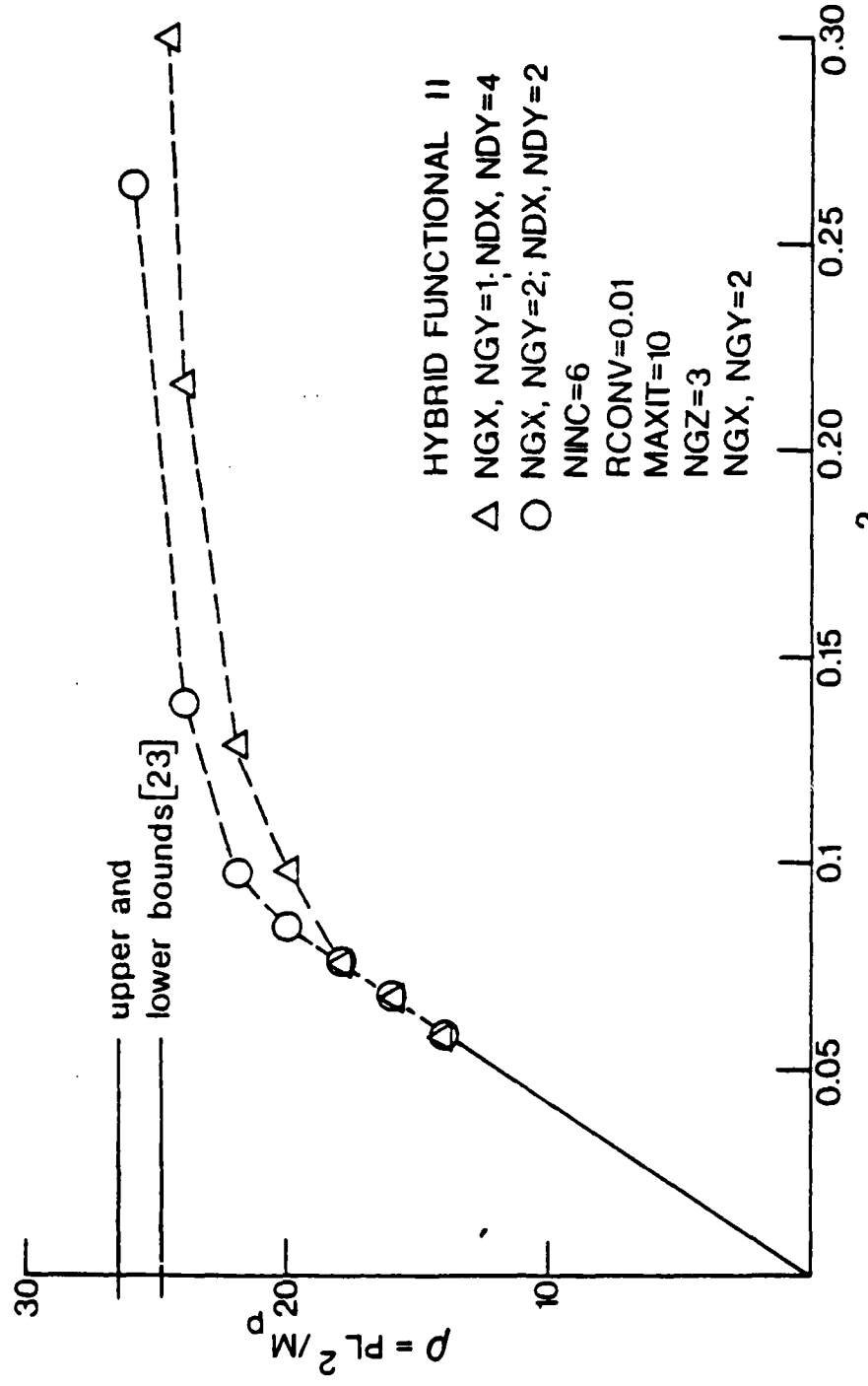

(a) Effect of Mesh and Inplane Integration Stations.

Figure 16. Effects of mesh and inplane integration rule for the plate problem.

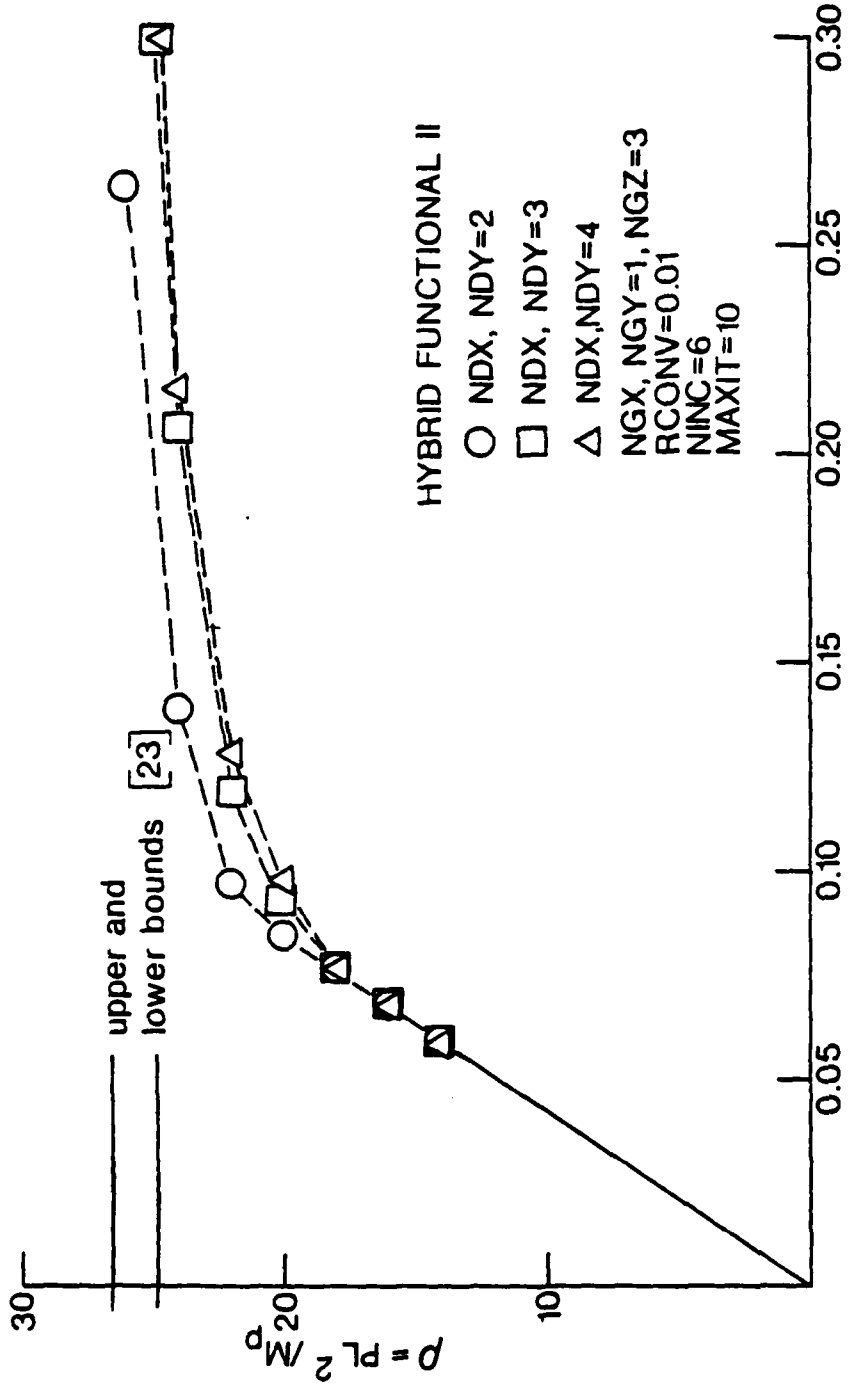

(b) Effects of Mesh with 1 Point Inplane Integration

Figure 16. (concluded)

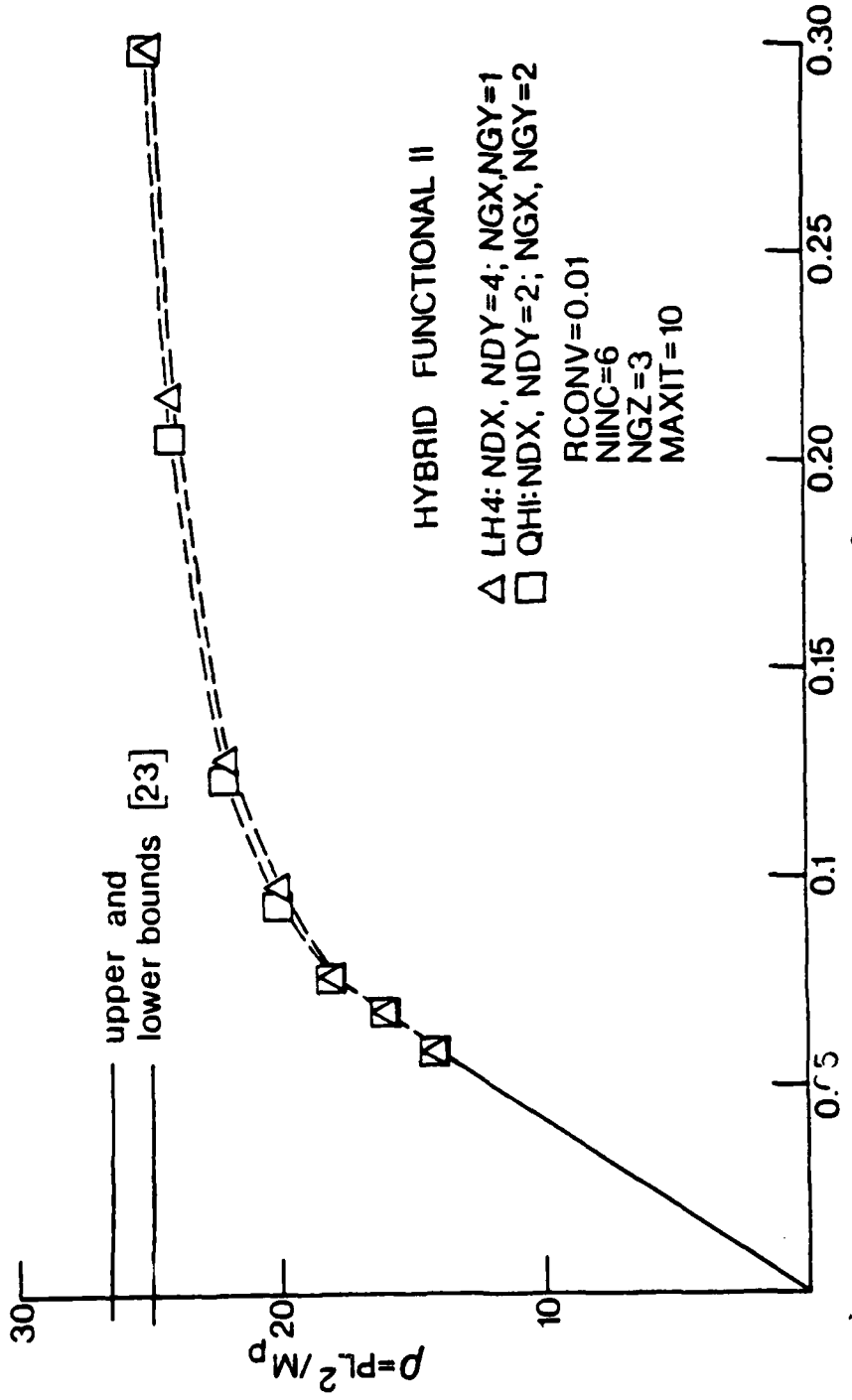

Figure 17. Comparison of results obtained using elements LH4 and QH1 for the plate problem.

8. Concluding Remarks

The elastic-plastic analysis of plates has been performed by using alternate hybrid-stress functionals based on the initial-stress approach for material nonlinearities. Accurate results have been obtained using both Π_{mc}^{I} with iteration scheme B, and Π_{mc}^{II} with iteration scheme A. In principle, Π_{mc}^{II} has the potential difficulty of requiring an intraelement displacement field. However, this poses no problems for the plate elements used here for which such interpolations are easily constructed. On the basis of computational effort, Π_{mc}^{II} is preferred over Π_{mc}^{I}.

Results obtained suggest that a 2 by 2 inplane and 3 point through-thickness integration rules are adequate for evaluation of the equivalent nodal loads corresponding to plasticity effects for the 4-node element. Although no such examples have been shown, the elements and procedure used here can also be applied to moderately-thick plates. Because the 4-node plate element produces good intraelement stress distributions, the use of a 2 x 2 inplane Gauss rule leads to improved results compared with a 1 point rule, for fixed mesh size. However, the 1 point rule, coupled with a more refined mesh may be more effective from a computation time versus accuracy viewpoint. Significant computational savings can also be realized for thin plates by using only the inplane stresses to compute the equivalent loads and bypassing the z=0 integration station of the 3-point through-thickness rule.

A single comparison between the 4-node element (LH4) and 8-node element (QH1) shows that the use of the simple LH4 element is more efficient computationally. However, for other loadings and boundary conditions, this observation could be reversed. In QH1, σ_z is included, whereas $\sigma_z = 0$ in LH4. If, for example, the present elements/analysis were extended to the material nonlinear analysis of multi-layer laminated composite plates, a QH1-type element should be preferred because of the dominant role of σ_z near free-surfaces for relatively thin laminated plates [24, 25].

9. References

1. O.C. Zienkiewicz, The Finite Element Method, McGraw Hill, Berkshire, England, 1977.

2. C.S. Desai and J.F. Abel, Introduction to the Finite Element Method, 1st ed., Van Nostrand Reinhold, New York, 1972.

3. Y. Yamanda, S. Nakagiri and K. Takatsuka, 'Elastic-Plastic Analysis of St. Venant Torsion Problem by a Hybrid Stress Method', Int. J. Numerical Methods in Engng. 5, 193-207 (1972).

4. C.H. Luk, 'Assumed Stress Hybrid Finite-Element Method for Fracture Mechanics and Elastic-Plastic Analysis', MIT ASRL TR 170-1 (1972).

5. R.L. Spilker, 'A Study of Elastic-Plastic Analysis by the Assumed-Stress Hybrid Finite-Element Model, with Application to Thick Shells Revolution', MIT ASRL TR 175-1 (1974).

6. T.H.H. Pian, R.L. Spilker, and S.W. Lee, 'Elastic-Plastic and Creep Analysis by Assumed Stress Finite Elements' Transactions Third International Conference on Sturctural Mechanis in Reactor Technology, London; September 1-5, Paper M2/1 (1975).

7. R.L. Spilker and T.H.H. Pian, 'Hybrid Stress Models for Elastic-Plastic Analysis by the Initial Stress Approach', Int. J. Num. Meth. Engng. 14, 359-378 (1979).

8. E. Horrigmoe and O.M. Eidsheim, 'Hybrid Stress Finite Element Model for Elastic-Plastic Analysis', Finite Elements in Nonlinear Mechanics, 1, 109-130, Tapir Publishers, Norway (1978).

9. A.J. Barnard and P.W. Sharman, 'Elastic-Plastic Analysis Using Hybrid Stress Finite Elements,' Finite Elements in Nonlinear Mechanics, 1, 131-148, Tapir Publishers Norway, (1978).

10. T.H.H. Pian, 'Variational Principles for Incremental Finite Element Methods', J. Franklin Institute 302, 473-488 (1976).

11. O.C. Zienkiewicz, S. Valliappan and J.P. King, 'Elasto-Plastic Solutions of Engineering Problems 'Initial Stress' Finite Element Approach', Int. J. Numerical Methods in Engng. 1, 75-100 (1969).

12. T.H.H. Pian and P. Tong, 'Finite Element Methods in Continuum Mechanics,' Adv. Appl. Mech., 12, Academic Press, New York, 1-58, (1972).

13. T.H.H. Pian, 'Hybrid Elements,' Numerical and Computer Methods in Structural Mechanics (edited by S.J. Fenves, N. Perrone, A.R. Robinson and W.C. Schnobrich), Academic Press, New York, 59-78 (1973).

14. R.L. Spilker, and N.I. Munir, 'The Hybrid Stress Model for Thin Plates', Int. J. Num. Meth. Engng., 15, 1239-1260 (1980).

15. R.L. Spilker and N.I. Munir, 'A Hybrid Stress Quadratic Displacement Mindlin Plate Bending Element', Computers and Structures, 12, 11-21 (1980).

16. R.L. Spilker and N.I. Munir, 'A Serendipity Cubic Displacement Hybrid Stress Element for Thin and Moderately Thick Plates', Int. J. Num. Meth. Engng., 15, 1261-1278 (1980).

17. G.N. White, Jr., 'Application of the Theory of Perfectly Plastic Solids to Stress Analysis of Strain Hardening Solid', Brown University Grad. Division of Applied Math. TR 51 (1950).

18. J.F. Besseling, 'A Theory of Plastic Flow for Anisotripic Hardening in Plastic Deformation of an Intially Isotropic Material', Rept. S410, Natl. Aeronautical Research Institute, Amsterdam, The Netherlands (1953).

19. B. Hunsaker, Jr., D.K. Vaughan, J.A. Stricklin and W.E. Haisler, 'A Comparison of Current Work Hardening Models Used in the Analysis of Plastic Deformations', Aerospace Engng. Dept., Texas A & M University (1973).

20. A. Mendelson, 'Plasticity Theory and Application', Macmillan, New York, (1968).

21. E. Hinton, F.C. Scott and R.E. Ricketts, 'Local Least Squares Stress Smoothing for Parabolic Isoparametric Elements, Int. J. Num. Meth. Engng., 9, 235-256 (1975).

22. J. Barlow, 'Optimal Stress Locations in Finite Element Models', Int. J. Num. Meth. Engng., 10, 243-251 (1976).

23. P.G. Hodge, Jr. and T. Belytschko, 'Numerical Methods for the Limit Analysis of Plates,' Trans. Am. Soc. Mecha. Engng., J. Appl. Mech., 35, 796-802, (1968).

24. R.B. Pipes and N.J. Pagano, 'Interlaminar Stresses in Composite Laminates Under Uniform Axial Extension', J. Comp. Materials, 4, 538, (1970).

25. N.J. Pagano, 'On the Calculation of Interlaminar Normal Stress in Composite Laminates', J. Comp. Materials, 8, 65 (1974).

EDGE SINGULARITIES IN ANISOTROPIC COMPOSITES

ABSTRACT

The stress singularity at the vertex of an anistropic wedge has the form $r^{-\xi}F(r,\vartheta)$ as $r \to 0$ where $0 < \xi < 1$ and F is a real function of the polar coordinates (r,ϑ). In many cases, F is independent of r. The explicit form of $F(r,\theta)$ depends on the eigenvalues of the elasticity constants, called p here, and on the order of singularity $\varkappa$. When $\varkappa$ is real, $\xi = \varkappa$. If $\varkappa$ is complex, ξ is the real part of $\varkappa$. The p's are all complex and consist of 3 pairs of complex conjugates which reduce to $\pm i$ when the material is isotropic. The function F depends not only on p and $\varkappa$, it also depends on whether p and $\varkappa$ are distinct roots of the corresponding determinants. In this paper we present the function $F(r,\vartheta)$ in terms of p and $\varkappa$ for the cases when p and $\varkappa$ are single roots as well as when they are multiple roots. The relationship between the complex variable z introduced in the analysis and the polar coordinates (r,ϑ) is interpreted geometrically. After presenting the form of F for individual cases, a general form of F is given in Eq. (64). We also show that the stress singularity at the crack tip of general anisotropic materials has the order of singularity $\xi = \frac{1}{2}$ which is a multiple root of order 3. The implication of this on the form $F(r,\vartheta)$ is discussed.

1. INTRODUCTION

For isotropic materials, use of the biharmonic function, or the Airy stress function, seems to be the universal approach in the analysis of stress singularities [1-4]. There appears to be no universal approach in analyzing the stress singularities in anisotropic materials. Lekhnitskii [5] introduced two stress functions to analyze general anisotropic materials. His approach was used by Wang and Choi [6] to study the thermal stresses at the interface in a layered composite. Green and Zerna [7] employed a complex function representation of the solution. Their approach was used by Bogy [8] and Kuo and Bogy [9] in conjunction with a generalized Mellin transform to analyze stress singularities in an anisotropic wedge. It should be mentioned that plane deformation was assumed in [7-9] and hence the material property was assumed to be symmetric with respect to the plane of deformation.

In this paper we use the approach of Stroh [10] whose analysis was further developed by Barnett and his co-workers (see [11], for example) to study the surface waves in anisotropic elastic materials. An excellent review article on surface waves in anisotropic elastic materials was given by Chadwick and Smith [12]. Although no stress singularities were studied in [10-12], their approach is used here to find the stress distribution at an anisotropic wedge. A recent study by Dempsey and Sinclair [3] on isotropic elastic wedge problems shows that the singularity analysis can be accomplished without resorting to the Mellin transform even when the boundary conditions are not homogeneous [4]. Following their analysis and using the approach of Stroh, we present here possible forms of stress distribution near the vertex of a wedge or a composite wedge of anisotropic materials.

The stress distribution near the vertex of a wedge or a composite wedge depends on whether the eigenvalues p of the elasticity constants are distinct. It also depends on whether the order of singularity κ is a single or multiple root. The purpose of this paper is to show how one can derive the form of stress distribution when p and/or κ are not single roots. We also show the geometrical meaning of the complex variable Z in terms of the polar coordinates (r,θ).

Finally, as an application, we consider the stress singularity at a crack tip of general anisotropic materials.

2. BASIC EQUATIONS

In a fixed rectangular coordinates x_i, $(i = 1,2,3)$, let u_i, σ_{ij} and ε_{ij} be the displacement, stress and strain, respectively. The continuity condition, the stress-strain law and the equations of equilibrium can be written as

$$\varepsilon_{ij} = (\partial u_i/\partial x_j + \partial u_j/\partial x_i)/2 \tag{1}$$

$$\sigma_{ij} = c_{ijk\ell}\,\varepsilon_{k\ell} \tag{2}$$

$$\partial \sigma_{ij}/\partial x_j = 0 \tag{3}$$

where

$$c_{ijk\ell} = c_{jik\ell} = c_{ij\ell k} = c_{k\ell ij} \tag{4}$$

are the elasticity constants of the anisotropic material. Unless stated otherwise, repeated indices imply summation.

We assume that u_i and σ_{ij} are independent of the x_3-coordinate. Hence we assume that

$$Z = x_1 + px_2 \tag{5}$$

$$u_i = \upsilon_i f(Z) \tag{6}$$

$$\sigma_{ij} = \tau_{ij} df(Z)/dZ \tag{7}$$

where f is an arbitrary function of Z and p is an eigenvalue of the elasticity constants to be determined shortly. υ_i and τ_{ij} are independent of x_1 and x_2 but they depend on the eigenvalue p. Substitution of Eqs. (6,7) into Eqs. (1-3) yields the results

$$\tau_{ij} = (c_{ijk1} + pc_{ijk2})\upsilon_k \tag{8}$$

$$D_{ik}\upsilon_k = 0 \tag{9}$$

where

$$D_{ik} = c_{i1k1} + p(c_{i1k2} + c_{i2k1}) + p^2 c_{i2k2} \tag{10}$$

For a non-trivial solution of υ_k, the determinant of D_{ik} must vanish. This provides the eigenvalues p. Equation (9) then provides the eigenvector υ_i.

3. EIGENVALUES AND EIGENVECTORS OF THE ELASTICITY CONSTANTS

In view of Eq. (4), $c_{ijk\ell}$ has only 21 constants. If we write Eqs. (2) and (4) as

$$\sigma_i = c_{ij}\varepsilon_j , \qquad c_{ij} = c_{ji} \tag{11}$$

where

$$\left.\begin{aligned} &\sigma_1 = \sigma_{11}, \quad \sigma_2 = \sigma_{22}, \quad \sigma_3 = \sigma_{33}, \\ &\sigma_4 = \sigma_{23}, \quad \sigma_5 = \sigma_{13}, \quad \sigma_6 = \sigma_{12}, \end{aligned}\right\} \tag{12}$$

$$\left.\begin{aligned} &\varepsilon_1 = \varepsilon_{11}, \quad \varepsilon_2 = \varepsilon_{22}, \quad \varepsilon_3 = \varepsilon_{33}, \\ &\varepsilon_4 = 2\varepsilon_{23}, \quad \varepsilon_5 = 2\varepsilon_{13}, \quad \varepsilon_6 = 2\varepsilon_{12}. \end{aligned}\right\} \tag{13}$$

the coefficients in Eq. (10) can be written as

$$\left.\begin{aligned} Q_{ik} = c_{i1k1} &= \begin{bmatrix} c_{11} & c_{16} & c_{15} \\ c_{61} & c_{66} & c_{65} \\ c_{51} & c_{56} & c_{55} \end{bmatrix} \\ R_{ik} = c_{i1k2} &= \begin{bmatrix} c_{16} & c_{12} & c_{14} \\ c_{66} & c_{62} & c_{64} \\ c_{56} & c_{52} & c_{54} \end{bmatrix} \\ T_{ik} = c_{i2k2} &= \begin{bmatrix} c_{66} & c_{62} & c_{64} \\ c_{26} & c_{22} & c_{24} \\ c_{46} & c_{42} & c_{44} \end{bmatrix} \end{aligned}\right\} \qquad (14)$$

Equation (10) can then be written as

$$D_{ik} = Q_{ik} + p(R_{ik} + R_{ki}) + p^2 T_{ik} \qquad (15)$$

and vanishing of the determinant D_{ik} means

$$\begin{vmatrix} c_{11}+2pc_{16}+p^2c_{66} & c_{16}+p(c_{12}+c_{66})+p^2c_{26} & c_{15}+p(c_{14}+c_{56})+p^2c_{46} \\ c_{16}+p(c_{12}+c_{66})+p^2c_{26} & c_{66}+2pc_{26}+p^2c_{22} & c_{56}+p(c_{25}+c_{46})+p^2c_{24} \\ c_{15}+p(c_{14}+c_{56})+p^2c_{46} & c_{56}+p(c_{25}+c_{46})+p^2c_{24} & c_{55}+2pc_{45}+p^2c_{44} \end{vmatrix} = 0 \qquad (16)$$

Eq. (16) provides six eigenvalues of p.

For each of p the associated υ_i's are obtained from Eq. (9). In general, υ_i, (i = 1,2,3) are all non-zero. Hence, u_1, u_2 and u_3 are coupled.

As to τ_{ij}, we let j = 1 and 2, respectively, in Eq. (8) and use the notations of Eq. (14) to obtain

$$\left.\begin{aligned} \tau_{i1} &= (Q_{ik} + pR_{ik})\upsilon_k \\ \tau_{i2} &= (R_{ki} + pT_{ik})\upsilon_k \end{aligned}\right\} \qquad (17)$$

It follows from Eqs. (9,15,17) that

$$\tau_{i1} + p\tau_{i2} = 0 \tag{18}$$

and hence

$$\tau_{12} = -p\tau_{22}\,, \quad \tau_{11} = p^2\tau_{22}\,, \quad \tau_{13} = -p\tau_{23} \tag{19a}$$

Therefore, of the six components τ_{ij}, all we need is τ_{22}, τ_{33} and τ_{23}. They are obtained from Eqs. (17) and (8) with the aid of Eq. (14). The results can be casted in the following form:

$$\tau_i = (c_{i1} + pc_{i6})\upsilon_1 + (c_{i6} + pc_{i2})\upsilon_2 + (c_{i5} + pc_{i4})\upsilon_3\,, \qquad (i = 2,3,4) \tag{19b}$$

where

$$\tau_2 = \tau_{22}\,, \quad \tau_3 = \tau_{33}\,, \quad \tau_4 = \tau_{23} \tag{19c}$$

Notice that since Q_{ik} and T_{ik} are symmetric, so is D_{ik}. Notice also that c_{3j}, $(j = 1,2,\ldots,6)$ are not present in Eq. (16). Therefore, the eigenvalues p are independent of these elastic constants. In fact, the stress singularities are also independent of these elastic constants.

Equation (16) is a sextic equation in p. If the strain energy is positive definite, it can be shown that p cannot be real [10,12]. Therefore, we would have 3 pairs of complex conjugate roots for p.

When the material property is symmetric with respect to the (x_2,x_3) plane or to the (x_1,x_3) plane, Eq. (16) reduces to a cubic in p^2 [10]. Since every cubic has at least one real root, one of the p's will be purely imaginary when (x_2,x_3) or (x_1,x_3) is a plane of symmetry.

4. UNCOUPLING OF u_3 FROM u_1 AND u_2

When the material property is symmetric with respect to the (x_1,x_2) plane, we have

$$c_{14} = c_{15} = c_{24} = c_{25} = c_{34} = c_{35} = c_{46} = c_{56} = 0 \tag{20}$$

Equation (16) then reduces to

$$\begin{vmatrix} c_{11}+2pc_{16}+p^2c_{66} & c_{16}+p(c_{12}+c_{66})+p^2c_{26} & 0 \\ c_{16}+p(c_{12}+c_{66})+p^2c_{26} & c_{66}+2pc_{26}+p^2c_{22} & 0 \\ 0 & 0 & c_{55}+2pc_{45}+p^2c_{44} \end{vmatrix} = 0 \qquad (21)$$

Therefore, instead of a sextic we have a quartic equation and a quadratic equation in p.

If p is a root of the quartic equation, we see from Eqs. (9,21) that $v_3 = 0$. Moreover, Eqs. (19) show that $\tau_{13} = \tau_{23} = 0$. Hence, we have a plane deformation.

Similarly, if p is a root of the quadratic equation, $v_1 = v_2 = 0$ and $\tau_{11} = \tau_{22} = \tau_{33} = \tau_{12} = 0$. This is an anti-plane deformation.

Therefore, when Eq. (20) holds, the plane deformation and the anti-plane deformation are uncoupled. Since the system is linear, we may consider them separately when Eq. (20) holds.

5. GEOMETRICAL INTERPRETATION OF $Z = x_1 + px_2$

Let α and β be, respectively, the real and imaginary part of p so that

$$p = \alpha + \beta i \ , \quad \beta > 0 \qquad (22)$$

We assumed $\beta > 0$ because the conjugate of p will have the negative imaginary part. Using the polar coordinates with the origin at $x_1 = x_2 = 0$, we have

$$x_1 = r\cos\theta \ , \quad x_2 = r\sin\theta \ . \qquad (23)$$

Hence,

$$Z = x_1 + px_2 = X + iY = re^{i\psi} \qquad (24)$$

where

$$\left.\begin{aligned} X/r &= \cos\theta + \alpha\sin\theta = \rho\cos\psi \\ Y/r &= \beta\sin\theta = \rho\sin\psi \\ \rho^2 &= (\cos\theta + \alpha\sin\theta)^2 + \beta^2\sin^2\theta \end{aligned}\right\} \tag{25}$$

It is not difficult to show from Eqs. (23-25) that a unit circle in the (x_1,x_2) plane maps an ellipse in the (X,Y) plane, Fig. 1. If the (x_1,x_2) plane is a stretchable sheet, one obtains the ellipse by first stretching the circle uniformly β units in the x_2-direction and then shear the sheet with the x_1-axis fixed until point b displaces α unit horizontally. From point a in (x_1,x_2) and (X,Y) planes we see the geometrical relationship between θ, ρ and ψ. From Eq. (25), notice that ρ and ψ depend on θ and p but are independent of r. Notice also that

$$\rho = 1 , \quad \psi = \theta , \quad \text{at} \quad \theta = 0 , \quad \pm\pi \tag{26}$$

If p is purely imaginary, we also have, in addition to Eq. (26),

$$\rho = \beta, \ \psi = \theta, \ \text{at} \ \theta = \pm\pi/2, \ \pm 3\pi/2 \ \text{ when } \alpha = 0 \tag{27}$$

For isotropic materials, $p = \pm i$ is a multiple root of order 3. Thus the ellipse in the (X,Y) plane reduces to a unit circle. Hence,

$$\rho = 1 , \quad \psi = \theta , \tag{28}$$

and

$$Z = x_1 + ix_2 = re^{i\theta} \tag{29}$$

which is the well-known complex coordinate for (x_1,x_2) in two-dimensional elasticity problems of isotropic materials.

6. STRESS DISTRIBUTION NEAR THE VERTEX WHEN p's ARE DISTINCT

To find the stress distribution and the stress singularities at the vertex of a wedge, we choose

$$f(Z) = \frac{1}{1-\kappa} Z^{1-\kappa} \tag{30}$$

where κ is the order of singularity to be determined by the boundary conditions. As we mentioned earlier, the eigenvalues p are all complex numbers and consist of three pairs of complex conjugates. In this section we assume that the eigenvalues are distinct. Using Eq. (30) in Eqs. (6,7) for all eigenvalues and forming a linear combination of them leads to

$$u_i = (A_1 v_i Z^{1-\kappa} + B_1 \bar{v}_i \bar{Z}^{1-\kappa})/(1-\kappa) + \ldots \tag{31}$$

$$\sigma_{ij} = A_1 \tau_{ij} Z^{-\kappa} + B_1 \bar{\tau}_{ij} \bar{Z}^{-\kappa} + \ldots \tag{32}$$

where $A_1, B_1, \ldots$ are constants which may be complex and an overbar denotes a complex conjugate. For simplicity only the terms associated with one pair of eigenvalues are written explicitly to avoid introducing an additional subscript for the eigenvalues. The dots denote terms associated with the remaining two pairs of eigenvalues.

It should be pointed out that v_k as given by Eq. (9) is not unique and can have an arbitrary multiplicative constant. The constants A_1 and B_1 in Eqs. (31,32) represent this arbitrary multiplicative constant.

For a wedge or a composite wedge, by substituting Eqs. (31,32) in the boundary conditions (which include the interface conditions if the wedge is a composite), one obtains a system of linear algebraic equations in A_1, $B_1, \ldots$, which may be written as

$$K_{ij} c_j = q_i \tag{33}$$

where K_{ij} is a square matrix which depends on κ, c_j is a column matrix whose elements are $A_1, B_1, \ldots$, and q_i is a column matrix which depends on the boundary conditions. If the boundary conditions are homogeneous, $q_i = 0$.

In this case, a nontrivial solution exists if the determinant of K_{ij} vanishes. The roots of this determinant provides the values for κ. Let

$$\kappa = \xi + \eta i \tag{34}$$

where ξ and η are real. If $0 < \xi < 1$, we have a singularity at $r = 0$.

Since u_i and σ_{ij} are real, only the real parts or the imaginary parts on the right-hand sides of Eqs. (31,32) should be considered. They will have different expressions depending on if the root κ is real or complex.

A. $\kappa = \xi$, Real

Since υ_i and τ_{ij} are in general complex, let

$$\upsilon_i = v_i e^{ia_i} \qquad \tau_{ij} = t_{ij} e^{ib_{ij}} \tag{35}$$

where v_i, a_i, t_{ij} and b_{ij} are real and repeated *indices do not imply* summation here. With Eqs. (24,35), the real parts of Eqs. (31,32) can be written as

$$u_i = (r\rho)^{1-\xi} v_i \{M_1 \cos[a_i + (1-\xi)\psi] + N_1 \sin[a_i + (1-\xi)\psi]\}/(1-\xi) + \ldots \tag{36}$$

$$\sigma_{ij} = (r\rho)^{-\xi} t_{ij} \{M_1 \cos(b_{ij} - \xi\psi) + N_1 \sin(b_{ij} - \xi\psi)\} + \ldots \tag{37}$$

where $M_1, N_1, \ldots$ are related to $A_1, B_1, \ldots$ and are real. The imaginary parts of Eqs. (31,32) provide no new expressions.

B. $\kappa = \xi + i\eta$, complex

When κ is a complex root there is no loss in generality in assuming $\eta > 0$ because if κ is a root, so is $\bar{\kappa}$. We then have

$$\begin{aligned} z^{-\kappa} &= (r\rho e^{i\psi})^{-\xi - i\eta} = (r\rho)^{-\xi} e^{\eta\psi} e^{-i\xi\psi} (r\rho)^{-i\eta} \\ &= (r\rho)^{-\xi} e^{\eta\psi} e^{-i(\xi\psi + \eta \ln(r\rho))} \end{aligned} \tag{38}$$

The real parts, or the imaginary parts of Eq. (32) now become

$$\sigma_{ij} = (r\rho)^{-\xi} t_{ij}\{e^{\eta\psi}(M_1^- \cos\phi_{ij}^- + N_1^- \sin\phi_{ij}^-) + e^{-\eta\psi}(M_1^+ \cos\phi_{ij}^+ + N_1^+ \sin\phi_{ij}^+)\} + \ldots \tag{39}$$

where

$$\phi_{ij}^{\pm} = b_{ij} - \xi\psi \pm \eta \ln(r\rho) \tag{40}$$

and $M_1^{\pm}$, $N_1^{\pm}$ are real constants and are related to A_1 and B_1. A similar equation may be written for u_i. We see that σ_{ij} is oscilatory and unbounded as $r \to 0$. As expected, Eq. (39) reduces to Eq. (37) when $\eta = 0$.

In the sequel, we will consider only the cases in which κ is a complex. The solution for a real κ is deduced by letting $\eta = 0$.

7. STRESS DISTRIBUTION NEAR THE VERTEX WHEN p IS A DOUBLE ROOT

When p is a double root of Eq. (16), we have only two pairs of distinct eigenvalues instead of three. It is not difficult to see that, if

$$u_i = \upsilon_i z^{1-\kappa}/(1-\kappa) \tag{41}$$

$$\sigma_{ij} = \tau_{ij} z^{-\kappa} \tag{42}$$

are the solutions corresponding to the double root p, so are

$$\left.\begin{aligned} u_i &= \frac{1}{1-\kappa}\frac{d}{dp}\{\upsilon_i z^{1-\kappa}\} \\ &= \frac{1}{1-\kappa}\upsilon_i' z^{1-\kappa} + \upsilon_i z^{-\kappa} x_2 \end{aligned}\right\} \tag{43}$$

$$\sigma_{ij} = \tau_{ij}' z^{-\kappa} - \kappa\tau_{ij} z^{-\kappa-1} x_2 \tag{44}$$

where a prime stands for differentiation with respect to p. Since

$$x_2 = (z-\bar{z})/(2p), \tag{45}$$

we have

$$u_i = (\frac{1}{1-\kappa}\upsilon_i' + \frac{1}{2p}\upsilon_i) z^{1-\kappa} - \frac{1}{2p}\upsilon_i \bar{z} z^{-\kappa} \tag{46}$$

$$\sigma_{ij} = (\tau_{ij}' - \frac{\kappa}{2p}\tau_{ij}) z^{-\kappa} + \frac{\kappa}{2p}\tau_{ij}\bar{z} z^{-\kappa-1} \tag{47}$$

U_i' is obtained by differentiating Eq. (9) with respect to p:

$$D_{ik}U_k' + D_{ik}'U_k = 0 \tag{48}$$

The existence of a solution for U_k and U_k' from Eqs. (9,48) will not be discussed here. Likewise, τ_{ij}' is obtained by differentiating Eq. (8) with respect to p.

Notice that U_k' and U_k obtained from Eqs. (9,48) are not unique. They both have a multiplicative constant, say A_1 and A_2, respectively. The $Z^{-\kappa}$ term in Eq. (47) together with the same term with p replaced by $\bar{p}$ is essentially similar to Eq. (32) and hence would yield an expression similar to Eq. (39). The last term in Eq. (47) will produce a second independent solution. This is obtained from

$$\sigma_{ij} = A_2 \frac{\kappa}{2p} \tau_{ij} Z\bar{Z}^{-\kappa-1} + B_2 \frac{\kappa}{2\bar{p}} \bar{\tau}_{ij} Z\bar{Z}^{-\kappa-1} \tag{49}$$

by taking the real or imaginary parts of the right-hand side. Therefore, when p is a double root, we have the following second independent solution for σ_{ij} in addition to Eq. (39):

$$\sigma_{ij} = (r\rho)^{-\xi} t_{ij}\{e^{\eta\psi}[M_2^- \cos(\phi_{ij}^- - 2\psi) + N_2^- \sin(\phi_{ij}^- - 2\psi)]$$
$$+ e^{-\eta\psi}[M_2^+ \cos(\phi_{ij}^+ - 2\psi) + N_2^+ \sin(\phi_{ij}^+ - 2\psi)] \tag{50}$$

where $\phi_{ij}^{\pm}$ are defined in Eq. (40) and $M_2^{\pm}$, $N_2^{\pm}$ are related to A_2, B_2, p and κ. Equation (50) applies to the case when κ is complex. For a real κ, we simply let $\eta = 0$.

8. STRESS DISTRIBUTION NEAR THE VERTEX WHEN p IS A TRIPLE ROOT

For isotropic materials, $p = \pm i$ is a triple root. However, since u_3 is uncoupled from u_1 and u_2 for isotropic materials, p is actually a double root when we consider u_1 and u_2 only. Hence the previous section on a double root p applies to isotropic materials.

We have not seen an example other than isotropic materials for which p is a triple root. If there is one, and if u_3 is not uncoupled from u_1 and u_2, we see that a third independent solution is

$$u_i = \frac{1}{1-\kappa} \frac{d^2}{dp^2} \{u_i z^{1-\kappa}\} \tag{51}$$

$$\sigma_{ij} = \frac{d^2}{dp^2} \{\tau_{ij} z^{-\kappa}\} \tag{52}$$

Following a similar procedure in deriving Eq. (50), the real expressions for the third independent solution when p is a triple root can be obtained from Eq. (50) with 2ψ replaced by 4ψ and the subscripts 2 replaced by 3.

9. STRESS NEAR THE VERTEX WHEN κ IS A DOUBLE ROOT

Up to now, we tacitly assumed that κ is a single root of the determinant of K_{ij} and hence, other than a multiplicative constant, the homogeneous equation of Eq. (33) has a unique solution for c_j whose elements are the coefficients $A_1, B_1, \ldots$ If κ is a multiple root, then $A_1, B_1, \ldots$ may not be unique and we have other new solutions.

Let κ be a double root of the determinant K_{ij} defined in Eq. (33) with $q_i = 0$. Then, not only Eqs. (31,32) are the solutions, but also are

$$u_i = \upsilon_i \frac{d}{d\kappa}\{\frac{A}{1-\kappa} z^{1-\kappa}\} + \bar{\upsilon}_i \frac{d}{d\kappa}\{\frac{B}{1-\kappa} \bar{z}^{1-\kappa}\} + \ldots \tag{53}$$

$$\sigma_{ij} = \tau_{ij} \frac{d}{d\kappa}\{A z^{-\kappa}\} + \bar{\tau}_{ij} \frac{d}{d\kappa}\{B \bar{z}^{1-\kappa}\} + \ldots \tag{54}$$

Since

$$\tau_{ij} \frac{d}{d\kappa}\{A z^{-\kappa}\} = \frac{dA}{d\kappa} \tau_{ij} z^{-\kappa} - A \tau_{ij} z^{-\kappa} \ln z, \tag{55}$$

the first term on the right is essentially the same as the first term of Eq. (32). The second term provides a new solution for σ_{ij} when κ is a double root:

$$\sigma_{ij} = A_2\tau_{ij}Z^{-\kappa}\ln Z + B_2\bar{\tau}_{ij}\bar{Z}^{-\kappa}\ln\bar{Z} \tag{56}$$

The real or imaginary parts of Eq. (56) have different expressions depending on whether p is a single root or a multiple root.

A. p is a single root

When p is a single root, the real or imaginary parts of Eq. (56) have the expression:

$$\begin{aligned}\sigma_{ij} = (r\rho)^{-\xi}t_{ij}\{&e^{\psi\eta}[M_2^-(\ln(r\rho)\cos\phi_{ij}^- - \psi\sin\phi_{ij}^-) \\ &+ N_2^-(\ln(r\rho)\sin\phi_{ij}^- + \psi\cos\phi_{ij}^-)] \\ &+ e^{-\psi\eta}[M_2^+(\ln(r\rho)\cos\phi_{ij}^+ - \psi\sin\phi_{ij}^+) \\ &+ N_2^+(\ln(r\rho)\sin\phi_{ij}^+ + \psi\cos\phi_{ij}^+)]\}\end{aligned} \tag{57}$$

As before, $\phi_{ij}^{\pm}$ are defined in Eq. (40) and $M_2^{\pm}$, $N_2^{\pm}$ are related to A_2 and B_2.

B. p is a multiple root

Let us consider first the case in which p is a double root. Then, in addition to Eq. (56), we also have the solution

$$\sigma_{ij} = A_2\frac{d}{dp}(\tau_{ij}Z^{-\kappa}\ln Z) + B_2\frac{d}{d\bar{p}}(\bar{\tau}_{ij}\bar{Z}^{-\kappa}\ln\bar{Z}) \tag{58}$$

However, since

$$\begin{aligned}\frac{d}{dp}(\tau_{ij}Z^{-\kappa}\ln Z) &= (\tau_{ij}' - \frac{\kappa}{2p}\tau_{ij})Z^{-\kappa}\ln Z \\ &+ \frac{1}{2p}\tau_{ij}(Z^{-\kappa} - \bar{Z}Z^{-\kappa-1}) + \frac{\kappa}{2p}\tau_{ij}\bar{Z}Z^{-\kappa-1}\ln Z\end{aligned} \tag{59}$$

where use has been made of Eq. (45), only the last term provides a new solution. The rest of the terms in Eq. (59) have appeared in Eqs. (56,32,47). Therefore, a new solution when p is a double root is

$$\sigma_{ij} = A_2 \frac{\kappa}{2p} \tau_{ij} \bar{z} z^{-\kappa-1} \ln z + B_2 \frac{\kappa}{2\bar{p}} \bar{\tau}_{ij} z \bar{z}^{-\kappa-1} \ln \bar{z} \tag{60}$$

The real or imaginary parts of Eq. (60) have the expression which is obtained from Eq. (57) with $\phi_{ij}^{\pm}$ replaced by $(\phi_{ij}^{\pm} - 2\psi)$.

Similarly, if p is a triple root, it is not difficult to show that the new solution is obtained from Eq. (57) by replacing $\phi_{ij}^{\pm}$ by $(\phi_{ij}^{\pm} - 4\psi)$.

We see from Eq. (57) that σ_{ij} has the singularity of $r^{-\xi} \ln r$. The existence of a solution of Eq. (57) depends on the existence of a solution for A and $dA/d\kappa$ in Eq. (55). Since A is an element of c_j in Eq. (33), the existence of A and $dA/d\kappa$ depends on the existence of a solution for c_j and $dc_j/d\kappa$ from the following equations

$$K_{ij} c_j = 0 \tag{61}$$

$$K_{ij} (dc_j/d\kappa) + (dK_{ij}/d\kappa) c_j = 0 \tag{62}$$

A discussion of the solution of Eqs. (61, 62) can be found in [3].

10. STRESS NEAR THE VERTEX WHEN κ IS A TRIPLE ROOT

When κ is a triple root, one can follow the same reasoning as in the previous section for a double root κ. Therefore, the new solution for a triple root κ is obtained by replacing $d/d\kappa$ by $d^2/d\kappa^2$ in Eqs. (53,54). Equation (56) then is replaced by

$$\sigma_{ij} = A_2 \tau_{ij} Z^{-\kappa} (\ln Z)^2 + B_2 \bar{\tau}_{ij} \bar{Z}^{-\kappa} (\ln \bar{Z})^2 \tag{63}$$

and Eq. (57) is modified by replacing $\ln(r\rho)$ by $[\ln(r\rho)]^2 - \psi^2$, which is the real part of $(\ln Z)^2$, and ψ by $2\psi \ln(r\rho)$, which is the imaginary part of $(\ln Z)^2$.

11. GENERAL EXPRESSION

We can summarize the results obtained so far in the following form. Let n_p be the multiplicity of p and m_κ be the multiplicity of κ. If we write

$$\sigma_{ij} = r^{-\xi} F_{ij}(r,\theta) \tag{64a}$$

then F_{ij} consists of a linear combination of the real and imaginary parts of the following expression

$$t_{ij}\rho^{-\xi} e^{\pm\psi\eta}\{\ln(r\rho)\pm i\psi\}^{m-1}\{\cos[b_{ij}-\xi\psi-2(n-1)\psi\mp\eta\ln(r\rho)] + i\sin[b_{ij}-\xi\psi-2(n-1)\psi\mp\eta\ln(r\rho)]\} \tag{64b}$$

for each p and for all integers m and n subjected to the limitations

$$1 \le m \le m_\kappa, \quad 1 \le n \le n_p \le 3 \tag{64c}$$

As we stated before, ρ and ψ depend on θ but not on r.

12. SINGULARITY AT A CRACK TIP FOR ANISOTROPIC SOLIDS

Consider an infinite anisotropic solid with a crack plane which is located at $x_1 < 0$ of the (x_1, x_3) plane. Hence, $\sigma_{2j} = 0$, $(j = 1,2,3)$ at $\theta = \pm\pi$. Using Eq. (26), Eq. (37) for $\theta = \pi$ and $-\pi$ reduces to

$$\left.\begin{aligned} t_{2j}\{M_1\cos(b_{2j}-\xi\pi) + N_1\sin(b_{2j}-\xi\pi)\} + \ldots &= 0 \\ t_{2j}\{M_1\cos(b_{2j}+\xi\pi) + N_1\sin(b_{2j}+\xi\pi)\} + \ldots &= 0 \\ (j = 1,2,3) & \end{aligned}\right\} \tag{65}$$

If we set $\xi = \frac{1}{2}$, we have

$$\left.\begin{aligned} t_{2j}\{M_1\sin(b_{2j})-N_1\cos(b_{2j})\} + \ldots &= 0 \\ t_{2j}\{-M_1\sin(b_{2j})+N_1\cos(b_{2j})\} + \ldots &= 0 \\ (j = 1,2,3) & \end{aligned}\right\} \tag{66}$$

Equation (66) consists of 6 equations for $M_1, N_1, \ldots$ and can be written in the form of Eq. (33) with $q_i = 0$. Since the first three equations are identical to the last three equations, $\xi = \frac{1}{2}$ is a triple root of the determinant. We can therefore let $\xi = \frac{1}{2}$, $\eta = 0$, $m_K = 3$ in Eqs. (64). Disregarding the dependence on θ, the singularities at the crack tip in a general anisotropic material are $r^{-\frac{1}{2}}$ and possibly $r^{-\frac{1}{2}} \ln r$ and $r^{-\frac{1}{2}} (\ln r)^2$. The existence of $r^{-\frac{1}{2}} \ln r$ and $r^{-\frac{1}{2}} (\ln r)^2$ depends on the existence of a solution for c_j, $dc_j/d\kappa$, $d^2c_j/d\kappa^2$ from Eqs. (61,62) and an equation obtained by differentiating Eq. (62) with κ.

13. SUMMARY AND CONCLUSION

We have presented here a means to determine the order of singularity κ at the free-edge of an interface in a layered composite in which each layer is anisotropic. Although the order of singularity does not depend on the stacking sequence of the layers in the composite, the coefficients of the singular terms which are related to the intensity factor do. These coefficients can be determined only by solving the complete boundary value problem. One may use a special finite element at the free-edge using the analyses presented here and regular finite elements elsewhere in solving the complete boundary-value problem.

REFERENCES

[1] Williams, M. L., "Stress singularities resulting from various boundary conditions in angular corners of plates in extension," J. Appl. Mech., Vol. 19, 526-528, 1952.

[2] Bogy, D. B., "On the problem of edge-bonded elastic quarter-planes loaded at the boundary," Int. J. Solids Structure, Vol. 6, 1287-1313, 1970.

[3] Dempsey, J. P. and Sinclair, G. B., "On the stress singularities in the plane elasticity of the composite wedge," J. of Elasticity, Vol. 9, 373-391, 1979.

[4] Dempsey, J. P., "The wedge subjected to tractions: A paradox resolved," J. of Elasticity, in press.

[5] Lekhnitskii, S. G., "Theory of elasticity on an anisotropic elastic body," (translated by P. Fern), Holden-Day, Inc., San Francisco, 1963.

[6] Wang, S. S., and Choi, I., "Boundary layer thermal stresses in angle-ply composite laminates," Modern Developments in Composite Materials and Structures, ed. by J. R. Vinston, ASME, 315-341, 1979.

[7] Green, A. E., and Zerna, W., "Theoretical Elasticity," Oxford, Ch. 6, 1954.

[8] Bogy, D. B., "The plane solution for anisotropic elastic wedges under normal and shear loading," J. Appl. Mech., Vol. 39, 1103-1109, 1972.

[9] Kuo, M. C. and Bogy, D. B., "Plane solutions for the displacement and traction-displacement problems for anisotropic elastic wedges," J. Appl. Mech., Vol. 41, 197-203, 1974.

[10] Stroh, A. N., "Steady state problems in anisotropic elasticity," The Journal of Mathematics and Physics, Vol. 41, 77-103, 1962.

[11] Barnett, D. M., and Lothe, J., "Synthesis of the sextic and the integral formalism for dislocations, Greens functions, and surface waves in anisotropic elastic solids," Phys. Norv., Vol. 7, 13-19, 1973.

[12] Chadwick, P. and Smith, G. D., "Foundations of the theory of surface waves in anisotropic elastic materials," Advances in Applied Mechanics, Vol. 17, 303-376, 1977.

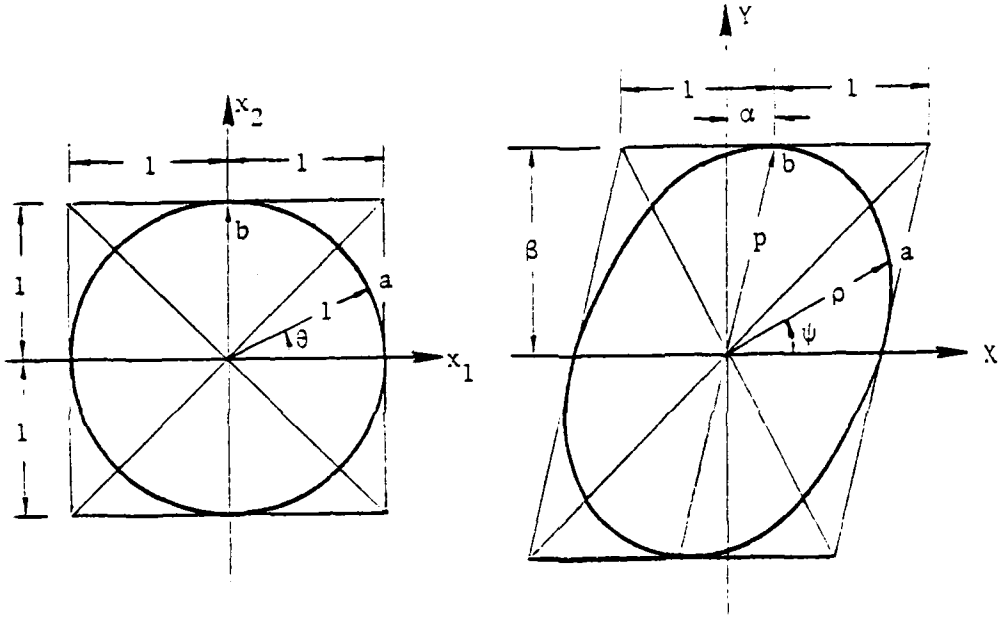

Fig. 1 Geometrical interpretation of $\Xi = x_1 + px_2 = re^{i\vartheta}$

CHAPTER 6

TRANSIENT WAVE PROPAGATION NORMAL TO THE LAYERING OF A FINITE LAYERED MEDIUM

ABSTRACT

Plane wave propagation in the direction normal to the layering of a periodically layered medium is studied. A period consists of two layers of homogeneous, isotropic, linear elastic or viscoelastic materials. The layered medium is of finite extent and hence consists of a finite number of layers. A theory is presented by which the layered medium is replaced by an "equivalent" linear homogeneous viscoelastic material such that the stress or the velocity in the latter and in the layered medium are identical at the centers of the alternate layers. Transient waves in the layered medium are then obtained by solving the transient waves in the "equivalent" homogeneous viscoelastic medium. Solutions at points other than the centers of the alternate layers are also presented. Numerical examples are given for transient waves in an elastic layered medium due to a step load applied at one of the boundary while the other boundary is fixed. Comparisons with the exact solutions by the ray theory show that the present theory can predict very satisfactorily transient waves in a finite layered medium. The theory of viscoelastic analogy applies to other cases for which exact solutions by the ray theory are not available, such as the case of finite layered medium with prescribed boundary conditions which are time-dependent.

1. INTRODUCTION

Most of the approximate theories for wave propagation in a layered medium focus on the determination of the dispersion relation or the frequency equation due to a harmonic oscillation [1-4], although some of the theories are able to predict the late-time asymptotic solution in a semi-infinite layered medium due to a step load applied at the boundary. For the latter, exact theories may be used to find the asymptotic solution and the wave-front solution [5-7].

To predict the transient response at points not necessarily far away from the impact end (where the asymptotic solution does not apply) and to points not necessarily near the wave-front, a new theory based on the analogy between the dynamic response of a semi-infinite layered medium and a semi-infinite homogeneous viscoelastic medium has been proposed recently by Ting and Mukunoki [8]. The fundamental idea is to characterize the layered medium by an "equivalent" homogeneous viscoelastic medium such that the dynamic response of the latter is identical to that of the layered medium at the centers of the alternate layers. Although the idea of modeling a composite by a viscoelastic medium is not new [9,10], the "theory of viscoelastic analogy" introduced in [8] succeeds in obtaining the exact form of the "equivalent" relaxation function for the layered medium.
Since wave propagation in a homogeneous linear viscoelastic medium can be solved easily by many known numerical schemes (see [11], for example), one can obtain the transient wave solution in a layered medium by solving the transient waves in the "equivalent" homogeneous viscoelastic medium.

The layered medium considered in [8] is of semi-infinite extent. In this paper we extend the theory to the case of a finite layered medium. First, we derive the general solution in the form of Laplace transform for

waves propagating normal to the layerings of a finite layered medium. The general solution, which is applicable to any point in the finite layered medium, contains two arbitrary coefficients which can be determined from the boundary conditions of the finite layered medium. Next, we apply the general solution to certain points in the layered medium, namely, the centers of each layer. We show that the general solution at the centers of each layer is analogous to the general solution for waves propagating in a homogeneous viscoelastic medium. From this analogy we obtain the viscoelastic relaxation function of the "equivalent" homogeneous viscoelastic medium. Several analogies can be made depending on whether one is interested in the stress response or the velocity response in the layered medium. The analogies obtained here are more general than that presented in [8] and can be applied to the semi-infinite medium as well. In finding a means for determining the response at points other than the centers of the layers, we inadvertently obtain a characteristic relation in an integral form for one-dimensional waves in homogeneous viscoelastic media. In the literature, this is in a differential form.

2. BASIC EQUATIONS

Consider a periodic layered medium as shown in Fig. 1 in which each period 2ω consists of two layers of homogeneous, isotropic, linear elastic or viscoelastic materials. The two different materials in the layers will be designated as material 1 and 2, respectively. Thus material 1 occupies layers 1, 3, 5... while material 2 occupies layers 2, 4, 6... The thicknesses of individual layers are denoted by $2h_i$ $(i = 1,2)$ where the subscripts 1 and 2 refer to material 1 and 2, respectively. We will assume that the layered medium is initially at rest and occupies the region $0 \leq x \leq \ell$. We choose the central surface of layer 1 as $x = 0$ and the other boundary, $x = \ell$,

AD-A098 683 ILLINOIS UNIV AT CHICAGO CIRCLE DEPT OF MATERIALS ENG--ETC F/G 11/4
STRESS ANALYSIS OF COMPOSITES.(U)
JAN 81 R L SPILKER, T C TING

UNCLASSIFIED

DAAG46-79-C-0045

AMMRC-TR-81-8

NL

3 OF 3

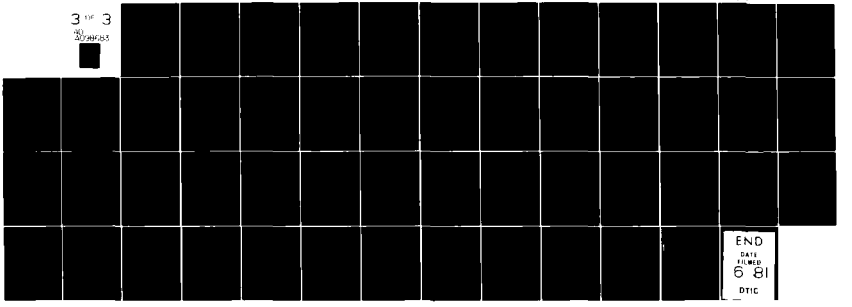

END
DATE FILMED
6 81
DTIC

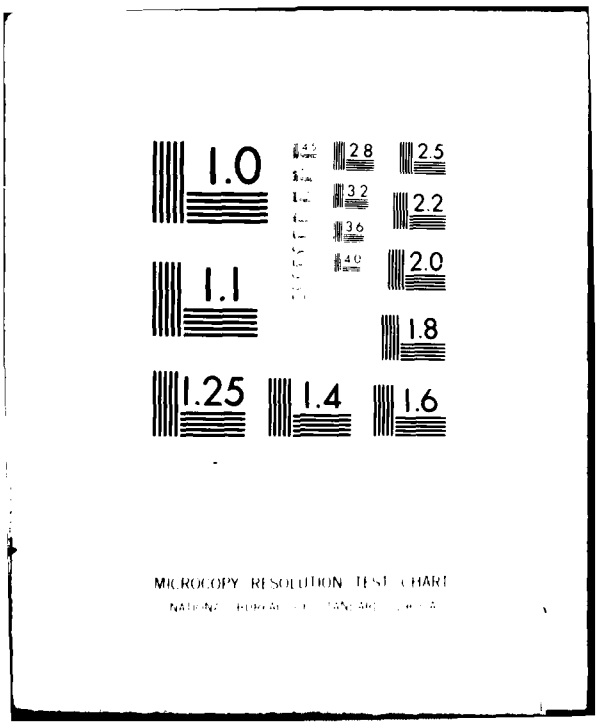
1.0
1.1
1.25
1.4
1.6
1.8
2.0
2.2
2.5
2.8
3.2
3.6
4.0
MICROCOPY RESOLUTION TEST CHART

is assumed to be at the central surface of layer N where N can be an even or odd integer. Hence,

$$\ell = (N - 1)\omega \tag{1}$$

We will consider plane wave propagation in the direction x in which the only non-vanishing component of the displacement is in the x direction. We therefore have a one-dimensional wave propagation problem in which the equation of motion and the continuity of the displacement are given by

$$\frac{\partial \sigma_i}{\partial x} = \rho_i \dot{v}_i \ , \qquad (i = 1,2) \tag{2}$$

$$\frac{\partial v_i}{\partial x} = \dot{\varepsilon}_i \ , \qquad (i = 1,2) \tag{3}$$

where a dot stands for differentiation with respect to the time t, and σ_i, ε_i, v_i, ρ_i $(i = 1,2)$ are the normal stress, normal strain, particle velocity and mass density, respectively. Let $\lambda_i(t)$ and $\mu_i(t)$ be the relaxation functions of the materials. For elastic materials, $\lambda_i(t)$ and $\mu_i(t)$ are independent of t and are identified as Lamé constants. The stress-strain relation can be written in the form of Stieltjes convolution

$$\sigma_i(x,t) = \int_{0^-}^{t} g_i(t - t')\, d\varepsilon_i(x,t') \ , \tag{4}$$

$$g_i(t) = \lambda_i(t) + 2\mu_i(t) \ , \tag{5}$$

where we have assumed that

$$\sigma_i(x,0^-) = v_i(x,0^-) = \varepsilon_i(x,0^-) = 0 \ . \tag{6}$$

3. GENERAL SOLUTIONS

The general solution to Eqs. (2-6) can be obtained by the method of Laplace transform and by the use of the Floquet theory. We define the Laplace

transform, $\bar{f}(p)$, of a function $f(t)$ by

$$\bar{f}(p) = \int_{0^-}^{t} f(t)e^{-pt}\, dt \tag{7}$$

After applying the Laplace transform to Eqs. (2-6), the general solution for the stress and the velocity in layers 1 and 2 can be written as

$$\bar{\sigma}_1(x,p) = \bar{A}_1 \cosh(k_1 x) + \bar{B}_1 \sinh(k_1 x) \tag{8a}$$

$$\bar{v}_1(x,p) = \frac{1}{m_1}\left\{\bar{A}_1 \sinh(k_1 x) + \bar{B}_1 \cosh(k_1 x)\right\} \tag{8b}$$

$$\bar{\sigma}_2(x,p) = \bar{A}_2 \cosh(k_2 x - k_2 \omega) + \bar{B}_2 \sinh(k_2 x - k_2 \omega) \tag{8c}$$

$$\bar{v}_2(x,p) = \frac{1}{m_2}\left\{\bar{A}_2 \sinh(k_2 x - k_2 \omega) + \bar{B}_2 \cosh(k_2 x - k_2 \omega)\right\} \tag{8d}$$

where

$$\left.\begin{aligned} \omega &= h_1 + h_2 \\ k_i &= \sqrt{\rho_i p/\bar{g}_i} \\ m_i &= \rho_i p/k_i = \sqrt{\rho_i p \bar{g}_i} \end{aligned}\right\} \tag{9}$$

$\bar{A}_i$ and $\bar{B}_i$ $(i = 1,2)$ are determined by the continuity condition at $x = h_1$

$$\begin{bmatrix} \bar{\sigma}_1 \\ \bar{v}_1 \end{bmatrix}(h_1,p) = \begin{bmatrix} \bar{\sigma}_2 \\ \bar{v}_2 \end{bmatrix}(h_1,p) \tag{10}$$

and the quasi-periodicity property of the solution together with the continuity condition at $x = 2\omega - h_1$

$$\begin{bmatrix} \bar{\sigma}_2 \\ \bar{v}_2 \end{bmatrix}(2\omega - h_1,p) = \begin{bmatrix} \bar{\sigma}_1 \\ \bar{v}_1 \end{bmatrix}(-h_1,p)\, e^{-2\omega\kappa} \tag{11}$$

where κ is the characteristic exponent [12]. Substitution of Eqs. (8) into Eqs. (10) and (11) leads to four homogeneous equations for $\bar{A}_i$ and $\bar{B}_i$. The

requirement for a non-trivial solution results in the following equation for the characteristic exponent κ:

$$\cosh(2\omega\kappa) = \theta \cosh(2k_1h_1 + 2k_2h_2) - (\theta-1)\cosh(2k_1h_1 - 2k_2h_2) \tag{12}$$

$$\theta = \frac{1}{4}\left(\frac{1}{m_1} + 2 + \frac{1}{m_2}\right) \tag{13}$$

Moreover, $\bar{A}_i$ and $\bar{B}_i$ are related by

$$\left.\begin{aligned} \frac{\bar{A}_2}{\bar{A}_1} &= p\bar{M}e^{-\omega\kappa} , & \frac{\bar{B}_2}{\bar{A}_1} &= -p\bar{R}m_2e^{-\omega\kappa} , \\ \frac{\bar{B}_1}{\bar{A}_1} &= -p\bar{L}_1 , & \frac{\bar{B}_2}{\bar{A}_2} &= -p\bar{L}_2 , \end{aligned}\right\} \tag{14}$$

where

$$\left.\begin{aligned} \bar{L}_1 &= m_1\bar{R}p\bar{M} , & \bar{L}_2 &= m_2\bar{R}/(p\bar{M}) \\ p\bar{M} &= \frac{m_1C_1C_2 + m_2S_1S_2}{m_1\cosh(\omega\kappa)} = \frac{m_2\cosh(\omega\kappa)}{m_2C_1C_2 + m_1S_1S_2} \\ p\bar{R} &= \frac{m_1C_1S_2 + m_2C_2S_1}{m_1m_2\sinh(\omega\kappa)} = \frac{\sinh(\omega\kappa)}{m_2C_1S_2 + m_1C_2S_1} \\ C_i &= \cosh(k_ih_i) , & S_i &= \sinh(k_ih_i) \end{aligned}\right\} \tag{15}$$

Notice that if we interchange the subscripts 1 and 2, the expression for $p\bar{R}$ remains unchanged while $p\bar{M}$ becomes $(p\bar{M})^{-1}$. Therefore, we can obtain the Stieltjes inversion of M(t) by simply interchanging the subscripts 1 and 2 in the expression for $p\bar{M}$ and applying the Laplace inverse transform.

With Eq. (14), the general solution in the layers 1 and 2 as expressed by Eq. (8) can now be reduced to a solution containing only one coefficient, say $\bar{A}_1$. The solutions in other layers are obtained by the quasi-periodicity relation:

$$\begin{bmatrix} \bar{\sigma}_i \\ \bar{v}_i \end{bmatrix} (2n\omega + x, p) = \begin{bmatrix} \bar{\sigma}_i \\ \bar{v}_i \end{bmatrix} (x, p)\, e^{-2n\omega\kappa} \tag{16}$$

where n is an integer. Moreover, we see from Eq. (12) that if κ is a characteristic exponent, so is $-\kappa$. Therefore, in addition to the general solution with $\bar{A}_1$ as the coefficient, we obtain the second general solution by changing the sign of κ. The coefficient of this second solution will be denoted by $\bar{A}_1'$. Consequently, the general solution for the stress and velocity at any point x in the layered medium can be written as, using Eqs. (8,14,16),

$$\bar{\sigma}_1(2n\omega + x_1, p) = \bar{A}_1 \left\{\cosh(k_1 x_1) - p\bar{L}_1 \sinh(k_1 x_1)\right\} e^{-2n\omega\kappa} + \bar{A}_1' \left\{\cosh(k_1 x_1) + p\bar{L}_1 \sinh(k_1 x_1)\right\} e^{2n\omega\kappa} \tag{17a}$$

$$\bar{v}_1(2n\omega + x_1, p) = \frac{\bar{A}_1}{m_1} \left\{\sinh(k_1 x_1) - p\bar{L}_1 \cosh(k_1 x_1)\right\} e^{-2n\omega\kappa} + \frac{\bar{A}_1'}{m_1} \left\{\sinh(k_1 x_1) + p\bar{L}_1 \cosh(k_1 x_1)\right\} e^{2n\omega\kappa} \tag{17b}$$

$$\bar{\sigma}_2(2n\omega + \omega + x_2, p) = \bar{A}_1 p\bar{M} \left\{\cosh(k_2 x_2) - p\bar{L}_2 \sinh(k_2 x_2)\right\} e^{-(2n+1)\omega\kappa} + \bar{A}_1' p\bar{M} \left\{\cosh(k_2 x_2) + p\bar{L}_2 \sinh(k_2 x_2)\right\} e^{(2n+1)\omega\kappa} \tag{17c}$$

$$\bar{v}_2(2n\omega + \omega + x_2, p) = \frac{\bar{A}_1}{m_2} p\bar{M} \left\{\sinh(k_2 x_2) - p\bar{L}_2 \cosh(k_2 x_2)\right\} e^{-(2n+1)\omega\kappa} + \frac{\bar{A}_1'}{m_2} p\bar{M} \left\{\sinh(k_2 x_2) + p\bar{L}_2 \cosh(k_2 x_2)\right\} e^{(2n+1)\omega\kappa} \tag{17d}$$

where

$$-h_i \le x_i \le h_i \quad , \qquad (i = 1,2) \tag{18}$$

When proper values for n and x_1 (or x_2) are chosen, Eqs. (17) can be used to determine solution at any point in the layered medium. The two coefficients $\bar{A}_1$ and $\bar{A}_1'$ are determined from the boundary conditions at $x = 0$ and $x = \ell$.

In the next section we will show how one can obtain the solution at the centers of the layers by solving the wave propagation problem in an "equivalent" homogeneous viscoelastic medium. Having found the viscoelastic analogy for the solution at the centers of the layers, we then show how one can obtain the solution at points other than the centers of the layers in terms of the solution at the centers of the layers.

4. SOLUTION AT CENTERS OF LAYERS

The stress and velocity at the centers of the layers have specially simple forms. By letting $x_1 = x_2 = 0$ in Eq. (17), we have

$$\left.\begin{aligned}
\tilde{\sigma}_1(2n\omega, p) &= \bar{A}_1 e^{-2n\omega\kappa} + \bar{A}_1' e^{2n\omega\kappa} \\
\tilde{v}_1(2n\omega, p) &= \frac{p\bar{L}_1}{m_1}\left(-\bar{A}_1 e^{-2n\omega\kappa} + \bar{A}_1' e^{2n\omega\kappa}\right) \\
\tilde{\sigma}_2(2n\omega + \omega, p) &= p\bar{M}\left(\bar{A}_1 e^{-(2n+1)\omega\kappa} + \bar{A}_1' e^{(2n+1)\omega\kappa}\right) \\
\tilde{v}_2(2n\omega + \omega, p) &= \frac{p\bar{L}_2}{m_2}\, p\bar{M}\left(-\bar{A}_1 e^{-(2n+1)\omega\kappa} + \bar{A}_1' e^{(2n+1)\omega\kappa}\right)
\end{aligned}\right\} \qquad (19)$$

We now consider a homogeneous, isotropic, linear viscoelastic medium which occupies $0 \le x \le \ell$ and which is at rest at $t = 0^-$ and is subjected to certain prescribed boundary conditions at $x = 0$ and $x = \ell$. Let Φ, η and V be the normal stress, normal strain and particle velocity, respectively. Also, let ρ and G be the "equivalent" mass density and the "equivalent" relaxation function of this homogeneous viscoelastic material.

The equation of motion, the continuity condition, the stress-strain relation and the initial conditions are

$$\left.\begin{aligned} &\frac{\partial \Phi}{\partial x} = \rho \dot{V} \\ &\frac{\partial V}{\partial x} = \dot{\eta} \\ &\Phi(x,t) = \int_{0^-}^{t} G(t-t')\, d\eta(x,t') \\ &\Phi(x,0^-) = V(x,0^-) = \eta(x,0^-) = 0 \end{aligned}\right\} \tag{20}$$

By applying the Laplace transform to Eqs. (20), the general solution for the stress and velocity will contain the exponential term

$$\exp\left(\pm \sqrt{\rho p/\bar{G}}\; x\right) \tag{21}$$

In view of the exponential terms in Eqs. (19), we will define the "equivalent" relaxation function $G(t)$ by the relation

$$\kappa = \sqrt{\rho p/\bar{G}} \tag{22}$$

We will also define the "equivalent" mass density ρ by the average mass density in the layered medium [4,8]:

$$\rho = (\rho_1 h_1 + \rho_2 h_2)/(h_1 + h_2) \tag{23}$$

With Eq. (22), the general solution to Eq. (20) can be written as

$$\bar{\Phi}(x,p) = \bar{a}\, e^{-\kappa x} + \bar{a}'\, e^{\kappa x} \tag{24a}$$

$$\bar{V}(x,p) = \frac{\kappa}{\rho p}\left(-\bar{a}\, e^{-\kappa x} + \bar{a}'\, e^{\kappa x}\right) \tag{24b}$$

where $\bar{a}$ and $\bar{a}'$ are arbitrary functions of p.

There are several ways to identify the analogy between Eqs. (19) and (24). If the stress in material 1 is of main interest, we may set

$$\bar{A}_1 = \bar{a} \ , \qquad \bar{A}_1' = \bar{a}' \tag{25}$$

we then have

$$\left.\begin{aligned} \bar{\sigma}_1(x,p) &= \bar{\Phi}(x,p) \\ \bar{v}_1(x,p) &= p\bar{J}_1\bar{V}(x,p) \end{aligned}\right\} \quad \text{for} \quad x = 2n\omega \tag{26a}$$

and

$$\left.\begin{aligned} \bar{\sigma}_2(x,p) &= p\bar{M}\bar{\Phi}(x,p) \\ \bar{v}_2(x,p) &= p\bar{M}\{p\bar{J}_2\bar{V}(x,p)\} \end{aligned}\right\} \quad \text{for} \quad x = (2n+1)\omega \tag{26b}$$

where

$$\bar{J}_i = \frac{\rho p\bar{L}_i}{\kappa m_i} \ , \qquad (i = 1,2) \tag{27}$$

It should be pointed out that while $\bar{\Phi}$ and $\bar{V}$ as given by Eq. (24) are defined for all x, Eqs. (26a) and (26b) apply only to $x = 2n\omega$ and $x = (2n+1)\omega$, respectively. By using the identity,

$$\bar{J}_1/\bar{J}_2 = (p\bar{M})^2 = m_2\bar{L}_1/(m_1\bar{L}_2) \tag{28}$$

the last of Eq. (26b) can be written as

$$\bar{v}_2(x,p) = \frac{1}{p\bar{M}}\{p\bar{J}_1\bar{V}(x,p)\} \ , \qquad x = (2n+1)\omega \tag{29}$$

With Eq. (29), we rewrite Eqs. (26) in the following form:

$$\sigma_1(2n\omega,t) = \Phi(2n\omega,t) \tag{30a}$$

$$v_1(2n\omega,t) = V^*(2n\omega,t) \tag{30b}$$

$$\sigma_2(2n\omega+\omega,t) = \int_{0^-}^{t} M(t-t')\, d\Phi\,(2n\omega+\omega,t') \tag{30c}$$

$$v_2(2n\omega+\omega,t) = \int_{0^-}^{t} M^{-1}(t-t')\, dV^*\,(2n\omega+\omega,t') \tag{30d}$$

where

$$V^*(x,t) = \int_{0^-}^{t} J_1(t-t')\, dV\,(x,t') \tag{30e}$$

and M^{-1} is the Stieltjes inverse of M. (See the discussion following Eq. (15) regarding the Stieltjes inverse of M.) Thus the stress and velocity at the centers of the layers are related to the stress Φ and velocity V in the "equivalent" homogeneous medium. In particular, the stress at the centers of the odd layers, $\sigma_1(2\omega,t)$, is identical to the stress Φ in the "equivalent" homogeneous viscoelastic medium.

As an illustration for the theory of viscoelastic analogy, we consider an elastic layered medium which is fixed at the center of the 14th layer (i.e., $\ell = 13\omega$) and subjected to a unit step stress applied at $x = 0$. Since the 14th layer is occupied by material 2, we have the following boundary conditions:

$$\sigma_1(0,t) = H(t) \quad , \qquad v_2(13\omega,t) = 0 \tag{31a}$$

where H(t) is the Heaviside step function. In view of Eqs. (30), the corresponding boundary conditions for the "equivalent" viscoelastic medium are:

$$\Phi(0,t) = H(t) \quad , \qquad V(13\omega,t) = 0 \tag{31b}$$

We now replace the elastic layered medium by the "equivalent" homogeneous viscoelastic medium whose mass density ρ and the relaxation function G(t) are given by Eqs. (23) and (22). Because of the complicated expression for κ as given by Eq. (12), analytical inversion of the Laplace transform $\bar{G}(p)$ from Eq. (22) does not appear feasible. We therefore resort to a numerical Laplace inversion of $\bar{G}(p)$, [13]. The result is shown in Fig. 2 along with the physical parameters of the elastic layered medium used in the calculation. The physical parameters are taken from [4]. Unlike for most real viscoelastic materials, the relaxation function for the "equivalent" viscoelastic medium is not a monotonically decreasing function of t. This was also predicted by Christensen [10] based on the dielectric theory. In

[8] one can find a discussion on the behavior of $G(t)$ as $t \to 0$ and $t \to \infty$ as well as the value of $\dot{G}(t)$ at $t = 0$.

With $G(t)$ given by Fig. 2 and the boundary conditions given by Eq. (31b), we integrate Eq. (20) numerically by the method of characteristics [14] for the stress Φ and velocity V in the "equivalent" homogeneous viscoelastic medium. The stress and velocity at the centers of the layers in the layered medium are then determined by using the viscoelastic analogy Eqs. (30). In Fig. 3 we present $\Phi(4\omega,t)$ which is the stress history at the center of the 5th layer. For this example, the exact solution in the elastic layered medium using the ray theory can be obtained numerically by keeping track of every reflected and transmitted waves at the interfaces of the layers [8]. This exact solution is also shown in Fig. 3 for comparison. It is seen that the agreement is excellent.

In Fig. 3 we also show the solution obtained by the effective modulus theory [15]. With this theory, the elastic layered medium is replaced by a homogeneous elastic medium whose effective modulus g_{eff} is given by

$$\frac{1}{g_{eff}} = \left(\frac{h_1}{g_1} + \frac{h_2}{g_2}\right) \Big/ \left(h_1 + h_2\right) \tag{32}$$

and whose effective mass density is identical to the "equivalent" mass density defined in Eq. (23).

In Figs. 4 and 5 we show, respectively, the velocity history at the center of the 5th layer and the stress history at the center of the 8th layer by using Eqs. (30b) and (30c). Since $\Phi(x,t)$ and $V(x,t)$ have already been determined, all we need is the functions $J_1(t)$ and $M(t)$ which are defined in Eqs. (27) and (15). $J_1(t)$ and $M(t)$ are obtained numerically by inverting their Laplace transforms. Again, the solutions by the ray theory

and the effective modulus theory are also shown in the figures for comparison.

The function J_i as well as functions M, R, and L_i, (i = 1,2) defined in Eq. (15) are called the "auxiliary" functions. Like G(t), the auxiliary functions depend only on the physical properties and the geometrical layering of the layered medium. They are independent of the boundary conditions. For the viscoelastic analogy given by Eqs. (30), only the functions J_1, M, and M^{-1} are needed. Of course, if $\sigma_1(2\omega,t)$ is the only quantity desired, no auxiliary functions are needed.

Before we study the solution at points other than the centers of the layers, we will discuss other forms of viscoelastic analogy in the next section.

5. OTHER FORMS OF VISCOELASTIC ANALOGY

In Eqs. (30) we present one form of viscoelastic analogy between Eqs. (19) and (24). The analogy, Eqs. (30), is convenient for the case when the stress in material 1 is of main interest because according to Eq. (30a) σ_1 is identical to Φ. If the stress in material 2 is of main interest, then the analogy given by Eq. (30c) requires a convolution integral with the auxiliary function M(t).

There are of course other forms of viscoelastic analogy which would be more convenient for other situations. If the stress in material 2 is of main interest, one may set

$$\left.\begin{aligned} p\bar{M}\bar{A}_1 &= \bar{a} \\ p\bar{M}\bar{A}_1' &= \bar{a}' \end{aligned}\right\} \tag{33}$$

Then the analogy between Eqs. (19) and (24) can be written as

$$
\left.
\begin{aligned}
\sigma_2(2n\omega+\omega,t) &= \Phi(2n\omega+\omega,t) \\
v_2(2n\omega+\omega,t) &= V^*(2n\omega+\omega,t) \\
\sigma_1(2n\omega,t) &= \int_{0^-}^{t} M^{-1}(t-t')\, d\Phi(2n\omega,t') \\
v_1(2n\omega,t) &= \int_{0^-}^{t} M(t-t')\, dV^*(2n\omega,t') \\
V^*(x,t) &= \int_{0^-}^{t} J_2(t-t')\, dV(x,t')
\end{aligned}
\right\} \qquad (34)
$$

With this analogy, the stress Φ in the "equivalent" viscoelastic medium is identical to σ_2 at $x = (2n+1)\omega$.

Likewise, if the velocity in material 1 is of main interest, the viscoelastic analogy can be written as

$$
\left.
\begin{aligned}
v_1(2n\omega,t) &= V(2n\omega,t) \\
\sigma_1(2n\omega,t) &= \Phi^*(2n\omega,t) \\
v_2(2n\omega+\omega,t) &= \int_{0^-}^{t} M^{-1}(t-t')\, dV(2n\omega+\omega,t') \\
\sigma_2(2n\omega+\omega,t) &= \int_{0^-}^{t} M(t-t')\, d\Phi^*(2n\omega+\omega,t') \\
\Phi^*(x,t) &= \int_{0^-}^{t} J_1^{-1}(t-t')\, d\Phi(x,t')
\end{aligned}
\right\} \qquad (35)
$$

Finally, if the velocity in material 2 is of main interest, we can write

$$
\left.
\begin{aligned}
v_2(2n\omega+\omega,t) &= V(2n\omega+\omega,t) \\
\sigma_2(2n\omega+\omega,t) &= \Phi^*(2n\omega+\omega,t) \\
v_1(2n\omega,t) &= \int_{0^-}^{t} M(t-t')\, dV(2n\omega,t')
\end{aligned}
\right\} \qquad (36)
$$

$$\left.\begin{aligned}\sigma_1(2n\omega,t) &= \int_{0^-}^{t} M^{-1}(t-t')\, d\Phi^*(2n\omega,t') \\ \Phi^*(x,t) &= \int_{0^-}^{t} J_2^{-1}(t-t')\, d\Phi(x,t')\end{aligned}\right\} \quad \begin{matrix}(36)\\ \text{Cont'd}\end{matrix}$$

Sometimes the boundary conditions may influence the choice of a viscoelastic analogy. For example, suppose that one is interested in the stress in material 1 for the problem in which the velocity is prescribed at $x = 0$ (i.e., $v_1(0,t)$ is known), and the other boundary $x = \ell$ is fixed. We could use either the analogy Eqs. (30) or the analogy Eqs. (35). If we use Eqs. (30), we obtain σ_1 directly from Φ but then we have to transform the boundary condition $v_1(0,t)$ to $V(0,t)$ by using Eqs. (30b,e),

$$V(0,t) = \int_{0^-}^{t} J_1^{-1}(t-t')\, dv_1(0,t') \tag{37}$$

before we solve for Φ and V in the "equivalent" homogeneous viscoelastic medium. If we use Eqs. (35), we can solve for Φ and V immediately since $V(0,t) = v_1(0,t)$, but to obtain σ_1 from Φ a convolution integral is required.

6. SOLUTION AT ARBITRARY POINTS

If we solve for $\bar{A}_1$ and $\bar{A}_1'$ from the first two equations of Eqs. (19) and substitute the results into Eqs. (17a,b), we have

$$\begin{aligned}\bar{\sigma}_1(2n\omega + x_1,p) &= \tfrac{1}{2}\left(e^{k_1x_1} + e^{-k_1x_1}\right)\bar{\sigma}_1(2n\omega,p) \\ &\quad + \tfrac{1}{2}\left(e^{k_1x_1} - e^{-k_1x_1}\right) m_1\bar{v}_1(2n\omega,p)\end{aligned} \tag{38a}$$

$$\begin{aligned}\bar{v}_1(2n\omega + x_1,p) &= \tfrac{1}{2}\left(e^{k_1x_1} + e^{-k_1x_1}\right)\bar{v}_1(2n\omega,p) \\ &\quad + \tfrac{1}{2}\left(e^{k_1x_1} - e^{-k_1x_1}\right)\frac{1}{m_1}\,\bar{\sigma}_1(2n\omega,p)\end{aligned} \tag{38b}$$

Similar results can be obtained for $\sigma_2(2n\omega + \omega + x_2, p)$ and $v_2(2n\omega + \omega + x_2, p)$.

We will define the Laplace transform of the functions $D_1(x_1,t)$, $E_1(x_1,t)$ and $F_1(x_1,t)$ by

$$\left.\begin{aligned} \bar{D}_1(x_1,p) &= \frac{1}{p} e^{-k_1 x_1} \\ \bar{E}_1(x_1,p) &= \frac{1}{pm_1} e^{-k_1 x_1} \\ \bar{F}_1(x_1,p) &= \frac{m_1}{p} e^{-k_1 x_1} \end{aligned}\right\} \tag{39}$$

D_1, E_1 and F_1 have the following physical interpretation. Suppose that material 1 occupies the semi-infinite space $x \geq 0$ and is initially at rest. Then $D_1(x_1,t)$ and $E_1(x_1,t)$ are, respectively, the stress and velocity history at $x = x_1$ due to a unit step normal stress applied at $x = 0$. $F_1(x_1,t)$ is the stress history at $x = x_1$ due to a unit step velocity applied at $x = 0$. We now rewrite Eq. (38a) as

$$\begin{aligned} \bar{\sigma}_1(2n\omega + x_1, p) = {} & \frac{1}{2}\left\{\bar{\sigma}_1(2n\omega,p)\, e^{px_1/c_{10}}\right\} p\left\{\bar{D}_1(-x_1,p)\, e^{-px_1/c_{10}}\right\} \\ & + \frac{1}{2}\left\{\bar{\sigma}_1(2n\omega,p)\, e^{-px_1/c_{10}}\right\} p\left\{\bar{D}_1(x_1,p)\, e^{px_1/c_{10}}\right\} \\ & + \frac{1}{2}\left\{\bar{v}_1(2n\omega,p)\, e^{px_1/c_{10}}\right\} p\left\{\bar{F}_1(-x_1,p)\, e^{-px_1/c_{10}}\right\} \\ & - \frac{1}{2}\left\{\bar{v}_1(2n\omega,p)\, e^{-px_1/c_{10}}\right\} p\left\{\bar{F}_1(x_1,p)\, e^{px_1/c_{10}}\right\} \end{aligned} \tag{40}$$

where

$$c_{i0} = \sqrt{g_i(0)/\rho_i}\,, \qquad (i = 1,2) \tag{41}$$

and $D_1(-x_1,t)$ is obtained from $D_1(x_1,t)$ by analytically extrapolating the later from $x_1 > 0$ to $x_1 < 0$. Similar definition applies to $F_1(-x_1,t)$. Equation (40) can now be inverted as

$$
\begin{aligned}
\sigma_1(2n\omega + x_1,t) = {} & \frac{1}{2}\int_{0^-}^{t} \sigma_1\left(2n\omega, t + \frac{x_1}{c_{10}} - t'\right) dD_1\left(-x_1, t' - \frac{x_1}{c_{10}}\right) \\
& + \frac{1}{2}\int_{0^-}^{t} \sigma_1\left(2n\omega, t - \frac{x_1}{c_{10}} - t'\right) dD_1\left(x_1, t' + \frac{x_1}{c_{10}}\right) \\
& + \frac{1}{2}\int_{0^-}^{t} v_1\left(2n\omega, t + \frac{x_1}{c_{10}} - t'\right) dF_1\left(-x_1, t' - \frac{x_1}{c_{10}}\right) \\
& - \frac{1}{2}\int_{0^-}^{t} v_1\left(2n\omega, t - \frac{x_1}{c_{10}} - t'\right) dF_1\left(x_1, t' + \frac{x_1}{c_{10}}\right)
\end{aligned} \tag{42}
$$

Equation (42) can be written in a compact form if we observe that $\sigma_1(2n\omega,t)$ and $v_1(2n\omega,t)$ vanish for $t < 0$, and $D_1(\pm x_1,t)$ and $F_1(\pm x_1,t)$ vanish for $t < \pm x_1/c_{10}$ and that $-h_1 \le x_1 \le h_1$ by Eq. (18). We have

$$
\begin{aligned}
\sigma_1(2n\omega + x_1,t) = {} & \frac{1}{2}\int_{(-h_1/c_{10})^-}^{t} \sigma_1(2n\omega, t - t')\, d\left\{D_1(-x_1,t') + D_1(x_1,t')\right\} \\
& + \frac{1}{2}\int_{(-h_1/c_{10})^-}^{t} v_1(2n\omega, t - t')\, d\left\{F_1(-x_1,t') - F_1(x_1,t')\right\}
\end{aligned} \tag{43a}
$$

By a similar argument, we obtain from Eq. (38b),

$$
\begin{aligned}
v_1(2n\omega + x_1,t) = {} & \frac{1}{2}\int_{(-h_1/c_{10})^-}^{t} v_1(2n\omega, t - t')\, d\left\{D_1(-x_1,t') + D_1(x_1,t')\right\} \\
& + \frac{1}{2}\int_{(-h_1/c_{10})^-}^{t} \sigma_1(2n\omega, t - t')\, d\left\{E_1(-x_1,t') - E_1(x_1,t')\right\}
\end{aligned} \tag{43b}
$$

When material 1 is elastic, m_1 is a constant and D_1, E_1 and F_1 are step functions:

$$\left.\begin{aligned} D_1(\pm x_1,t) &= H\left(t \mp \frac{x_1}{c_{10}}\right) \\ E_1(\pm x_1,t) &= \frac{1}{m_1} H\left(t \mp \frac{x_1}{c_{10}}\right) \\ F_1(\pm x_1,t) &= m_1 H\left(t \mp \frac{x_1}{c_{10}}\right) \end{aligned}\right\} \tag{44}$$

Equations (43) then reduce to (when material 1 is elastic)

$$\begin{aligned} \sigma_1(2n\omega + x_1,t) &= \frac{1}{2}\left\{\sigma_1\left(2n\omega,t + \frac{x_1}{c_{10}}\right) + \sigma_1\left(2n\omega,t - \frac{x_1}{c_{10}}\right)\right\} \\ &\quad + \frac{m_1}{2}\left\{v_1\left(2n\omega,t + \frac{x_1}{c_{10}}\right) - v_1\left(2n\omega,t - \frac{x_1}{c_{10}}\right)\right\} \end{aligned} \tag{45a}$$

$$\begin{aligned} v_1(2n\omega + x_1,t) &= \frac{1}{2}\left\{v_1\left(2n\omega,t + \frac{x_1}{c_{10}}\right) + v_1\left(2n\omega,t - \frac{x_1}{c_{10}}\right)\right\} \\ &\quad + \frac{1}{2m_1}\left\{\sigma_1\left(2n\omega,t + \frac{x_1}{c_{10}}\right) - \sigma_1\left(2n\omega,t - \frac{x_1}{c_{10}}\right)\right\} \end{aligned} \tag{45b}$$

This is nothing more than the familiar characteristic relation for one-dimensional waves in a homogeneous elastic medium. As such, Eq. (43) may be regarded as the characteristic relation in an integral form for one-dimensional waves in a homogeneous viscoelastic medium.

After finding the stress and velocity at the center of the 5th layer in Figs. 3 and 4, we use Eq. (45a) to find the stress history at the interface between the 4th and the 5th layers by letting $n = 4$ and $x_1 = -h_1$. The result is shown in Fig. 6 along with the exact solution by the ray theory.

7. DISCUSSION AND CONCLUDING REMARKS

Several analogies between the solutions of transient waves in a finite layered medium and in a finite homogeneous viscoelastic medium are established.

The analogies between the solutions apply to the centers of the alternate layers in the layered medium. Solutions at points other than the centers of the alternate layers are obtained in terms of the solutions at the centers of the alternate layers through the use of convolution integrals with auxiliary functions introduced in the paper. The materials in the individual layer of the layered medium can be elastic or viscoelastic, although numerical examples are given for an elastic layered medium.

The viscoelastic analogies derived here lead us to an exact expression $\bar{G}(p)$, which is the Laplace transform of the relaxation function $G(t)$ for the "equivalent" homogeneous viscoelastic medium. The relaxation function $G(t)$ is obtained by numerically inverting its Laplace transform using the method outlined in [13,14]. The method used in [13,14] tends to provide the value of $G(t)$ only at a finite number of t's which are close to $t = 0$. It provides poor information on $G(t)$ for large t. Fortunately, our relaxation function approaches rapidly to the equilibrium relaxation modulus G_∞ so that the inversion obtained by the method in [13,14] is adequate for most cases. One could certainly obtain a better numerical inversion of a Laplace transform by using other techniques such as the fast Fourier transform [16].

Even though the relaxation function $G(t)$ obtained here is quite crude, we have reached an excellent agreement between the solutions by the viscoelastic analogy and by the exact ray theory. The differences in the solutions are caused mainly from the numerical Laplace inversion of the relaxation function $\bar{G}(p)$ and the auxiliary functions $\bar{M}(p)$ and $\bar{J}_1(p)$. For those solutions which require no auxiliary functions, the differences in the solutions are less noticeable. Some of the auxiliary functions, namely, M, R, L_1 and L_2 defined in Eq. (15) can be determined exactly when the

constituents of the layered medium are elastic. With the use of exact auxiliary functions, the differences between the solutions by the viscoelastic analogy and by the ray theory can be made smaller [14].

One might ask the relative advantages of the viscoelastic analogy over a direct numerical computation of the original layered problem. In a direct computation of waves in the original layered medium, the calculations are feasible when the boundary conditions are constant in time and the individual layers are elastic. Moreover, keeping track of every reflection and transmission of waves at the interfaces between the layers may soon exhaust the storage capacity of the computor, not to mention the computing time. The situation is particularly acute when there are a large number of layers involved as in a real composite. These shortcomings are not present in the theory of viscoelastic analogy. One possible shortcoming of the theory of viscoelastic analogy approach is the less accurate result for the solution at points other than the centers of the layers. This shortcoming is not serious in practical applications when the individual layers are very thin such that the solution at the center of a layer and at other points in the layer are practically the same.

In connection with the present work on transient waves in a finite layered medium, we would like to point out that harmonic waves in a finite layered medium has been considered by Herrmann, Beaupre and Auld [17]. In contrast to the normal stress waves studied here, the harmonic waves considered in [17] are horizontally polarized shear waves. However, one can see from the analyses presented here that if we replace the normal stress and the normal displacement by the shear stress and the transverse displacement, respectively, the analyses presented here apply to the transient shear waves in finite layered media as well.

REFERENCES

[1] Sun, C. T., Achenbach, J. D. and Herrmann, G., "Continuum Theory for a Laminated Medium," J. Appl. Mech., Vol. 35, 1968, 467-475.

[2] Stern, M., Bedford, A. and Yew, C. H., "Wave Propagation in Viscoelastic Laminates," J. Appl. Mech., Vol. 38, 1971, 448-454.

[3] Drumheller, D. S. and Bedford, A., "On a Continuum Theory for a Laminated Medium," J. Appl. Mech., Vol. 40, 1973, 527-532.

[4] Hegemier, G. A. and Nayfeh, A. H., "A Continuum Theory for Wave Propagation in Laminated Composites, Case 1: Propagation Normal to the Laminates," J. Appl. Mech., Vol. 40, 1973, 503-510.

[5] Peck, J. C. and Gurtman, G. A., "Dispersive Pulse Propagation Parallel to the Interfaces of a Laminated Composite," J. Appl. Mech., Vol. 36, 1969, 479-484.

[6] Sve, C., "Stress Wave Attenuation in Composite Materials," J. Appl. Mech., Vol. 39, 1972, 1151-1153.

[7] Chen C. C. and Clifton, R. J., "Asymptotic Solutions for Wave Propagation in Elastic and Viscoelastic Bilaminates," Proc. 14th Midwestern Mech. Conf., Univ. of Oklahoma, 1975, 399-417.

[8] Ting, T. C. T. and Mukunoki, Isao," A Theory of Viscoelastic Analogy for Wave Propagation Normal to the Layering of a Layered Medium," to appear in J. Appl. Mech.

[9] Barker, L. M., "A Model for Stress Wave Propagation in Composite Materials," J. Composite Materials, Vol. 5, April 1971, 140-162.

[10] Christensen, R. M., "Wave Propagation in Layered Elastic Media," J. Appl. Mech., Vol. 42, 1975, 153-158.

[11] Glauz, R. D. and Lee, E. H., "Transient Wave Analysis in a Linear Time-Dependent Material," J. Appl. Phys., Vol. 25, Aug. 1954, 947-953.

[12] Ince, E. L., "Ordinary Differential Equations," Dover Pub., 1956, 381-384.

[13] Bellman, R., Kalaba, R. E. and Lockett, Jo Ann, "Numerical Inversion of the Laplace Transform: Applications to Biology, Economics, Engineering and Physics," American Elsevier Pub., 1966, 22-47.

[14] Mukunoki, Isao, "A Theory of Viscoelastic Analogy for Wave Propagation in Elastic and Viscoelastic Layered Media," Ph.D. Thesis, University of Illinois at Chicago Circle, Chicago, Illinois (under preparation).

[15] Postma, G. W., "Wave Propagation in a Stratified Medium," Geophysics, Vol. 20, 1955, 780-806.

[16] Durbin, F., "Numerical Inversion of Laplace Transform: An Efficient Improvement to Dubner and Abate's Method," Computer Journal, Vol. 17, No. 4, Nov. 1974, 371-376.

[17] Herrmann, G., Beaupre, G. S. and Auld, B. A., "Applicability of Floquet-Type Solutions to Bounded Layered Composites," to appear in the Symposium Proceedings Honoring Professor Eric Reissner's 65th Birthday.

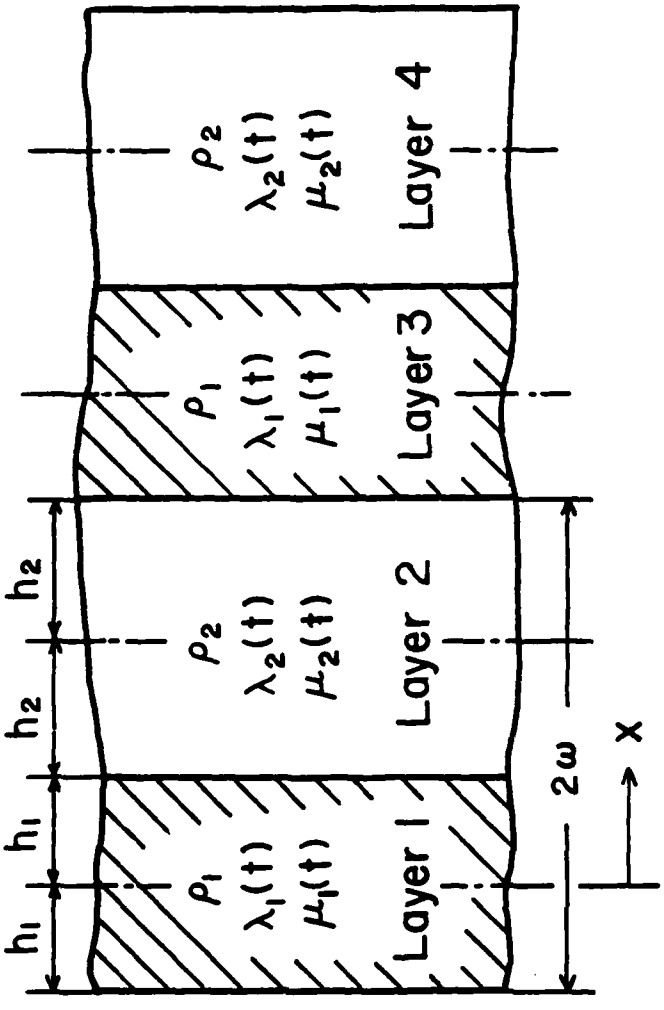

Fig. 1 Geometry of the Layered Medium

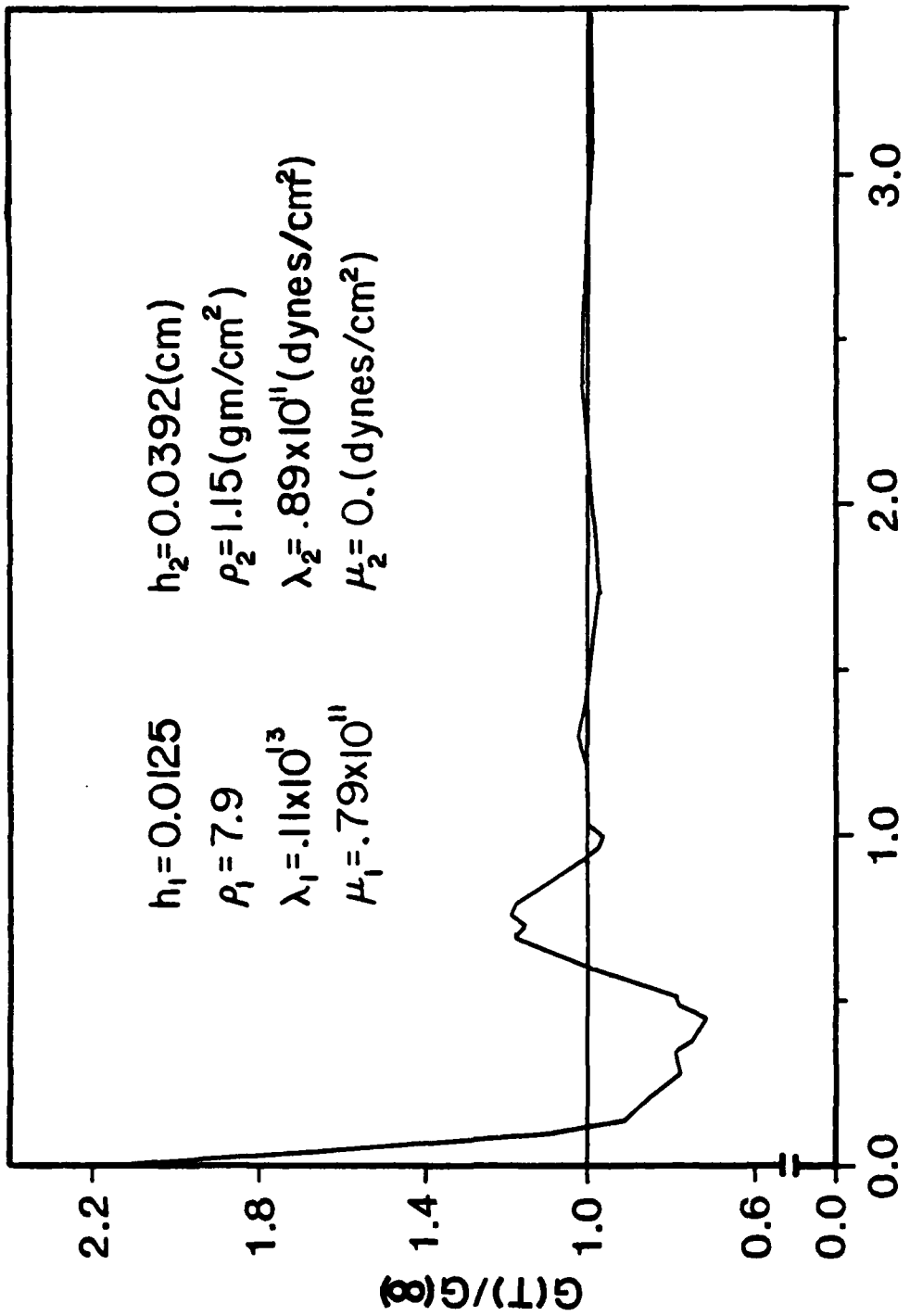

Fig. 2 "Equivalent" Viscoelastic Relaxation Function G(t)

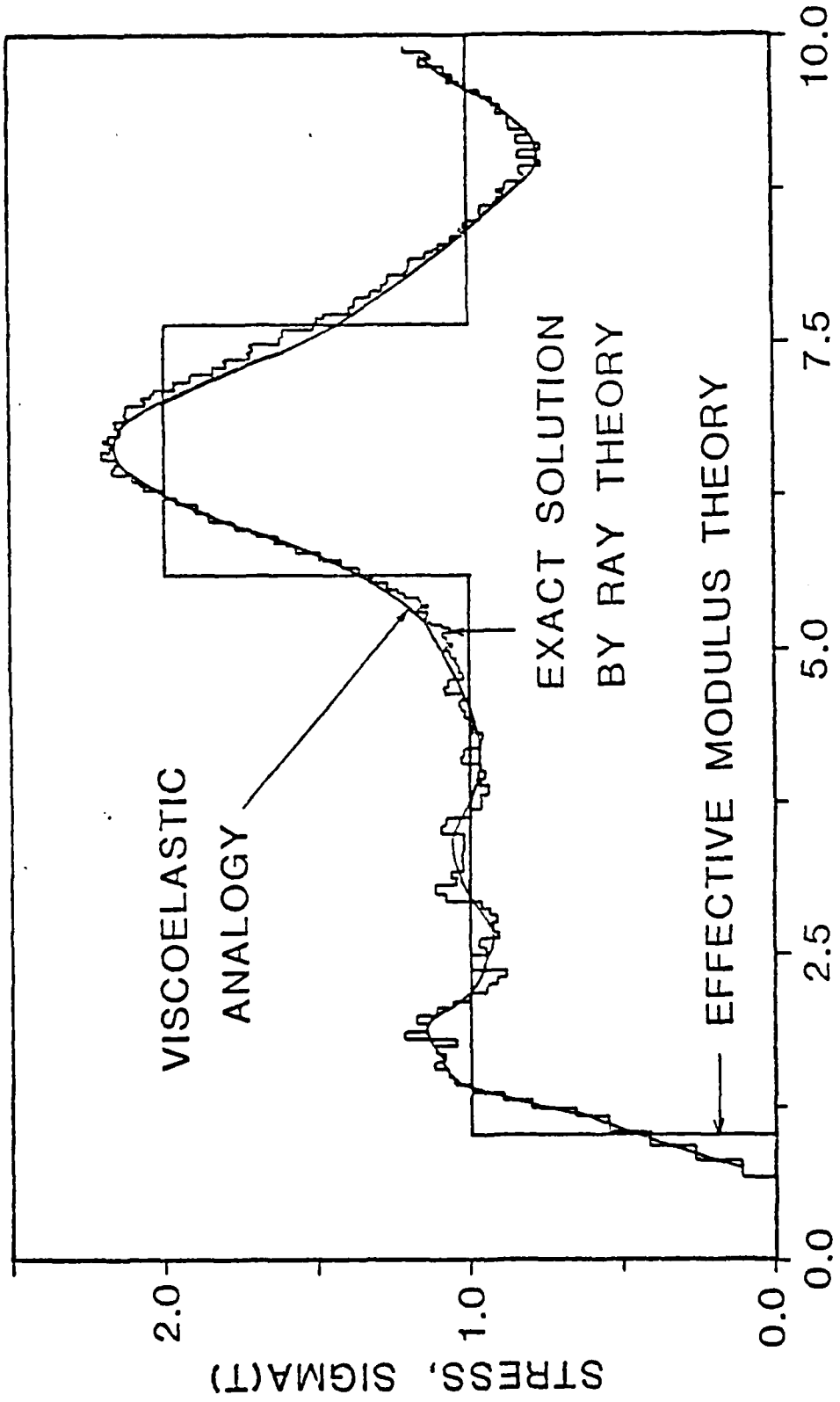

Fig. 3 Stress at the center of the 5th layer due to a unit step stress applied at the center of the first layer while the center of the 14th layer is fixed.

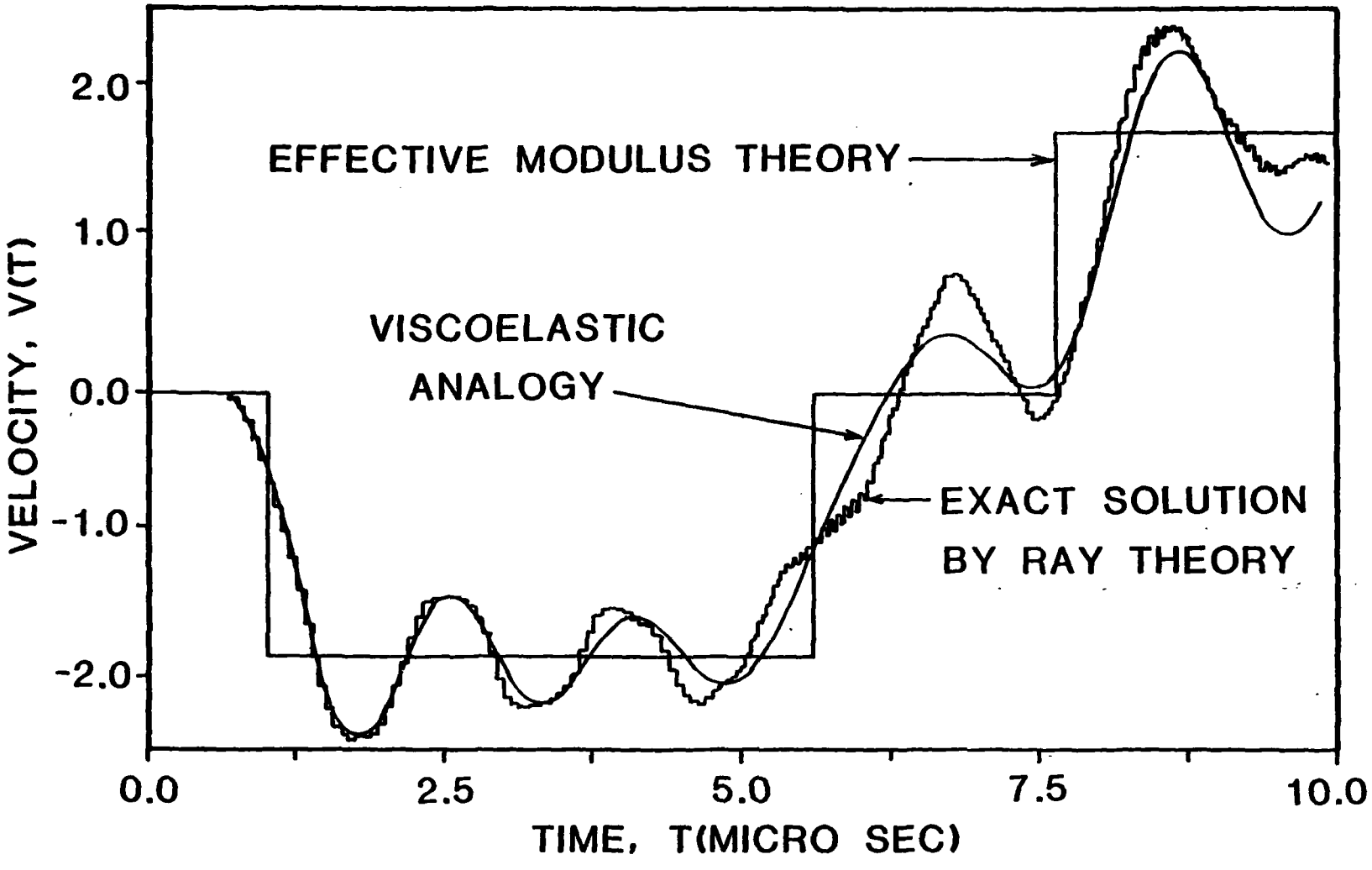

Fig. 4 Velocity at the center of the 5th layer due to a unit step stress applied at the center of the first layer while the center of the 14th layer is fixed.

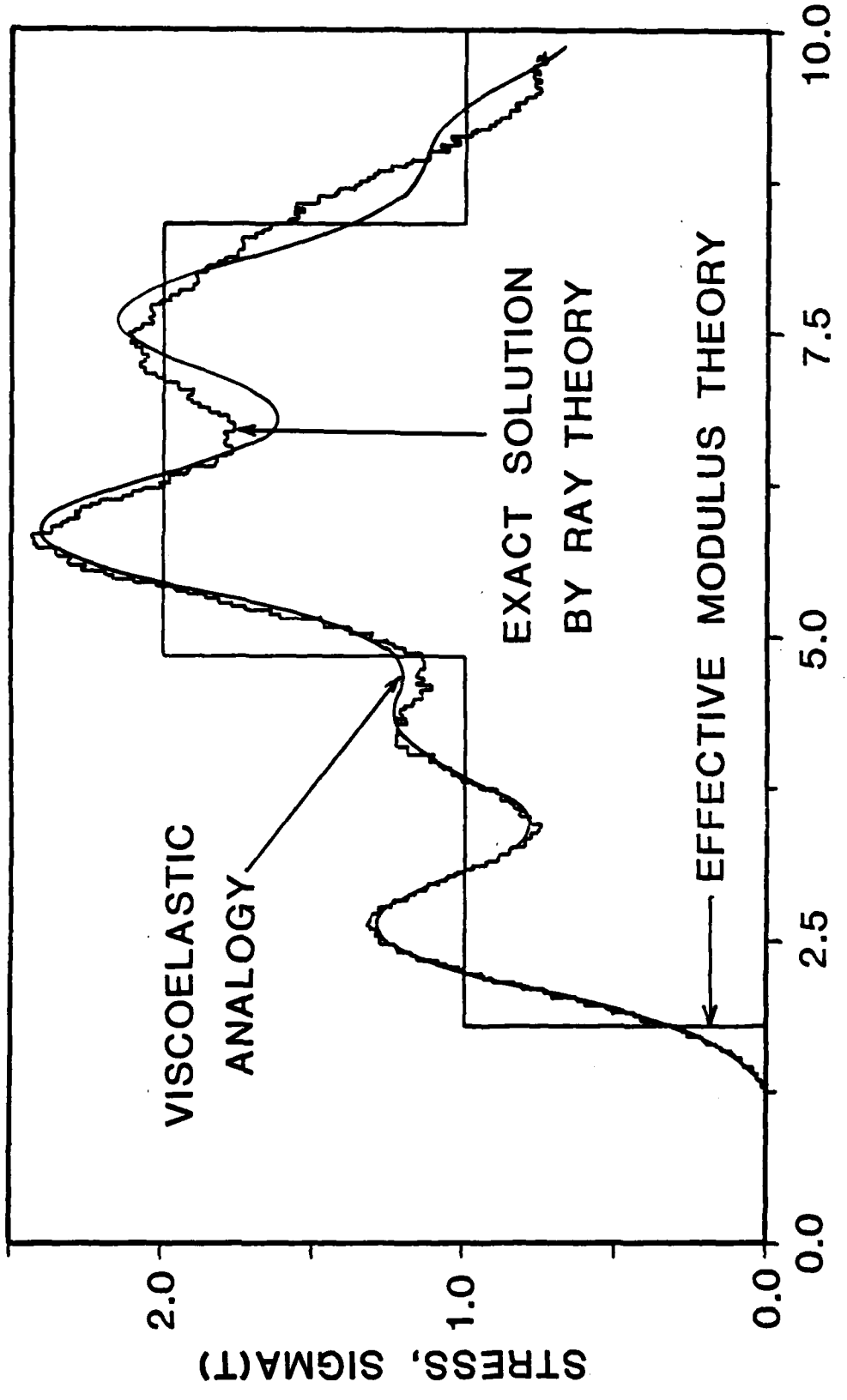

Fig. 5 Stress at the center of the 8th layer due to a unit step stress applied at the center of the first layer while the center of the 14th layer is fixed.

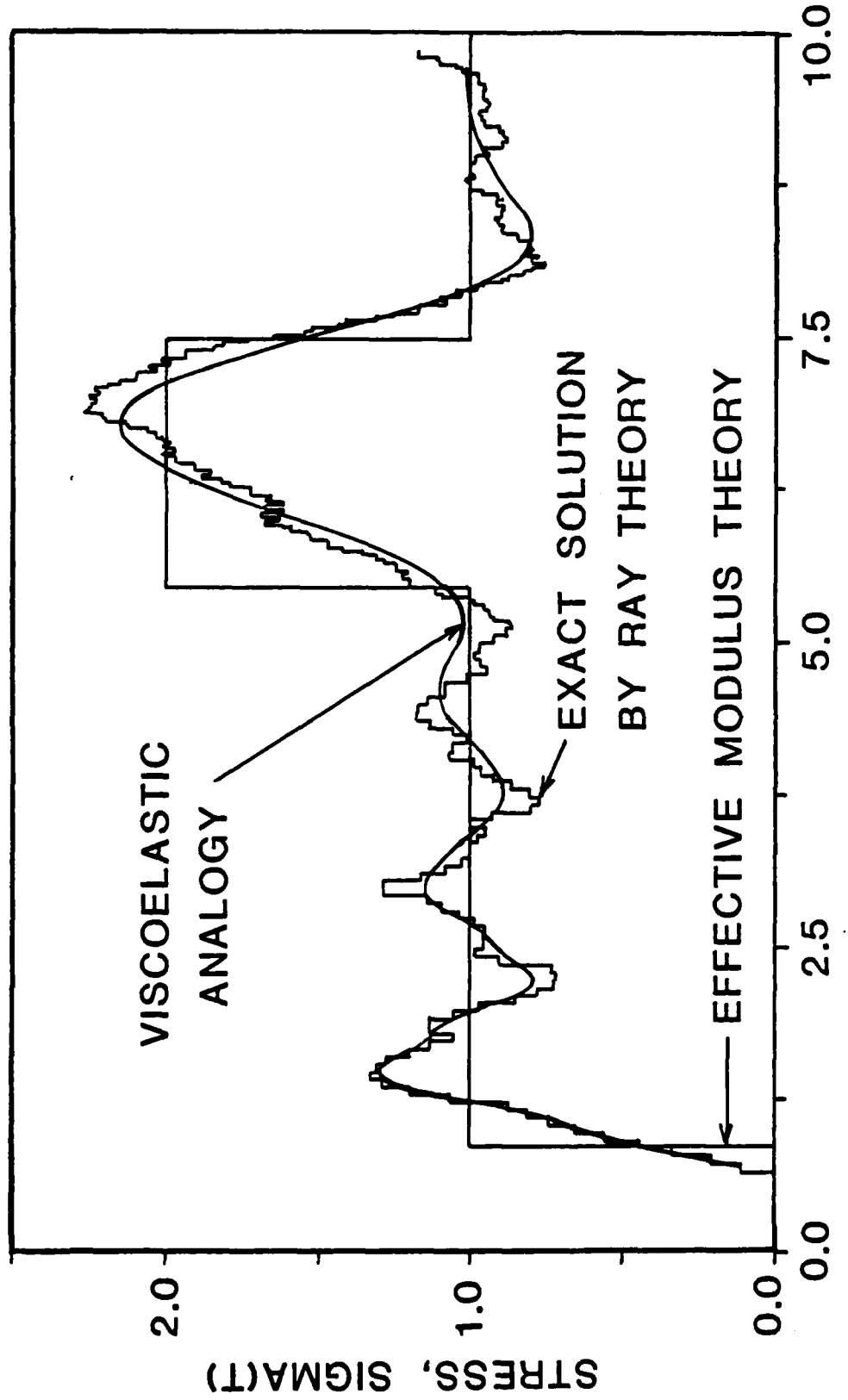

Fig. 6 Stress at the interface between the 4th and 5th layers due to a unit step stress applied at the center of the first layer while the center of the 14th layer is fixed.

CHAPTER 7

THE EFFECTS OF DISPERSION AND DISSIPATION ON WAVE PROPAGATION IN VISCOELASTIC LAYERED COMPOSITES

ABSTRACT

In Chapter 6, stress response at a finite distance from the impact end in an elastic or viscoelastic layered composite is studied. In this Chapter, the stress response at a large distance from the impact end of a viscoelastic composite is investigated. If the distance is not large enough, the stress response is oscillatory due to the dispersive nature of the composite. As the distance increases, the dissipation effect of the viscoelastic materials becomes pronounced and eventually wipes out completely the oscillatory response. The transition from the oscillatory response to the monotonic response is controlled by a parameter γ which contains (a) the impedence mismatch of the composite which contributes to the dispersion, (b) the dissipative properties of the viscoelastic materials and (c) the distance traveled by the wave.

1. INTRODUCTION

Consider a semi-infinite periodic layered composite as shown in Fig. 1 in which each period 2ω consists of two layers of homogeneous, isotropic, linear viscoelastic materials. The thickness of individual layers are $2h_i$ $(i=1,2)$ where the subscripts 1 and 2 refer to materials 1 and 2, respectively. We will consider plane wave propagation in the direction x which

is normal to the layers. For the problem considered here, the surface $x = 0$ need not be the central surface of the first layer. We will assume, however, that the first layer in which $x = 0$ is located is occupied by material 1.

The composite is initially at rest and at time $t = 0$, time-dependent, uniformly-distributed normal and shear stresses are applied at the surface $x = 0$. Since the problem considered is linear, the solutions due to the applied normal stress and the shear stress can be treated separately. The two solutions are mathematically identical. Therefore, we will consider only the solution due to the applied normal stress at $x = 0$. Moreover, we will assume that the applied normal stress at $x = 0$ is the Heaviside unit step function in time t, because the solution for a more general applied normal stress can be obtained by a linear superposition.

The stress response at a position x which is sufficiently large can be obtained by an asymptotic analysis. When both layers are elastic, the solution can be expressed in terms of an integral of an Airy function [1,2]. The stress, as a function of time t, oscillates around the Heaviside step function. When one or both layers are viscoelastic, the asymptotic solution can be expressed in terms of an error function [1,2]. The stress response is no longer an oscillatory function of t, but a monotonically increasing function of t which approaches to the unit stress as t increases.

Since elastic materials are special cases of viscoelastic materials, one might ask how a monotonic solution becomes an oscillatory solution when the viscoelastic materials become elastic. Alternately, one might ask what would be the behavior of the asymptotic solution if the relaxation functions of the viscoelastic materials are nearly step functions. Clearly, when the position x is not large enough, the dissipative effect of the viscoelastic materials does not have enough time to prevail and the stress response is

essentially governed by the dispersive nature of the composite which causes the solution to be oscillatory. As x increases, the dissipative effect, no matter how small, becomes prominent and dampens the dispersive mechanism so that the solution is non-oscillatory. The purpose of this paper is to study the effects of the dispersion, dissipation and the distance of wave propagation have on the wave profile. To simplify the analysis, we will consider only solutions at $x = 2\omega N$ where N is an arbitrary positive integer.

It should be pointed out that a similar problem was studied by Sve [1] for two special viscoelastic materials. The imaginary part of the wave number for the special materials is assumed to be proportional to the absolute value of the frequency or proportional to the square of the frequency. Hegemier [3] obtained asymptotic solutions for elastic composites as well as viscoelastic composites. However, his solutions differ from that obtained here and in [2]. A discussion on the differences will be given later.

2. SOLUTION FOR $x = 2\omega N$

The equations of motion and the continuity of the displacement are given by

$$\frac{\partial \sigma_i}{\partial x} = \rho_i \dot{v}_i \ , \qquad (i = 1,2) \qquad (1)$$

$$\frac{\partial v_i}{\partial x} = \dot{\varepsilon}_i \ , \qquad (i = 1,2) \qquad (2)$$

where σ_i, ε_i, v_i, ρ_i $(i = 1,2)$ are the normal stress, normal strain, normal particle velocity and mass density, respectively. A dot stands for differentiation with respect to time t. The initial and boundary conditions are

$$\sigma_i(x,0^-) = v_i(x,0^-) = \varepsilon_i(x,0^-) = 0 \qquad (i = 1,2) \qquad (3)$$

$$\sigma_i(\infty,t) = 0 \qquad (i = 1,2) \tag{4}$$

$$\sigma_1(0,t) = H(t) \tag{5}$$

where $H(t)$ is the Heaviside unit step function. The relation between σ_i and ε_i is written in the form of Stieltjes integral

$$\sigma_i(x,t) = \int_{0^-}^{t} g_i(t-t')\, d\varepsilon_i(t') \qquad (i = 1,2) \tag{6}$$

where $g_i(t)$ are the relaxation functions of the viscoelastic layers.

Let $\bar{f}(p)$ be the Laplace transform of $f(t)$:

$$\bar{f}(p) = \int_{0^-}^{\infty} f(t)e^{-pt}\, dt \tag{7}$$

Equations (1-6) then reduce to

$$\frac{\partial^2 \bar{\sigma}_i}{\partial x^2} = k_i^2 \bar{\sigma}_i \tag{8}$$

$$\bar{\sigma}_i(\infty,p) = 0 , \qquad \bar{\sigma}_1(0,p) = \frac{1}{p} \tag{9}$$

where

$$k_i = \sqrt{\rho_i p/\bar{g}_i} \quad . \tag{10}$$

Since k_i is periodic in x with periodicity 2ω, by using the Floquet theory [4] the solution for $x = 2\omega N$ where N is an arbitrary positive integer is

$$\bar{\sigma}_1(x,p) = \frac{1}{p}\, e^{-\kappa x} \tag{11}$$

where κ is the characteristic exponent given by (see [2,5,6])

$$\cosh(2\omega\kappa) = \vartheta \cosh(2k_1h_1 + 2k_2h_2) - (\vartheta-1)\cosh(2k_1h_1 - 2k_2h_2) \tag{12}$$

$$\theta = \frac{1}{4}\left(\frac{\rho_1 k_2}{\rho_2 k_1} + \frac{\rho_2 k_1}{\rho_1 k_2} + 2\right) \tag{13}$$

Therefore, the solution for $x = 2\omega N$ is

$$\sigma_1(x,t) = \frac{1}{2\pi i}\int_{Br} \frac{1}{p} e^{pt-\kappa x}\, dp \tag{14}$$

For a large x, the main contribution to the Bromwich contour integral of Eq. (14) appears to come from the values of integrand near $p = 0$. Hence we must study the behavior of κ near $p = 0$ before we evaluate Eq. (14) for large x.

3. BEHAVIOR OF κ NEAR $p = 0$

For most viscoelastic materials, the relaxation function $g_i(t)$, $(i = 1,2)$ is a monotonically decreasing function of t. Let $g_{i\infty}$ be the value of $g_i(t)$ at $t = \infty$. For most viscoelastic solids $g_{i\infty}$ is non-zero. If $\bar{g}_i(p)$ is the Laplace transform of $g_i(t)$,

$$\begin{aligned} p\bar{g}_i(p) &= p\int_0^\infty g_i(t)e^{-pt}\, dt \\ &= g_{i\infty} + p\int_0^\infty [g_i(t) - g_{i\infty}]e^{-pt}\, dt \end{aligned} \tag{15}$$

For small p, $e^{-pt} = 1 - pt + \ldots$ Hence

$$p\bar{g}_i(p) = g_{i\infty}(1 + a_i p - a_i T_i p^2 + \ldots) \tag{16}$$

where

$$\left.\begin{aligned} a_i g_{i\infty} &= \int_0^\infty [g_i(t) - g_{i\infty}]\, dt \\ T_i &= \frac{1}{a_i g_{i\infty}}\int_0^\infty [g_i(t) - g_{i\infty}]t\, dt \end{aligned}\right\} \tag{17}$$

It is seen that $a_i g_{i\infty}$ is the area between the curve $g_i(t)$ and the horizontal line $g_i(t)=g_{i\infty}$ while T_i is the distance of the centroid of this area from $t = 0$. According to [7], a_i provides a measure of the "viscosity" of the viscoelastic materials. An example of relaxation function which yields Eq. (16) is the standard linear viscoelastic solid

$$g_i(t) = g_{i\infty}\left(1 + \frac{a_i}{T_i} e^{-t/T_i}\right) \tag{18}$$

Using Eqs. (16), (10) and (13), the right-hand side of Eq. (12) can be expanded into power series in p. If we assume that, for small p, κ can be expressed as

$$c_\infty \kappa = p - \frac{\upsilon}{2!} p^2 - \frac{\beta}{3!} p^3 + \ldots \tag{19}$$

and use of this to expand the left-hand side of Eq. (12) into power series in p, we can determine the constants c_∞, υ and β by comparing the coefficients of same powers of p on both sides of Eq. (12). After a lengthy algebra, one obtains

$$c_\infty^2 = g_\infty/\rho \ , \tag{20}$$

$$\upsilon = g_\infty\left(\frac{a_1 n_1}{g_{1\infty}} + \frac{a_2 n_2}{g_{2\infty}}\right) \tag{21}$$

$$\begin{aligned}\beta = (\omega n_1 n_2 c_\infty)^2 \left(\frac{\rho_1}{g_{2\infty}} - \frac{\rho_2}{g_{1\infty}}\right)^2 - \frac{3}{4} g_\infty \Bigg[& \frac{a_1 n_1}{g_{1\infty}} (3a_1 + 4T_1) \\ & + \frac{a_2 n_2}{g_{2\infty}} (3a_2 + 4T_2) + g_\infty \frac{n_1 n_2}{g_{1\infty} g_{1\infty}} (a_1 - a_2)^2 \Bigg]\end{aligned} \tag{22}$$

where

$$\left.\begin{aligned} n_i &= h_i/\omega \ , \qquad n_1 + n_2 = 1 \\ \rho &= \rho_1 n_1 + \rho_2 n_2 \ , \qquad \frac{1}{g_\infty} = \frac{n_1}{g_{1\infty}} + \frac{n_2}{g_{2\infty}} \end{aligned}\right\} \tag{23}$$

We see that ρ and g_∞ are, respectively, the effective mass density and the effective equilibrium modulus of the composite.

When both layers are elastic, $a_i = 0$ and hence $\upsilon = 0$. Moreover, only the first term of β remains and $\beta \geq 0$. Notice that the first term of β is proportional to the difference in the impedances of the two layers and becomes zero when the difference in the impedances is zero. Since the dispersive nature of the composite comes from the impedance mismatch, the first term of β is responsible for the oscillatory nature of the stress response.

When one or both of the layers are viscoelastic, υ is positive and non-zero while β can be positive, negative or zero. Not only is υ responsible for the dissipative nature of the stress response, the second part of β is also responsible for the dissipation.

The case when both υ and β vanish will not be considered here.

4. ASYMPTOTIC SOLUTIONS

From Eqs. (19) and (14), we have

$$\sigma_1(x,t) = \frac{1}{2\pi i} \int_{Br} \frac{1}{p} \exp \left\{ \left(t - \frac{x}{c_\infty}\right) p + \frac{x}{2c_\infty} \left(\upsilon p^2 + \frac{1}{3} \beta p^3 + \ldots\right) \right\} dp \quad (24)$$

We will assume that x is sufficiently large that the terms denoted by the dots can be ignored. We will also assume that $\beta \neq 0$. The case $\beta = 0$ will be discussed later. Let

$$\left.\begin{aligned} b &= \left(\frac{x|\beta|}{2c_\infty}\right)^{1/3}, \qquad \tau = \left(t - \frac{x}{c_\infty}\right) \Big/ b, \\ \gamma &= b \frac{\upsilon}{|\beta|} = \left(\frac{x\upsilon^3}{2c_\infty \beta^2}\right)^{1/3}. \end{aligned}\right\} \quad (25)$$

Equation (24) then takes the form

$$\sigma^{\pm}(\gamma,\tau) = \frac{1}{2\pi i}\int_{Br} \frac{1}{p}\, e^{\tau p + \gamma p^2 \pm \frac{1}{3}p^3}\, dp \tag{26}$$

where the subscript 1 of σ has been omitted and the $+$ sign is for $\beta > 0$ and $-$ sign for $\beta < 0$.

By taking the Bromwich contour L_1 as shown in Fig. 2, it is not difficult to show that

$$\sigma^{+}(\gamma,\tau) + \sigma^{-}(\gamma,-\tau) = 1 \tag{27}$$

We will therefore consider only the case $\beta > 0$ and hence the integral

$$\sigma(\gamma,\tau) = \frac{1}{2\pi i}\int_{Br} \frac{1}{p}\, e^{\tau p + \gamma p^2 + \frac{1}{3}p^3}\, dp \tag{28}$$

Using the identity

$$\frac{1}{p}\, e^{\tau p} = \frac{1}{p} + \int_0^{\tau} e^{sp}\, ds \tag{29}$$

the integral in Eq. (28) can be divided into two parts:

$$\sigma(\gamma,\tau) = I_1 + I_2\ , \tag{30}$$

$$I_1 = \frac{1}{2\pi i}\int_{Br} \frac{1}{p}\, e^{\gamma p^2 + \frac{1}{3}p^3}\, dp\ , \tag{31}$$

$$I_2 = \int_0^{\tau} ds \left\{ \frac{1}{2\pi i}\int_{Br} e^{sp + \gamma p^2 + \frac{1}{3}p^3}\, dp \right\}\ . \tag{32}$$

Notice that $I_1 = \sigma(\gamma,0)$ and hence is the magnitude of stress at $t = x/c_\infty$. By taking the Bromwich contour L_2 of Fig. 2, one obtains

$$I_1 = \frac{1}{3} + \frac{1}{\pi}\int_0^\infty \frac{1}{r} e^{-\frac{1}{2}\gamma r^2 - \frac{1}{3}r^3} \sin\left(\frac{\sqrt{3}}{2}\gamma r^2\right) dr$$

$$\cong \frac{1}{3} + \frac{\sqrt{3}}{2\pi}\left\{3^{-1/3}\Gamma\left(\frac{2}{3}\right)\gamma - 3^{1/3}\Gamma\left(\frac{4}{3}\right)\frac{\gamma^2}{2!} + \ldots\right\} \tag{33}$$

where $\Gamma(x)$ is the Gamma function. If γ is very large, we take the Bromwich contour L_1 and obtain

$$I_1 = \frac{1}{2} - \frac{1}{\pi}\int_0^\infty \frac{1}{r} e^{-r^2} \sin\left(\frac{\delta}{3} r^3\right) dr$$

$$\cong \frac{1}{2} - \frac{\delta}{12\sqrt{\pi}}\left\{1 - \frac{35}{144}\delta^2 + \ldots\right\} \tag{34}$$

where

$$\delta = \gamma^{-3/2} = \left(\frac{2c_\infty \beta^2}{xU^3}\right)^{1/2} \tag{35}$$

We now turn to the integral I_2. By replacing the variable p by

$$p = z - \gamma \ , \tag{36}$$

Equation (32) can be written as

$$I_2 = \int_0^\tau e^{-s\gamma + \frac{2}{3}\gamma^3} ds \left\{\frac{1}{2\pi i}\int_{Br} e^{(s-\gamma^2)z + \frac{1}{3}z^3} dz\right\} \tag{37}$$

or

$$I_2 = \int_0^\tau e^{-s\gamma + \frac{2}{3}\gamma^3} \mathrm{Ai}(-s + \gamma^2)\, ds \tag{38}$$

where the Airy function is defined as [8]

$$\mathrm{Ai}(s) = \frac{1}{2\pi i}\int_{L_2} e^{-sz + \frac{1}{3}z^3} dz \tag{39}$$

$$= \frac{1}{\pi} \int_0^\infty \cos\left(sr + \frac{1}{3} r^3\right) dr \qquad (39)$$
(Cont'd)

Two extreme cases of $\gamma = 0$ and $\gamma = \infty$ have been studied in the literature. Before we evaluate σ for arbitrary γ, we will obtain these two extreme cases from Eq. (30).

(1) $\underline{\gamma = 0}$

For elastic composites, $\upsilon = 0$ and hence $\gamma = 0$. Equations (30), (33) and (38) then yield

$$\sigma(0,\tau) = \frac{1}{3} + \int_0^\tau \mathrm{Ai}(-s)\, ds \qquad (40)$$

This is precisely the asymptotic solution obtained in [1,2]. The stress σ is an oscillatory function of τ (see Fig. 3).

(2) $\underline{\gamma = \infty}$

For viscoelastic composites, $\upsilon \neq 0$ and β of Eq. (24) may or may not be zero. In [2] the term containing β was ignored. This is equivalent to assuming that $\beta = 0$ and hence $\gamma = \infty$. For a very large γ, the Airy function has the expression [8]:

$$\mathrm{Ai}(s) \cong \frac{1}{2\sqrt{\pi}} \frac{1}{s^{1/4}} e^{-\frac{2}{3}s^{3/2}} \qquad (41)$$

Use of this expression in Eq. (38) results in

$$I_2 \cong \frac{1}{2\sqrt{\pi}} \int_0^\tau e^{-\left(\frac{s}{2\sqrt{\gamma}}\right)^2} d\left(\frac{s}{\sqrt{\gamma}}\right) = \frac{1}{2} \mathrm{erf}\left(\frac{\tau^*}{2}\right) \qquad (42)$$

where

$$\left.\begin{aligned} \tau^* &= \left(t - \frac{x}{c_\infty}\right)\Big/ b^* , \qquad b^* = b\sqrt{\gamma} = \sqrt{\frac{xU}{2c_\infty}} , \\ \operatorname{erf}(x) &= \frac{2}{\sqrt{\pi}} \int_0^x e^{-s^2}\, ds \end{aligned}\right\} \tag{43}$$

Therefore, when $\beta = 0$, (i.e., $\gamma = \infty$ or $\delta = 0$), Eqs. (34), (42) and (30) yield the following asymptotic solution obtained in [1,2] :

$$\sigma = \tfrac{1}{2}\left\{1 + \operatorname{erf}(\tau^*/2)\right\} \tag{44}$$

The stress σ is a monotonically increasing function of τ^*, Fig. 4.

5. NUMERICAL RESULTS AND DISCUSSION

For an arbitrary γ, the stress σ as a function of τ may be obtained from Eq. (30) where I_1 is given by Eq. (33) or (34) and I_2 is given by Eq. (38). Since both I_1 and I_2 require a numerical integration, it might be simpler to evaluate σ directly from Eq. (28). If we take L_2 of Fig. 2 as the Bromwich contour, Eq. (28) reduces to

$$\sigma(\gamma,\tau) = \frac{1}{3} + \frac{1}{\pi} \int_0^\infty \frac{1}{r}\, e^{\frac{1}{2}(\tau r - \gamma r^2) - \frac{1}{3} r^3} \sin\left[\frac{\sqrt{3}}{2}\,(\tau r + \gamma r^2)\right] dr \tag{45}$$

For the contour L_1, we have

$$\sigma(\gamma,\tau) = \frac{1}{2} + \frac{1}{\pi} \int_0^\infty \frac{1}{r}\, e^{-r^2} \sin\left(\tau^* r - \frac{\delta}{3}\, r^3\right) dr \tag{46}$$

where τ^* and δ are defined in Eqs. (43) and (35). Notice that

$$\tau = \tau^* \qquad \text{when} \qquad \gamma = \delta = 1 . \tag{47}$$

Notice also that because of the factor $(1/r)e^{-r^2}$ in the integrand of Eq. (46), the absolute value of the integrand diminishes rapidly as r increases. For instance, at $r = 2$, $(1/r)e^{-r^2} \cong 9\times10^{-3}$ and at $r = 3$,

$(1/r)e^{-r^2} \cong 4\times10^{-5}$. Therefore, the infinite integral can be replaced by an integral of finite interval say $0 \le r \le 3$. A similar argument applies to the integral in Eq. (45).

Equation (45) is used to calculate σ for $\gamma = 0$, 0.1, 0.3, 0.6 and 1.0. The results are shown in Fig. 3. Equation (46) is used to calculate σ for $\gamma = 1$ and $\gamma = \infty$, (i.e., $\delta = 1$ and $\delta = 0$), Fig. 4. We see that the stress response differs very little for $\gamma = 1$ and $\gamma = \infty$.

The example of stress response at the 30th layer considered in [2] has a negative value of β and $\gamma = 0.58$. On the other hand, the example considered on p. 110 of [3] has a positive value of β and $\gamma = 0.68$.

For a given viscoelastic composite, υ and β are known and fixed. γ then depends on x and increases as x increases. We see from Fig. 3 that the oscillatory nature of the stress diminishes as γ increases. Since for $\gamma \ge 1$ the oscillation is practically non-existence, we may say that for

$$x \ge \frac{2c_\infty \beta^2}{\upsilon^3} \tag{48}$$

the stress response is monotonic.

The asymptotic solution for viscoelastic composite derived in [3] is different from Eq. (24). Using the notations of Eqs. (20-22), the asymptotic solution derived in [3] is based on the equation

$$\sigma(x,t) = \frac{1}{2\pi i} \int_{Br} \frac{1}{p} \exp\left\{ tp + \frac{\upsilon x}{2c_\infty} p^2 - \frac{xp}{c_\infty}\left(1 + \frac{\beta}{3} p^2\right)^{-1/2} \right\} dp \tag{49}$$

If we expand the last term in the exponent into a power series in p and ignore the terms of order higher than p^3, Eq. (49) is identical to Eq. (24). We are able to verify that υ in [3] is identical to the one obtained in Eq. (21). However, β in [3] appears to be different from the expression in Eq. (22).

6. CONCLUSION

The parameter γ defined in Eq. (25) consists of the variables υ, β and x. The dissipative nature of the viscoelastic material is represented by υ and a part of β, while the remaining part of β represents the dispersive nature of the composite. The distance traveled by the wave is represented by x. Thus γ contains the influences on the wave profile due to dissipation, dispersion and the distance traveled by the wave. With γ determined from Eq. (25), Figs. 3 and 4 provide the wave response.

REFERENCES

[1] Sve, C., "Stress Wave Attenuation in Composite Materials," J. Appl. Mech., Vol. 39, 1972, 1151-1153.

[2] Chen, C. C. and Clifton, R. J., "Asymptotic Solutions for Wave Propagation in Elastic and Viscoelastic Bilaminates," Proc. 14th Midwestern Mech. Conf., University of Oklahoma, 1975, 399-417.

[3] Hegemier, G. A., "On a Theory of Interacting Continua for Wave Propagation in Composites," in Dynamics of Composite Materials, ed. by E. H. Lee, ASME, 1972, 70-121.

[4] Ince, E. L., "Ordinary Differential Equations," Dover Pub., 1956, 381-384.

[5] Ting, T. C. T. and Mukunoki, I., "A Theory of Viscoelastic Analogy for Wave Propagation Normal to the Layering of a Layered Medium," J. Appl. Mech., Vol. 46, 1979, 329-336.

[6] Mukunoki, I. and Ting, T. C. T., "Transient Wave Propagation Normal to the Layering of a Finite Layered Medium," to appear in Int. J. Solids Structures.

[7] Pipkin, A. C., "Lectures on Viscoelasticity Theory," Springer-Verlag, New York, 1972, 36-37.

[8] Abramowitz, M. and Stegnun, I. A., "Handbook of Mathematical Functions," National Bureau of Standards, AMS 55, 1964, 446-448.

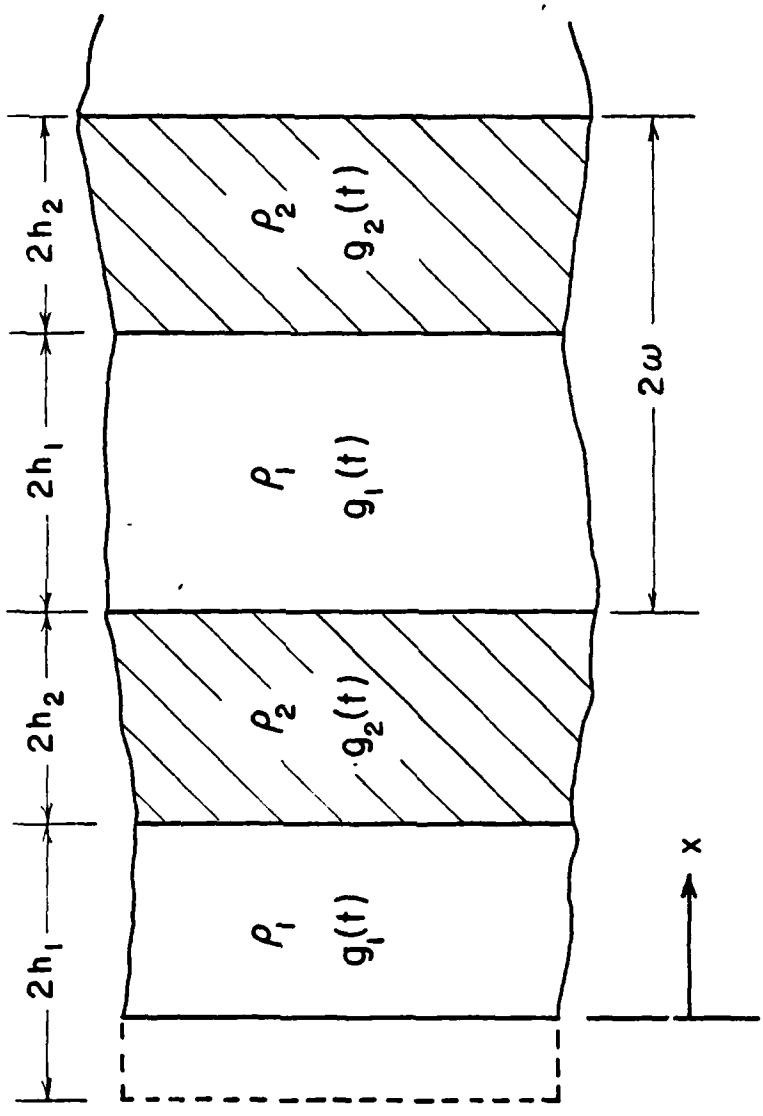

Fig. 1 Geometry of the Viscoelastic Layered Composite

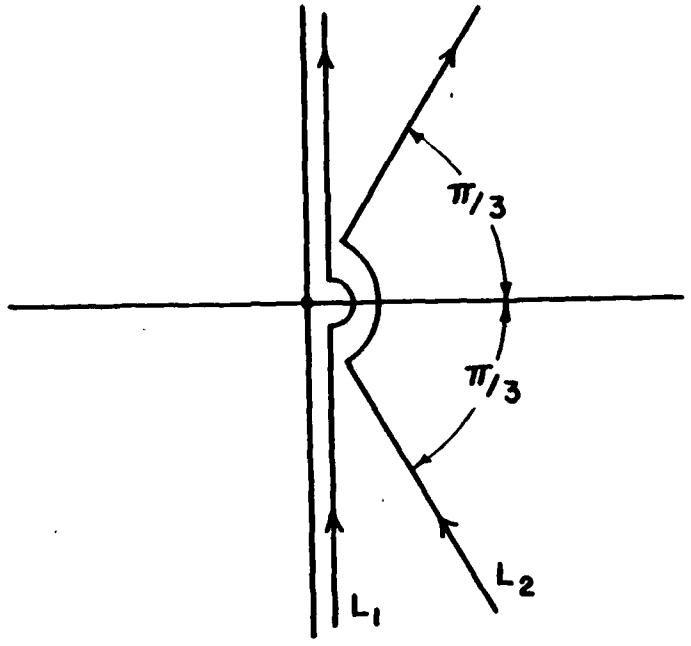

Fig. 2 Bromwich Contours for Eqs. (28,31,32)

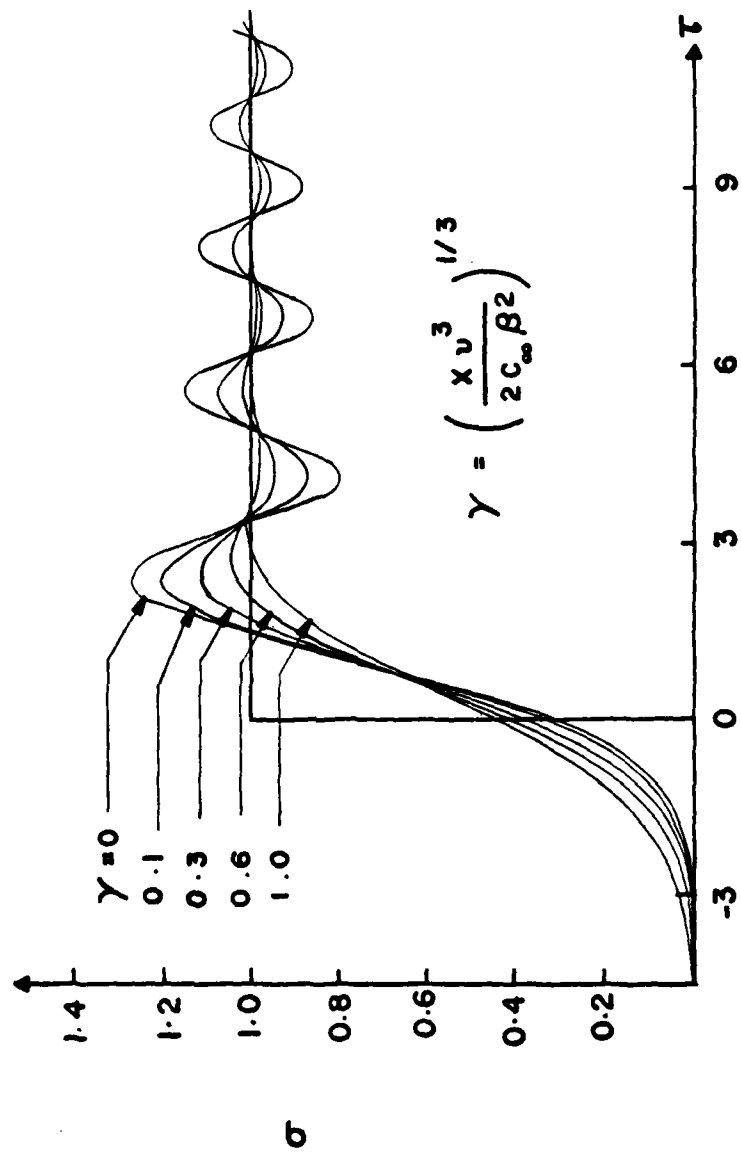

Fig. 3 Asymptotic Solution for $0 \leq \gamma \leq 1$

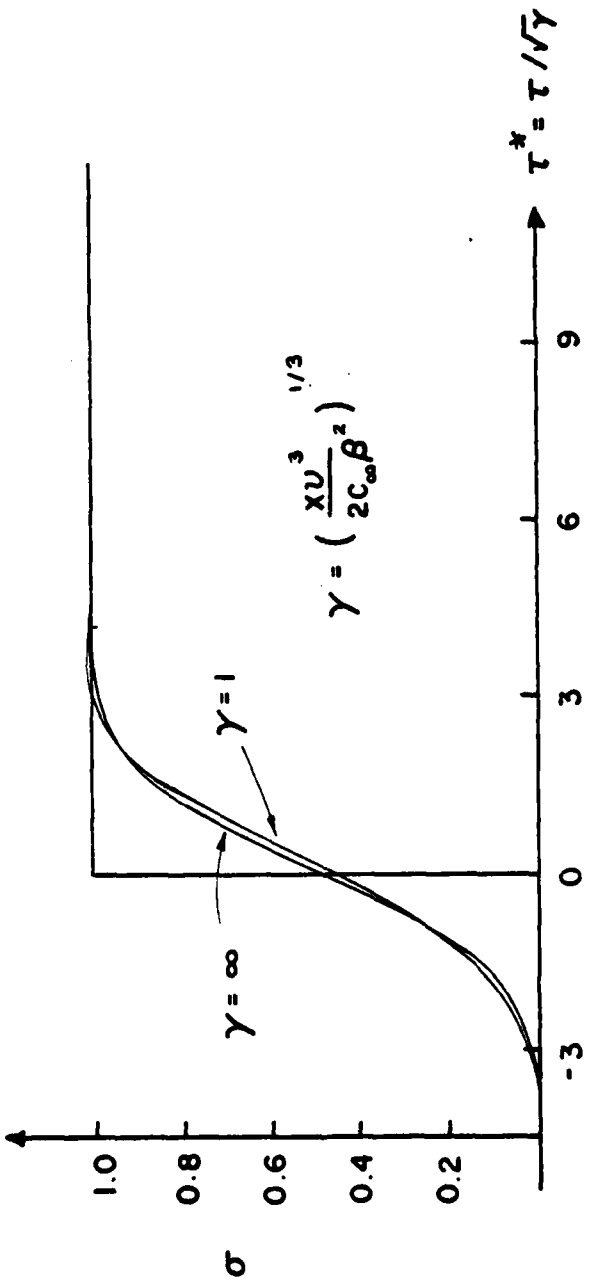

Fig. 4 Asymptotic Solution for $1 \leq \gamma \leq \infty$

CHAPTER 8

CONCLUSIONS

Static and dynamic analyses of multilayer composite laminates and/or pilot studies leading toward such analyses have been presented in this report. Detailed summaries and conclusions have been included with each chapter. The present chapter is intended to briefly summarize these conclusions and, where possible, to make suggestions for further investigations.

Three approaches were investigated in Chapter 2 for the finite-element analysis of edge-effects in symmetric laminates under prescribed inplane strain. Although these approaches produce essentially identical results away from the free edge, some differences are noted in the magnitude, and in selected cases the form, of the stress distributions near the free-edge. Until further analytic results are available it is not possible to conclude which of the strain continuity or traction-free-edge approaches is the more accurate. Some insight into this comparison may be obtained by combination of the stress predictions with appropriate failure criteria; the better analysis should be capable of consistent predictions of laminate first-failure in comparison with experimental results.

Of the 8-node single layer plate bending elements with a straight traction-free edge, developed in Chapter 3, the best element is identified as one based on a 21β stress-field. This element produced displacement and stress predictions which were, in general, superior to all other elements tested. Although the superiority of this element over a standard hybrid-stress plate element is not evident in all cases, it is expected that the superiority will be

apparent in examples where free-edge effects are dominant, such as in multilayer laminates. In the development of an 8-node multilayer plate element, a layer stress field analagous to that used in the 21β element is recommended.

In Chapter 4, alternate initial-stress approaches based on the hybrid-stress model were compared for the elastic-plastic analysis of single layer plates. Results obtained for selected example problems suggest that hybrid functional II, coupled with iteration scheme A, is the preferred approach. This approach should therefore be used in extension to include material nonlinear effects in multilayer laminated plates.

Chapter 5 provides a means for analysing the nature of singularities at the free edge of a composite whose individual layers are anisotropic. The results obtained can be used to formulate a hybrid-stress singularity element for the free-edge point.

The two dynamic problems studied in Chapters 6 and 7 contributed significantly to the literature of dynamic response of composites. A theory of viscoelastic analogy presented in Chapter 6 offers a reliable way to predict the transient response of a layered composite at finite times. Moreover the dimension of the layered composite is finite. This problem was not solved successfully before.

The other dynamic problem, namely the transient response of a viscoelastic layered composite studied in Chapter 7, sheds much light on the nature of interaction between the effects of dispersion, dissipation and the distance traveled by the wave. The results show how an oscillatory wave approaches a monotonic wave as the distance traveled by the wave increases.

DISTRIBUTION LIST

	No. of Copies
Office of Deputy Under Secretary of Defense for Research and Engineering (ET) ATTN: Mr. J. Persh, Staff Specialist for Materials and Structures (Room 3D1089) The Pentagon Washington, DC 20301	1
Office of Deputy Chief of Research Development and Acquisition ATTN: DAMA-CSS/Dr. J. I. Bryant (Room 3D424) The Pentagon Washington, DC 20310	1
Commander U.S. Army Materiel Development and Readiness Command ATTN: DRCLDC, R. Gonano, Office of Laboratory Management 500 Eisenhower Avenue Alexandria, VA 22333	1
Director Ballistic Missile Defense Systems Command ATTN: BMDSC-TEN, Mr. N. J. Hurst BMDSC-H BMDSC-T BMDSC-AOLIB P. O. Box 1500 Huntsville, AL 35807	1 1 1 1
Ballistic Missile Defense Program Office ATTN: DACS-BMT DARCOM Bldg., Seventh Floor 5001 Eisenhower Avenue Alexandria, VA 22333	1
Director Ballistic Missile Defense Advanced Technology Center ATTN: ATC-X, Dr. J. Carlson ATC-X, Col. J. W. Gillespie ATC-M, Mr. M. Whitfield ATC-M, Dr. D. Harmon ATC-M, Mr. J. Papadopoulos P. O. Box 1500 Huntsville, AL 35807	1 1 1 1 1

	No. of Copies
Director Defense Nuclear Agency ATTN: SPAS, Mr. D. Kohler Washington, DC 20305	1
Director Army Ballistic Research Laboratories ATTN: DRDAR-BLT, Dr. N. J. Huffington, Jr. DRDAR-BLT, Dr. T. W. Wright DRDAR-BLT, Dr. G. L. Moss Aberdeen Proving Ground, MD 21005	 1 1 1
Commander Harry Diamond Laboratories ATTN: DRXDO-NP, Dr. F. Wimenitz 2800 Powder Mill Road Adelphi, MD 20783	1
Commander U.S. Army Combat Development Command Institute of Nuclear Studies ATTN: Technical Library Fort Bliss, TX 79916	1
Commander Air Force Materials Laboratory Air Force Systems Command ATTN: LNE/Dr. W. Kessler LNC/Dr. D. Schmidt Wright-Patterson Air Force Base, OH 45433	 1 1
Commander BMO/ABES Office ATTN: BMO/MNRT, Col. R. Smith BMO/MNRTE, Maj. J. Sikra BMO/MNRTE, Maj. K. Yelmgren Norton Air Force Base, CA 92409	 1 1 1
Commander Air Force Materials Laboratory ATTN: AFML/MBM, Dr. S. W. Tsai Wright-Patterson Air Force Base, OH 45433	1

	No. of Copies
Commander Naval Ordnance Systems Command ATTN: ORD-03331, Mr. M. Kinna Washington, DC 20360	1
Commander Naval Surface Weapons Center ATTN: Dr. C. Lyons Dr. W. Messick Silver Springs, MD 20910	1 1
Lawrence Livermore Laboratory ATTN: Dr. E. M. Wu P. O. Box 808 (L-342) Livermore, CA 94550	1
Los Alamos Scientific Laboratory ATTN: GMX-6, Dr. J. W. Taylor P. O. Box 1663 Los Alamos, NM 87544	1
Sandia Laboratories ATTN: Dr. Frank P. Gerstle, Jr. Dr. L. D. Bertholf Dr. J. Lipkin P. O. Box 5800 Albuquerque, NM 87115	1 1 1
Aerospace Corporation ATTN: Dr. R. Cooper P. O. Box 92957 Los Angeles, CA 90009	1
AVCO Corporation Government Products Group ATTN: Dr. W. Reinecke Mr. P. Rolincik 201 Lowell Street Wilmington, MA 01997	1 1
ETA Corporation ATTN: Mr. D. L. Mykkanen P. O. Box 6625 Orange, CA 92667	1

	No. of Copies
Effects Technology, Inc.	1
ATTN: Dr. R. Wengler	1
Dr. R. Parisse	1
Mr. J. Green	
5383 Hollister Avenue	
Santa Barbara, CA 93111	
Fiber Materials, Inc.	1
ATTN: Mr. M. Subilia, Jr.	1
Mr. L. Landers	1
Mr. G. Williams	1
Mr. P. Marchol	
Biddeford Industrial Park	
Biddeford, ME 04005	
General Electric Company	
Advanced Materials Development Laboratory	
ATTN: Mr. K. Hall	1
Mr. J. Brazel, Room 4466	1
Ms. B. McGuire	1
Mr. L. Gilbert	1
3198 Chestnut Street	
Philadelphia, PA 19101	
General Dynamics Corporation	
Convair Division	
ATTN: Mr. J. Hertz	1
Mr. H. McCutcheon, Jr.	1
5001 Kearny Villa Road	
San Diego, CA 92138	
General Dynamics Corporation	
ATTN: Dr. D. J. Wilkins, Mail Zone 2884	1
P. O. Box 748	
Fort Worth, TX 76101	
Kaman Sciences Corporation	
ATTN: Mr. F. Shelton	1
P. O. Box 7463	
Colorado Springs, CO 80933	
Ktech	
ATTN: Dr. D. Keller	1
911 Pennsylvania Avenue, N.E.	
Albuquerque, NM 87110	

	No. of Copies
Lockheed Missiles and Space Company ATTN: Mr. D. Aspinwall P. O. Box 504 Sunnyvale, CA 94088	1
Martin Marietta Aerospace ATTN: Mr. V. Hewitt Mr. Frank H. Koo P. O. Box 5837 Orlando, FL 32805	1 1
McDonnell Douglas Corporation ATTN: Dr. L. Cohen Mr. H. Parachanian 5301 Bolsa Avenue Huntington Beach, CA 92647	1 1
Prototype Development Associates, Inc. ATTN: Mr. J. Schultzler Mr. N. Harrington 1740 Garry Avenue, Suite 201 Santa Ana, CA 92705	1 1
R&D Associates ATTN: Dr. A. Field 525 Wilshire Blvd. Santa Monica, CA 90025	1
Radkowski Associates ATTN: Dr. P. Radkowski P. O. Box 5474 Riverside, CA 92507	1
Southwest Research Institute ATTN: Mr. A. Wenzel 8500 Culebra Road San Antonio, TX 78206	1
Stanford Research Institute ATTN: Dr. D. Curran Dr. L. Seaman 333 Ravenswood Avenue Menlo Park, CA 90250	1 1

	No. of Copies
Terra Tek, Inc. ATTN: Dr. A. H. Jones 420 Wakara Way Salt Lake City, Utah 84108	1
TRW Systems Group ATTN: Mr. D. Gamble One Space Park Redondo Beach, CA 90278	1
Stanford University Department of Applied Mechanics ATTN: Professor E. H. Lee Stanford, CA 94305	1
Lehigh University Institute of Fracture and Solid Mechanics ATTN: Dr. George C. Sih Bldg. #19, Packard Lab. Bethlehem, PA 18015	1
Defense Technical Information Center Cameron Station, Bldg. 5 5010 Duke Station Alexandria, VA 22314	2
Director Army Materials & Mechanics Research Center ATTN: DRXMR-H, Mr. J. F. Dignam	1
DRXMR-H, Dr. S. C. Chou	1
DRXMR-H, Mr. L. R. Aronin	1
DRXMR-H, Dr. D. P. Dandekar	1
DRXMR-AP	1
DRXMR-PL	2
DRXMR-PR	1
DRXMR-PD Watertown, MA 02172	1
Department of Transportation T. S. C., 743 ATTN: Dr. Pin Tong Kendal Square Cambridge, MA 02142	1

Army Materials and Mechanics Research Center
Watertown, Massachusetts 02172
STRESS ANALYSIS OF COMPOSITES
R. L. Spilker and T. C. T. Ting
Department of Materials Engineering
University of Illinois at Chicago Circle
Chicago, IL 60680
Technical Report AMMRC TR 81-5, March 1981, 240 pp
Illus.-tables, Contract DAAG46-79-C-0045
D/A Project: 8X363304D215;
AMCMS Code: 633304.21500.03
Final Report, August 1979 to August 1980

AD ____________
Unclassified
Unlimited Distribution

Key Works

Composite materials
Finite Element
Stress analysis
Wave propagation
Plastic analysis
Viscoelasticity
Transient responses

Static and dynamic stress analysis of laminated composites is studied. In the static analysis, the hybrid-stress finite element model is used for (1) the study of edge effects in symmetrically-stacked laminates subject to prescribed inplane strain, (2) the development and evaluation of 8-node single-layer plate bending elements for which the traction-fee conditions are satisfied along a straight edge, and (3) the elastic-plastic analysis of single layer plates. An analytic study is also presented to determine the nature of the potential 2-D singularity at the intersection of a bimaterial interface and a free edge. In the dynamic analysis, the stress response in a laminated composite due to a unit step load applied at the boundary is obtained for points which are (a) at a finie distance, and (b) at a large distance, from the impact end. For the case (a), the composite may consist of a finite number of layers.

Army Materials and Mechanics Research Center
Watertown, Massachusetts 02172
STRESS ANALYSIS OF COMPOSITES
R. L. Spilker and T. C. T. Ting
Department of Materials Engineering
University of Illinois at Chicago Circle
Chicago, IL 60680
Technical Report AMMRC TR 81-5, March 1981, 240 pp
Illus.-tables, Contract DAAG46-79-C-0045
D/A Project: 8X363304D215;
AMCMS Code: 633304.21500.03
Final Report, August 1979 to August 1980

AD ____________
Unclassified
Unlimited Distribution

Key Works

Composite materials
Finite Element
Stress analysis
Wave propagation
Plastic analysis
Viscoelasticity
Transient responses

Static and dynamic stress analysis of laminated composites is studied. In the static analysis, the hybrid-stress finite element model is used for (1) the study of edge effects in symmetrically-stacked laminates subject to prescribed inplane strain, (2) the development and evaluation of 8-node single-layer plate bending elements for which the traction-fee conditions are satisfied along a straight edge, and (3) the elastic-plastic analysis of single layer plates. An analytic study is also presented to determine the nature of the potential 2-D singularity at the intersection of a bimaterial interface and a free edge. In the dynamic analysis, the stress response in a laminated composite due to a unit step load applied at the boundary is obtained for points which are (a) at a finie distance, and (b) at a large distance, from the impact end. For the case (a), the composite may consist of a finite number of layers.

Army Materials and Mechanics Research Center
Watertown, Massachusetts 02172
STRESS ANALYSIS OF COMPOSITES
R. L. Spilker and T. C. T. Ting
Department of Materials Engineering
University of Illinois at Chicago Circle
Chicago, IL 60680
Technical Report AMMRC TR 81-5, March 1981, 240 pp
Illus.-tables, Contract DAAG46-79-C-0045
D/A Project: 8X363304D215;
AMCMS Code: 633304.21500.03
Final Report, August 1979 to August 1980

AD ____________
Unclassified
Unlimited Distribution

Key Works

Composite materials
Finite Element
Stress analysis
Wave propagation
Plastic analysis
Viscoelasticity
Transient responses

Static and dynamic stress analysis of laminated composites is studied. In the static analysis, the hybrid-stress finite element model is used for (1) the study of edge effects in symmetrically-stacked laminates subject to prescribed inplane strain, (2) the development and evaluation of 8-node single-layer plate bending elements for which the traction-fee conditions are satisfied along a straight edge, and (3) the elastic-plastic analysis of single layer plates. An analytic study is also presented to determine the nature of the potential 2-D singularity at the intersection of a bimaterial interface and a free edge. In the dynamic analysis, the stress response in a laminated composite due to a unit step load applied at the boundary is obtained for points which are (a) at a finie distance, and (b) at a large distance, from the impact end. For the case (a), the composite may consist of a finite number of layers.

Army Materials and Mechanics Research Center
Watertown, Massachusetts 02172
STRESS ANALYSIS OF COMPOSITES
R. L. Spilker and T. C. T. Ting
Department of Materials Engineering
University of Illinois at Chicago Circle
Chicago, IL 60680
Technical Report AMMRC TR 81-5, March 1981, 240 pp
Illus.-tables, Contract DAAG46-79-C-0045
D/A Project: 8X363304D215;
AMCMS Code: 633304.21500.03
Final Report, August 1979 to August 1980

AD ____________
Unclassified
Unlimited Distribution

Key Works

Composite materials
Finite Element
Stress analysis
Wave propagation
Plastic analysis
Viscoelasticity
Transient responses

Static and dynamic stress analysis of laminated composites is studied. In the static analysis, the hybrid-stress finite element model is used for (1) the study of edge effects in symmetrically-stacked laminates subject to prescribed inplane strain, (2) the development and evaluation of 8-node single-layer plate bending elements for which the traction-fee conditions are satisfied along a straight edge, and (3) the elastic-plastic analysis of single layer plates. An analytic study is also presented to determine the nature of the potential 2-D singularity at the intersection of a bimaterial interface and a free edge. In the dynamic analysis, the stress response in a laminated composite due to a unit step load applied at the boundary is obtained for points which are (a) at a finie distance, and (b) at a large distance, from the impact end. For the case (a), the composite may consist of a finite number of layers.


DATE
ILMED
8